Julius-Maximilians-Universität Würzburg
Institut für Informatik
Lehrstuhl für Kommunikationsnetze
Prof. Dr. P. Tran-Gia

Modeling and Optimization Methods for Wireless Sensor and Mesh Networks

Barbara Staehle

Würzburger Beiträge zur
Leistungsbewertung Verteilter Systeme

Bericht 01/11

Würzburger Beiträge zur Leistungsbewertung Verteilter Systeme

Herausgeber

Prof. Dr. P. Tran-Gia
Universität Würzburg
Institut für Informatik
Lehrstuhl für Kommunikationsnetze
Am Hubland
D-97074 Würzburg

Tel.: +49-931-31-86631
Fax.: +49-931-31-86632
email: trangia@informatik.uni-wuerzburg.de

Satz

Reproduktionsfähige Vorlage der Autorin.
Gesetzt in LaTeX Computer Modern 9pt.

ISSN 1432-8801

Modeling and Optimization Methods for Wireless Sensor and Mesh Networks

Dissertation zur Erlangung des
naturwissenschaftlichen Doktorgrades
der Julius–Maximilians–Universität Würzburg

vorgelegt von

Barbara Staehle

aus

Ansbach

Würzburg 2011

Eingereicht am: 10.05.2011
bei der Fakultät für Mathematik und Informatik
1. Gutachter: Prof. Dr.-Ing. P. Tran-Gia
2. Gutachter: Prof. em. Dr.-Ing. Dr. h.c. mult. Paul J. Kühn
3. Gutachter: Prof. Dr.-Ing. Christoph Mecklenbräuker
Tag der mündlichen Prüfung: 28.07.2011

Danksagung

Dank für die Sonne, Dank für den Wind,
Dank für die Menschen, die um mich sind.
Dank für die Freunde, die mit mir gehn,
und Dank für alle, die mich verstehn.

Johannes Jourdan (1923 -)

Diese Arbeit ist das Resultat fünfjähriger Forschungsarbeit am Lehrstuhl für Kommunikationsnetze, während derer ich nicht nur Höhen sondern auch Tiefen erlebt habe. Im Folgenden möchte ich daher all den Menschen danken die mir während dieser Zeit in vielfältiger Weise beigestanden sind.

Mein erster Dank gebührt natürlich meinem Doktorvater Prof. Dr.-Ing. Phuoc Tran-Gia dessen Impulse und Denkanstöße meiner Arbeit die richtige Richtung gaben und der mir die Freiheit gab, die Ideen zu verwirklichen, die ich spannend fand. Weiteren Dank schulde ich Prof. em. Dr.-Ing. Dr. h.c. mult. Paul J. Kühn und Prof. Dr.-Ing. Christoph Mecklenbräuker für die Begutachtung meiner Arbeit und ihre wertvollen Kommentare. Ein Dankeschön geht außerdem an Prof. Dr. Klaus W. Wagner für die souveräne Leitung meiner Disputation und an Prof. Dr. Reiner Kolla der sich als weiterer Prüfer zur Verfügung stellte.

Herrn Prof. Tran-Gia habe ich es zu verdanken dass ich im Zuge der Mitarbeit an Projekten und Konferenzteilnahmen Kontakte zu anderen Wissenschaftlern knüpfen und so meinen Horizont in vielen Richtungen erweitern konnte. Insbesondere bin ich Dr. Norbert Vicari und Michael Bahr für praxisrelevante Einsichten in die IEEE 802.15.4 und IEEE 802.11s Standards dankbar. Je me sais redevable de m'avoir permis partager leurs connaissances en géometrie stochas-

tique à Prof. Dr. Bartłomiej Błaszczyszyn et Prof. Dr. François Baccelli. I also owe many thanks to Prof. Dr. Michał Pióro, Dr. Mateusz Żotkiewicz, and Prof. Dr. Di Yuan for showing me new dimensions of optimization methodologies.

Den Studenten deren Bachelor- oder Diplomarbeiten ich betreut habe, verdanke ich neue Sichtweisen auf Problemstellungen, Technik, oder Präsentationsmethoden. Insbesondere sind hier Matthias Kuhnert, Markus Weiß, Viktor Wendel, Matthias Hirth, Desheng Fu, Sebastian Deschner, Johann Scherer, Andreas Wendl, Markus Leimbach, David Stezenbach und Andreas Blenk zu nennen.

Unabdingbar für meinen wissenschaftlichen Erfolg war jedoch auch das Klima das Prof. Tran-Gia an seinem Lehrstuhl geschaffen hat und in dem ich mich sehr wohl gefühlt habe. Meinen Kollegen bin ich dafür dankbar dass sie mich als eine der ihren akzeptiert und mir mein Leben durch sehr viele technische, fachliche, und programmiertechnische Hilfestellungen oder schlichtes Zuhören erleichtert haben. Viele Kollegen sind auch zu Freunden geworden mit denen ich sehr viele schöne Stunden außerhalb des Lehrstuhls beispielsweise mit Feiern, Radfahren, Laufen, Cachen oder Klettern verbracht habe.

In fachlicher Hinsicht bin ich am meisten den Kollegen schuldig, die vor mir ihre Doktorarbeit abgeschlossen. Insbesondere gilt mein Dank hier Dr. Dirk Staehle der sehr oft meine fachliche Dunkelheit wie ein leuchtendes Feuer erhellte. Von Dr. Andreas Binzenhöfer, Dr. Andreas Mäder, Dr. Tobias Hossfeld, Dr. Kenji Leibnitz und Dr. Rastin Pries lernte ich nicht nur fachliche Details, sondern auch viel über die korrekte wissenschaftliche Sprache, Interpretation und Aufbereitung von Ergebnissen, den Umgang mit Projektpartnern, Marathontaktik oder Skitechnik. Dr. Robert Henjes und Dr. Simon Oechsner möchte ich besonders dafür danken dass sie immer ein offenes Ohr für mich hatten und mir mit Rat und Tat zur Seite standen. Meinem CTO Florian Wamser habe ich es zu verdanken dass alle Bewohner unseres AquareYoums aufs Vortrefflichste harmonierten. Daniel Schlosser danke ich für seinen unerschütterlichen Optimismus dass schon alles gut werden würde, Thomas Zinner für unzählige virtuelle zusammen gerauchte Zigaretten, Michael Duelli für manch strafenden Blick über den Rand seiner Brille dem meist ein wertvoller Rat folgte. Meinen Mitbewohnern

Dr. Rüdiger Martin und Dominik Klein schulde ich tiefsten Dank für ihre Toleranz des Zustandes meiner Bürohälfte. Meinen Seilpartnern Matthias Hartmann und Frank Lehrieder danke ich dafür dass sie mich an ihrem Wissen teilhaben lassen und dass ich ihnen mein Leben anvertrauen kann so wie sie mir ihres anvertrauen. Für die Beantwortung technischer Fragen bin ich insbesondere meinen jüngeren Kollegen Steffen Gebert, Matthias Hirth, David Hock, Michael Jarschel und Christian Schwartz dankbar.

Nicht vergessen möchte ich Frau Gisela Förster deren organisatorische Unterstützung mir das Leben erleichtert hat. Frau Susann Schmitt ist es zu verdanken dass ich nicht an den letzten Hürden vor der Disputation gescheitert bin.

Außer Frage steht dass die Unterstützung meiner Familie einen wesentlichen Beitrag an dieser Arbeit hat. Vor allem meinen Eltern Monika und Dr. Leonhard Emmert kann ich es nie vergelten dass sie immer an mich geglaubt haben, besonders in den Zeiten in denen ich dies selbst nicht tat. Das Wissen dass sie immer vier offene Ohren, frisches Gemüse und einen Platz am Feuer für mich haben war und ist eine beruhigende Konstante in meinem Leben.

Mein Mann Dirk Staehle freut sich wahrscheinlich ebenso sehr über die Vollendung dieser Arbeit wie ich, da er mich oft an Abenden und Wochenenden mit der Wissenschaft hat teilen müssen. Zum Glück hat er hierfür, genauso wie für alle meine durch die Arbeit verursachten guten und schlechten Launen, immer großes Verständnis gezeigt. Während ich diese Arbeit erstellt habe, hat er immer zu mir gehalten und wenn er es auch nicht immer geschafft hat mich aufzumuntern, hat er doch stets für mein leibliches Wohl gesorgt. Dafür dass er mich insbesondere in letzter Zeit in Liebe ertragen und so das Band des Friedens zwischen uns bewahrt hat, bin ich ihm über alle Maßen dankbar.

Contents

1 Introduction

A journey of a thousand miles begins with a single step.
Confucius (604 BC - 531 BC)

The last decades have been blurring the line between the physical and the digital world. The most obvious trace of this process is that today, 72 % of the German population is using the Internet [29]. In contrast, the early Internet adopters have been a small group of computer scientists only. Likewise, the early-day Internet has been used for communication purposes only, whereas today, the typical Internet applications go far beyond data and email exchange. A plethora of daily life activities like looking for the weather forecast, accessing multi-media content, shopping, staying in touch with friends, booking travels, organizing or even having business meetings, have migrated from the physical to the digital world. And lastly, the Internet has grown beyond the structures dictated by workstations, desktop PCs and the wired infrastructure. Thanks to laptops, smartphones, or personal digital assistants, it has instead become close to ubiquitous.

Most probably the next decades will see an even tighter integration of the Internet in the real world. This will on the one hand be achieved by enhancing it with the ability to perceive, and on the other hand by loosening the chains of the wired backbone. In any case, the people-centric communication paradigm will be complemented by an ubiquitous communication among people and devices [30], or even a communication between devices [31]. Enabling this *future Internet* requires a research effort resembling to the journey of a thousand miles, Confucius speaks from. The problem is that the current Internet protocols and structures,

having their origin in the 1970s or 1980s, are unsuitable for coping with the resulting increased user mobility, number of traffic sinks, and sources, and amount and variance of data traffic. Actually integrating the Internet more seamlessly into the real world, and making the vision of an efficient omnipresent Internet access reality, requires additional efforts in the *wireless* networking domain. *Cellular* wireless networking technologies like GSM, UMTS, or LTE enable high data rates, and a high degree of coverage, but require an expensive infrastructure. This monograph therefore makes one step of the thousand mile journey towards the future Internet, by presenting modeling and optimization methods for two types of *non-cellular* networks which seem most promising for accomplishing the Internet's omnipresence.

Enhancing the Internet by including perceptions is achieved by integrating *wireless sensor networks* (WSNs), whereas *wireless mesh networks* (WMNs) are responsible for offering simple and convenient access possibilities beyond the reach of the wired backbone. WSNs consist of small devices, so called *sensor nodes* equipped with a number of sensors and a wireless communication unit. Sensor nodes are either battery-powered, or gather their energy from their surroundings, hence do not need wires and may be deeply embedded into the environment. Thereby, a variety of previously impossible scientific, agricultural, health care, safety, or leisure applications like soil-moisture based vineyard irrigation, or assisted ambient living environments, become possible.

For assuring the connection between the WSN data sinks and the Internet, or between a user and the Internet, their flexibility and adaptability make WMNs a convenient solution. WMNs are composed of mains-powered so called *mesh nodes*, or *mesh routers*. WMNs are very similar to the "traditional", well-known wireless local area networks (WLANs), where access points (APs) are the center of a star topology and provide Internet access to a number of clients. In contrast to the WLAN APs, mesh nodes cooperate in providing a wireless multi-hop backbone and thereby covering a larger geographical area where client devices may exchange data, and access the Internet. As there is no "free lunch", this increase in coverage comes at the price of more complex topologies, which in turn

requires efficient, distributed resource management schemes for guaranteeing a minimum degree of quality to the clients.

At first glance, the smallest common denominator of wireless sensor and mesh networks seems to be that both are wireless networks and that they are indispensable for the future Internet. The applications WSNs and WMNs are enabling, and consequently also the used technologies, protocols, and evaluation criteria differ however strongly: The main purpose of WSNs is to deliver data gathered from the environment while minimizing maintenance overhead and maximizing lifetime, consequently, energy-efficiency is a must. In contrast, the main WMN use case is to provide Internet access. Hence, energy-efficiency is less important, but offering maximal throughput, and service guarantees play a significantly larger role. What is however again common to both network types is the problem that traditional network engineering metrics and techniques are insufficient and new approaches on both fields are mandatory. Adequate WSN and WMN performance models foster the understanding of these increasingly important network types, but additionally are a prerequisite for WSN and WMN specific optimization approaches, which are in turn of utmost importance for realizing a seamless integration of both network types into the Internet.

1.1 Contribution

Accepting the challenge to proceed towards the future Internet creates new opportunities, too. For enhancing the Internet by perceptions, and for increasing its ubiquity, novel modeling and optimization methods for the two enabling network types, WSNs, and WMNs, are necessary. Each of the four elements of the resulting problem space corresponds to one contribution of this monograph. This is summarized by Figure 1.1, illustrating that on the one hand, integrating WSNs into the Internet necessitates a thorough understanding and modeling of the energy consumption process. This first contribution, depicted on the lower left, enables the second one, depicted on the upper left, which increases the energy efficiency of IEEE 802.15.4, thereby enabling standards-based WSNs. On the

other hand, WMN Internet access networks can be operated more efficiently, if link rates are assigned in a dedicated manner. This fourth contribution, depicted on the upper right, is enabled by the third one, depicted on the lower right, which introduces WMN evaluation metrics reflecting the quality needs of the customers.

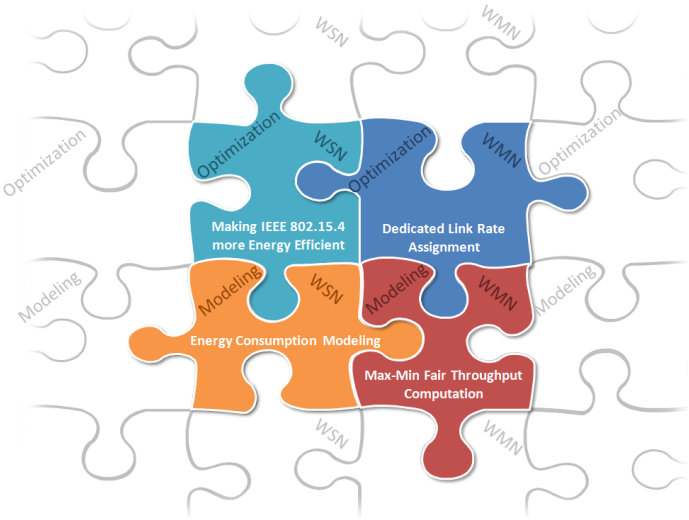

Figure 1.1: *Contributions of this monograph*

Let us now discuss the four issues more thoroughly. The first contribution of this work addresses the importance of *energy consumption modeling* in the context of wireless sensor networking. Before the advent of the WSN paradigm, energy efficiency was already in the focus of network engineering, but a question of minor interest. WSN performance evaluation and optimization can however only be done under the additional constraint of energy efficiency. Consequently, the sensor networking pioneers had to come up with adequate energy modeling approaches. Since then, many analytical works just adopted these models without wondering whether this still allows statements about networks consisting of state-

of-the art hardware, or if more detailed, hardware-oriented models, are necessary. From the networking perspective, the transmission energy consumptions are of highest interest, as only those costs may be influenced by tuning the communication behavior. An exhaustive discussion of different approaches for modeling these costs is hence one part of the first contribution. The second part arises from the need for energy efficiency, which makes the minimization of sensor node activity times under the constraint of guaranteeing a reliable multi-hop data delivery the major task of any WSN medium access control (MAC) protocol. Various researchers picked up this gauntlet and contributed WSN MAC protocols, each following a different operation principle and having a different degree of efficiency. Including this MAC layer efficiency in the analysis of a sensor node's daily energy consumptions has never been done before, examining the impact of both factors on analytical WSN engineering is hence an important step towards fully understanding WSN processes.

The second contribution of this monograph concerns *WSN optimization*, and identifies, and overcomes three inhibitors for low-power multi-hop standards-based wireless sensor networks. This is an urgent need as one of the reasons why WSNs have not yet been fully accepted by the mass market is the lack of a standardized communication layer. Out of the existing IEEE wireless communication standards, IEEE 802.15.4 [32], targeting at low-rate wireless personal area networks (WPANs), together with the higher layer protocol stack ZigBee [33] is the most promising possibility for enabling standards-based wireless sensor networks. The problem with these standards is however that the energy-saving mechanisms work for one-hop star topologies only, an organization form which is not feasible for large-scale WSNs.

Third, this monograph contributes suitable *WMN capacity models*. For analytically assessing the capacity of a wireless network, first of all, two questions have to be answered: It has first to be known which nodes must not transmit in parallel, and second how the load of a link is determined. Similar to the WSN energy modeling issue, the literature provides two different approaches for each of the two problems, but no holistic solution suitable for state-of-the-art WMNs,

where fairness guarantees have to be provided, exist. This lack is hence the motivation for contributing quickly computable algorithms which yield the max-min fair network throughput, and thereby an upper bound capacity for WMNs. An additional value of these algorithms is that they allow to compare the impact of the previously mentioned transmission constraint, and load definitions.

The final contribution of this monograph is an extensive study of one optimization possibility which has been neglected by research so far. The possibility of adapting the modulation and coding scheme (MCS), and thereby the transmission rate to the channel conditions arises from the way how bits are transmitted over the air interface: Using MCS with less information bits per symbol means a higher degree of robustness against interference at the price of a smaller data rate. If now, in contrast to the common praxis, a smaller data rate than the maximal feasible one is used, this allows for more concurrent transmissions. As a result, the per-link throughput is decreased, but the overall network throughput might increase. In order to thoroughly evaluate the costs and benefits of systematically assigning more robust MCS, first an analytical framework for link rate assignment is derived. This framework is then put to work for examining the impact of link rate assignment on the max-min fair WMN throughput, for a contention based channel access scheme, and under optimality conditions.

1.2 Outline

The previously discussed contributions are organized in the following manner: Chapter 2 is dedicated to discussing the impact of energy modeling on sensor network analysis. Giving an overview on the field of sensor networking, and introducing approaches to modeling the WSN energy consumptions, it additionally establishes the background necessary for understanding this and the following chapter. At the example of energy efficient routing topology establishment, which is a typical sensor networking engineering problem, the chapter subsequently studies the impact of transmission energy consumption modeling decisions. The analytical framework enabling this examination furthermore introduces an ab-

straction for the MAC layer efficiency and for the traffic patterns arising in a multi-hop topology, and thereby allows to assess the daily radio-related energy consumptions. This chapter is based on [8].

Chapter 3 proceeds from WSNs in general to the specific IEEE 802.15.4 and ZigBee technologies. Both are prospective WSN techniques, but as they originally aim at applications which do not require large networks consisting of regularly sleeping sensor nodes, there are three main inhibitors on the way to making them fully accepted WSN standards. The first problem lies at the beginning of the WSN lifetime: each IEEE 802.15.4 network has to complete the so-called association phase before it can become functional, a mechanism which is not working for low-power multi-hop networks. For the operational phase, ZigBee proposes a self-organizing routing protocol which is not working efficiently in the presence of sleeping nodes. Finally, there has to be a coordination of the sensor node duty cycles, otherwise no multi-hop data delivery with acceptable packet delivery rates is possible. The chapter addresses and solves each of the problems in a standards-compliant way and summarizes the results of [6, 11, 13].

The part on wireless mesh networks is introduced by Chapter 4 which establishes the background required to understand this and the following chapter. This is achieved by surveying mesh networking in general, and then discussing how a WMN can be formally described. Moreover, an overview on works related to the problem of WMN capacity estimation is given. The existing contributions are now extended so that two algorithms, each using a different analytical load definition, emerge. These enable the computation of the WMN throughput under max-min fairness. A comparison of the network throughputs achieved if the two algorithms are used with different interference models completes this chapter which is based on [20].

The last contribution of this monograph can be found in Chapter 5, which investigates in how far link rate assignment is suitable for increasing the WMN performance. After a review of works related to the problem of using link rate assignment for WMN optimization, the idea of link rate assignment is formalized. Subsequently, it is shown that assigning slightly slower data rates than neces-

sary is suitable for increasing the max-min fair network throughput. For a WMN with a random channel access, without fairness mechanisms, stochastic geometry allows to derive a link rate assignment scheme which is suitable for avoiding collisions. A simulation study however points out, that this is not beneficial in terms of end-to-end throughput. Finally, this chapter introduces a mixed integer programming formulation which allows to find an optimal solution for the joint problem of transmission scheduling and link rate assignment. This chapter extends the contributions of [2, 16, 22].

Finally, this monograph is summarized in Chapter 6. Additionally it provides conclusions and insights emerging from the findings of this work.

2 Modeling Wireless Sensor Network Energy Consumptions

Energy and persistence conquer all things.
Benjamin Franklin (1706 - 1790)

While the idea of wireless sensor networking inspires the research community since the turn of the millennium (see e.g. [34–36]), WSN applications have been, in contrast, not yet fully adopted by the mass market. Similarly, the Internet of Things first described by Gershenfield et al. [37] in 2004, has yet to become reality. One important reason why WSNs do not yet help in coping with questions of the everyday life are monetary costs. In 2000, Rabaey et al. [38] called setting up cheap, self-organizing, low-energy wireless sensor networks and making them easily accessible to end-users "one of the most compelling challenges of the next decade". According to the authors, having not only small low-power, but primarily cheap sensor nodes is vital for successfully addressing this challenge. While the energy demand of the sensor nodes, as well as their size have been reduced, device prices below 1 $ mentioned by [38] are still far from becoming reality.

Another consequence of the still rather high device costs is that the vision of large, very dense WSNs consisting of randomly deployed sensor nodes dropped from an air plane, which was very popular during the first years of WSN research (see e.g. [39]), has also not yet become reality. In contrast, WSNs have to be carefully planned and engineered in order to allow for a successful operation. To maximize the network survivability and hence the quality and quantity of the

assembled data, a WSN has however to be designed in the most energy-efficient manner as possible. As discussed in the last chapter, are traditional network engineering metrics and techniques inadequate for this purpose, as they do not bother about performance evaluation and optimization under the additional constraint of energy efficiency. Consequently, much work has been dedicated to the design of highly energy-efficient WSN algorithms and protocols resulting in a plethora of algorithms a WSN designer can choose from.

More optimization potential lies in the sensor node duty cycle, the spatial distribution of the sensor nodes, the number and positions of sink nodes, or in application layer parameters like the use of data aggregation. Due to the large design space, it is not possible to test all possible configurations in the field. It is therefore vital to rate the reasonableness of an intended deployment *before* actually bringing out the nodes, as any setting which already shows weaknesses on the drawing-board, will not perform better under harsh environment conditions.

If now the energy efficiency of a WSN configuration shall be determined by means of analysis or simulation, it is necessary that results match the reality. For this purpose, realistic simulations for determining energy consumption and the lifetimes of battery operated nodes would yield the most accurate results, but require a highly detailed model of the sensor nodes and their behavior. As those fine grained models are computationally expensive and time-consuming, analytical methods are preferable, especially, if a quick estimation is required, or if a set of design alternatives for a large scale deployment has to be analyzed.

Analytical approaches for predicting the energy consumption in sensor networks have to find adequate abstractions and descriptions for the sensor node behavior. The possibilities for abstractions are countless, this chapter therefore aims at assessing the influence of energy consumption modeling on engineering decisions and identifies the critical parameters describing the communication costs. This contribution is in accord with the seminal work of Heinzelman et al. [35] who pointed out that different assumptions on the communication costs alter the advantages and disadvantages of each energy-efficient protocol. The insights presented in the following are however insofar novel and important as most

WSN optimization works opt for one energy model only and do not comment in how far the results would still be valid if another model was used. The second contribution of this chapter is the inclusion of the MAC layer efficiency in the analysis of the energy consumptions, a factor which has never been considered before but which is definitively relevant for the outcome of this metric.

This chapter is structured as follows: Section 2.1 establishes the background for this and the following chapter. This is achieved by giving an overview on sensor networking and thereby illustrating the manifold purposes sensor networks are used for and the resulting variety of network architectures and shapes. Secondly, approaches for modeling the transmission-related energy consumptions as well as the amount of energy, a sensor nodes radio unit consumes per day, are introduced. Note that beyond this introduction, this section does not contain related work, as the scientific community has up to now neglected discussing the impact of energy consumption modeling.

The heart of this chapter, i.e. the analytical framework which allows to compare the impact of modeling decisions on the transmissions costs, and to estimate the impact of the MAC layer efficiency on the daily sensor node energy consumptions is introduced in Section 2.2. The modularity of the framework allows to exchange the different components of the transmission costs one by one and thereby enables computing different variations of these costs.

In Section 2.3 this framework is put to work and used for producing a number of numerical results illustrating the large energy consumption variety arising from the resulting different per-bit energy consumption models. A subsequent comparison of minimum-energy topologies created according to the different energy consumption models shows that this difference applies to the topologies, too. These results as well as the preceding section are based on [8]. Concluding remarks can finally be found in Section 2.4.

2.1 Background

This section is on the one hand the key to understanding the content of this chapter, highlighting the impact of energy consumption modeling on wireless sensor networks in general. On the other hand, it also establishes the background knowledge for the following chapter which focuses on IEEE 802.15.4-based WSNs. Therefore, it starts with an introductory survey on WSNs, before a basic introduction to WSN energy consumption modeling is given.

2.1.1 A Survey on Wireless Sensor Networks

While *sensors*, i.e. devices which measure characteristics of the physical world like temperature, humidity, vibration, or acceleration have been around since long, it was not before the year 2000 that technological advances made it possible to build *sensor nodes*, sometimes also called *motes*, consisting of several sensors, a microprocessor, a memory chip and a communication unit. In one of the elementary contributions to WSN research, Intanagonwiwat et al. [40] pointed out that this allows to deploy a large number of sensor nodes carrying out specific tasks within the phenomenon to observe instead of heaving either intelligent nodes far away or dumb sensors in the region of interest.

In addition to the benefits, Langendoen [41] identifies a number of challenges resulting from this tight integration in the environment. In general, sensor nodes are not mains-powered but are supplied by batteries, or have to gather their energy from the environment. Exchanging batteries is always critical, sometimes even infeasible, and perpetual energy sources are not easily accessible. Hence, nodes have to operate for a number of years with the same battery, or with very scarce resources, and energy efficiency is a must. Furthermore, WSNs have to operate autonomously, even in the presence of hardware failures.“Traditional” communication protocols like IP, TCP, or UDP, or even adaptations for wireless networks are unsuitable for sensor networks as they do not strive for energy efficiency. Consequently, many researchers picked up the gauntlet by contributing

propositions for WSN specific hardware designs, deployment algorithms, architectures, and protocols for all layers of the networking stack.

In the remainder of this section, an overview on some typical fields of applications for sensor networking is given, illustrating the amount of challenges, WSNs have to cope with. Afterwards, the typical WSN network architecture is discussed and, an overview on enabling technologies is given. An exhaustive survey of all contributions to WSN research can e.g. be found in the survey paper of Akyildiz et al. [39], or the newer work of Yick et al. [42].

Use Cases

Out of the many ideas for the usage of sensor networks, only a fraction has left the drawing board and has been realized as a prototype or in commercially available products. In order to illustrate the versatility of the sensor networking paradigm, in the following, some of these potential fields of applications are reviewed.

One important WSN use case is *structural health monitoring* which allows to estimate the state and to detect changes in the structure of civil infrastructure like large buildings, bridges, or streets. Immediate warnings in the case of dramatic changes are as vital as continuous monitoring to assess the impact of long term effects. A platform for the indirect detection of structural damages using measurements of ambient vibrations and strong motions has e.g. been proposed by Kim et al. [43], who established a structural health monitoring system on the Golden Gate Bridge. *Disaster management* is another public safety application where it is necessary to collect and aggregate data from as many information sources as possible. An example for such a disaster management sensor network is the FireBug network, described by Doolin and Sitar [44], which aims at collecting real-time data from wildfires. The possibility of real-time data collection is obviously also highly interesting for military *surveillance missions and target tracking* applications. According to He et al. [45], who investigated the feasibility of such a target tracking network within the VigilNet project, the objective of ground or battlefield surveillance missions is to inform the military command and

control unit about passing tanks or troops, mine deployments, or target positions.

Security applications are however also interesting for civilians and private individuals. Wittenburg et al. [46] for instance, describe the design of a wireless sensor network which allows to monitor a fence and thereby to detect illegal intruders. Non-military applications are also in the focus of the ZigBee alliance (see Section 3.1.2 for a more extensive description). The main use cases of the ZigBee standard are *home, building, and industrial automation* applications. The use of WSNs for automation purposes offers a higher degree of automation, and a more flexible management of ambient control systems like heating or cooling[1].

In the scientific domain, WSNs have been used for a number of projects: A growing number of *environmental sensor networks* (ESNs) help in studying and understanding environmental processes. Hart and Martinez [47] list over 50 different application examples of ESNs, delivering complex seismological, meteorological, or oceanographic data, as well as simple temperature, light level, airflow, snow accumulation, water conductivity, or air humidity measurements. The collection of likewise data also enables *precision agriculture*, whereof the goal is optimizing agricultural processes, using information concerning not only the macroscopic environment conditions but also minuscule in-field variabilities. An exemplary such WSN deployment is reported in [48], where Goense et al. describe a setup where data from sensor nodes deployed in a potato field on the soil temperature, or humidity levels enables to fight a fungus disease more efficiently.

Observe that the previously mentioned applications are all feasible with a fixed set of sensor nodes deployed on the ground or on the structures to monitor. Relaxing these requirements by introducing mobile nodes makes sensor networking an interesting option for *health care* purposes. One example for this is AlarmNet, described by Virone et al. [49]. This system integrates heterogeneous devices, some wearable on the patient and some placed inside the living space, thereby enabling assisted living, monitoring, and home automation systems for the elderly and disabled. Another example is Code Blue proposed by Lorincz et al. [50]. It extends the applications of wireless sensor network technology to a range of med-

[1] http://www.zigbee.org/, last accessed 04/2011

ical applications, which require more urgent attention including pre-hospital and in-hospital emergency care, disaster response, and stroke patient rehabilitation.

For WSNs including mobile nodes, more optimization challenges, but also more opportunities, arise. The same holds for more specific WSN types surveyed by the group around Akyildiz, like underwater [51], or underground sensor sensor networks [52]. While most statements for "traditional" WSNs are applicable to those specialized WSNs, the inverse is in general not true. Consequently, the remainder of this work is dedicated to terrestrial sensor networks without mobile components.

Network Architecture

The main conclusion of the previous discussion is that describing a *typical* WSN is not trivial, as *the* typical WSN use case does not exist. What is however common to all WSNs is that the intelligence is mainly at the edge of the network as the sensor nodes deployed in the field are kept as simple as possible in order to guarantee a maximal length of maintenance free operation. Hence, processing and storage capabilities are reduced to a minimum. State-of-the art sensor nodes like e.g. the IRIS mote from MEMSIC [53], have microcontrollers which are up to 8 MHz fast and have a RAM of up to 8 kB. This is already a significant improvement in comparison to the early day motes, but not enough for carrying out complex queries, or for offering an ergonomic user interface.

Consequently, sensor nodes are only meant to capture data, sometimes carry out some simple operations and then deliver the measurements to a more powerful *sink node* which either offers a user interface, or which forwards the data over the Internet, see e.g. [39]. This results in the typical WSN architecture, whereof an example is depicted in Figure 2.1. Due to the rather low range of the sensor node transceivers, not all sensor nodes are able to directly reach the sink node. Hence, each sensor node which is not a leaf in the resulting routing tree has to forward data on behalf of other nodes in order to ensure that all measurement data reach the sink nodes. Observe that except for this forwarding traffic, there

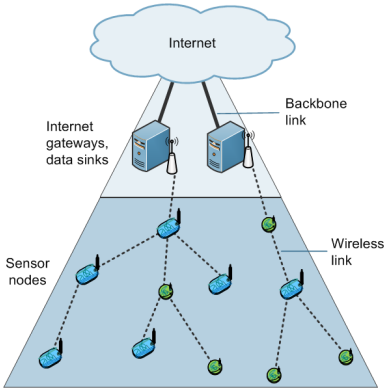

Figure 2.1: *A typical two-tiered WSN architecture*

is no communication between the sensor nodes. The traffic flows are strongly restricted: The sensor nodes send their measurement packets to the sink nodes, requests for specific pieces of data are traveling in the other direction.

Technologies

In Figure 2.1, intentionally, two different types of sensor nodes are shown to illustrate the manifold shapes and sizes sensor motes come in. This diversity is due to the previously discussed diversity of sensor networking applications, operation conditions, and the different approaches for coping with the demand of energy efficiency. In the following, let us hence traverse the ISO/OSI stack and analyze how this need is solved at the different layers.

Starting with the physical layer, one discovers that in contrast to wireless *mesh* networks, which will be the topic of Chapters 4 and 5, there is no widely accepted communication standard for wireless *sensor* networks. None of the existing standards, like IEEE 802.11 [54] or IEEE 802.16 [55] are suitable for low-power, low-complexity WSN hardware. The IEEE 802.15.4 standard [32] discussed

in Chapter 3 might one day play this role, but even if there is a growing number of sensor nodes with a IEEE 802.15.4-compliant radio, this standard is not yet fully accepted. Moreover is IEEE 802.15.4 not suited for all imaginable WSN operating conditions, and, additionally involves a rather high MAC layer overhead. Hence, many sensor nodes use a proprietary radio protocol, operating in one of the unlicensed ISM bands.

For the WSN MAC layer, the main challenge is the reduction of the so-called *idle-listening* overhead. If the IEEE 802.11 CSMA/CA protocol is used, a node in a multi-hop network always has to listen to the channel as it does not know when it will receive a message [41]. To remedy this and other deficiencies of CSMA/CA, a large number of protocols have been proposed which allow to find a trade-off between throughput, latency, and fairness on the one hand and a reduction in energy consumptions, thereby an increase in network lifetime on the other hand. Most of them claim their own letter, which results in a "MAC Alphabet Soup"[2] of over 50 different WSN specific MAC protocols. Following Langendoen [41], it is possible to classify them according to the channel access. If a *random access* scheme is used, the nodes do not organize but content for channel access. The advantage is the low organization overhead which comes at the price of increased collision probability. *Slotted access* schemes minimize the collision probability, but are slightly more complex, as all nodes have to agree upon a common time when to wake up and to communicate. *Frame-based access* protocols have the highest degree of complexity, as they organize in which slot of a time frame which node is allowed to send to which node. In the optimal case, this allows a collision free operation, but is very sensitive to drifting clocks. *Hybrid protocols* at combining the advantages and disadvantages of random and frame-based access schemes.

Moving up to the networking layer, we find a similar picture of a large zoo of existing protocols. Despite the need for energy efficiency, there is a number of other reasons which make routing in wireless sensor networks more challenging than routing in other wireless networks, see e.g. the work of Al-Karaki and

[2] http://pds.twi.tudelft.nl/ koen/MACsoup, last accessed 04/2011

Kamal [56]. The most important reason why IP based routing schemes are unsuitable for WSNs is the absence of a global naming scheme. Hence, a data-centric instead of an address-centric routing paradigm is more suitable. While this problem could be overcome by the introduction of IPv6, this protocol is still to heavy-weight for typical sensor nodes. Consequently, it is the goal of the IETF 6lowpan working group[3] to solve the various problems arising from the transmission of IPv6 packets in low-power wireless networks. However, the working group is still far from achieving its goal, and the lack of addressing schemes is still a problem for sensor networking.

The necessity of coping with these and similar problems and of adapting to the large variety of sensor network applications has lead to a huge number of routing protocols which are specifically adapted to the needs of WSN routing, and also to the application. Several works, e.g. [39, 56, 57], give an overview of the existing proposals and discuss different classification approaches: Akkaya and Younis [57] present a number of protocols which are classified according to the way in which the routes are determined. According to the authors this can e.g. be data-centric, wherefore directed diffusion [40] is the most prominent example. In this case the sink disseminates interests for certain pieces of data which propagate through the network. The measurement data is then sent back on the same path the interest has traveled. Another option is a hierarchical routing structure which has been first realized by the LEACH protocol [35]. Here, a subset of the sensor nodes are selected as cluster heads which serve as relays for the other sensor nodes, aggregating, and then forwarding their data. The other most frequently used variant is location-based routing. The GEAR protocol [58] has been the first approach to implement this paradigm where data is routed in order to minimize the geographical distance to the destination.

In most WSN stacks, the transport layer protocol is omitted, as retransmissions are handled by the MAC layer, and congestion is no problem. Obviously, this saves processing power, and thereby energy, but comes at the price of a decreased end-to-end reliability. Recall that some WSN applications target security-relevant

[3] http://datatracker.ietf.org/wg/6lowpan, last accessed 04/2011

purposes and hence require a reliable message delivery. However, for those networks, the energy constraint holds, too. Therefore, TCP and its adaptations are too heavy-weight for WSNs, and a number of transport layer protocols tailored to WSNs exist which are reviewed by Jones and Atiquzzaman [59].

Additionally, a number of other sensor networking problems exist, which Yick et al. [42] summarize to be energy-efficient localization, synchronization, guaranteeing the coverage of the area to monitor, data compression and aggregation, and finally privacy and security. In a nutshell, the requirement for energy efficiency, is integral to WSN design on all layers. Hence, let us concentrate a bit more on the energy aspect in the following.

2.1.2 Modeling Energy Consumptions

Despite all attempts to save energy, a truly autonomous WSN operation is still not feasible. As the main cause for this, Paradiso and Starner [60] identify the battery capacity not growing according to Moore's law. They show that while disk capacity, CPU speed, available RAM, and wireless transfer speed are growing near to exponentially, this is not the case for battery energy density. As a consequence, they point out the need to exploit renewable energy sources, especially for highly power constrained sensor networks. According to the authors, the principle of *energy harvesting* (also known as *power harvesting* or *energy scavenging*) guarantees a prolonged or even perpetual functioning of the network. Several energy harvesting possibilities are seen to be suitable for wireless mobile devices, and also sensor nodes, which e.g. include gathering energy from ambient radiation, or light sources, via heat transfer, from vibrations, or from movements [60] .

The downside of such approaches is their high price and their rather low energy conversion efficiency. Hence, energy efficiency is still a vital driving force for WSN engineering, which makes in turn assessing the energy consumption of a network design or algorithms indispensable. The interest of the networking community is on layer 3 and below, consequently, the energy consumptions of the transceiver are the mainly important evaluation metric. Those *radio-related*

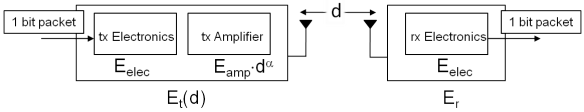

(a) Following Heinzelman et al. [64]

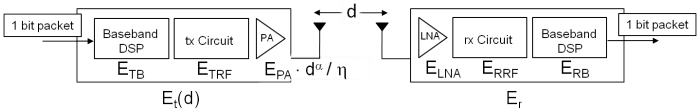

(b) Following Wang et al. [65]

Figure 2.2: *Modeling the energy required for transmitting a bit*

energy consumptions consist of both, the energy consumed for receiving and transmitting packets, and of the amount of energy which is consumed during the rest of the time. Models for both problems will be reviewed in the following.

Radio energy dissipation models

The most widely used energy model for analyzing radio operations in sensor networks (see e.g. [61–63]), has been proposed by Heinzelman et al. in [35] and later been refined in [64]. As illustrated by Figure 2.2(a), the authors model the amount of energy required for a transmission over a distance d as the sum of a constant and of the required transmission output power. The latter scales with a power of d, accounting for the path loss, the former represents the constant energy consumptions of the transmitter (tx) and receiver (rx) electronics.

Applying results from the model introduced above to a real world sensor network deployment results in two problems: On the one hand, typical sensor node transceivers, as e.g. Texas Instruments' CC1000 [66], or CC2420 [67] do not enable a continuous variation of transmission output powers, but have only a discrete set of power levels. On the other hand, the assumption that the distance dependent power consumptions of the transmitter hardware is the same as the

required transmission output power is not true. This has been pointed out by Wang et al. [65] who develop a radio energy dissipation model accounting for the characteristics of typical low-power sensor node transceivers. Comparing the representation of this model, shown in Figure 2.2(b) to the one proposed by [64] depicted in Figure 2.2(a) illustrates the higher level of detail of this model.

Apart from the more accurate model of the electrical components, the main difference of this model is in the distance related transmission costs. According to Wang et al. [65], the *drain efficiency* η of the power amplifier of the sensor node radio chip, i.e. the ratio of transmission output power and the consumed DC input power, is at most 50 %. Additionally is it not constant, but increases with the output power. Apart from the constant processing and reception costs, this effect makes long transmissions more energy efficient than multiple short hops, as the impact of the path loss exponent is attenuated, an observation which has earlier been made by Haenggi [68].

Estimating the daily radio-related energy consumptions

Assessing the transmission-related energy consumptions is vital, but does not suffice. In order to evaluate the performance of an algorithm, or a network configuration, the question when which node will run out of energy, or how long a given percentage of sensor nodes might survive is of higher interest. Hence, a more holistic sensor node model, including more sensor node activities is necessary. Landsiedel et al. [69] attack the problem of energy consumption modeling by creating a sensor network emulator which predicts the energy consumptions of specific applications. A similar, but analytical approach is proposed by Polastre et al. [70], who evaluate the performance of their MAC protocol by estimating sensor node lifetimes. For this purpose, the node energy consumptions are computed as the sum of the energy needed for the node activities, which are described as transmitting, receiving, sleeping, channel scanning, and sampling data.

The interest of this work is on the communication-related aspects, therefore it focuses on estimating the energy consumptions of the transceiver. For this

purpose, the idea of abstracting the sensor node radio unit to a state machine is used, where each state has a dedicated power consumption. Based on this state machine, the daily energy consumptions are obtained as the sum of the times spent in the different states multiplied by the corresponding power consumptions. Among the first authors to use this approach are Bougard et al. [71] who analyze the energy efficiency of the IEEE 802.15.4 standard. In the following, an extension of this model will be introduced incorporating the results of Wang and Yang [72] which propose to additionally include the energy consumptions required for transitions between the states.

Wang and Yang [72] suggest to use a finite-state machine for abstracting the most important control states of the sensor node radio unit. As this finite-state machine models a hardware component, which has a limited number of states only, the adjective "finite" will be omitted in the following. This state machine reflects the energy consumptions of sensor node transceivers required in different states or transitions between states and can be used for analyzing the sensor node energy consumptions. The authors also show that extracting values for energy consumptions and times required in states or for state transitions from data sheets is exact enough for an analysis, besides the time required for starting up the sensor node, which is found by measurements [72].

In Figure 2.3 the state machine corresponding to TI's CC2420 [67] radio control states is shown. The indicated durations and power consumptions of states and transitions are taken from [67] or estimated as the average of the two initial and final state for the transition [72]. Using this model, and establishing an adequate temporal model of the sensor node behavior, it is now possible to asses the energy consumptions of the sensor node transceiver in a very accurate manner.

2.2 Framework for Energy Consumption Modeling

In the following, an analytical framework will be presented which introduces a unified notation for the transmission cost models established in the last section. Moreover, this model allows to exchange the different components of the trans-

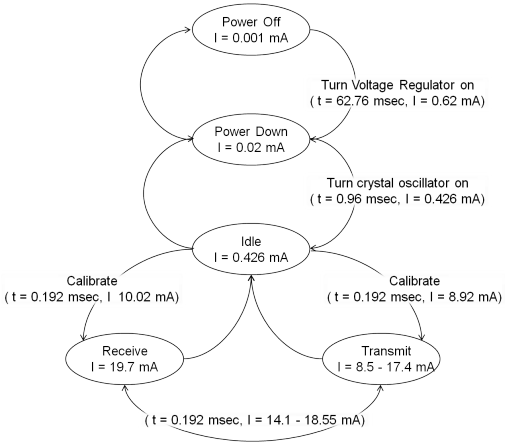

Figure 2.3: *Finite-state machine abstracting CC2420*

mission costs one by one and therefore enables a detailed analysis of the different components' impact. In Section 2.3 this framework will be used to compare routing topologies created with the so computed different communication costs. One of the benchmarks used for this comparison will be the daily energy consumptions with regard to the MAC layer efficiency and the routing topology.

2.2.1 Radio Operation Costs

Seeking a unifying description for the models of [64] and [65], shown in Figure 2.2, results in the following expression for the energy required for transmitting one bit over a distance d:

$$E(d) = E_0 + \frac{E_t(c,d)}{\eta(c,d)} + E_r. \tag{2.1}$$

E_0 represents the energy consumption in the transmitters' signal processing and front-end circuits. This term is constant for transmissions over all distances, and is computed as the product of the time the transceiver needs for handling a bit, t_{bit} and the corresponding transmitter power consumptions. $E_t(c, d)$, the required transmission energy is computed as the product of the transmission output power required for achieving the distance d, P_t, and t_{bit}. The value of P_t depends on the channel characteristics, represented by the radio propagation model, and the receiver sensitivity. This is captured by the variable c.

Furthermore, does $\eta(c, d)$ denote the drain efficiency of the power amplifier, which is the ratio of transmission output power to DC input power [65]. As discussed earlier, η varies with the transmission output energy consumptions, E_t and thus depends on c and d as well. Finally, E_r represents the reception energy consumption, which is again distance independent. Please note that Equation (2.1) is not suitable for actually calculating the operational energy consumption of a packet radio as it neglects the overhead of packet headers, and footers. For comparing the different links in a network it is however suitable.

To compare the influence of the two discussed transmission cost models on minimum energy routing trees, Equation (2.1) is parameterized according to two different models. The *theoretical model (TM)* is based on the work of Heinzelman et al. [64] and the *hardware oriented model (HM)* is inspired by the insights presented by Wang et al. [65]. The parameters for the latter model are chosen to capture the characteristics of the earlier mentioned sensor node transceiver CC1000 transmitting in the 868 MHz band as it is used in MICA2 [73].

The theoretical model

This model captures the characteristics of the energy consumption model shown in Figure 2.2(a) proposed by [64]. This results in $E_0 = E_r = 50$ nJ/bit and

$$E_t(c, d) = \begin{cases} c_1 d^2 & \text{if } d < d_0 \\ c_2 d^4 & \text{if } d \geq d_0, \end{cases} \tag{2.2}$$

with $c_1 = 10$ pJ/(bit·m^2) and $c_2 = 0.0013$ pJ/(bit·m^4) models receiver sensitivity and free space or multipath signal propagation respectively [64]. No numerical value for d_0 is given, it is therefore set to the value wherefore the path loss exponents of 2 and 4 yield the same result, i.e. $d_0 = \sqrt{\frac{c_1}{c_2}} = 87.71$ m. Recall from the discussion in Section 2.1.2 that Heinzelman et al. [64] assume a direct relation of transmission output power and required DC input power. This translates to a distance independent $\eta(c, d) \equiv 1$.

The hardware-oriented model

According to Wang et al. [65], the non-distance related power consumptions in the transmission circuit are slightly smaller than the power amplifier consumptions for the smallest transmission output power. Using this approximation and the figures from CC1000's data sheet [66] yields $E_0 = 671.875$ nJ/bit and $E_r = 750$ nJ/bit. Note that these constant costs are over ten times higher than under TM. The reason for this is that at the time of writing of [35], Bluetooth[4] has been a prospective wireless sensor networking technology. Consequently, the authors parametrized their model according to Bluetooth characteristics, which is a low-power communication technique enabling data rates of up to 700 kbps. Turning Bluetooth radios on and off is both energy and time consuming. Consequently, this technology has never become popular for sensor networking. Moreover, the high Bluetooth data rates have never been realized by sensor node transceivers, which achieve at most 76.8 kbps (CC1000), or 250 kbps (CC2420). Consequently, the time for transmitting a bit, t_{bit} used by Heinzelman et al. in 2000 [35], is by magnitudes smaller than the one Wang et al. [65] assumed 6 years later. As now the values for the *energy consumptions* are computed as a product of the current draw, the voltage, and t_{bit}, this results in higher non-distance related energy requirements for HM.

For computing the transmission output power P_t required to span a distance d, the empirical ground plain channel model for WSNs operating in the 868 MHz

[4] http://www.bluetooth.com, last accessed 04/2011

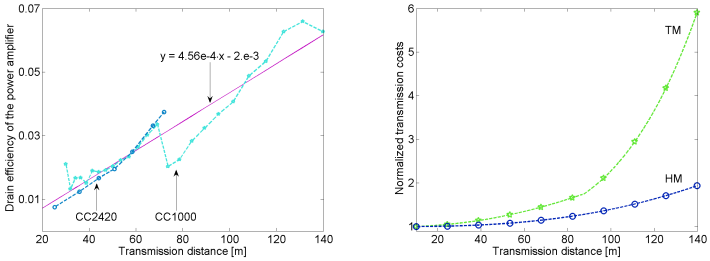

(a) Drain efficiency

(b) Normalized transmissions costs

Figure 2.4: *Drain efficiency and its impact on the transmission costs*

band proposed by Molina-Garcia-Pardo et al. [74] is used. Multiplying the transmission output power by t_{bit} gives the energy required for transmitting a bit as

$$E_t(c,d) = \begin{cases} c_1 d^{2.35} & \text{if } d < d_0 \\ c_2 d^{3.6} & \text{if } d \geq d_0, \end{cases} \tag{2.3}$$

where $d_0 = 6.2$ m, $c_1 = 0.0152$ pJ/(bit·m$^{2.35}$) and $c_2 = 0.0016$ pJ/(bit·m$^{3.6}$).

Recall from Section 2.1.2 that Wang et al. [65] report typical sensor node transceivers to have a drain efficiency, i.e. ratio of transmission output power to DC input power smaller than one. Additionally, the drain efficiency is increasing with the transmission output power. As a consequence, for HM a distant dependent η is used. The drain efficiency of the considered CC1000 in dependence of the transmission distance is shown in Figure 2.4(a). The considered MICA2 mote disposes of 26 different transmission output powers increasing in steps of 1 dBm from -20 to 5 dBm. The drain efficiency of the transceiver is now simply computed as the fraction of the possible output powers and the corresponding power consumptions of the transceiver. The latter is computed as a product of the typical current consumptions given in CC1000's data sheet [66] and a constant operating voltage of 3 V. To obtain the interdependency between d and η,

the channel model from Equation (2.3) is used. Along with the so obtained discrete values of η, a simple linear fit is shown. In addition, the figure visualizes the drain efficiency of the IEEE 802.15.4-compliant CC2420 [67] which will be used in the evaluation section of Chapter 3.

While the precise behavior of η depends strongly on the specific chip, and the channel conditions, the trend of linear increase with the transmission distance is not only observable for the two considered, but for most existing transceivers. Consequently, $E(d)$ does scale with the transmission distance d to the power of the path loss minus 1. This small difference makes on the one hand long transmissions more energy efficient than multiple short ones and on the other hand does not allow to directly derive the transmission costs from the transmission distance, as in reality, the drain efficiency is non-linear. In Figure 2.4(b) the former fact, i.e. the stronger increase of $E(d)$ with the distance is visualized by comparing the *normalized transmission costs* $E_{norm}(d) = E(d)/E(d_1)$ resulting from the TM and the HM model, where $d_1 = 6$ is the smallest considered distance for this figure. This normalization is necessary, as $E(d)$ computed by HM with $\eta < 0.05$ is significantly larger than $E(d)$ computed by TM with $\eta \equiv 1$.

2.2.2 Daily Radio-Related Energy Consumptions

The focus of this work is on communication related aspects, hence affects the sensor node transceiver only and not the other components of the sensor board. The subsequently introduced model capturing the daily energy consumptions of the sensor node transceiver is hence suitable for comparing the efficiency of different communication protocol configurations. It is based on a rough abstraction of the radio unit state cycle and is similar to the approach presented by [70].

Once active, the radio unit of sensor node i is either transmitting, receiving data, listening for incoming packets or sleeping. The latter is most commonly implemented by putting the sensor node transceiver to the power down state, as going to power off requires a lengthy recalibration of the crystal clock (cf. Figure 2.3). In order to listen to the channel, the sensor node transceiver has to be

in the receive state, listening therefore consumes the same amount as receiving data. The duty cycle therefore reduces to the states receiving (r), transmitting (t) and sleeping (s). Focusing on situations where all nodes operate at a regular schedule, node i has the same duties during all time units. The mentioned state cycle translates thus to the following partition of a time unit T:

$$T = t_i^t + t_i^r + t_i^s. \tag{2.4}$$

For the case where the WSN consists of homogeneous nodes, i.e. where each node is equipped with the same radio unit, all nodes have the same typical *electrical* power consumptions, denoted by the exponent "*el*", $P_t^{el}(P_t)$, P_r^{el} and P_s^{el} which are required for transmissions with an output power P_t, receptions and sleeping respectively. The electrical energy node i needs for radio activities during one time unit T can thus be calculated as

$$E_i^{radio} = t_i^t P_t^{el}(P_t) + t_i^r P_r^{el} + t_i^s P_s^{el}, \tag{2.5}$$

where the question which output power P_t is used depends on the routing topology, and also on the application characteristics.

The time each sensor node spends in transmit, receive or sleep state depends on several factors. One is of course the radio's data rate which determines how fast packets are transmitted and received. Another factor influencing the part of the time a node spends sending and receiving data is its load which is given by application demands and the routing topology. To account for the impact of these characteristics, the number of measurement packets each node creates and sends to the sink per time unit have to be taken into account. In dependence on the purpose the WSN is used for, this traffic pattern can be arbitrarily complex. Including the influence of the application layer characteristics is out of scope of this analysis. Hence, the assumption that all nodes create exactly λ packets during T, abstracting a typical monitoring application, is used in the following.

Let us start establishing a model for the amount of time node i spends in the

different states with the time spent in transmit state. This of course depends on the number of packets Π_i, sent by node i during one time unit T, which is in turn influenced by the number of nodes using i as a relay towards the sink. Π_i could be a random variable, if packet losses, collisions or data aggregation are modeled and increases if acknowledgments and retransmissions are considered. To reduce the degree of complexity of this analysis, let us assume that this is not the case. Π_i is thus just the sum of the number of measurement data packets generated by i and its children in the routing tree: $\Pi_i = \lambda(\xi_i + 1)$, where ξ_i represents the number of children node i has. If i is not relaying data, $\xi_i = 0$. Under the assumption that all data packets have the same size, they can be sent and received within t_{dat} each. The part of T node i is busy with sending is thus given by

$$t_i^t = \Pi_i t_{dat} = \lambda(\xi_i + 1)t_{dat}. \tag{2.6}$$

For computing the time a sensor node spends in receive state, we need to have a closer look at the WSN MAC layer functionality. Saving energy is one of the key requirement of WSNs, consequently, a MAC protocol running on a sensor node is responsible for putting the transceiver to sleep mode as often as possible. In order to enable a multi-hop communication, mechanisms allowing the sensor node to receive the packets whereof it is the recipient have to be implemented. The strategies of the existing MAC protocols, whereof some have been reviewed in Section 2.1.1, are different and so is their efficiency. Obviously, a perfect MAC protocol would allow that a node's radio unit is just active for the time it requires for transmitting its own packets and receiving the packets it shall receive. To model a smaller degree of efficiency, the following abstraction is used: Sensor nodes in the radio range of a sending node are forced to overhear this transmission unless their radio is in sleep state. As soon as a node overhearing an unwanted transmission recognizes that it is not the intended receiver, it can discard the packet. Again, the costs for discarding such unwanted packets depend strongly on the deployed protocol, but a worst case approximation is to allow the radio unit of a not addressed sensor node to return to sleep state after heaving read the

address field of the packet, i.e. after an amount of time t_{disc}. The *effectiveness* of the MAC protocol, $\varepsilon \in [0, 1]$, now gives the fraction of unwanted transmissions a sensor node could theoretically receive, the node actually *has* to receive and to discard. $\varepsilon = 0$ describes the ideal situation, where no sensor node overhears unwanted transmissions. $\varepsilon = 1$ would signify that all nodes are overhearing the communication of all their neighboring nodes, all other values indicate better or worse energy saving strategies.

Let $\Xi_i = \lambda\xi_i$ be the number of data packets i receives per time unit, and let us neglect protocol overhead and assume that all transmissions succeed. Then, we obtain the part of a time unit i is busy with receiving as

$$\begin{aligned} t_i^r(\varepsilon) &= \Xi_i t_{dat} + \varepsilon \sum\nolimits_{j\in\mathcal{N}} \Pi_j \vartheta_{ji} t_{disc} \\ &= \lambda[\xi_i t_{dat} + \varepsilon \sum\nolimits_{j\in\mathcal{N}} (c_j + 1)\vartheta_{ji} t_{disc}]. \end{aligned} \tag{2.7}$$

The boolean variable ϑ_{ji} expresses, whether the messages sent by j are overheard by i: $\vartheta_{ji} = 1$, if i overhears transmissions of j and it is 0 otherwise. Furthermore $\vartheta_{ii} = 0$ for all sensor nodes i.

Note that an energy consumption analysis ignoring the broadcast nature of wireless transmissions would assume $\varepsilon \equiv 0$. It would hence ignore the second term in Equation (2.7), representing the time i needs for receiving and discarding unwanted packets. Obviously, the main influence factor on this term is the node's position with respect to the sink: If i could theoretically overhear all transmissions from and to the sink, its unnecessary reception time will increase, as all data packets generated in the entire sensor network have to be forwarded to the sink. Moreover, this overhearing time will increase with the network density and the transmission output power, which both increase the number of nodes which are within the receiving range of a sending node. Finally, the amount of time the radio unit of node i spends sleeping is given by

$$t_i^s(\varepsilon) = T - (t_i^r(\varepsilon) + t_i^t). \tag{2.8}$$

Evaluating Equations (2.5) – (2.8) for a specific specific node i in a given network topology yields only an absolute lower bound for the *total* energy consumptions of the sensor node: This model does neither include factors like energy consumptions required for data sensing, processing or other purposes, nor does it account for battery discharge characteristics. Furthermore, retransmissions due to collisions or packet losses are negeglected. Despite its simplicity, this model is however suitable to capture the energy consumptions of the radio unit, and is a novel contribution to WSN research, as the efficiency of the MAC protocol and the impact of a node's neighborship have never been considered by analytical models. Moreover, this model is appropriate for illustrating the effects of energy modeling parameter choices on routing topologies, an analysis which will be presented in following.

2.3 Influence of Energy Consumption Modeling

The previously established framework is now applied to both point out the differences between the transmission energy consumption models TM and HM, and to evaluate their impact on the design of an energy efficient routing topology.

2.3.1 Transmission Costs

A glance back at Equation (2.1) shows that the transmission costs, i.e. the amount of energy required for transmitting one bit over a certain distance depends on the four building blocks E_0, E_r, c, and η, representing the constant part of the transmission costs, the reception costs, the channel model and the efficiency of the power amplifier. To examine the influence of modeling decisions, $E(d)$ is composed by choosing these building blocks as variants between TM and HM. This means that for both models, Equation (2.1) is evaluated, but with one of the four parameters set according to the other metric. Additionally, variations with $E_r = 0$, are investigated as this is also a wide-spread modeling assumption. As an example: for the variation denoted as "TM, c HM", Equation (2.1)

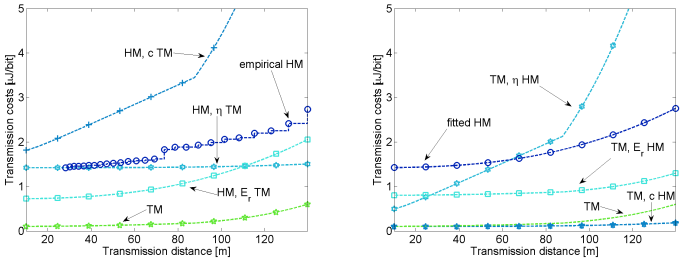

(a) Variations of HM

(b) Variations of TM

Figure 2.5: *Transmission costs for different energy consumption models*

is parameterized as discussed for TM, with the exception of the channel characteristics, which are taken from HM. Thus, $E_0 = E_r = 50$ nJ/bit, $\eta(c, d) \equiv 1$, $c_1 = 0.0152$ pJ/(bit·m$^{2.35}$) and $c_2 = 0.0016$ pJ/(bit·m$^{3.6}$).

Most of the 10 resulting parameter combinations result only in small variations of the energy required for receiving and transmitting one bit in dependence of the transmission distance. An analysis of the entire parameter space is not the goal, instead, the impact of the different factors is of interest. Hence, only some examples of the resulting combinations are depicted in Figure 2.5(a) and Figure 2.5(b). Note that the x-axis of this figure is limited to 140 m, as the maximal transmission distance for the considered chip according to [74] is 139.8 m.

In both figures, the costs resulting from the pure HM and TM metrics are shown. For HM, Figure 2.5(b) illustrates the transmission costs resulting from the use of a fit of the empirical drain efficiency depicted in Figure 2.4(a). Note that due to the nonlinear nature of the drain efficiency, this curve is much smoother than the one for the transmission costs obtained using the empirical values for η shown in Figure 2.5(a), but does not differ much otherwise. Hence, it is used for computing the costs resulting for variations of HM in the following.

Looking now at the curves resulting from a variation of the constant costs, i.e. E_r and E_0 confirms that changing the transmission costs by a constant factor

results in mere linear variations of the pure metric. In contrast, changes in the channel model and in the mapping of transmission output power to transmission costs, i.e. the parameters c and η affect the costs in a more interesting manner. Analyzing this effect in more detail shows that in both figures, the most steeply increasing curve depicts the combination of the channel characteristics proposed by TM (having a larger path loss exponent than the HM model) and the output power dependent drain efficiency model proposed by HM, i.e. "HM, c TM" and "TM, η HM" respectively. Note however that although both curves are increasing dramatically, the earlier discussed smaller normalized transmission cost decrease, caused by η, holds in this case, too.

In contrast, the combination of the channel model from HM and a direct mapping of transmission output power to necessary DC input power, i.e. "TM, c HM" and "HM, η TM" yields to seemingly distance independent transmission costs compared to the other metrics. This is however not the case, as the costs for this metric do also increase exponentially, but the use of $\eta \equiv 1$ introduces a reduction of a factor between 15 and 45. If one now plots this curve on the same axis as the curves representing the other metrics, it seems to be linear.

All in all is apparent, that the model of the channel characteristics has a major influence on the analysis of transmission related energy consumptions. Moreover, the parametrization of η, i.e. the mapping of transmission output power to consumed DC input power has to be done carefully, as this parameter has an major influence, too. These insights are quite natural and have already been mentioned in the literature, e.g. [65, 75]. However, the practical impact of those different transmission costs on sensor network analysis has not been examined. Using the example of energy minimizing topologies, the next section will hence illustrate that the abstraction of transmission costs has a huge influence on analytical work.

2.3.2 Energy Efficient Routing Trees

To obtain insights in the impact of energy consumption modeling on sensor network design, let us take a well known, widely studied problem as an example for

the various existing WSN research problems: If the batteries of all nodes may regularly be exchanged or if the nodes are able to gather energy from the environment, a minimum total energy tree (MTE), minimizing the per-transmission energy consumptions, is an interesting option for minimizing the energy required for collecting measurement data and thereby make optimal use of the resources.

For a numerical evaluation, the Monte Carlo simulation technique is applied. More precisely, network snapshots consisting of a set of identical sensor nodes randomly deployed in a quadratic area of size l^2 are considered. The location of the sensor nodes follows a spatial Poisson process with density ϱ. The application layer is abstracted by letting all nodes periodically send measurement data to one sink node. Between any two nodes i and j, a link exists if the distance between them, $d_{i,j}$ is smaller than the maximal feasible link length of 139.8 m predicted by the used channel model [74]. For each network snapshot, the MTE for TM, HM and their considered variations are obtained with the Dijkstra algorithm. The "costs" of each link which are used as a metric for the routing algorithm are obtained as follows: to each link of length d the per bit transmission costs $E(d)$, computed according to Equation (2.1), where the components are parameterized as outlined in the last section, are assigned. Recall that the considered CC1000 chip has only a limited set of output powers. Implementing an energy-efficient transmission paradigm is hence done by using for each link the smallest transmission output power which is required for reaching the destination. Consequently, the used $E(d)$ function is not continuous, but a step function.

For comparison purposes, additionally, two minimum hop topologies where all nodes operate with transmission output powers fixed to the minimum or maximum possible value are considered. For the CC1000, these are -20 and 5 dBm respectively, which translates to maximal reachable distances of 28.25 and 139.8 m [74]. For all considered scenarios with varying l and ϱ, and sink positions, the obtained results show comparable trends. Therefore, only results for topologies obtained in the setting with $l = 400$ m and $\varrho = 0.02$ and the sink placed in the upper left corner, are shown.

In order to illustrate the impact of the energy models on the resulting routing

trees, the results discussed in the following will tackle both topological characteristics and the resulting daily energy consumptions.

Topological characteristics

The more hops a data packet has to travel until it reaches the sink node, the longer the application has to wait for the outcome of a measurement event. Hence, the length of the routing paths is a good metric for comparing routing topologies as it determines the freshness of the data. Moreover, for the considered setting where no data is aggregated, an increase in hops means an increase of consumed bandwidth. Hence, both the times required for sending and receiving data and the risks of collisions and data losses are growing with the length of the routing paths. Furthermore, the relaying load of the nodes within one hop distance of the sink is growing if paths with longer hops are the majority. To analyze the path length distributions in the considered MTE topologies, let us compare the cumulative distribution function (CDF) resulting from the variations of HM and TM. These CDFs are shown in Figure 2.6(a) and Figure 2.6(b), respectively.

Additionally, the CDFs of the path lengths occurring in the minimum hop topologies with the maximal or minimal output power are shown and labeled by "minH$^+$" and "minH$^-$", respectively. Observe that these CDFs give clear lower and upper bounds for path length distributions reached in the MTE topologies. While in the minH$^-$ topology, up to 25 hops are necessary to reach the sink node, and the CDF is clearly below all other CDFs, the path length distribution of minH$^+$, representing topologies with the minimal possible number of hops, is nearly identical to several variations of both HM, and TM.

A closer look at Figure 2.6(a) shows that only two of the considered variations result in topologies with near to maximal link lengths, and therefore near to minimal path lengths. More precisely is the variation of η the only parameter of HM which does not influence the distribution of the path length. The reason for this is that under HM the constant per hop costs, E_r and E_0 are significantly larger than the distance dependent costs. Consequently, reducing or even neglecting the con-

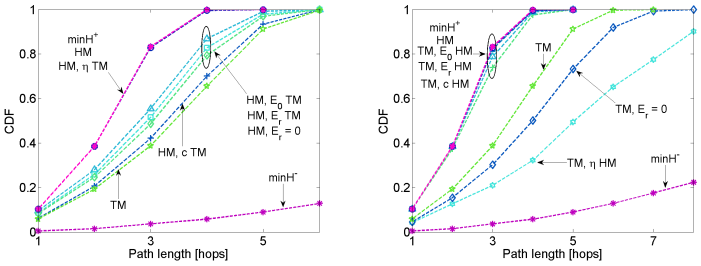

(a) Variations of HM (b) Variations of TM

Figure 2.6: *Impact of energy models on the MTE path lengths*

stant costs makes several shorter hops more energy efficient than one long hop and leads to topologies with more hops. Another interesting fact is that using the channel model of TM instead of HM has the strongest impact on the path lengths, as using a smaller path loss exponent makes long transmissions more expensive. Observe moreover that none of the variations of HM results in a MTE with as many hops as in the MTE resulting from the pure TM.

Figure 2.6(b) reveals that TM is more sensitive to changes: The curves representing "TM, η HM" and "TM, $E_r = 0$" illustrate that the number of hops increases, if distance related transmission costs are higher, or the reception costs are neglected respectively. Both makes more shorter hops more efficient, while increasing the constant costs, i.e. E_r and E_0 and decreasing the path loss coefficient, i.e. changing c, makes but less longer hops more favorable. This results in path length distributions very similar to the one of HM.

The insights gained from the analysis of the path length distribution hold also for two other topological characteristics. This is illustrated by Figure 2.7 which depicts statistics on the per node forwarding load and the link lengths. Figure 2.7(a) shows the CDF of the forwarding load, i.e. the number of children ξ_i each node has in some selected topologies. The curve of the "minH$^-$" for instance illustrates that the advantage of shorter links, and thereby smaller trans-

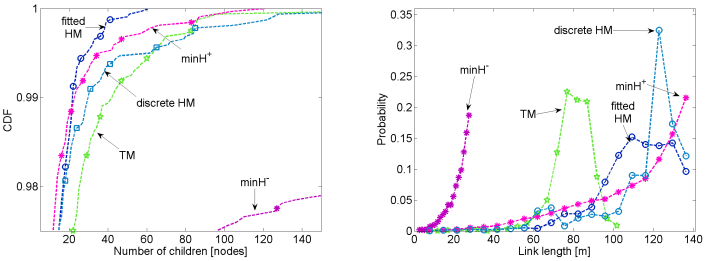

(a) Forwarding load (b) Link lengths

Figure 2.7: *Impact of energy model on forwarding load and link lengths*

mission error probability of longer paths comes at the price of a higher more varying forwarding load. The latter fact is a consequence of the tree-shaped routing topology structure, where the few nodes in reach of the sink node have to forward the packets of all other nodes. More interesting is the observation that the load distribution in the topologies resulting from the use of the fitted and the empirical η for HM differ strongly. This is in contrast to Figure 2.6 which shows that the distributions of the path length could not be distinguished. Hence, although the continuous cost metric fitted HM predicts not achievable link costs, it is better suited for breaking ties and therefore yields a more homogeneous forwarding load distribution. Together with the earlier made observation, this fact should be kept in mind for the case of battery operation, as highly loaded nodes will be the first ones to run out of battery.

Another topological comparison metric which follows from the path length distribution is the length of the links used for routing purposes. Therefore, Figure 2.7(b), shows the probability distribution of the link lengths, i.e. the distance between one sensor node and its next hop on the path towards the sink. Again, the link lengths occurring in the minH$^-$ and minH$^+$ topologies give the lower and upper bound of the link length occurring in the MTE topologies. The comparison of the curves for those topologies illustrates again that due to the higher

path loss exponent and the low reception costs under TM, shorter hops than under HM are preferred. A more interesting fact is the existence of local maxima corresponding to link lengths which are especially energy efficient according to the used metric. This again illustrates the importance of a correct energy consumption modeling as computing an MTE topology for a WSN deployment with a wrongly parameterized metric will result in a decreased system lifetime.

Observations following from the analysis of the transmission output powers used in the different energy efficient topologies are in accord with the earlier discussed findings. Especially the local maxima of the link length distribution which are visualized in Figure 2.7(b) can also be found in the CDFs of the transmission output powers. The earlier observed fact that the MTE established for TM results shorter hops, thereby longer routing paths, moreover also directly translates to the distribution of the output transmission power. Hence, for TM, smaller transmission powers compared to the topology emerging from the use of HM are dominating. Altering components of HM always results in less or equal transmission powers, whereas only assuming $E_r = 0$, causes the same effect for TM. All other changes make higher transmission output powers more likely.

All in all, this analysis hence illustrates that insofar topological characteristics are concerned, altering the model of the transmission energy consumptions results in near to arbitrary topologies. As outlined earlier, energy efficiency is the most relevant WSN metric. In the following, let us hence discuss if and how these topologies differ also with regard to this criterion.

Daily energy consumptions

The last three figures of this section are dedicated to analyzing the energy efficiency of the created topologies, and, on the impact of the MAC layer efficiency represented by the factor ε. For this purpose, let us compare the different routing topologies with the help of the estimated daily radio related energy consumptions, E_i^{radio} obtained from the model presented in Section 2.2. To obtain numerical results, a setting with sensor nodes that have MICA2's [73] and CC1000's [66]

characteristics, i.e. the radio chip needs 0.6 μW in sleep state, 28.8 mW for receiving and between 25.8 and 76.2 mW for a transmission with a voltage of 3 V, is assumed. The application running on top of the WSN is modeled so that per $T = 1$ minute, each node has to create and send measurement packet towards the sink node with a rate of $\lambda = 1$ min^{-1}. All transmitted data packets carry 10 Byte of measurement data, 4 Byte are needed for addressing purposes. To illustrate the influence of the MAC efficiency, results for an idealistic MAC protocol, where no sensor node overhears foreign transmissions, and for the case where everything is overheard, i.e. $\varepsilon = 0$ and $\varepsilon = 1$, respectively, are considered.

The six subfigures of Figure 2.8 show the average daily radio-related energy consumptions of a sensor node in the considered routing topologies. All shown values are obtained as averages over the considered random topologies. Together with the average values, the 95 % confidence intervals are shown. Their sizes indicate on the one hand that E_i^{radio} is varying strongly within the network, but on the other hand also that the mean E_i^{radio} is a metric suitable for cross-topology comparisons as the intervals do not overlap. Comparing the left ($\varepsilon = 0$) and the right ($\varepsilon = 1$) subplot of each subfigure of Figure 2.8 shows that the estimated energy consumptions which are roughly 20 times lower for the case of a perfectly efficient MAC layer. This huge difference illustrates the necessity of a proper inclusion of the MAC layer efficiency, if reasonable results shall be obtained. Please note that abstracting any realistic MAC protocol will result in a value of ε somewhere in between these two extremes.

For analyzing the differences between the topologies, let us first compare the minimum hop topologies and the MTE routing structures. This comparison is shown in Figure 2.8(a), where E_i^{radio} resulting in MTEs created with respect to the pure HM and TM are compared against E_i^{radio} resulting in the minH$^+$ and minH$^-$ topologies. The left figure describes the ideal situation of $\varepsilon = 0$ and illustrates that under this assumption higher transmission output powers, and thereby a smaller number of longer hops, result in smaller per node energy consumptions. This is mainly due to the smaller amount of consumed bandwidth and has been observed earlier [75]. In contrast, if all transmissions have to be overheard, the

situation depicted on the right, the estimated energy consumptions are in general nearly ten times higher. Additionally, topologies with smaller transmission output power seem more favorable now. The reason for this is that the number of potentially overheard messages increases with the transmission power. If all messages are overheard, i.e. if $\varepsilon = 1$, this leads to a significant reduction of sleep time and hence an increase of energy consumptions. This factor is in first line affecting the energy consumptions in the minH$^+$ and minH$^-$ topologies, but holds to a weaker degree for the MTE topologies created according to TM or HM, too. Note moreover that the energy consumptions in the MTEs created according to the discrete, or to the pure HM are nearly the same.

After this basic analysis, let us concentrate on Figures 2.8(b) and 2.8(c), where the average estimated daily per node energy consumptions for MTEs created according to variations of HM and TM are shown. This allows to make observations similar to the previously obtained results: E_i^{radio} for the topologies resulting from variations of HM does not vary strongly, the energy consumptions are thus rather similar, if $\varepsilon = 0$ is assumed. The right figure of Figure 2.8(b) demonstrates however, that differences are more visible, if overhearing is taken into account. Again, the statements reverse: "HM, c TM", which is the least favorable variation of HM for the idealistic case promises the smallest average per node energy consumption if overhearing is considered. This effect is also observable in Figure 2.8(c). If $\varepsilon = 0$, the topology created with a path loss exponent of 4 and the distance dependent drain efficiency, "TM, η HM", for instance, results in the highest average per node energy consumptions, as the percentage of nodes operating with a high transmission output power is larger than under all other variations. If $\varepsilon = 1$ is assumed, this topology seems much more favorable.

The used model allows only for a very rough estimation of the daily radio related energy consumptions. It however allows to illustrate that the energy efficiency of the different topologies is varying strongly. Moreover are these statements strongly depending on the MAC layer efficiency: Considering mere transmission and reception costs ($\varepsilon = 0$) leads to totally different conclusions than the ones obtained including overhearing costs ($\varepsilon = 1$). Both observations together

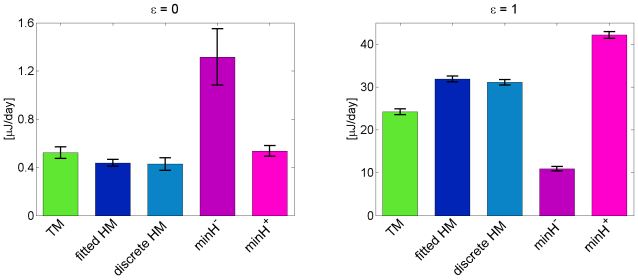

(a) MTE vs. minH^- and minH^+

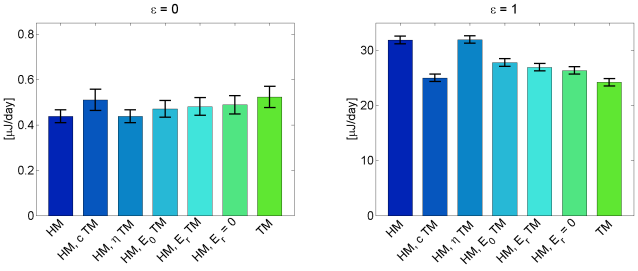

(b) MTE resulting from variations of HM

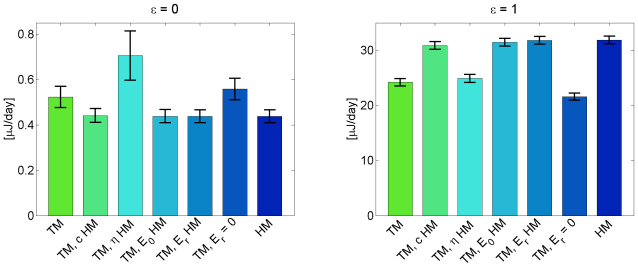

(c) MTE resulting from variations of TM

Figure 2.8: *Estimated daily energy consumptions*

hence again illustrate the necessity of using an energy model which captures the characteristics of the deployment the optimization is intended for.

2.4 Concluding Remarks

The sensor networking paradigm entered the stage with the promise of more seamlessly integration of Internet in the every day life. Although the research community has worked towards the goal of integrating the world's physical characteristics into the Internet for the last ten years, corresponding applications are only slowly available for the average Internet user. The reason for this lies in the WSN hardware and protocol complexity which necessitates an enormous engineering effort for designing efficiently working applications.

For WSN engineering, energy efficiency is the key challenge, as it directly translates to a lower maintenance overhead of the mostly battery powered sensor nodes. Hence, for any analytical work, one model out of the numerous existing energy consumption abstractions has to be chosen. Contradicting Heinzelman et al.'s [35] statement made at the beginning of the WSN research era that any energy efficient engineering holds for the chosen energy model only, most works just chose one energy model and do not comment on the impact of selecting other parameters. This exactly is the goal of this chapter which compares the impact of different energy models, on a well known analytical problem. Namely it investigates in how far the shape of analytically designed energy efficient routing trees for a large sensor network deployment varies with the used energy consumption metric. To examine the influence of different modeling assumptions, a modular framework has been introduced allowing to exchange the four components of the transmission costs. The findings illustrate that the abstractions of channel characteristics and the mapping of transmission output power to required DC input power influence the analysis of transmission energy consumptions most heavily.

As the most important metric, the daily energy consumptions in the created topologies have been analyzed. This analysis revealed that the per node energy consumptions vary strongly with the efficiency of the MAC protocol, i.e. the

number of unwanted transmissions a sensor node is forced to overhear. This often neglected factor is also responsible for a possibly wrong estimation of energy consumptions: if an ideal MAC protocol is assumed, i.e. no node is forced to overhear foreign transmissions, topologies which favor a few long hops over several short hops for multi-hop paths, are rated to be by far more energy efficient than topologies which contain more short hops. This statement does not hold any more if the effect of overhearing is considered, as for larger transmission ranges, more energy may be consumed for discarding unwanted messages. Thus, for any statement concerning per node energy consumptions, the consideration of the MAC layer and the structure of the routing topology is vital.

All in all, the findings of this chapter illustrate that energy models used for the design and analysis of real world sensor network deployments have to be chosen with care and with respect of the used hardware, as a bad design choice may lead to incorrect routing decisions. The contributions of this chapter are hence not only an important self-contained contribution for WSN research, but also a methodological foundation for the following chapter.

3 Enabling Standards-Based Wireless Sensor Networks

If you obey all the rules, you miss all the fun.
Katharine Hepburn (1907-2003)

The introductory discussion in Section 2.1.1 of use cases for WSNs revealed applications as different as habitat monitoring, environmental surveillance, cargo tracking, industrial automation, intrusion detection or health monitoring. Specific requirements and challenges are manifold and so are the types of deployed WSN hardware, radio communication techniques and higher layer protocols. This diversity inhibits architectures spanning different WSN deployments which are necessary for realizing ideas like the "Internet of Things", envisaged by Gershenfeld et al. [37], or "Integrating the Physical with the Digital World", an European Integrated Project[1]. A unified standardized communication layer providing clearly defined interfaces is hence a key enabler for these and similar concepts as the non-compatibility of proprietary communication techniques prevent truly pervasive and ubiquitous computing environments.

A number of wireless standards out of the IEEE 802 family provide data rates and ranges which seem suitable for wireless sensor networking. Taking the communication related energy consumptions into account, the IEEE 802.15.4 standard seems to be the most promising one for WSN purposes as it specifies a physical (PHY) and a medium access control (MAC) layer enabling cheap wireless networking for applications with limited battery power and small throughput

[1] http://www.sensei-project.eu/, last accessed 04/2011

and range requirements [32]. Together with higher layer protocol stacks like ZigBee [33] or WirelessHART [76], IEEE 802.15.4 has become popular for industrial purposes, as well as for monitoring and control applications and is seen as a prospective wireless sensor networking standard.

An indication for this statement is the bulk of sensor motes which are promoted to be "IEEE 802.15.4-compliant". Examples for this standard compliance are Tmote Sky from Sentilla [77], SmartMesh-XT M2135 from Dust Networks [78] or TelosB [79], IRIS [53], MICAZ [80] and Imote2 [81] from Memsic. This popularity is also illustrated by the hardware installation of the European WISEBED project which interconnects several WSN testbeds. Here, 559 out of the 779 deployed nodes and even 39 out of the 41 mobile nodes or 71% and 95% respectively have a IEEE 802.15.4-compliant radio [82].

The downside of IEEE 802.15.4, ZigBee, WirelessHART, and similar standards is that they are designed for scenarios where only one hop star topologies, are applicable. In this case it is possible to run the network in the so called *beacon-enabled* mode, where one central device informs its surrounding devices about periods which may be spent in power-down mode. For the case of WSNs, it is not admissible to assume that all sensor nodes are in reach of one central entity. Consequently the *nonbeacon-enabled* mode, providing no energy saving routines, is easier to realize. This lack causes all WSNs, which are part of the earlier mentioned WISEBED, to replace the IEEE 802.15.4 MAC layer by a WSN specific energy-efficient MAC protocol. Fully standard-compliant sensor networks should however implement all standard specifications and specifically use the non-energy-efficient IEEE 802.15.4 CSMA/CA channel access. This in turn necessitates additional mechanisms enabling the sensor nodes to sleep regularly while still allowing the successful data delivery over multiple hops.

The remainder of this chapter therefore describes a number of mechanisms required for enabling the energy-efficient operation of standards-based multi-hop topologies. It is structured as follows: Section 3.1 reviews IEEE 802.15.4 and the higher layer protocol family ZigBee and gives an overview on literature related to the problems of optimizing IEEE 802.15.4 and ZigBee for low power WSNs.

The next three sections address three major challenges on the way towards the energy-efficient operation of standards-based WSNs.

The first challenge is at the beginning of the WSN lifetime: Each IEEE 802.15.4 network can only become functional after the *association procedure* has been successfully executed. The association procedure requires that each node exchanges a number of messages with an already associated node. The case that one of these messages is lost is not handled by the standard [32], but occurs in contrast with high probability in a multi-hop network. Consequently, Section 3.2 introduces a number of modifications to the association procedure to efficiently start up a low-power multi-hop IEEE 802.15.4 network. This section is based on results published in [13].

The second challenge is in the operational phase of the network, where a distributed routing protocol has to enable data delivery. Such protocols work less efficiently in the presence of sleeping nodes since phases of inactivity may not be distinguished from node failures. Section 3.3 thus shows how to modify the routing layer in order to remedy this deficiency, a contribution which summarizes [6].

The third challenge arises from the combination of sleeping and multi-hop routing: If the sensor nodes sleep independently and ignore their surrounding, a multi-hop data delivery is not possible since a node forwarding data on behalf of another node has to share wake time with this node. Therefore, Section 3.4 introduces an efficient routing-layer aware sleep scheduling mechanism working above the IEEE 802.15.4 MAC layer. The contributions of this section are based on [11]. Finally, Section 3.5 concludes this chapter.

3.1 Background and Related Work

This section establishes the technical background required for the remainder of the chapter by traversing the ISO/OSI stack. First, an overview on the IEEE 802.15.4 PHY and MAC layer is provided before, the higher layers specified by ZigBee are introduced. As the networking functionality of ZigBee is the most relevant one for WSNs, a special focus lies on the ZigBee network layer.

Subsequently, the literature relevant for this chapter is summarized.

3.1.1 An Overview on IEEE 802.15.4

The IEEE 802.15 working group focuses on creating PHY and MAC layer specifications for (wireless) personal area networks ((W)PANs). From seven different task groups, TG 4 seems especially promising for wireless sensor networking purposes, which is illustrated by its self-description[2]:

> *The IEEE 802.15 TG4 subgroup was chartered to investigate a low data rate solution with multi-month to multi-year battery life and very low complexity. It is operating in an unlicensed, international frequency band. Potential applications are sensors, interactive toys, smart badges, remote controls, and home automation.*

Before giving an overview on IEEE 802.15.4 functionality relevant for the remainder of this chapter, this section shortly discusses the historical evolution of the IEEE 802.15.4 standards and amendments.

Existing and upcoming IEEE 802.15.4 standards

In 2003, IEEE 802.15 TG4 developed it's first standard. IEEE 820.15.4-2003 [83] specifies one direct sequence spread spectrum (DSSS) PHY layer with binary phase shift keying (BPSK) for the 868/915 MHz band and one DSSS PHY layer with offset quadrature phase shift keying (O-QPSK) for the 2.45 GHz MHz band. In Europe, only one channel on the 868 MHz frequency band is available, allowing a data rate of 20 kbps, while in the US, the 915 MHz frequency band offers 10 channels and a data rate of 40 kbps. In contrast, on the 2.45 GHz band, 16 channels are available worldwide and offer a data rate of 250 kbps. Consequently, this band is by far the most popular one. Additionally, IEEE 820.15.4-2003 specifies a number of MAC layer functionalities which will be discussed below.

[2] http://www.ieee802.org/15, last accessed 04/2011

Three years later, IEEE 820.15.4-2006 [32] was published, proposing specific enhancements and corrections while being backwards compatible with IEEE 820.15.4-2003. The main purpose of IEEE 820.15.4-2006 is to increase the applicability of IEEE 802.15.4 and the acceptance of the 868/915 MHz band. IEEE 820.15.4-2006 introduces more modulation schemes for the 868/915 MHz frequencies and a number of MAC layer extensions and modifications. With the 2006 revision, two more DSSS PHY layers in the 868/915 MHz frequency band became available. Amplitude shift keying (ASK) and O-QPSK enable data rates of 250 kbps and 100/250 kbps respectively. Moreover the number of available channels is increased to 3 (868 MHz) and 30 (915 MHz).

In 2007, an amendment to IEEE 820.15.4-2006, IEEE 802.15.4a-2007, was approved [84]. It specifies two more PHY layers for applications requiring location awareness, extended range, enhanced robustness and mobility. The first one is a chirp spread spectrum (CSS) PHY layer in the 2.45 GHz band. Differential quadrature phase shift keying (DQPSK) and 8-ary or 64-ary bi-orthogonal coding enable data rates of 1 Mbps and 250 kbps respectively. In addition to the DSSS channels, 14 partially overlapping channels became available. The second PHY layer implementation is an ultra-wide band (UWB) PHY layer enabling data rates of 0.11, 0.85, 6.81, and, 23.24 Mbps and providing 16 non-overlapping channels. The basic idea of UWB is similar to the Morse code. So called pulses, low power radio energy transmissions, occupy a large amount of bandwidth which may cover the frequencies of several “traditional” narrowband transceivers as their power is too low to disturb transmissions in this band. The information the pulses shall carry is modulated on the time when the pulses are transmitted. The IEEE 802.15.4a-2007 UWB PHY layer specifies, a sub-gigahertz band (250-750 MHz), a low band (3.1-5 GHz), and a high band (6-10.6 GHz).

Two years later, two amendments for the Chinese and Japanese market were approved. IEEE 802.15.4c-2009 defines two alternative DSSS PHY layers and modifications to the MAC needed to make IEEE 802.15.4 compliant with Chinese regulations [85]. 8 channels for the 780 MHz band are defined and data rates of 250 kbps with m-ary phase shift keying (MPSK) and O-QPSK are achievable.

The IEEE 802.15.4d-2009 amendment specifies two new PHY layers and introduces changes to the MAC layer for the Japanese 950 MHz band [86] in order to allow coexistence with passive tag systems. One PHY layer specifies DSSS together with BPSK and offers a data rate of 20 kbps, the other specifies Gaussian frequency-shift keying (GFSK). GFSK does not need a spreading technology and allows a data rate of 100 kbps. IEEE 802.15.4d-2009 introduces 22 channels.

The work on IEEE 802.15.4 is ongoing. TG4e is working on MAC layer enhancements for a better support of applications like factory and process automation or asset tracking and to permit a better compatibility with the Chinese WPAN. TG4f has the task of defining PHY layers and MAC layer extensions for active RFID systems. TG4g develops PHY layer amendments facilitating large scale smart utility networks allowing the smart grid to become reality. The purpose of TG4h is to correct errors, inconsistencies, and ambiguities in IEEE 820.15.4-2006. TG4i has the goal of combining the contents of the previously published IEEE 802.15.4 standards and amendments into an all-embracing standard. At the time of writing are TG4j, and TG4k focusing at medical body area networks, and low energy critical infrastructure monitoring, respectively the youngest IEEE 802.15.4 task groups[3].

The IEEE 802.15.4 MAC layer functionality

The IEEE 802.15.4 functionality which is most relevant for WSNs is specified by IEEE 820.15.4-2003 [83] and IEEE 820.15.4-2006 [32]. Both standards specify the popular 2.45 GHz PHY layer which is used by most existing IEEE 802.15.4-compliant sensor node transceivers and the MAC layer functionality. In contrast to the comparably simple PHY layer, the MAC layer provides many interesting features which will be reviewed in the following. On functional level, the differences between IEEE 820.15.4-2003 and IEEE 820.15.4-2006 are small, and IEEE 820.15.4-2006 is backward compatible to IEEE 820.15.4-2003. In the following, the term “IEEE 802.15.4“ is therefore used as shorthand for

[3] http://www.ieee802.org/15/, last accessed 04/2011

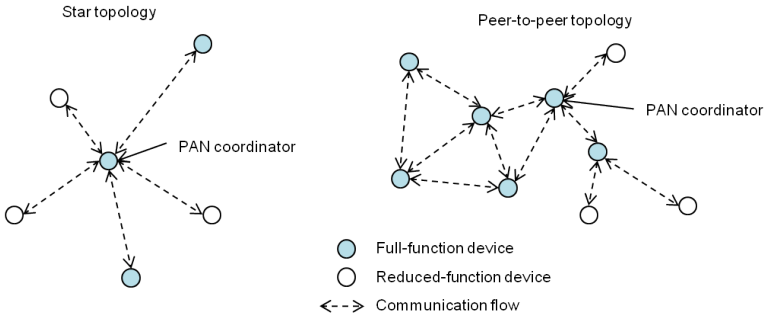

Figure 3.1: *Network topologies supported by IEEE 802.15.4*

"IEEE 820.15.4-2003 and IEEE 820.15.4-2006".

Let us start discussing the MAC layer functionality with the IEEE 802.15.4 network structure. Each IEEE 802.15.4 network, also called PAN, has exactly one *PAN coordinator* which should be mains-powered, as it has to be always active. IEEE 802.15.4 distinguishes two types of devices: *full-function devices* (FFDs) and *reduced-function devices* (RFDs). FFDs may communicate with both FFDs and RFDs, are able to relay packets on behalf of other nodes, and can become the PAN coordinator. RFDs can only communicate with one FFD and may be very simple devices like light switches. Each device wanting to join a PAN must associate, i.e. exchange a sequence of messages, with the PAN coordinator or an already associated FFD. In large networks the standardized procedure is not working as no mechanisms for the case where this message exchange fails are specified. Therefore, Section 3.2 describes some modifications for the association procedure and reviews the standardized mechanism in detail in Section 3.2.1.

The difference between RFDs and FFDs is illustrated in Figure 3.1, where the two topology types supported by IEEE 802.15.4, the star and the peer-to-peer topology, are depicted. In the latter topology type, RFDs may only be used at the edge of the routing topology, where FFDs may additionally forward data

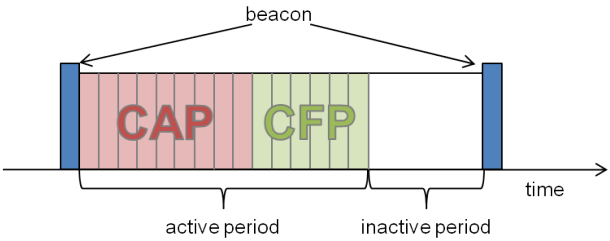

Figure 3.2: *Beacon-enabled IEEE 802.15.4 superframe structure*

on behalf of other nodes. Clearly, the star topology is most suitable for home automation, gaming and health care purposes, where one central machine collects and evaluates data from near-by sensors. WSNs in contrast may be spread over a larger area and not all sensor nodes are in reach of their data sink. In this case, the peer-to-peer topology should be used. Note that this requires that all sensor nodes must be FFDs in order allow for a flexible and resilient network formation.

IEEE 802.15.4 specifies carrier sense multiple access with collision avoidance (CSMA/CA) as channel access scheme. To increase the transfer reliability, the MAC layer acknowledges each transmission. To allow for an energy-efficient operation, IEEE 802.15.4 offers the possibility of organizing time into consecutive superframes which in turn are divided into 16 equally sized slots. The structure of a single superframe is illustrated in Figure 3.2. Such an organization works only in a *beacon-enabled* PAN where the PAN coordinator emits *beacons* in the first slot of each superframe. Each beacon contains information on the organization of the superframe and is used for synchronizing the network devices. It is possible (as e.g. depicted by Figure 3.2), that a superframe does not only contain an active but also an inactive part, where the PAN coordinator disables its receiver and consequently its associated devices can also enter sleep mode. The active phase is furthermore divided into a contention access period (CAP) and a contention free period (CFP). In the CAP, all devices may compete for channel access using slot-

ted CSMA/CA. In order to support applications with low-latency or bandwidth requirements, it is possible to reserve dedicated portions of the CFP, so called guaranteed time slots (GTS), for nodes which have to send time-critical data.

The drawback of the superframe structure is that it works flawlessly only for the case where all nodes are able to receive the beacons of the PAN coordinator. In order to realize the beacon-enabled mode in a multi-hop topology, FFDs are capable of sending out beacons and thereby establishing their own superframe structure for all nodes within their reach. In IEEE 802.15.4, such a structure is called *cluster tree* and proposed as a possible organization form for larger topologies. The question how the communication between the cluster heads is organized is however less trivial and additionally neither discussed by [83] nor by [32]. For such topologies and for typical WSN applications, which do not have strict latency or synchronization requirements, IEEE 802.15.4 specifies the *nonbeacon-enabled* mode which does not require periodic beacon transmissions. The price for this reduced overhead is that it is not possible to maintain the superframe structure in nonbeacon-enabled PANs and the channel access is done via unslotted CSMA/CA. Moreover, no energy-saving periods of inactivity are provided. Thus, nodes wishing to communicate in a peer-to-peer topology have either to synchronize their periods of inactivity or to always enable their receiver.

A problem which is common to both the beacon-enabled and the nonbeacon-enabled mode is the small packet size. A IEEE 802.15.4 packet may at most contain 127 B whereof at least 15 B and at most 31 B are occupied by PHY and MAC layer headers and footers [32]. The actually feasible payload size hence varies between 96 B and 112 B.

IEEE 802.15.4 performance studies

Since IEEE 820.15.4-2003 was published, many authors tried to answer the question whether it is able to keep its promise of being suitable for low-power low-rate applications. Zheng and Lee [87] are the first authors to report on results from an extensive performance evaluation of IEEE 802.15.4. Their study confirm the

standard's suitability for low-power low-rate applications. The authors report that for these applications, the packet delivery ratio of IEEE 802.15.4 is comparable to the one of IEEE 802.11 while the control overhead is smaller. Additionally, the authors investigate various specific aspects like the efficiency of slotted and unslotted CSMA/CA during the CAP of an IEEE 802.15.4 superframe. The *ns-2* IEEE 802.15.4 implementation used for this work is still the base of the IEEE 802.15.4 stack implemented in the *ns-2* versions published after 2004[4]. Since 2007, this stack additionally includes the extensions of Ramachandran et al. [88] introducing a more realistic energy and node state model in order to analyze the CAP and the influence of radio-shutdowns on the energy consumptions.

While the previously mentioned studies mainly focus on the MAC layer functionality, Petrova et al. [89] dedicate more effort to the physical layer. Measurements with the IEEE 802.15.4 compliant Telos mote allowed to develop a signal propagation model which is used for calibrating the *ns-2* physical layer model. Additionally, the authors show that the interference between IEEE 802.15.4 and IEEE 802.11 networks is negligible if the channels are chosen appropriately. Another experimental performance evaluation is reported by Lee [90]. The author evaluates the performance of a star topology with one IEEE 802.15.4-compliant PAN coordinator and four IEEE 802.15.4-compliant devices. He shows that due to the MAC layer overhead the effective data rate is significantly smaller than the theoretically achievable 250 kbps. This effect is stronger in the beacon-enabled mode, as the superframe structure significantly reduces the transmission opportunities. This overhead is smaller for the nonbeacon-enabled mode, but due to the small packet size, the bandwidth efficiency is still rather low. This is in any case the outcome of an analytical study of Latré et al. [91] who determine maximum throughput and minimum delay for a single connection.

Most of the previously mentioned studies focus on the beacon-enabled mode. The reason for this is that the IEEE 802.15.4 nonbeacon-enabled MAC is barely more than plain CSMA/CA while the beacon-enabled MAC offers interesting energy saving mechanisms. As multi-hop IEEE 802.15.4 topologies are best estab-

[4] http://www.isi.edu/nsnam/ns/, last accessed 04/2011

lished as nonbeacon-enabled networks, this is also the reason why IEEE 802.15.4 multi-hop topologies have not attracted the interest of the research community. One rare work on multi-hop topologies has been contributed by Kohvakka et al. [92] who study the cluster tree topology as possibility for building IEEE 802.15.4-based WSNs. The authors establish models for the device energy consumptions and goodput in beacon-enabled cluster tree topologies and obtain results allowing to choose two key IEEE 802.15.4 superframe parameters for increasing the network performance and energy efficiency. The question how the cluster heads are coordinated is however not discussed and the results additionally apply to the beacon-enabled mode only. Studies on the suitability of IEEE 802.15.4 nonbeacon-enabled multi-hop topologies for WSN applications do not exist. This is exactly the gap this chapter tempts to close.

3.1.2 An Introduction to ZigBee and AODV

The ZigBee Alliance[5] is an association consisting of currently more than 300 companies cooperating to enable standard compliant, reliable, cheap, low-power, wireless monitoring and control products. This cooperation has resulted in a number of ZigBee specifications using the IEEE 802.15.4 PHY and MAC layers as foundation. The latest ZigBee specification is ZigBee-2007 [33].

The ZigBee protocol stack, depicted in Figure 3.3 contains a network layer (NWK) and an application layer (APL) [33]. The APL layer in turn consists of the application support sub-layer (APS), the application framework and the ZigBee device objects (ZDO). The application framework enables manufacturers to implement application objects which share APS and NWK services with the ZDO. The ZigBee NWK layer is responsible for starting a network and for letting devices join and leave. It provides security mechanisms and additionally discovers and maintains routes for ensuring a multi-hop data delivery.

The responsibilities of the APS sub-layer include mechanisms for matching two devices based on their services and requirements, as well as forwarding mes-

[5] www.zigbee.org, last accessed 04/2011

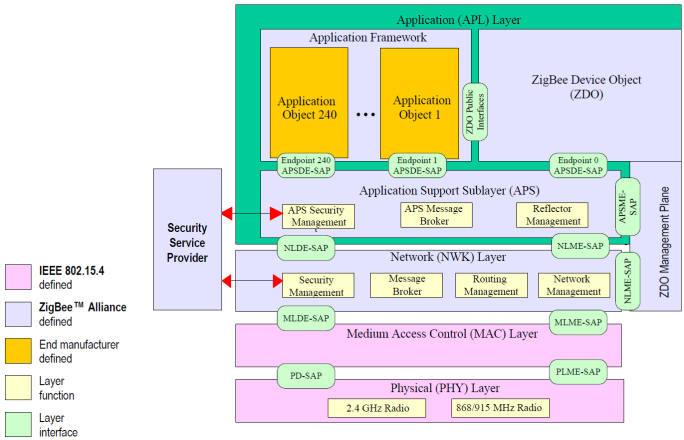

Figure 3.3: *The ZigBee stack architecture [33]*

sages. The main responsibility of the ZDO is defining the role of the device within the network (PAN coordinator, FFD, or RFD). In order to facilitate creating applications, the ZigBee alliance additionally defines a number of application profiles regulating the data transmission and data processing. The currently existing and upcoming ZigBee application profiles aim at target markets like health care, home and building automation, as well as energy metering [33]. For this reason the ZigBee stack contain various security services and configurable application parameters which are not relevant in the sensor networking context. For an exhaustive discussion of all details of the ZigBee stack, please refer to [33].

Instead, let us focus on the ZigBee networking layer which is the most relevant layer for sensor networking purposes. It supports star, tree, and mesh topologies which correspond to the IEEE 802.15.4 star, cluster tree and peer-to-peer topologies. For establishing large WSNs with homogeneous node capabilities only the last topology type is interesting, as the star topology does not support multi-hop structures, and the tree topology assumes a hierarchical routing structure where

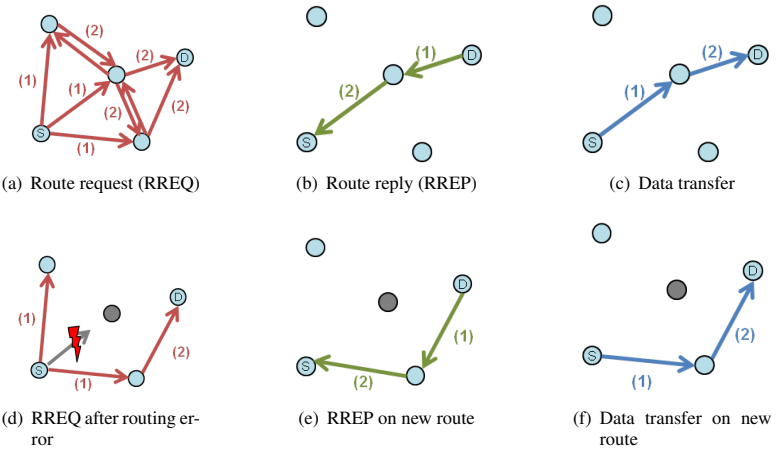

(a) Route request (RREQ)

(b) Route reply (RREP)

(c) Data transfer

(d) RREQ after routing error

(e) RREP on new route

(f) Data transfer on new route

Figure 3.4: *AODV route establishment and maintenance*

the cluster heads bear a higher load than their children. The main functionality of the mesh topology routing protocol is borrowed from AODV proposed by Perkins et al. [93]. AODV is a reactive routing protocol intended for networks with mobile nodes and dynamic link conditions. Therefore, paths are established on-demand and maintained only as long as they are required. For each destination IP address a node knows of, it stores a routing table entry containing a number of information whereof the next hop, the number of hops to this destination, and a unique sequence number are the most important ones.

Route establishment and maintenance under the AODV variant implemented by the ZigBee NWK layer is shown by Figure 3.4 for a part of the peer-to-peer topology illustrated in Figure 3.1. Figures 3.4(a) – 3.4(c) depict the AODV route discovery process: A PAN member (S) is the data source and wants to send data to the PAN coordinator (D) acting as data destination. S does not have a valid entry for D in its routing table. Consequently, it either initializes the

sequence number for D to 0 or increments the value in the routing table by 1. Next, it broadcasts a route request (RREQ) message, containing the address of both source (S) and destination (D) of this request, the sequence number for D, a hop count field set to 0 and some other information (cf. Figure 3.4(a)). Each node which receives this request first adds or updates the entry for S in its routing table using the information contained in the RREQ. Then, it checks if it has an entry for D. If it has no entry, and has not yet received this RREQ, it rebroadcasts it with an increased hop count field. As soon as the RREQ reaches D, it adds S to its routing table. Then, D sends a route reply (RREP) back to S along the same path the RREQ has traveled and uses the same sequence number and a hop count field of 0 for this RREP (cf. Figure 3.4(b)). Each intermediate node increases the hop count field and adds D to its routing table. As soon as S receives the RREP, it may begin to forward its data packets to D (cf. Figure 3.4(c)). If a node, which is not D, receives the RREQ, but has an entry for D in its routing table with a sequence number that is newer than the one in the RREQ, it sends a RREP back to S containing this newer sequence number. Sequence numbers are used for avoiding routing loops and additionally allow S to choose among different RREPs. In this case, the RREP with the larger sequence number or, if the numbers are equal, the one with the smaller hop count is chosen.

If a node on the path from S to D is damaged or sleeping, S's transmission fails. In this case where the failure happens in the middle of the path from S to D, AODV proposes to send a route error (RERR) message back to S [93]. All intermediate nodes mark this route as invalid and S restarts the procedure of finding a route. As this method causes a large amount of overhead, the ZigBee specification proposes the intermediate node to start a local repair, i.e. the intermediate node starts the procedure of RREQ and RREP exchange. If this is successfully completed, the data is sent on the newly found route (cf. Figures 3.4(d) – 3.4(f)). Note that AODV includes a large number of additional features which are however not adopted by the ZigBee specification [33,93] and therefore not described.

ZigBee performance studies

As IEEE 802.15.4 defines the two lower layers of the ZigBee architecture, many authors study aspects of the IEEE 802.15.4 PHY or MAC layer and call their work "ZigBee study". In addition to the previously reviewed studies [92, 94], the works of Shin et al. [95] and Lee et al. [96] are examples for this approach. Both studies claim to examine ZigBee features but concentrate on PYH and MAC layer aspects like packet error rate under interference or throughput efficiency and energy consumptions, respectively.

The work of Pinedo-Frausto and Garcia-Macias [97] is an exception to this rule. The authors identify the lack of experimental evaluations of commercially available ZigBee compliant hardware as a challenge for potential ZigBee users. Therefore, they conduct various experiments testing parameters like data integrity, response time or network size. For this purpose, a ZigBee test profile is used, and both indoor and outdoor settings are considered. The outcome of this study is that ZigBee is well suited for open loop control, monitoring and logging purposes, but does not meet the responsiveness and reliability criteria of emergency and closed-loop control applications.

3.1.3 Related Work

This section contains literature related to the chapter's three contributions. First, works related to the problem of optimizing the association phase are summarized before an overview on studies on routing in ZigBee compliant networks is given. Finally, contributions related to the problem of efficiently sleep scheduling in IEEE 802.15.4 networks are discussed.

Optimizing the IEEE 802.15.4 association procedure

In Section 3.1.1 it became clear that most studies analyze and optimize aspects of the IEEE 802.15.4 beacon-enabled mode. Most authors additionally do not consider the early stage of the network life time which is adequate if the steady

state system behavior is of interest, see e.g. Law and Kelton [98]. As a result of both facts, the contributions to the problem of optimizing the nonbeacon-enabled association procedure are rare.

Some authors have examined the early stages of the sensor network lifetime, a period when the sensor nodes have to learn about the sink nodes. Mathew and Younis [99] propose e.g. a distributed protocol which allows the sink nodes to announce their presence to the sensor nodes. This is achieved by letting the sink nodes take turn in broadcasting their presence to the sensor nodes. Upon the reception of an announcement, the sensor nodes send an identification message back to this sink. This algorithm is however not suitable for a multi-hop scenario, as the authors assume all sensor nodes to be in communication distance of the sink node. Barsi et al. [100] thoroughly investigate what they call training a WSN. During the training process, the sink follows a precomputed schedule for broadcasting messages at different transmission output powers. The sensor nodes follow their own schedule to listen to the channel. By analyzing in which slot they receive or do not receive a transmission, they learn in which of k concentric circles around the sink node they are in. The problems with this idea is again that the sink node has to be able to reach all sensor nodes. The work of Staehle et al. [23] considers multi-hop networks, but described mechanisms which allow all sink nodes to announce their presence to all sensor nodes. This contribution is however also not applicable for the nonbeacon-enabled association procedure, as in this case, the sensor nodes must take the initiative.

The seminal performance evaluation performed by Zheng and Lee [87] is one of the few works covering the initial IEEE 802.15.4 network stage. The authors study the association procedure for the case of beacon-enabled networks, point out that it has to be modified if it shall work in larger topologies and propose an optimization which will be discussed in Section 3.2.1. Zhang et al. [101] show how to speed up the association procedure in beacon-enabled networks. The authors propose to reduce the number of primitives sent and thereby the collision probability of command messages. This approach is however suitable for beacon-enabled star topologies only, as sending less primitives decreases the probability

of a successful association in nonbeacon-enabled multi-hop networks.

As a non-associated sensor node is excluded from an IEEE 802.15.4 PAN, efficiently carrying out the association procedure is the fundament of a successful network operation and routing tree establishment [87]. This idea was extended by Cuomo et al. [102] who exploit the parent-child relationship resulting from the association procedure for establishing a routing tree rooted in the PAN coordinator. As no additional overhead for initial route establishment is required, HERA, as this algorithm is called, outperforms AODV in simulations in terms of packet loss, delay and energy consumptions. The association procedure was not considered in this study, but of course heavily influences HERA's performance.

Routing in ZigBee compliant duty cycling WSNs

Recall from Section 3.1.2 that the ZigBee peer-to-peer routing protocol based on AODV is hence appropriate for multi-hop WSNs. WSNs have often less harsh operation conditions than the networks AODV is intended for, e.g. do most WSN deployments not have mobile nodes. Therefore, the large amount of messages AODV needs to maintain routes under dynamic link conditions is unnecessary and reduces the throughput in a WSN with mainly static link conditions. Consequently, many AODV variants promising to increase the performance of WSNs by reducing the AODV route maintenance overhead exist. One example for this approach is AODVjr proposed by Chakeres and Klein-Berndt [103]. This simplified ADOV variant is based on two main ideas: Firstly does only the destination of a RREQ answers to the first RREQ it receives with a RREP. As the fastest route is always considered to the best one, neither hop counts nor sequence numbers are used. Secondly, no HELLO or RERR messages are used for route maintenance. The source of a route simply triggers a new RREQ message, if it does not receive messages from the destination any more. Tao et al. [104] propose to use AODVjr augmented by a multi-path mechanism for routing in ZigBee WSNs. Their idea is to let the recipient of a RREQ send a RREP on each of the paths it received a copy of the RREQ. This increases the overhead for path finding but enables load

balancing and a faster route recovery after intermediate-load failures.

Most existing AODV variants have been tested on IEEE 802.15.4-compliant hardware and are therefore suitable for ZigBee-compliant WSNs. What is however common to all previously mentioned studies is the assumption of always active sensor nodes. This is clearly not feasible if the nodes are battery-powered and duty cycling is mandatory, a node behavior which reduces the probability of a correct packet delivery and thereby negatively affects the network performance. This chapter outlines how AODV has to be modified in order to efficiently operate in the presence of sleeping nodes and therefore attempts to fill in this void.

Saving energy in nonbeacon-enabled IEEE 802.15.4 networks

Out of the two operation modes of IEEE 802.15.4, the beacon-enabled mode offers energy-saving mechanisms but is not suitable for multi-hop topologies, whereas the nonbeacon-enabled mode is more suitable for multi-hop topologies but does not contain energy saving routines. Therefore, Khayyat and Safwat [105] advocate to introduce a third IEEE 802.15.4 operation mode which enables low-power multi-hop WSNs, the so called synchronized peer-to-peer mode. This realizes the superframe structure available in the beacon-enabled mode including periods of inactivity and GTS for delay sensitive data in a distributed fashion. The downside of this idea is that it is not IEEE 802.15.4-compliant. Moreover is it not clear if the benefits of this operation mode hold in the real world since for the performance evaluation the assumption of a perfect time synchronization has been used and neither the required overhead nor the effects of a non-perfect synchronization have been included.

For reducing the energy consumptions in a nonbeacon-enabled IEEE 802.15.4 WSN, the three possibilities Anastasi et al. [106] identified as suitable for saving energy in WSNs are more viable. The authors propose to reduce unnecessary data transmissions, to balance the energy consumptions of forwarding nodes by using mobile sinks, or to apply duty cycling. In most networks, however, only the latter possibility is feasible, as the amount of data to deliver is given by application

constraints and the sink nodes are static. Duty cycling in turn can be done on network or on node level. The former idea exploits the existence of redundant nodes which take turn in covering certain areas or paths of the network. For sparse networks without redundancies, or where the application requires data from all sensor nodes, only the idea of putting the transceiver, a sensor node's most energy-consuming component, to sleep as often as possible, remains.

For transceiver duty cycling, again, two possibilities exist. The first one is to use one of the WSN MAC protocols surveyed by Langendoen [41]. The problem with this approach is that most WSN MAC protocols run on IEEE 802.15.4 compliant hardware, but replace the IEEE 802.15.4 MAC layer. An example for this is the SCP MAC protocol [107]. Its authors, Ye et al., show that it enables sensor node duty cycles below 0.1% and enables multi-hop streaming with a small end-to-end delay only. SCP runs on IEEE 802.15.4 compliant radios, but replaces the CSMA/CA channel access by a synchronized adaptive channel polling scheme. The large number of existing energy saving WSN MAC protocols is the motivation for Park et al. [108] to propose power saving mechanisms for the nonbeacon-enabled mode as emulations of low-power WSN MAC protocols. While these emulations enable an energy efficient operation, it does not get clear in how far such a mechanism is IEEE 802.15.4-compliant.

The second possibility, having a sleep scheduling protocol working atop the MAC layer is more promising for realizing a IEEE 802.15.4 compliant WSN. In multi-hop networks, sleep scheduling has to take care that a data delivery over multiple hops remains possible. In order to achieve this, Giusti et al. [109] propose a solution for scheduling the activity of nodes in a tree-based sensor network. To optimize the temporal coverage area of a WSN, i.e. the probability that an event is detected by at least one not sleeping node, a decentralized scheme which enables each sensor node to optimize its active time with respect to its neighbors is proposed. The authors show that if each node keeps track about its neighbors' activity and distance to the sink and uses this information for data forwarding, fast data delivery is guaranteed. For the case where the routing structure is given by the ZigBee-compliant AODV, this scheme is however not applicable.

A similar approach which is closer to the idea introduced in this chapter has been presented by Anastasi et al. [110]. ASLEEP, as their protocol is called, runs atop the IEEE 802.15.4 nonbeacon-enabled CSMA/CA channel access and enables the sensor nodes to dynamically adapt their duty cycle in dependence on the number of messages they have to send and to receive in the data gathering tree. In contrast to ASLEEP, the contribution of this chapter is tailored to systems where a fixed duty cycle is dictated by the application running atop the WSN and is moreover suitable for systems where the routing structure is not predetermined but maintained by a routing algorithm like AODV.

3.2 Optimizing the IEEE 802.15.4 Nonbeacon-enabled Association Procedure

A IEEE 802.15.4 WSN can not become functional before the association procedure has been carried out successfully. The association mechanism is designed for beacon-enabled star topologies and thus less effective, if even working, in large duty cycling nonbeacon-enabled multi-hop topologies. Despite its fundamental importance for the network functionality, it has never been considered in depth how a nonbeacon-enabled IEEE 802.15.4 network can start up efficiently. Therefore, this section provides a description of the association procedure revealing issues and propositions for optimizing large low-power networks. Subsequently, the methodology for evaluating the different optimization possibilities is introduced, before insights on the individual and combined effects of the considered parameters are presented.

3.2.1 Standard and Enhanced Asssociation Procedure

In the following, the key facts of the nonbeacon-enabled association mechanism as defined by IEEE 802.15.4 [32, 83] are reviewed. Subsequently, the optimizations for low-power WSNs are introduced.

The IEEE 802.15.4 - conform association mechanism

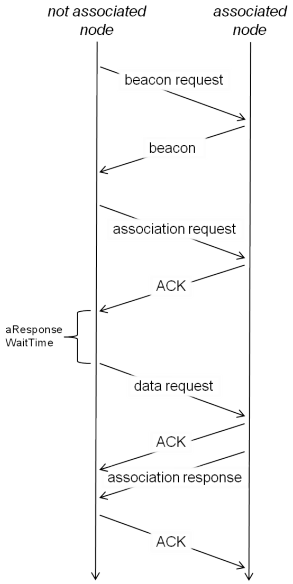

Figure 3.5: *Message exchange*

A starting PAN coordinator chooses one out of the available channels to operate the PAN it is going to coordinate. A node x, willing to *associate* to this PAN, executes an active channel scan, i.e., it broadcasts a beacon request to all available channels. If the PAN coordinator or an already associated FFD receives such a request, it answers by sending a beacon. This beacon request and all subsequently exchanged messages are summarized in Figure 3.5. After having sent the beacon request, x waits $0.015 \cdot (2^{ScanDuration} + 1)$ sec for a response [32]. For $ScanDuration$, no default value is given by [32], as this value has to be adapted to the network size and dynamics. This study therefore follows the seminal work of Zheng and Lee [87] who propose to use $ScanDuration = 4$, resulting in 0.26 sec per channel and to save energy by scanning 3 channels only. Together with processing times and state transitions, x spends $t_{scan} = 0.78$ sec for a channel scan.

After the scan, x sends an association request command message to one of the devices from which it received a beacon. Neither the IEEE 820.15.4-2003 [83] nor the IEEE 820.15.4-2006 [32] standard specify which out of several beacon senders to choose. For this study, the most straight-forward idea, again proposed by Zheng and Lee [87], to let x send the association request to the quickest respondent y is applied. After having received the association request, y immediately sends back an acknowledgment, which x answers by a data request

command after $aResponseWaitTime = 0.49$ sec. Meanwhile, y has to check whether x may associate. If yes, y sends an acknowledgment and an association response command frame back to x which in turn is acknowledged. Conditions for rejection are not mentioned in the standard [32], in this study, all nodes are therefore always allowed to associate.

Association mechanism extension for low-power WSNs

The case where x receives no beacon in response to its beacon request is not supposed to happen and consequently neither handled by [83] nor by [32]. For large low-power WSN deployments which have only one sink or Internet gateway acting as PAN coordinator, it may in contrast occur quite frequently that a node receives no answer to its channel scan and consequently fails to associate. Possible reasons are that the PAN coordinator is out of reach, already associated FFDs are in sleep mode or packets are lost. Zheng and Lee [87] identify this problem and propose that each node failing to associate should retry to associate after having waited for an *association retry interval* $a = 1$ sec. For beacon-enabled multi-hop topologies where nodes are always active, this mechanism is indeed suitable for allowing all nodes to associate [87].

In contrast, if nodes alternate between sleep and wake state in order to save energy, this solution may cause sensor nodes to try and retry to associate during their neighbors inactivity phases. An analysis of the association procedure yields four ideas which are suitable for adapting it to multi-hop duty cycling topologies: The first improvement is a *randomization* the association retry interval a which allows to let a node to become active in different temporal neighborships. The *length* of a has clearly also an influence on the association procedure performance. In addition, two extensions for the node behavior might be beneficial: The *greedy* behavior causes a sensor node to immediately retry to associate after an unsuccessful channel scan, i.e. to restart the channel scan after it has not received a response to its beacon requests. The *altruistic* behavior causes a successfully associated node to listen to the channel some time before starting its

regular sleep-wake cycle. If the node receives any beacon requests, it starts to sleep as soon as it has completed all associations it participated in, otherwise the node starts to sleep after the *altruistic period* t_{alt}.

3.2.2 Evaluation Framework

Many factors influence the performance of a WSN and especially the association procedure in nonbeacon-enabled IEEE 802.15.4 WSNs. Therefore, the environmental conditions and design choices are abstracted by a set of factors which are discussed in the following. After this discussion, the metrics used for this evaluation are introduced.

Considered factors

The goal of this section is to improve the performance of an IEEE 802.15.4 WSN deployment by adapting the association procedure. This problem abstracts to optimizing a network characterized by a set of *hard factors* describing the existing application requirements and environmental conditions. The degree of freedoms for tuning the association procedure are represented by a set of *soft factors*.

The considered hard and soft factors are summarized in Table 3.1. The soft factors have been explained in Section 3.2.1, the meaning of the hard factors is discussed in the following. The factor dep, i.e. the strategy by which the positions of the sensor nodes is chosen can be either random or planned by an algorithm similar to the ones discussed by Younis and Akkaya [111]. The number of nodes each sensor node may on average communicate with is denoted by θ. It is determined by the transceiver transmission output power and the density of the node deployment. A starting WSN is modeled by letting each sensor node to become active a randomly distributed time after the PAN coordinator has been switched on. The coefficient of variation of the node activation time σ captures the variety of the node starting time distribution. It is computed as the fraction of the node activation time standard deviation and the average node activation time and therefore only then equal to zero if all nodes are activated at the same time. The

Factor Name	Factor Meaning
Hard Factors	
dep	Node deployment
θ	Average node degree
σ	Coefficient of variation of node activation time
T	Network clock
ν	Node activity factor
T_0	Initial tolerance time
Soft Factors	
a	Length of association retry interval
$rand$	Randomization of a
gr	Greedy association
alt	Altruistic association

Table 3.1: *Considered hard and soft factors*

network clock T determines the responsiveness of the WSN. The sensor node *activity* factor $0 < \nu \leq 100\,\%$ captures a simple abstraction of a duty cycling scheme: all sensor nodes are active for νT and sleep for $(1 - \nu)T$. Finally, T_0 indicates the amount of time after which the WSN has to be functional at the latest.

Performance metrics

For their study of the association process, Zheng and Lee propose two metrics: the *successful association rate* giving the percentage of devices which succeeded to associate and the *association efficiency*, indicating how much attempts the devices have to make until the association is completed [87]. In the following, an extension of this framework is used which includes three different network level metrics: The *association success* s_A is equal to 1 if all nodes of the PAN could associate during T_0, and 0 otherwise. The *association time* t_A denotes the amount of time which passes until the last node of the PAN has associated. If not all nodes could associate, $t_A = T_0$. Finally, E_A denotes the *association energy consumptions* which is defined as the energy consumptions of the node

which required the largest amount of energy for associating. E_A does not include the energy consumptions required for sending out association responses, but captures the energy each node consumes until it is successfully associated and until the optional altruistic phase is terminated. Recall from Section 2.1.2 that an exact calculation of E_A has to include characteristics on all mote subsystems. As the improvements of the association mechanism focus on reducing the communication related energy consumptions, only the energy consumption of the transceiver is of interest. For this purpose, the extension of the state machine model proposed by Wang and Yang [72] introduced in Section 2.2.2 is used.

3.2.3 Association Mechanism Performance Evaluation

For an evaluation of the effects of the proposed association procedure extensions, the *ns-2.33* IEEE 802.15.4 stack is extended to include the ideas discussed in Section 3.2.1. In order to gain an overview on the impact of the considered factors, a 2^k factorial design study is carried out. As the greedy and the altruistic mechanism prove to be especially promising, this section additionally contains a study on an association mechanism optimization using different parameterizations of these two mechanisms.

2^7 factorial design setup

Examining the performance of the association procedure for each combination of all considered 10 different hard and soft factors is an intractable task, especially as the range of possible values is continuous. A so called 2^k *factorial design*, see e.g. the description of Law and Kelton [98], is a more economical strategy for obtaining an initial insight in the effects and interactions of k factors. For this purpose, a representative low (-) and high (+) value or *level* is chosen for each factor and simulation runs for each of the resulting 2^k different factor combinations or *design points* are executed.

The WSN topology has a strong influence on the network performance, as the way how the nodes are arranged decides over communication success or failure.

Factor	θ [nodes]	c	ν [%]	a	$rand$	alt	gr
Level (-)	1.8	0	1	$0.1T$	no	no	no
Level (+)	6	1	25	$5.1T$	yes	yes	yes

Table 3.2: *Considered experimental factors and their levels*

The network density, represented by the average node degree θ, is the most influential network characteristic. Therefore the factor dep is not considered for the factor screening study and the impact of the other factors' influences is examined in a simple topology with varying node densities. Nine sensor nodes and one PAN coordinator are arranged on a line, with the PAN coordinator at the left edge. To abstract a typical non-time critical WSN application, $T_0 = 5$ min and $T = 1$ sec are used as values for the initial tolerance time and the network clock, respectively. The experiments showed that other values for these parameters do not change the effects of the 7 remaining free factors, for which (+) and (-) levels are summarized in Table 3.2.

In the simulation, the radio stack is configured to model the IEEE 802.15.4-compliant CC2420 chip. The radio propagation is abstracted as a disc model, and the two-ray ground propagation model proposed by [87] is used. Under the assumption that each node uses the highest possible output power (0 dBm) and has a typical receiver sensitivity of -95 dBm [67] this causes each transmission within 20 m to succeed. To obtain varying node degrees, two different line topologies with inter-node spacings of 20 and 5 m are used, each node can thus communicate with 1 or 4 neighbors per direction. Averaged over 10 nodes, this results in a low value of $\theta = 1.8$ and a high value of $\theta = 6$. Startup times distributed with $\sigma = 0$ stand for all nodes starting exactly 30 sec after the PAN coordinator, $\sigma = 1$ corresponds to an exponential distribution with the same mean value. $\nu = 1\,\%$ and $\nu = 25\,\%$ reflect a good lower and an absolute upper bound for a low-power network duty cycle. The association retry interval a is chosen in dependence of the system clock and varies between a very small and a very large value. a is randomized by multiplying it with a random variable which is uni-

formly distributed in the interval (0,1]. Low and high values for the factors rand, gr and alt correspond to using these features or not. If the altruistic mechanism is used, t_{alt} is set to be slightly longer than the time required for a channel scan, $t_{alt} = t_{scan} \cdot 1.1 = 0.86$ sec. Other choices for this and the other levels are imaginable, but the experiments show that using other level values just slightly changes the quantitative results and does not change the qualitative statements.

The performance of the association mechanism for each of the resulting 2^7 design points is evaluated by the following simulation run: at time 0, the PAN coordinator is activated. As specified by [32], it is always active during the simulation run. Each of the sensor nodes is activated at a randomly distributed time with mean 30 seconds and coefficient of variation as specified by σ. As soon as a node has been activated, it tries to associate with the parameters set for this design point. After having successfully associated and after an optional altruistic period, the node starts its regular sleep and wake cycle. At the end of each simulation run, the *system responses*, i.e. the metrics s_A, t_A and E_A are collected. To obtain statistically significant results, the responses for each design point are averaged over 100 simulation runs.

Main effects

The influence of factor x on the system performance in terms of metric y is characterized by its *main effect*, $e_x(y)$. It is obtained as the average change in y which results if x is changed from (-) to (+) while all other factors are kept fixed:

$$e_x(y) = \frac{1}{2}(\bar{y}_{x+} - \bar{y}_{x-}), \tag{3.1}$$

where $\bar{y}_{x+}$ and $\bar{y}_{x-}$ denote y averaged over all design points where x is at its high level and low level, respectively [98].

A visualization of the 7 different considered factor main effects can be found in Figure 3.6. The main effects on the considered system responses s_A, t_A, and E_A are shown in Figures 3.6(a) – 3.6(c). In each subfigure, the three bars at

the left show the hard factor's, the four bars on the right the soft factor's main effects. Together with the main effects, their 95%-confidence intervals are shown to verify that only some of the effects are not statistically significant, as their confidence intervals include 0.

Let us first discuss the system responses averaged over all 2^7 design points, whereof the value is shown in each figure. The association success s_A is the probability that all nodes associate within T_0. This is zero if only one node is not able to associate, s_A averaged over all design points and 100 runs results hence in the surprisingly low probability of 0.8 given the large amount of available tolerance time. The reason for this is that if a is not randomized it may happen that a node never succeeds to associate since it sends its association requests always during the sleep phases of its neighbors. This is also the reason why the average t_A is so large. In contrast, the average association energy consumption correspond to less than 0.01% of the theoretical capacity of two AA batteries[6] and seems to be neglibigle when compared to the energy consumptions during the WSN lifetime. However, already in this simple topology the minimal and maximal E_A of 0.2 J and 10.4 J differ strongly, the inherent energy saving potential of the association phase should thus not be underestimated. The average values therefore already illustrate the necessity of a suitable association mechanism configuration.

The way towards promising optimization directions is pointed out by the main effects of the factors shown in Figure 3.6. Obviously, some factors have a stronger influence than others and the factor impact strongly differs between the metrics. A closer look reveals that the hard factors θ and ν have a larger influence than all other parameters: the association procedure will succeed with high probability, rather quick and at low energy costs in dense and highly active networks. While this is quite evident, the influence of a randomized startup point characterized by σ's main effect is ambiguous. $\sigma > 0$ is suitable for increasing the association success as it decreases the probability of packet collisions, but results in a slightly increased time and energy consumption.

As the hard parameters can in general not be influenced, the analysis of the

[6] http://data.energizer.com/Static.aspx?Name=AppManuals, last accessed 04/2011

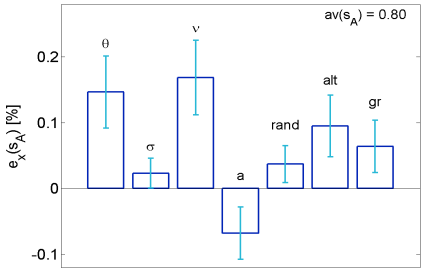

(a) Association success s_A

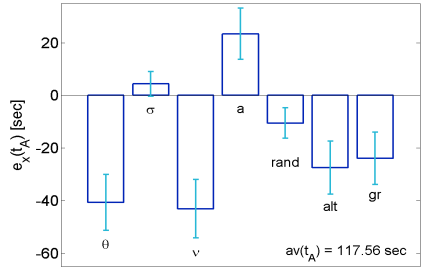

(b) Association time t_A

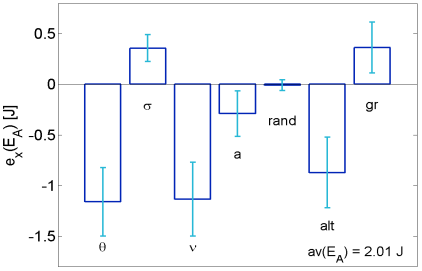

(c) Association energy consumptions E_A

Figure 3.6: *Main effects of the considered factors on the different metrics*

soft parameters is more important for the goal of an association optimization. Observe that the the altruistic mechanism is the only soft parameters which has an entirely positive influence on all three considered metrics. The energy saving potential of the altruistic mechanism is quite large as the energy savings of nodes which associate earlier outweigh the energy consumption of nodes altruistically delaying their transition to power save mode. The randomization of the association retry interval has no effect on the energy consumptions, but is an interesting option as it increases on average the association success and speed. The greedy mechanism and a small association retry interval increase the association success and the association speed but lead to increased energy consumptions by triggering too many unnecessary channel scans.

Interaction effects

Considering just the main effects of the factors for deciding upon the parametrization of the association mechanism would lead to wrong decisions if interactions between factors exist, i.e. if the influence of one factor varies in dependence of the behavior of other factors. It is possible that all combinations of factors interact, but the *two-way interaction effect* of factors x and z on the system response y, $e_{xz}(y)$ is the most important one. It is computed as the average difference of x's effect when z is at its (+) level and the effect of x when z is at its (-) level:

$$e_{xz}(y) \quad = \quad \frac{1}{2}((\bar{y}_{x^+z^+} - \bar{y}_{x^-z^+}) - (\bar{y}_{x^+z^-} - \bar{y}_{x^-z^-})), \tag{3.2}$$

where analogously to Equation (3.1), $\bar{y}_{x^+z^+}$ denotes y averaged over all design points where both x and z are at their (+) levels [98].

The interaction effects on all considered responses are similar, the illustration of the interactions on s_A shown in Figure 3.7 is therefore a representative example for the interaction effects on E_A and t_A. The key to the figure matrix is the following: In the subfigure which is at row z and column x, a solid line is drawn between the average system response when x is at its (-) and (+) level, while z is at is (-) level, $\bar{s_{A}}_{x^-z^-}$ and $\bar{s_{A}}_{x^+z^-}$, while a dashed line connects the aver-

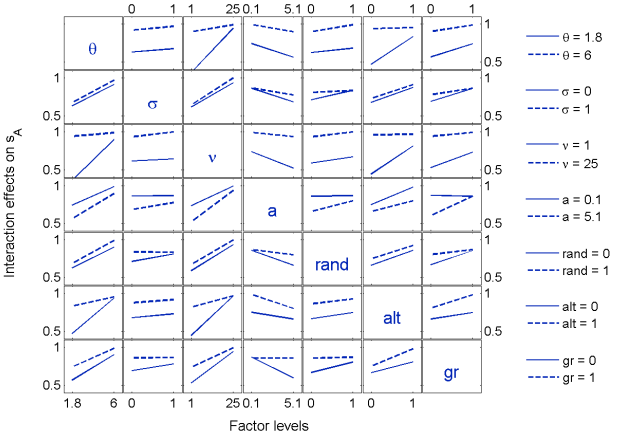

Figure 3.7: *Interaction effects on the association success* s_A

age system response when x is at its (-) and (+) level, while z is at is (+) level, $\bar{s_A}_{x^-z^+}$ and $\bar{s_A}_{x^+z^+}$. For a more compact representation, units for the factor levels on the axis are omitted.

Non-parallel lines represent interactions between two factors. This allows to see that nearly all factors are interacting. A comparison between Figures 3.6 and 3.7 yields moreover that factors with strong main effects also have strong interactions. Often a factor's effect is amplified or reduced by another factor's level, as it is e.g. the case for the altruistic behavior and all other soft factors which have a nearly negligible effect if the activity is high and the network is dense. Interactions exist however also between the soft factors. The greedy mechanism is e.g. suitable for increasing the association success (c.f. Figure 3.6). An analysis of the interactions depicted in Figure 3.7 shows however that this positive effect is significantly stronger if a is not randomized, as a greedy behavior may for some nodes be the only chance to find a node to associate with. All in all, the

analysis of interactions demonstrates, that any deeper analysis of the association mechanism has to be done considering different network configurations. Also sparse and low-duty cycled network designs need to be optimized more carefully. The analysis of higher level interactions goes beyond the scope of this study, but the magnitude of the two-way interactions demonstrate that this is necessary for an optimal association mechanism configuration.

Out of the soft factors the greedy and the altruistic mechanisms have the strongest effects on the s_A and t_A (c.f. Figure 3.6). Additionally, the altruistic mechanism amplifies the positive effects of the greedy mechanism on s_A (c.f Figure 3.7). This positive interaction is observable for t_A and E_A, too. In the following it will therefore be verified if this holds for larger topologies, too.

Combining the greedy and the altruistic mechanism

Let us consider an exemplary monitoring application, where an area of 60×60 m is covered with 24 sensor nodes and one sink node acting as PAN coordinator. Small energy consumptions together with acceptable responsiveness are abstracted by $\nu = 1\%$ and $T = 1$ sec. To examine the influence of the node deployment two types of randomly generated topologies are used. A connected graph with 25 nodes results either from choosing positions on a grid with 12 m in between or from uniformly distributing nodes over the square to cover. In both cases, one random position is chosen to be the position of the sink. Averaging the mean node degree over 100 different random and grid topologies results in $\theta = 6$ and $\theta = 3.2$ respectively. To analyze the benefits of the altruistic and greedy mechanisms, the association retry interval is not randomized and set to $a = 0.5T$. Different possibilities for activating the sensor nodes are abstracted by choosing different distributions for t_0 which have a coefficient of variation $\sigma \in \{0, 1e^{-3}, 1e^{-2}, 1e^{-1}, 0.577, 1, 2\}$ and mean 30 sec. For a closer examination of the altruistic mechanism, values for $t_{alt} = \{0, t_{scan}, t_{scan} + T, t_{scan} + 2T, t_{scan} + 5T, t_{scan} + 10T\}$ are used.

The association success is clearly increasing with t_{alt} as the probability that a

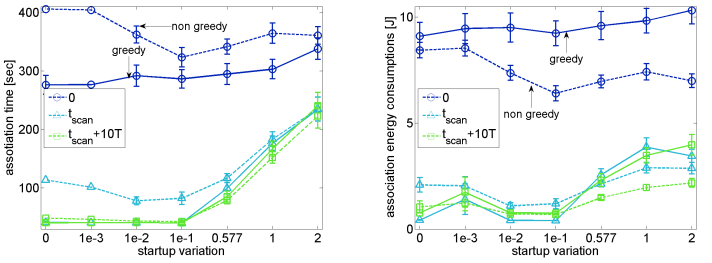

(a) Association time t_A

(b) Association energy consumptions E_A

Figure 3.8: *Effects of the combined altruistic and greedy mechanism*

node is able to associate increases with the time an associated node does not go to sleep, especially if the activity time ν is small. Hence, the trade-off between association speed and energy consumptions in dependence of the startup variation and the interactions with the greedy mechanism are more interesting. For this purpose, T_0 is set to 10 minutes which allows all nodes in the considered topologies to associate in nearly all cases. Results from this experiment for both topology types are similar, but due to the smaller node degree, stronger for the grid topologies and shown in the following. t_A and E_A averaged over 100 simulation runs together with their 95% confidence intervals are plotted against σ in Figure 3.8. Different values of t_{alt} are distinguished by different markers. For sakes of clarity, however, not all considered values of t_{alt} are shown. The greedy and the non greedy behavior are shown with solid and dashed lines, respectively.

The most obvious result is that $t_{alt} = 0$, i.e. a non altruistic behavior, leads to the slowest association and highest energy consumption. Observe also that in both subfigures the gap between the curves representing $t_{alt} = 0$ and $t_{alt} > 0$ is larger than the one between the representation of the greedy and non-greedy behavior, the altruistic mechanism is hence improving the performance more than the greedy mechanism. The benefits of the latter are moreover strongly depending on the startup variation: While the greedy behavior together with a small

$t_{alt} > 0$ increases the association speed and decreases the association energy consumption in networks with small startup variation, this does not hold anymore if the startup variance increases. If $\sigma \geq 0.577$, the greedy mechanisms consumes more energy than a non-greedy association regardless the configuration of the altruistic mechanism, although it is still faster than the non-greedy behavior. This demonstrates, that for the exact parameterization of t_{alt} a balanced solution between association speed and energy consumption has to be found. The association speed always increases with t_{alt}, but if $t_{alt} > t_{scan}$ is chosen *too* large, too much energy is wasted by unnecessarily listening to the channel. All in all, Figure 3.8 demonstrates that in the considered scenarios, adapting the usage of the greedy and altruistic mechanism to the WSN deployment enables accelerations of over 300 sec and energy savings of over 5 J. We may hence be confident that comparable numbers will result from topologies of the same size and that the optimization potential will even grow with the topology size.

3.3 Routing in Duty Cycing ZigBee Networks

Having successfully completed the association procedure, the next challenge arises: An IEEE 802.15.4 WSN should use AODV as routing mechanism in order to be ZigBee-compliant. If AODV works in a duty cycling network, it causes an enormous amount of overhead, as each time a transmission fails due to a sleeping next hop, a route repair mechanism is triggered. In order to examine and solve this problem, this section introduces two simple duty cycling possibilities working atop the IEEE 802.15.4 stack. Afterwards, the *smooth AODV* protocol is introduced which is better adapted to duty cycling networks than the classical AODV which is proved by means of a simulation study.

3.3.1 Two Simple Sleep Scheduling Possibilities

The most intuitive idea of an energy-saving mechanism working atop the IEEE 802.15.4 MAC layer is to let each node independently decide when to wake

up to send packets and go to sleep afterwards. In multi-hop topologies, this idea can however not be applied, as a node does not know if and when it has to receive and relay packets on behalf of other nodes.

Another simple method is to implement the sensor node duty cycle as an on-off-process. This model has already been assumed in the last section, and will be refined now: Each node in the network is awake for the same fraction ν of a constant time interval T and spends the rest in sleep state. If the sensor node activity $\nu = 100\,\%$, the nodes are always active. The exact value of the network clock T depends on the speed requirements of the application running atop the WSN. To decide which part of T the node is sleeping, two strategies are straightforward: The sensor node activity can either be *random* or *synchronized*. In the first case, the nodes go active for νT at randomly distributed times at the beginning of the WSN lifetime, then sleep for $(1 - \nu)T$ and so on. In the second case, the entire network is either on or off at the same time. These two paradigms clearly mark the worst and the best cases for sleep scheduling possibilities and are therefore suitable mechanisms for benchmarking the performance of AODV in the presence of sleeping nodes.

Note that, under the random paradigm, especially if $\nu < 50\,\%$, it is possible that some nodes will not be able to communicate as they are never awake when their neighbors are. The physically connected network will hence be temporally partitioned. The drawback of the synchronized paradigm is that it is not be feasible in realistic networks with potentially drifting clocks and that the collision probability is increased as all nodes try to send during the small activity period.

3.3.2 Smooth AODV

Recall from Section 3.1.2, that for establishing multi-hop networks, the ZigBee specification proposes an algorithm which is very similar to AODV [33]. For analysing the feasibility of duty cycling ZigBee multi-hop networks, it is thus sufficient to take the existing *ns-2* AODV implementation and to include the proposed ZigBee modification to jitter the route request broadcast [33]. This idea

means that each node randomly delays the forwarding of an AODV RREQ packet in order to decrease the probability of packet collisions. The *smooth AODV* mechanism introduced in this section includes this idea and a more tolerant failure handling which will be described in the following.

AODV recognizes a link failure either if no periodic HELLO messages are received any more or by using link layer feedback (LLF) [93]. As HELLO messages cause a large amount of overhead, the latter method is more advantageous for low-power networks. After three acknowledgments which have not been received, i.e. three failed MAC layer retransmissions, a failed transmission is announced. The link is considered as broken, and the route error mechanism is started. This mechanism basically consists of starting a local repair as illustrated in Figures 3.4(d) – 3.4(f). The cause for the outstanding ACKs could not only be a dead destination, but also a sleeping one or a packet collision. If a local repair is started after each LLF, some of those local repairs are potentially unnecessary as a failure occurred due to a sleeping not a dead node. As those superfluous messages decrease the system performance, the ZigBee specification [33] proposes a more tolerant mechanism which does not react upon on each LLF.

Smooth AODV implements this idea and is summarized in Figure 3.9. The main difference between smooth AODV and AODV specified by [93], which is called *regular* AODV in the following, is that smooth AODV ignores all LLFs following a first LLF within a *guard interval* g. It additionally only assumes a link failure, if the number of LLFs n_c exceeds the *LLF threshold* L_T.

3.3.3 Evaluation Framework

The suitability of smooth AODV for duty cycled nonbeacon-enabled 802.15.4 sensor networks is demonstrated by comparing its performance against the performance of the same network running regular AODV. The simulation uses a rough sensor node abstraction which simplifies the application layer to a constant bit rate (CBR) traffic pattern, where each node sends a packet of $p_l = 50\,\mathrm{B}$ to the sink every $\Delta t = 50\,\mathrm{sec}$. For modeling the ZigBee communication stack,

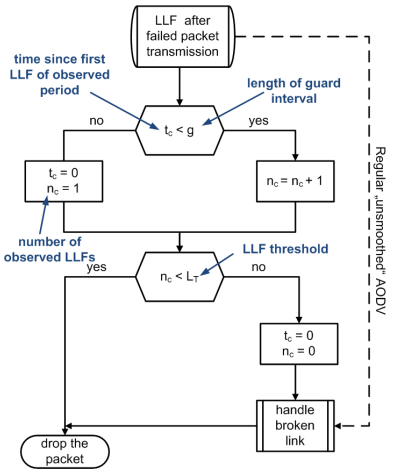

Figure 3.9: *Modified LLF handling under smooth AODV*

a similar *ns-2* simulation framework as described in Section 3.2.3 is used. The simulation framework used in this section is based on the IEEE 802.15.4 *ns-2.29* implementation and follows more closely the code of [87] and [94]. Moreover does the simulation environment contain a PHY layer model which is parameterized slightly different than the one used in Section 3.2.3.

The radio propagation follows the *ns-2* two-ray ground propagation model with transmission powers and receiver sensitivities conform to IEEE 802.15.4. The resulting radio range is 12 meters. The experiments show that the network topology has a strong influence on the network performance. Therefore a simple network topology consisting of 49 nodes arranged on a 7×7 grid with an inter-node spacing of 5 meters is used, allowing each node to communicate with up to 2 neighbors per grid direction. For maximizing the path lengths, the PAN coordinator, playing the role of the traffic sink, is in one of the grid's corners. The necessary multi-hop paths are established using smooth and regular AODV.

In order to quantify the performance of the four different combinations of sleep scheduling and routing, simulation runs with a duration of $t_{sim} = 10000$ sec are executed. The system is configured with $T = 1$ sec. The guard interval g and the LLF threshold L_T can be used for adapting smooth AODV to the network dynamics and traffic patterns. For this study, $g = 12$ sec and $L_T = 3$ are used. In order to obtain statistically significant results while being able to investigate a large number of configurations, each simulation run is repeated 5 times.

For the performance comparison, a number of metrics are used whereof the packet delivery ratio (PDR) is the most important one. For each node, it is computed as the number of APL packets received at the sink divided by the number of APL packets the node sent. The effectiveness of the routing algorithms are captured by the overhead resulting from finding and maintaining the routing paths. This is expressed by the number of AODV packets each node has to send, n_A.

For WSNs, energy efficiency is a key requirement, therefore the amount of energy used per successfully received bit, E_b, is an additional metric. As described in Section 3.2.3 it is obtained by configuring the standard *ns-2* energy model to represent state-of-the-art sensor node hardware similar to the one introduced in Section 2.2.2. Besides the fact that the energy required for transitions between states is neglected, it implements a sensor node state machine similar to the one shown in Figure 2.3. The node energy consumptions are obtained by multiplying the amount of power the sensor node consumes for sleeping, transmitting and receiving or listening to the channel respectively by the amount of time it spends in the corresponding states. WSN applications need not only to be energy efficient, but should also fulfill certain quality requirements. Therefore, the end-to-end (e2e) delay δ, i.e., the time required for transmitting a data packet to the sink node, is therefore considered as exemplary application layer metric.

3.3.4 Comparison of Smooth and Regular AODV

The aforementioned metrics packet delivery ratio, AODV overhead, per-bit energy and e2e delay enable a comprehensive performance comparison of smooth

and regular AODV in the considered scenario. The remainder of this section will hence discuss these metrics one-by-one.

Packet delivery ratios

A comparison of the PDRs resulting from the use of the different sleep scheduling and routing mechanisms allows to get an overview on their impact on the system performance. In the following, the four different possible scenarios resulting from the combination of AODV variant and sleep scheduling policy are denoted by regular rand, regular sync, smooth rand, and smooth sync. The sensor node PDRs obtained from five simulation runs in dependence on their distance to the sink are shown in Figure 3.10 for an activity ratio of $\nu = 90\%$. For all other activity ratios, the difference between the four different combinations is similar, while a higher percentage of sleeping time significantly decreases the PDR if the nodes are not synchronized. This is illustrated by Figure 3.11, where the CDF of the average PDR values for each node is shown for $\nu \in \{50\%, 90\%, 100\%\}$.

Let us first take a look at the results provided by Figures 3.10(b) and 3.10(d). They show that if the activity phases are synchronized, the PDR is nearly 100 % for each node independent of the node's distance to the sink. In this case, smooth AODV increases the PDR only marginally, if at all, compared to regular AODV. If, in contrast, the nodes are active in a random fashion, the PDR drastically decreases with an increasing distance to the sink (cf. Figures 3.10(a) and 3.10(c)). Observe however that this decrease is less severe in Figure 3.10(c), which is due to the smooth AODV algorithm. For the case of random sleep scheduling smooth AODV outperforms regular AODV, as it especially increases the PDR of nodes which are no one-hop neighbors of the sink. The variation of the PDRs is an additional indicator for the instability of the WSNs operating under the random sleep schedule. This together with the small PDR which is already unacceptable for a high activity ratio of 90 %, motivate the need for more sophisticated sleep scheduling strategies like the one which will be introduced in Section 3.4.

The need for an efficient sleep scheduling solution is also underlined by the

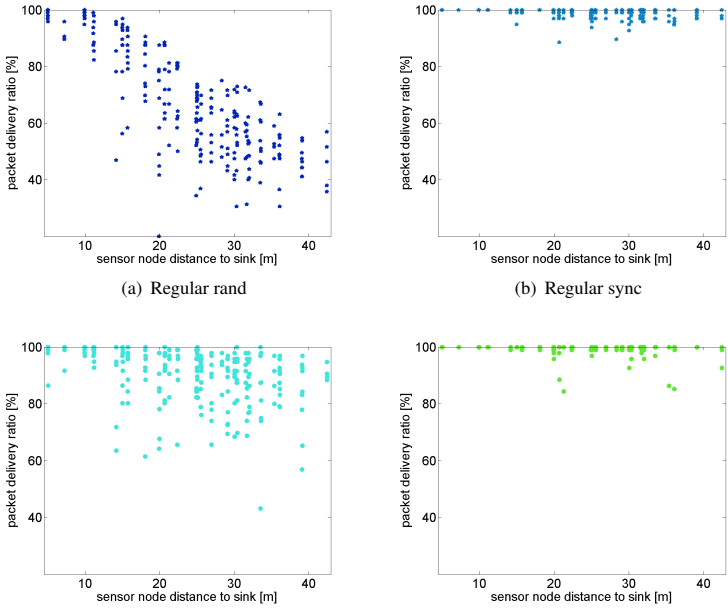

(a) Regular rand (b) Regular sync

(c) Smooth rand (d) Smooth sync

Figure 3.10: *Packet delivery ratio for ν=90% activity ratio*

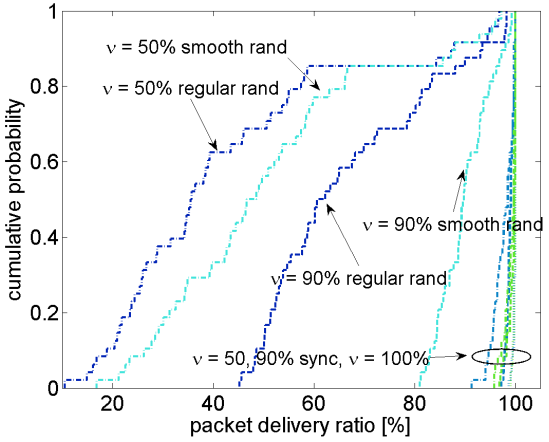

Figure 3.11: *Packet delivery ratio for* $\nu = 50\%, 90\%, 100\%$

results depicted in Figure 3.11. If the nodes are always on, i.e. $\nu = 100\,\%$, or if the nodes are synchronized, nearly all transmissions succeed. Under the random sleeping schedule in contrast, the average PDR significantly reduces as soon as the nodes are sleeping only 10% of the time, i.e. $\nu = 90\,\%$. In this case, the difference between smooth and regular AODV is significant. For shorter online periods with $\nu = 50\,\%$, the difference of the PDR between regular and smooth AODV narrows, and leads to very small PDRs in the random case. The reason for the less beneficial effect of smooth AODV under smaller duty cycles is the previously discussed temporal partitioning of the network. For the case where $\nu = 50\,\%$, a larger amount of packets are lost since nodes are simply not awake at the same time. If, in contrast, $\nu = 90\,\%$, the cause for loosing packet is not that the destination is not awake but that the channel is occupied by one of the packets regular AODV sends for route maintenance.

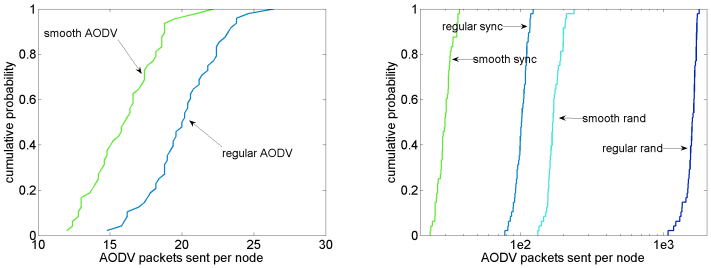

(a) ν=100% activity ratio (b) ν=90% activity ratio

Figure 3.12: *Sent AODV packets* n_A

AODV overhead

An explanation for this duty cycle dependent effect on the PDR is given by an analysis of the number of sent AODV packets n_A in dependence of the activity ratio. This analysis is visualized by Figure 3.12 which shows the CDFs of n_A for the case where the nodes are always on (cf. Figure 3.12(a)) and where the nodes are active for 90 % of the time (cf. Figure 3.12(b)), respectively. Let us discuss the insights provided by Figure 3.12(a), first. In the considered idealistic scenario neither node nor transmission failures occur. If the nodes are alway online, a node does not need to change its once found route to the sink, unless a collision causes a packet failure which accidentally triggers AODV's error mechanism. Smooth AODV reacts intentionally slower to packet failures, i.e. it does not try to find a new route for each failed data transmission and is thereby more efficient than regular AODV avoiding those unnecessary route finding operations.

For the case of an activity ratio of $\nu = 90\,\%$, smooth AODV is also suitable for reducing the overhead, but the sleep scheduling strategy has a stronger impact on n_A. This is illustrated by Figure 3.12(b) where the CDFs of n_A under the four different configurations are shown. As n_A averaged over all nodes is 1557, 102, 173, and 30 for regular rand, regular sync, smooth rand, and smooth sync,

respectively, the x-axis of Figure 3.12(b) is logarithmically scaled.

The reason why a random sleep scheduling causes so much AODV packets to be sent already for a high activity ratio of $\nu = 90\,\%$ is explained by probability calculus: For a random observer a node is inactive with a probability of $1 - \nu$. For a route with h hops between source and sink, the probability that all nodes on the route are online is thus ν^h. In the considered grid, each path has on average 4 hops and at most 7 hops. In the worst case, i.e. $h = 7$, the packet is routed successfully with a probability of $\nu^h = 48\,\%$ only. Each packet sent to a sleeping node is considered as lost, as the receiver is not able to send an acknowledgment. As a consequence, regular AODV immediately starts the local repair mechanism and a large number of AODV packets are unnecessarily sent. This in turn increases the channel occupancy and thereby the packet delivery success. Smooth AODV alleviates this problem by reducing the overhead and is hence especially suited for scenarios with duty cycling nodes.

Repeating the same experiments for other values of ν shows that for all duty cycle percentages, smooth AODV reduces n_A by a constant factor in comparison to regular AODV. For the case of a heavier loaded system, i.e. shorter inter-packet send times, the number of collisions and thereby n_A increases under both regular AODV and smooth AODV. Still, the overhead resulting from the use of smooth AODV is significantly smaller than the overhead caused by regular AODV.

Per-bit energy consumptions and end-to-end delay

An analysis of the influence of ν on δ and E_b allows to examine the sensitivity of smooth AODV's with respect to the sensor node activity ratio. Note that the per-bit energy consumption implicitly describes the PDR. The reason for this are the transceiver energy consumptions which are by magnitudes smaller if the sensor node is in sleep state than if the sensor node is transmitting or receiving. Consequently, the total node energy consumptions are just linearly related to ν. As the power consumptions for sending and receiving are nearly the same, E_b does moreover not capture the amount of hops a packet has to travel or the number

of retransmissions it has to suffer, but mainly depends on the node activity. For each sensor node it can be estimated as the fraction of the energy consumptions and the number of bits arrived at the sink node during the simulation:

$$E_b = \frac{t_{sim} \cdot \nu \cdot P}{PDR \cdot p_l \cdot t_{sim}/\Delta t} \ . \tag{3.3}$$

The energy used during the active time is $t_{sim}\nu P$, with the average power consumption required for transmitting and receiving, P, is the same for all nodes with the same ν. The number of successfully received bits at the sink is computed as $PDR \cdot p_l \cdot t_{sim}/\Delta t$.

E_b and δ averaged over the simulation runs differ strongly between the sensor nodes. That is why the representation of the obtained values is done using the box plot which is depicted in Figure 3.13. All values lie within the interval given by the minimum and the maximum, i.e. by the lower and upper triangle, respectively. 50 % of all observed values lie within the box given by the 25 % and 75 % quantile. The length of this box is thus a measure for the statistical dispersion of the observed test values. The positions of the mean and the median values furthermore characterize the skewness of the distribution: If both are roughly on the same position in the middle of the box, the mass of the distribution lying above the mean value is equal to the mass lying below the mean. If, in contrast the median is not equal to the mean, as it is the case in Figure 3.13, this is an indicator for statistical outliers, i.e. a small number of extremely large (or small) values.

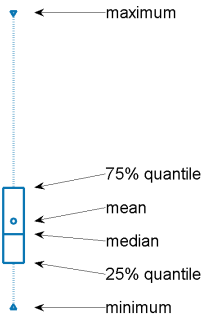

Figure 3.13: *Explanation of a box plot*

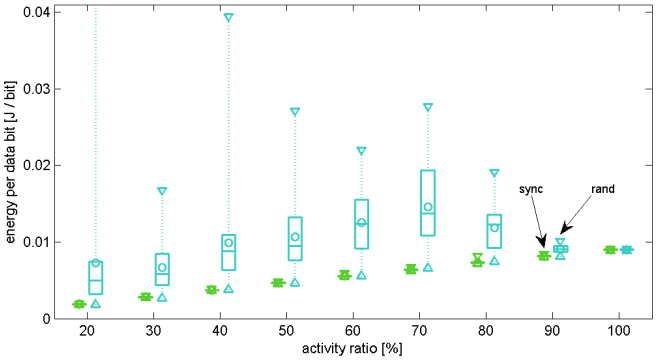

(a) Amount of energy consumed per successfully transmitted bit

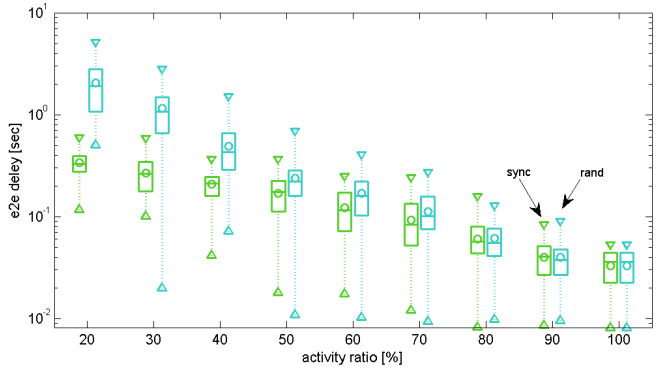

(b) E2e delay of successfully delivered packets

Figure 3.14: *Impact of activity ratio on smooth AODV*

The amount of energy required for transmitting a bit under smooth AODV for the synchronized and random sleep scheduling, respectively, are shown in Figure 3.14(a). For all considered values of ν, the node energy consumption is summarized in one box. Observe first that the boxes representing E_b for the synchronized case show a very small variance and a linear dependency on ν. This is also the case for the minimum E_b observed under the random sleep scheduling. In these cases the PDR is 100 % and E_b depends on ν and t_{sim} only (cd. Equation (3.3)) and hence linearly increasing with ν.

We saw in Figure 3.10(c) that for the case of the random sleep scheduling, the PDR for nodes far away from the sink is significantly decreased and heavily varying. Accordingly, the per-bit energy consumptions of those nodes vary strongly. This is also illustrated by the fact that the maximal value of $E_b = 0.05$ J/bit for $\nu = 20\,\%$ is not shown in order to make the presentation more readable. As small PDR implies a large per-bit energy consumption, as more retransmissions, thereby more time and energy are required for delivering a bit. This is the reason why the average E_b is not decreasing with a decreasing node activity.

The cost of duty cycling is depicted in Figure 3.14(b), where the e2e delay of successfully delivered application packets is visualized. Note that both under synchronized and under random sleep scheduling, the packets sent by one hop neighbors of the sink encounter the minimum network wide e2e delay. This is on the one hand very small and on the other hand not dependent on the sleep scheduling strategy, but only on the random time which lies between the arrival of the application layer data send request and the time when the transceiver is activated. For all other nodes, δ is significantly larger which necessitates a logarithmic scale of the y-axis. This variance is caused by the transmission over multiple hops which is additionally delayed by duty cycling, especially under the random sleep scheduling. As the activity ratio ν impacts the amount of packet collisions and the resulting retransmissions of packets, the e2e delay decreases with an increasing ν. Under the synchronized sleeping schedule, no packets have to be retransmitted because the destination has not been awake, a reason for the difference between the two sleeping policies.

3.4 Sleep Scheduling in ZigBee Multi-hop Networks

The results of the last section demonstrated that AODV and any other distributed routing algorithm do not work flawlessly in the presence of duty cycling nodes as long as the routing layer is not aware about the activity times of the sensor nodes. This section therefore introduces the *cross-layer sleep scheduling* algorithm CLS which allows to optimize the sleep and wake schedule of the sensor nodes with regard to the communication and routing problem. In the following, CLS is described in detail before the framework used for a performance evaluation of CLS and the results from this experiment are introduced.

3.4.1 Cross-Layer Sleep Scheduling

The goal of any WSN MAC protocol or sleep scheduling solution which has to work in the presence of a multi-hop routing structure is to minimize the percentage of time the node transceiver is on, while still allowing each node to communicate with its neighbors. Therefore, CLS consists of two components. The *neighbor aware communication* (NAC) mechanism introduces a NWK-MAC layer interaction allowing to postpone packets to sleeping neighbors. The *adaptive resynchronization* (AR) functionality enables the nodes to adapt their activity schedule to their neighbors' schedules.

Neighor aware communication

In the last section we saw that low duty cycles, i.e. short activity times, and reliable data delivery are not achievable if the sensor nodes are not aware of their next hop's duty cycle, as many packets are sent to sleeping nodes and consequently lost. The NAC mechanism, therefore lets each node send a wakeup signal (WS), as soon as it goes from sleep to active state to announce its activity to its neighbors. WSs are small, hence have a negligible impact on the network load. Note that in a network implementing the entire ZigBee specification, the link status

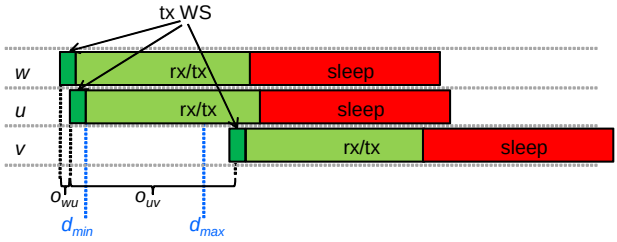

Figure 3.15: *Node u, its successor v and its predecessor w*

frames each FFD has to periodically send to its neighbors can moreover play the role of a WS [33]. Another overhead reduction can be applied for the case of static networks where it is sufficient to send this small signal each third time a node wakes up to allow all nodes to maintain a neighbor list containing their neighbors' states. Clearly, this frequency can be adapted to the network dynamics in order to guarantee a good trade-off between overhead and adaptiveness.

When a node u receives a WS from node v, it updates its neighbor list by adding v's identifier along with the offset o_{uv} to its own wakeup time. o_{uv} is computed as the amount of time between the times when u and v wake up (cf. Figure 3.15). o_{uv} indicates how much communication time u shares with its so-called *successsor* v. In contrast, u only becomes aware of its so called *predecessor* w which wakes up before u, if w sends a packet to u. Predecessors are also included in the neighbor list, but without an exact offset value.

The information included in the neighbor list enables NAC. If u has to send a unicast data packet to its successor v, u can simply delay the transmission until v is awake. Otherwise, it will send the packet immediately as it would have done without the cooperation of MAC and routing layer. Recall that AODV uses broadcasts for establishing and maintaining routing paths [93]. In order to increase the performance of the routing mechanism, a node using NAC maximizes the number of receivers of a broadcast message, by sending it at a time when it

knows the maximum number of its successors to be active.

Adaptive resynchronization

NAC alone is already suitable for increasing the PDR in networks following the random sleep scheduling strategy, but the performance improvements are limited. Especially in networks operating at a very low random duty cycle, it may happen, that two neighboring nodes are never awake at the same time, and the physically connected network is temporally partitioned. The goal of the AR algorithm is therefore to increase the number of a sensor node's *temporal* neighbors by allowing each node to adapt its duty cycle to the ones of its surrounding nodes. The focus of AR is establishing a temporal connectivity in a physically connected network layout, the adjective "temporal" is therefore omitted in the following.

The example of Figure 3.15 illustrates that a node's neighborship allows to file it in one of four different classes: Either it has (1) both successors and predecessors (node u), it has (2) only successors (node w), (3) only predecessors (node v) or it has (4) no neighbors at all. In the last case, the node is totally separated from the rest of the network and consequently has to *search for successors*. This is done by delaying its next waking up by a significant fraction of νT, thereby potentially finding communication partners. If a node falls in class (3), i.e., has only predecessors in its neighbor list, this is insofar problematic as the amount of waketime shared with the predecessors is not known and the communication is hence not reliable. In order not to lose the connection to their predecessors, while finding successors, those nodes delay their waking up by a small period only, thereby allowing their predecessors to adapt to their new duty cycle.

Nodes belonging to the classes (1) and (2) may also be forced to adapt their duty cycle: If a node has successors in its neighbor list, but the resulting offsets do not allow reliable communication, the node has to *adapt to its successors*. This adaptation may be necessary due to two reasons which are illustrated by the example of Figure 3.15: either the node and its successor share too much of the waketime which leads to collisions of the WS (nodes w and u), or the overlap is

too small to allow a reasonable communication (nodes u and v). In the first case, u, being the nearest temporal neighbor of node w wakes up too shortly after w, i.e. $o_{wu} < d_{min}$. Node w has thus to schedule its next waking up earlier. In contrast, the closest successor of u, v, becomes active shortly before u is going to sleep, i.e. $o_{uv} > d_{max}$. u thus has to wake up later the next time. Different values of d_{min} and d_{max} may be used to optimize the system performance. The simulation study whereof results are presented in Section 3.4.3 therefore uses different values for these thresholds to illustrate the impact of parameter choices on the system performance. Note that the mains-powered not sleeping sink sends WSs according to a constant schedule and therefore acts as an "anchor" in order to avoid an endless oscillation of the AR mechanism.

3.4.2 Evaluation Framework

The simulation methodology used for evaluating the performance of CLS is the same as in Section 3.3.4. A rough sensor node abstraction capturing the IEEE 820.15.4-2003 stack of a 7×7 grid WSN running smooth AODV allows to obtain results which are applicable to various WSN deployments.

Recall that for the case of a duty cycling multi-hop IEEE 802.15.4-compliant WSN, the amount of energy consumed for communication purposes depends mainly on the time the node's radio unit spends in sleep state. The energy consumptions of all nodes in an arbitrary simulation run are hence roughly the same and just linearly increasing with the duty cycle ν. In Section 3.3.4 we additionally saw that he amount of energy per consumed bit just mirrors the PDR. Energy related curves are therefore omitted. It is evident that ν has to become as small as possible as long as the PDR and the e2e delay are still acceptable.

The effects of CLS on the system performance are analyzed by considering three different scenarios, i.e. WSN configurations, namely synchronized sleep scheduling, random sleep scheduling and random sleep scheduling together with CLS. Recall from Section 3.3.4 that in the synchronized network, whereof the performance serves as an upper benchmark, all nodes are either on or off at the

same time and that this behavior is not achievable without an enormous amount of synchronization overhead. In the random network, which can be considered as the worst case, each node activates its radio unit for νT at a randomly chosen time during the first 50 sec of a simulation run, then sleeps for $(1 - \nu)T$ and so on. If CLS is used, NAC and AR allow to adapt each node's communication behavior and the schedule of its duty cycle with respect to its neighbors.

3.4.3 CLS Performance Evaluation

The most important metric for comparing the performance of the three different sleep scheduling strategies is the PDR. As an additional application layer metric the e2e delay δ is considered.

Packet delivery ratios

The PDR averaged over all data packets sent by the nodes in the network in dependence on the duty cycle ν is shown in Figure 3.16(a). As a CBR traffic pattern and a perfect wireless channel are assumed, the system is stable, i.e. all nodes have associated and all routes are established, after an initial period of 1000 sec. In contrast to the previous section, here the steady state system behavior is of interest. Therefore the following results are obtained from simulation runs of 3000 sec repeated 50 times after this transient period, an approach which has e.g. been proposed by Law and Kelton [98]. 50 runs are sufficient for obtaining satisfyingly small 95 % confidence intervals.

Figure 3.16(a) confirms the results obtained in the last section: the performance of the random network without CLS breaks down to 50 % if the nodes sleep only 25 % of the time. In contrast, the performance of the synchronized network is only slightly affected by a decreasing ν. In practice, however, the synchronization comes along with high costs. The fact that CLS achieves almost the same performance with respect to the PDR in an initially not synchronized network while requiring no synchronization effort hence demonstrates the attractiveness of this solution.

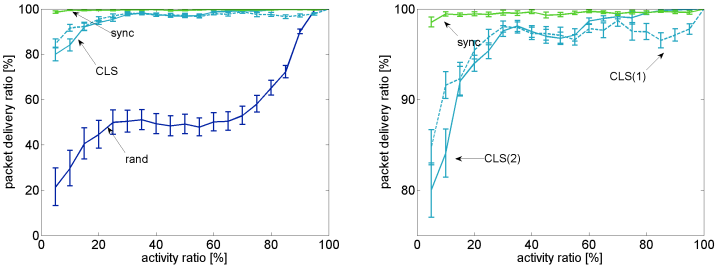

(a) Random, synchronized, and CLS (b) A closer look at CLS and synchronized

Figure 3.16: *Effects of different sleep scheduling mechanisms on the PDR*

d_{min} and d_{max} are lower and upper bounds for the temporal distance between node u and its successor v (cf. Figure 3.15). These parameters can be used to optimize the system performance with respect to the environmental conditions. This is illustrated by the PDRs achieved by CLS under different duty cycles running with parameter set (1) $d_{min} = 0.05\nu T$ and $d_{max} = 0.5\nu T$ and (2) $d_{min} = 0.01\nu T$ and $d_{max} = 0.9\nu T$. To ease the comparison Figure 3.16(b), shows the same analysis as Figure 3.16(a) but zooms in the y-axis.

Observe that for the smallest considered activity ratio $\nu = 5\,\%$, even the synchronized system has a PDR significantly smaller than 100 %. This is sign that the activity times are not large enough to always finish all necessary transmissions. This effect is more severe for the case of the random system operation with CLS where the nodes are additionally not perfectly aligned and consequently roughly 15 % more packets are lost. Note however that this is still by far better than the PDR of 22 % achieved for the case without CLS (cf. Figure 3.16(a)). Moreover, the performance difference is quickly decreasing with increasing ν. The comparison of the curves representing the different CLS parameterizations resulting in smaller (1) and larger (2) allowed neighbor offsets shows that it is possible to optimize d_{min} and d_{max} with respect to the network activity. Parameter set (1), e.g., is more advantageous in systems operating under low duty

cycles, as the nodes activity times overlap more thereby increasing the packet transmission success. Parameter set (2) in contrast is able to guarantee a high PDR in networks operating at high duty cycles, as it allows for longer communication periods thereby reducing the packet collision probability.

End-to-end delay

Besides the PDR, the e2e delay is another important metric for a WSN application, as the end user wants to receive information within a certain delay bound. A comparison of the e2e delay δ averaged over all packets successfully received at the sink shown in Figure 3.17(a), illustrates the drawbacks of CLS. The e2e delay for the case of a system operating under CLS is clearly larger than in the synchronized case. With CLS the e2e delay is moreover influenced by the parameters of the AR algorithm, where tight bounds for the offset between two temporal neighbors (i.e. parameter set (1)) yield a much less homogeneous e2e delay than looser bounds (parameter set (2)). Additionally, the non-monotonic behavior of δ under CLS is striking, which is the motivation for the subsequently presented analysis.

For the case of duty cycled networks, δ consists of three different components. There is a *base delay*, δ_1, required for transmitting a packet through the network, accounting for random backoff intervals due to the contention avoidance mechanism, the propagation speed and processing delays at intermediate nodes. δ_1 is varying with the network characteristics and traffic patterns. For each network configuration it is given by $\delta_1 = \delta(100\,\%)$ or the average e2e delay observed in the case of an "always on" network.

In a system operating with a duty cycle of $\nu < 100\%$, *intra-* and *inter-node delays* can occur. The intra-node delay $\delta_2(\nu)$ is the amount of time between the APL send request and the time the transceiver can actually transmit the packet. The inter-node delay $\delta_3(\nu)$ is non-zero, if the nodes in the network are not sleeping at the same time or the packet arrives very shortly before all nodes go to sleep. In both cases, a packet may encounter a small delay at each forwarding node, as NAC delays the packet until the next hop is awake.

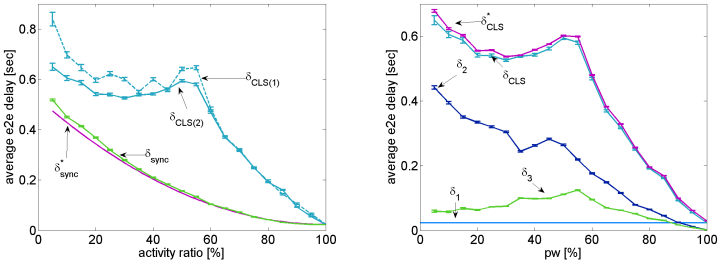

(a) Synchronized and CLS (b) CLS(2)

Figure 3.17: *Effects of different sleep scheduling mechanisms on the e2e delay* δ

Putting all components together allows to break down the average e2e-delay encountered by successfully delivered application layer packets into

$$\delta(\nu) = \delta_1 + \delta_2(\nu) + (h(\nu) - 1)\delta_3(\nu), \tag{3.4}$$

where $h(\nu)$ denotes the average number of hops on each data path, if the network is running with a duty cycle of ν.

For computing δ, let us first focus on the synchronized sleep scheduling policy. In this case, all nodes are either active or sleeping. Except for very rare cases, where a send request arrives shortly before all nodes go to sleep state, packets can be forwarded immediately and $\delta_{3_{sync}}(\nu)$ can be approximated by zero.

By means of probability theory, deriving the average delay at the source node, $\delta_{2_{sync}}(\nu)$, is straightforward: Out of p packets arriving at the sink during one simulation run, νp of the corresponding APL layer send requests encountered an active radio unit. For those packets, the intra-node delay $\delta_{2_{sync}}(\nu)$ will be infinitely small and can be approximated by zero. The remaining $(1 - \nu)p$ APL layer requests in contrast, had to wait until the radio unit is active. An APL layer packet facing a sleeping radio unit encounters with equal probability a worst

case waiting time of $(1-\nu)T$, a best case zero waiting time or something in between. The average time an application layer request encountering a sleeping radio unit has to wait, is thus given by $\frac{(1-\nu)T}{2}$. The sleep schedules of the nodes are synchronized, the next hop of the node is hence awake at the same time, and the packet can be sent as soon as the radio unit is active. This yields

$$\delta_{2_{sync}}(\nu) = (1-\nu)\frac{(1-\nu)T}{2} \tag{3.5}$$

as an average intra-node delay. Putting an experimentally obtained δ_1, Equation (3.5), and $\delta_{3_{sync}}(\nu) = 0$ in Equation (3.4) results in an e2e delay approximation δ^*_{sync} which matches very well the simulation results (cf. Figure 3.17(a)).

For the average e2e delay resulting from the use of CLS, Equation (3.4) holds, too, but computing its components is much more complex. Figure 3.17(b) visualizes for the case of parameter set (2), that the interdependency between the components $\delta_{2_{CLS}}(\nu)$ and $\delta_{3_{CLS}}(\nu)$, which are obtained from simulation traces and the duty cycle ν is more difficult to describe than for the synchronized case, as the corresponding curves show a zigzag behavior.

Both issues are a direct consequence of the not strictly synchronized sleeping periods. For the average delay encountered at the source node Equation (3.5) does not hold anymore, as in some cases, packets will additionally have to wait until the next hop is awake, i.e. $\delta_{2_{CLS}}(\nu) = \delta_{2_{sync}}(\nu) + \delta_x(\nu)$. This additional waiting time $\delta_x(\nu)$ is difficult to capture. While the AR mechanism makes it possible to obtain bounds for the offset to the nearest *temporal* neighbor v of a node u, v is not necessarily the next *routing* hop of u. The reason for this is that CLS is not coupled to the routing protocol. As a consequence, CLS is open towards other routing mechanisms, but a probabilistic estimation of δ_x and thereby also of $\delta_{2_{CLS}}(\nu)$ is difficult. The independence of CLS and routing is also the reason why it is not possible to give a closed-form expression for $\delta_{3_{CLS}}(\nu)$. Putting values for $\delta_{2_{CLS}}(\nu)$ and $\delta_{3_{CLS}}(\nu)$ obtained from simulation traces into Equation (3.4) allows however to calculate the approximation δ^*_{CSL}, which shows again a good match and thereby confirms the correctness of the

analysis (cf. Figure 3.17(b)).

Let us now come back to discussing the behavior of $\delta_{CLS}(\nu)$. In systems operating at low duty cycles, where d_{max} is sufficiently large and d_{min} is small (e.g. parameter set (2)), the time a packet has to wait until the next hop is awake is nearly uniformly distributed over the active time νT. Under parameter set (1) in contrast, the "allowed" sending time is smaller which results in an slightly increased and also less homogeneous e2e delay (cf. Figure 3.17(a)), as collisions causing retransmissions are more likely.

In contrast to the intra-node delay, the inter-node delay $\delta_{3_{CLS}}(\nu)$ is not monotonically increasing with decreasing ν but has a local maximum at $\nu = 55\,\%$, thereby causing a local maximum for δ_{CSL}. The reason for this is again the independence of CLS and routing. A node's next routing hop is not necessarily its nearest successor but chosen among its temporal neighbors. With an increasing node activity, the temporal neighborship of the nodes become larger and the probability that a node chooses a neighbor with a small offset as next routing hop is decreasing. Consequently, the probability that $\delta_{3_{CLS}}(\nu)$ is large and thereby also the average value increases. The reason why $\delta_{3_{CLS}}(\nu)$ decreases for $\nu > 55\,\%$ is caused by another phenomenon which overlaps this effect. For $\nu > 55\,\%$, the sleep times are shorter than the active times and it is possible that a node has its next hop both as successor and as predecessor, as their activity times overlap not only once but twice. Consequently a node has two opportunities for forwarding a packet which of course decreases the forwarding delay.

3.5 Concluding Remarks

A standardized communication stack would lower the barriers for interconnecting and accessing existing and future WSN deployments and therefore pave the way towards a truly ubiquitous computing environment. Despite the number of promising ideas, no standardized technology has yet been fully accepted for wireless sensor networking. The theoretically suitable standards IEEE 802.15.4 and ZigBee are not able to play the role of such enabling technologies as they are

not targeted at scenarios where battery powered nodes participate as routers in a multi-hop topology. This is however a key requirement for any long-lasting WSN deployment and results in three inhibiting reasons for standards-based WSNs which have been addressed in this chapter.

The first identified inhibitor lies in the beginning of the WSN lifetime: Each IEEE 802.15.4 network has to successfully carry out the association procedure before it can become operational. Neither the IEEE 820.15.4-2003 standard nor the IEEE 820.15.4-2006 standard however specify an association procedure which is working in nonbeacon-enabled duty cycling multi-hop WSNs. In order to solve this problem, four enhancements have been proposed and extensively studied. The results of the simulation study show that the influence of factors given by the application tends to be larger than the improvements achievable by tuning the association mechanism. However, especially the newly introduced altruistic and the greedy behavior are promising possibilities for optimizing the association procedure with respect to the network characteristics.

The second inhibitor is the ZigBee routing protocol. It is very similar to the well known AODV protocol and causes an exorbitant amount of routing overhead if the sensor nodes are regularly in power saving mode, therefore causing transmission failures which in turn cause AODV to trigger repair mechanisms. For this purpose, the idea of "smoothening" AODV, i.e., to make AODV more tolerant in the face of transmission failures, has been investigated. We saw that smooth AODV is suitable for significantly reducing the AODV overhead and therefore improving the system performance.

The third inhibitor for IEEE 802.15.4-based WSNs is the non-existence of energy saving possibilities in the nonbeacon-enabled mode. The simulation study conducted for the performance evaluation of smooth AODV showed that the idea of letting each sensor node independently decide over its activity should not be applied to multi-hop WSNs as the system performance becomes unacceptable even for rather high duty cycles. As a solution to this issue, the CLS mechanism has been introduced which avoids sending packets to sleeping nodes and allows each sensor node to adapt its duty cycle to its neighbors. The performance

of CLS regarding the packet delivery ratio proves to be similar to the one of a synchronized sleep scheduling but does not require out-band synchronization.

Together, the mechanisms introduced in this chapter allow to run a IEEE 802.15.4 and ZigBee based sensor network under low duty cycles in a robust and efficient manner. The introduced extensions of the association mechanism allow to lay the foundations for a successful and efficient WSN operation. Building on this foundation, CLS and smooth AODV allow to carry out the operational phase in an energy-efficient manner. Even if there is still a long way to go until all those extensions are accepted within the bodies of standardization, this chapter should make us confident that IEEE 802.15.4 is suitable for becoming 'the" WSN standard as IEEE 802.11 has become "the" wireless LAN standard.

4 Assessing the Max-Min Fair Wireless Mesh Network Throughput

Fairness is what justice really is.
Potter Stewart (1915-1985)

Wireless mesh networks share with the previously discussed wireless sensor networks the ability to be self-organizing, self-configuring, and self-healing. Consequently, WMN protocols, residing in the middle of the ISO/OSI stack, are similar to the corresponding WSN protocols. The key differences between the two network types lie at the bottom and the top of the protocol stack: WSNs are supposed to deliver as much data from the environment as possible while operating with a single pair of batteries or the scavenged energy as long as possible. WMNs in contrast have become popular as fast, reliable, and cost-effective wireless networks facilitating the storage, sharing, and exchange of information, and for enabling an ubiquitous Internet access [112]. Hence, the WSN hardware and also the communication technology used for wireless sensor networking has energy efficiency and cost reduction as a primary goal, while data rates are of secondary importance. For wireless mesh networking in contrast, the energy efficiency is a minor issue, while the achievable end-to-end throughput shall be maximized and quality of service (QoS) guarantees are relevant.

As a consequence, the study on WSN energy consumption models conducted

in Chapter 2 is not relevant to mesh networks. WMNs are a special type of a mobile ad hoc network (MANETs), therefore it seems reasonable to use MANET metrics for the WMN performance evaluation. This approach is however also not suitable as MANETs target emergency and battlefield situations where a fast network startup and a dynamic network adaptation are vital for guaranteeing a wireless communication in the absence of infrastructure. WMNs in contrast, operate under less harsh conditions and have more stable traffic patterns. Addressing the lack of suitable WMN metrics, this chapter breaks new ground by contributing quickly computable, upper bound capacity estimation algorithms for WMNs.

As typical traffic demands in WMNs are time varying, a fair bandwidth allocation is able to capture the main traffic characteristic of WMN - the aggregates of mesh clients attached to mesh routers are usually consuming as much contents as possible. The key WMN performance evaluation challenge is hence to determine the capacity of a wireless mesh networks under certain fairness constraints. Due to the traffic uncertainty, an exact a priori evaluation of the actual performance of mesh networks is typically not feasible. The evaluation of the performance of an idealized mesh network is however suitable for giving a first estimate what performance the deployed mesh network might achieve. Consequently, this challenge has been accepted by the research community, but a final solution has still not been found. In the following, an answer to this problem will be provided which gives firstly more insights in the theoretical understanding of mesh networks, secondly may be directly applied to assigning resources in centralized scheduling schemes, and thirdly is useful for planning mesh networks.

The objective of this chapter is to develop algorithms for computing a *max-min fair* (MMF) rate allocation for the flows in a mesh network. Following Bertsekas and Gallager [113], a solution is max-min fair if no rate can be increased without decreasing another rate. Max-min fairness hence means to maximize the minimum per flow throughput in a network. For a WMN where all non-gateway nodes serve as access points for clients, and therefore have a saturated best effort-flow from the Internet, MMF rate allocation translates to finding (application layer) flow rates which are feasible with respect to the used routing paths and link rates

and fulfill the definition of max-min fairness.

Two major contributions to the research on MMF rate allocations in WMNs are made by this chapter. Firstly, it establishes a framework allowing to determine the max-min fair throughput in a multi-gateway, multi-radio, multi-rate, multi-hop mesh network with static routing, channel and rate allocation. Secondly, it considers two possibilities for defining collision domains, i.e. the set of all links which must not be used in parallel, namely the asymmetric and the symmetric case [114]. Moreover, the impact of nominal [114] and effective [115] load definitions are considered.

The remainder of this chapter is structured as follows. In Section 4.1, the background necessary for this and the following chapter is established. It starts with an introduction to the topic of mesh networking. Next, a formal framework for abstracting a specific WMN instance and a methodology for generating random WMN instances and thereby enabling Monte Carlo simulation studies is introduced. Finally, this section reviews contributions related to the problem of WMN capacity estimation and more precisely works on MMF throughput computation.

After this introductory discussion, Section 4.2 describes max-min fair rate allocation algorithms for WMNs which have been introduced and evaluated in [20]. They are on the one hand a self-contained contribution to WMN research and will on the other hand be used as performance metrics in Chapter 5. This section consists of two parts. Firstly, the existing MMF algorithms which deliver the basic building blocks for this chapter's contribution are discussed in detail. Secondly, extensions are presented which allow to determine the MMF throughput under more realistic conditions including the asymmetric and the symmetric collision domain and both the effective and the nominal load definition.

The MMF rate allocations resulting from the four different considered combination of load and collision domain definitions are compared in Section 4.3. The discussion of an example network allows to clarify the impact of the collision domain and load definition, which are stochastically verified by analyzing the rate allocations in a number of randomly generated network snapshots. Finally, concluding remarks can be found in Section 4.4.

4.1 Background and Related Work

This section is not only the cornerstone for the contributions of this chapter on max-min fair throughput computation for WMNs but also for the following chapter where WMN optimization possibilities will be investigated. Therefore, it includes a survey on wireless mesh networking, before an analytical framework for abstracting a WMN and a methodology for generating random WMN topologies are introduced. Finally, this section reviews contributions related to the problem of WMN capacity determination.

4.1.1 A Survey on Wireless Mesh Networks

In order to get an overview on the field of wireless mesh networking, let us first answer the question what a WMN actually is and discuss its typical architecure, before we focus on the typical WMN technologies and use cases. For a more exhaustive introduction to mesh networking, the reader is referred to the works of Bruno et al. [116] or Akyildiz et al. [112].

Network architecture

Searching the literature for a formal definition of a wireless mesh network results in most authors, e.g. Bruno et al. [116], Akyildiz et al. [112], Conti and Giordano [117] defining a WMN as a special type of a mobile ad hoc network. The RFC 2501 [118] issued by the IETF MANET working group defines a MANET to consist of mobile devices or *nodes* which are free to move and to arbitrarily leave and join the network. In the absence of an infrastructure or a central managing entity, the network nodes cooperate to forward packets in an ad hoc fashion in order to ensure a multi-hop data delivery within the MANET or to another network, e.g. the Internet. This enables building large networks in areas without infrastructure and is hence an interesting option for military or disaster recovery scenarios. In those scenarios, monetary costs are not the issue which makes typical MANET technology less attractive for users seeking an affordable reliable

wireless networking platform providing Internet access. According to [116, 117], this is the main reason why MANETs did not enter the market despite the enormous research effort dedicated to MANET engineering during the last 20 years.

Wireless mesh networks relax one of the key MANET characteristics, namely the lack of infrastructure. Introducing a wireless backbone into the network allows to increase the degree of reliability and robustness while still enabling a dynamic network structure [116] which is the most probable explanation for the increasing spreading of mesh networks. Another consequence of introducing a wireless backbone is that in contrast to MANET nodes, not all nodes of a WMN are equal, but *mesh routers* build an infrastructure for *mesh clients*. As a result, a typical WMN architecture like the one depicted in Figure 4.1 consists of three tiers [112]. The wireless backbone is represented by the upper two tiers of this architecture. A subset of the mesh routers is connected to the Internet via a wired or wireless backhaul link and therefore called *(Internet) gateway*. Another subset of the mesh routers serves as access points (APs) for the mesh clients forming the lowest tier of the hierarchy. Observe that although the mesh backbone is built by *wireless* links, clients may connect either over the air or via Ethernet [112].

Following Akyildiz et al. [112], this architecture describes only one WMN type, namely the *infrastructure WMNs*. The authors furthermore mention *client WMNs*, being a peer-to-peer network among mesh clients, and *hybrid WMNs*, being a mixture of the other two types. The infrastructure WMN architecture is however by far the most popular one, and besides the previously mentioned [116, 117], most authors identify a WMN with an infrastructure WMN, a position which is adopted by this monograph. Consequently, the adjective "infrastructure" is omitted in the following.

Technologies

According to [112] and also to a recent white paper from Calsoft Labs [119], the key characteristics of a WMNs are the following. In a similar way as MANETs, wireless mesh networks are multi-hop networks which significantly extend the

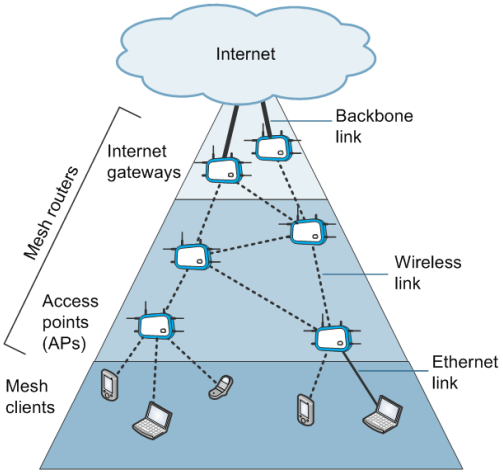

Figure 4.1: *A typical three-tiered WMN architecture*

coverage of infrastructure networks consisting of a single access point only. Removing the need for the wired infrastructure means that WMNs can extend their coverage to terrains where no "normal" wired backbone can be set up, or to rural areas where it does not pay to install DSL lines. The routing structure has self-* properties, i.e. it is self-forming, -healing, and -organizing. The popularity of mesh networking has its reasons also in the low technological requirements. Setting up mesh networks does not require specialized hardware. Serrano et al. [120] e.g. report on a wireless mesh testbed which consists of 12 off-the-shelf wireless routers which are normally used in home and office environments. Similarly, any device with a IEEE 802.11 or Ethernet interface can connect to a mesh router and consequently become a mesh client.

Let us now move to a more technical level. Currently, most mesh networks use the random channel access IEEE 802.11a/b/g technology and establish the routing structure on IP layer by protocols like AODV [93], OLSR [121] or

B.A.T.M.A.N [122]. The key issue for routing in wireless networks is to account for the reduced reliability and time variance of the wireless links. Information for link metrics going beyond the hop count hence have to include MAC layer information. According to Hiertz et al. [123], this is the main motivation for developing an IEEE 802.11 amendment addressing the needs of mesh networking. Since 2004 the IEEE task group s is busy with this task. The publication of the amendment is envisaged for 2011, at the time of writing, IEEE P802.11s/D9.0 [124] is the most recent draft version.

The main contribution of IEEE 802.11s will be to introduce routing capabilities at the MAC layer which is referred to as *path selection* in order to differentiate it from "normal" IP routing. Other important contributions are extensions to the MAC layer which enable service differentiation and QoS support for large scale networks. Furthermore, the MAC functionality supports congestion control mechanisms. Congestion is a definitive issue in mesh networks as nodes at the edge of the network have a higher probability of sensing an idle channel and therefore have a higher transmission probability than nodes at the core of the network. This in turn may now result in the stations in the middle of the network to congest and consequently to drop packets. Fu et al. [27] show that IEEE 802.11s compliant congestion control mechanisms are suitable for avoiding this packet loss and therefore to increase the network throughput. Other IEEE 802.11s features enable security mechanisms which is necessary for increasing the acceptance of mesh networking.

As a member of the IEEE 802.11 WLAN family, IEEE 802.11s targets *local* area mesh networks. Within the IEEE there are also two other working groups dedicated to mesh networking for networks with a different range. The goal of IEEE 802.15.5 [125] is to provide mesh networking capabilities to *personal* area networks using an IEEE 802.15.4 or IEEE 802.15.3 PHY and MAC layer going beyond the already included features described in Section 3.1.1. According to Lee et al. [126] IEEE 802.15.5 concentrates on the network formation, introducing basic meshing functions like tree formation, address allocation, and routing. It moreover introduces power-saving and multicasting options for IEEE 802.15.4

meshes and QoS support for IEEE 802.15.3 mesh networks.

At the other end of the spectrum there is IEEE 802.16 mesh networking which aims at *metropolitan* area networks. As a cellular networking technology, and working with a TDMA channel access, the purpose of the IEEE 802.16 mesh mode is only specified in addition to the "normal" point-to-multipoint (PMP) mode where one base station transmits data to several clients. The mesh mode shall facilitate the information exchange between the clients and extend the network range beyond the line of sight of the base station. The IEEE 802.16 mesh mode has however never been fully accepted, as it is not compatible with the PMP mode, and consequently specified by the older IEEE 802.16-2004 [127] only. The mesh mode is not included in the newer IEEE 802.16-2009 [55].

Looking at the real mesh networking world illustrates that neither the mesh paradigm specified by IEEE 802.15.5 nor by IEEE 802.16 has come to greater acceptance. At the moment, IEEE 802.11 is the mesh networking technology of choice, even if in the future other wireless communication standards will very likely adopt the mesh networking paradigm.

Use cases

In the survey papers written at the beginning of the wireless mesh network research era [112, 116, 117], several WMN use cases are identified, but all authors agree that providing Internet access is the most important task for WMNs. Today, this is still valid. According to Calsoft Labs [119], wireless mesh networks are indispensable for providing seamless and affordable wireless Internet access.

In [112], distributed information and sharing within the WMN for purposes like gaming, file sharing, backup storage, or establishing and maintaining social structures is identified as a further WMN use case. And indeed, this is a vital goal of the German Freifunk initiative[1] which aims at establishing the freedom of wireless communication without needing to rely on telecommunication service providers. The basic idea of this and other *community mesh networks* is that

[1] http://start.freifunk.net/, last accessed 04/2011

everybody makes his own private WLAN router available for other people, see e.g. Sombrutzki et al. [128]. Together, the coverage of the individual access points can be increased to a significantly larger area thereby enabling not only the previously mentioned data exchange, but also as a not unwelcome side effect a near to ubiquitous free Internet access.

While mesh networks are already popular for those two applications, there are also other less popular use cases which will be reviewed shortly. According to [116, 117] WMNs are also a key technology for intelligent transportation systems which shall provide real time information to passengers. Public safety applications are mentioned by [116, 117, 119] where WMNs shall build a wireless backbone to which mobile devices carried by policemen or municipal workers can easily connect. Finally, [119] mentions that the interest of military hardware manufacturers has shifted from MANETs to mesh networks due to the advantages introduced by an infrastructure combined with a flexible network formation.

4.1.2 Formal Description of a Wireless Mesh Network

Any analytical work on WMNs needs an abstraction. In the following, a description of a mesh network along with the details on the setting considered in the remainder of this work is introduced. A suitable abstraction of WMN is a graph, where the vertices are represented by the set of mesh nodes $\mathcal{N}$ and the edges are given by the set of links $\mathcal{L}$. The set of links consists of all pairs of nodes $i, j \in \mathcal{N}$ which are able to directly communicate. $r_{i,j}$ is the data rate of link (i, j). The set of nodes consists of two subsets: $\mathcal{N} = \mathcal{G} \cup \mathcal{F}$, where the set of gateways $\mathcal{G}$ contains the nodes which are connected to the Internet and hence serve as Internet gateways for the non-gateway mesh nodes contained in the set $\mathcal{F}$. All nodes in $\mathcal{F}$ are used as access points for end-users and hence the destination of a best effort downlink flow from the Internet. In the scenario considered in this work, $\mathcal{G} \cap \mathcal{F} = \emptyset$ does hold, but this is not necessary in general.

The direction from the Internet to the mesh nodes is denoted as *downlink*, the reverse direction as *uplink*. In order to simplify the notation, only downlink data

flows are considered. Another simplification is the abstraction of a dynamic self-healing WMN routing protocol to the existence of a set of static routing paths $\mathcal{P}$. As a non-multi-path setting is considered, each $f \in \mathcal{F}$ has one routing path $p_f \in \mathcal{P}$ to one dedicated gateway node $g \in \mathcal{G}$. The resulting routing structure is hence a forest consisting of routing trees rooted in the gateway nodes. Furthermore, the contributions of this chapter are applicable to multi-channel, multi-radio mesh networks, i.e. every link (i, j) is assigned a channel $q_{i,j}$ out of a set of non-overlapping channels.

The power received at node j when i is transmitting, $P_r^{i,j}$, is computed by a simplified path loss model proposed e.g. by Goldsmith [129]:

$$P_r^{i,j} = P_t P_g^{i,j} = P_t K [\frac{d_0}{d_{i,j}}]^{\alpha} = P_t \beta d_{i,j}^{-\alpha}, \tag{4.1}$$

where the node transmission power, P_t, is the same for all nodes. $P_g^{i,j}$ denotes the path gain between i and j which is considered to be time invariant. It is computed using the unitless constant K capturing the antenna characteristics and the average channel attenuation, the reference distance d_0 and the path loss exponent α. The variable $\beta = K d_0^{\alpha}$ simplifies this notation.

A measure for the average channel quality between i and j is the *signal to noise ratio* (SNR) [129]

$$\gamma'_{i,j} = \frac{P_r^{i,j}}{N_0}, \tag{4.2}$$

where N_0 denotes the ambient noise power. If other nodes are transmitting at the same time and on the same channel as i, this produces a certain amount of interference which disturbs the transmission of i. The probability that j can decode i's transmission is hence only then large enough if i's signal is strong compared to the other transmissions on the channel. Formally, this is the case, if the *signal to interference and noise ratio* (SINR), $\gamma_{i,j}$, is large enough. It is computed as [129]

$$\gamma_{i,j} = \frac{P_r^{i,j}}{N_0 + I_{i,j}} = \frac{P_r^{i,j}}{N_0 + \sum_{z \in \mathcal{Z}} P_r^{z,j}}, \tag{4.3}$$

where the time varying interference, $I_{i,j}$, is computed as the sum of the powers received from the nodes z which are transmitting on channel $q_{i,j}$ at the same time as i, $z \in \mathcal{Z} \subset \mathcal{N}$. Obviously, the values of both, SINR and interference depend on the time of observation, a more exact notation would thus be $\gamma_{i,j}(t)$ and $I_{i,j}(t)$. For reasons of readability, the variable t is only used if necessary. Observe that if the interference is zero, i.e. no node is transmitting at the same time as i, then $\gamma_{i,j} = \gamma'_{i,j}$, otherwise $\gamma_{i,j} < \gamma'_{i,j}$.

Transmission power, received signal strength, and background noise are given in mW and consequently, both, SNR and SINR are ratios without a unit. In addition to those *linear* units, the *logarithmic* units dBm for transmission power, received signal strength, and background noise and dB for SNR and SINR are used, where the relation between a linear value $\hat{V}$ and its logarithmic pendant V are as follows [129]

$$V = 10 \log_{10} \hat{V} \qquad \hat{V} = 10^{V/10}. \tag{4.4}$$

In the remainder of this work, a parameterization of channel model introduced by Equation (4.1), which is suitable for an imaginable IEEE 802.11g mesh network setting, is used which follows [129]. In decibel scale for a reference distance of $d_0 = 10\,\text{m}$, assuming the 2.45 GHz IEEE 802.11g frequency band, and a path loss exponent of 4, the power received by j if i is transmitting is

$$P_r^{i,j} = P_t + P_g^{i,j} = P_t - 140.046 - 40 \cdot \log_{10}(d_{i,j}), \tag{4.5}$$

where $d_{i,j}$ is the distance of nodes i and j in km and the transmission power is assumed to be $P_t = 100$ mW $= 20$ dBm for all nodes of the network. For computing the SNR, and the SINR, i.e. evaluating Equations (4.2) and (4.3), the ambient noise N_0 is set to the product of the thermal noise spectral density -174 dBm/Hz and the system bandwidth 20 MHz, i.e. to $N_0 = -101$ dBm.

Any wireless mesh networking technology allows to trade off transmission robustness and speed by offering a discrete set of modulation and coding schemes.

MCS	data rate	SINR threshold	maximal distance
BPSK 1/2	6 Mbps	3.5 dB	273.5 m
BPSK 3/4	9 Mbps	6.5 dB	230 m
QPSK 1/2	12 Mbps	6.6 dB	228 m
QPSK 3/4	18 Mbps	9.5 dB	193.67 m
16-QAM 1/2	24 Mbps	12.8 dB	160.2 m
16-QAM 3/4	36 Mbps	16.2 dB	131.7 m
64-QAM 2/3	48 Mbps	20.3 dB	103.8 m
64-QAM 3/4	54 Mbps	22.1 dB	93.5 m

Table 4.1: *IEEE 802.11g MCS, FER $\leq$ 1%, 1.5 kB payload, and Equation (4.5)*

As a representative example for the set of available MCS $\mathcal{M}$, this monograph uses the modulation and coding schemes available in IEEE 802.11g. Table 4.1 shows the required SINR γ_m^* and the maximal feasible transmission distances which allow to meet a frame error rate (FER) of 1% when an IP packet with 1500 Bytes payload is transmitted over an additive white Gaussian noise (AWGN) channel.

4.1.3 Wireless Mesh Network Topology Generation

The WMN performance is heavily affected by the node locations, the channel conditions, and the routing structure. For a thorough contribution to the understanding of mesh networks, Monte Carlo simulation techniques allowing to examine randomly generated network instances are hence a suitable means.

Each WMN consists of mesh nodes which are distributed over a certain area. This can be abstracted by modeling the location of the mesh nodes as point process $\Phi = \{X_i\}$, where the node locations are given by $\{X_i\}$. For a discussion on stochastic geometry see e.g. Stoyan et al. [130]. The main purpose of WMNs is to provide Internet access to a number of clients. Mesh nodes are either used as access points or for establishing the connection between access points and the Internet gateways. As mesh nodes have a monetary value, each planned WMN deployment aims at minimizing the number of required nodes and each unplanned WMN consists of access points contributed by users living in differ-

ent places. Hence, each two nodes are separated by a certain minimum distance which makes the most popular and well-understood point process model, the Poisson point process, unsuitable for creating realistic mesh topologies, as two points in a Poisson field may be arbitrarily close. Moreover, topologies emerging from a Poisson point process have a varying number of nodes, a fact which complicates the comparison between results achieved in the different topologies.

As a solution to both issues, the positions of mesh access points and gateway nodes are chosen according to a binomial point process on a grid. The positions of the $F = |\mathcal{F}|$ non-gateway nodes or access points are randomly chosen grid points of a grid with grid length l_F. For choosing the locations of the $G = |\mathcal{G}|$ gateway nodes, another grid with grid length l_G is used. Gateways are more expensive than non-gateway nodes and consequently tend to be separated by larger distances than non-gateway mesh nodes. l_G is hence by a factor $F/G > 1$ larger, i.e. there is a smaller number of grid points for choosing the location of the gateways. In the studied topologies the gateways are assumed to not be the bottleneck of the Internet connection and to be connected to the backbone with 100 Mbps.

The assumption that all nodes transmit on the same channel, i.e. $q_{i,j} = q$ for all $(i, j) \in \mathcal{L}$ reduces the computational complexity, the results presented in the following however hold for multiple channels as well. For deciding if a link between two nodes i and j in the randomly generated topology is existing and which MCS is used, the results provided by Table 4.1 are used. For each pair of nodes, the SNR is computed using Equations (4.2) and (4.5). If this SNR is smaller than the SINR requirement of the most robust MCS BPSK 1/2, i and j may not communicate directly. However, their transmissions may interfere with each other. Note that this binary condition for existence or non-existence of a link is on a very high abstraction level, as in reality, a transmission suffering a FER of more than 1 % could nevertheless succeed. In turn could a transmission fail despite a FER smaller than 1 %. In order to model the adaption of the link rate to the channel conditions, for each link (i, j) the MCS k is chosen which has an SINR requirement γ_k^* that is just smaller than the link's SNR $\gamma_{i,j}$. Correspondingly, the data rate $r_{i,j}$ corresponds to the data rate r_k of the MCS k that has the largest

SINR requirement below $\gamma_{i,j}$. A more thorough discussion on the challenges and benefits involved in the problems of link rate selection and link rate assignment schemes going beyond this simplistic approach is provided by Chapter 5.

4.1.4 Related Work

For estimating the capacity of a wireless network it is crucial to know which nodes can successfully communicate and which transmissions can concurrently take place. One of the first authors studying the wireless network capacity is Abramson [131] in 1970. The network where his newly introduced random channel access protocol ALOHA is running is a star topology with stations transmitting packets to a central coordinator in an unsynchronized manner. If two stations transmit at the same time, the packets collide and have to be sent again. By modeling this behavior, Abramson is able to prove that the ALOHA computer network can support up to 162 users sending on average 2 packets per minute.

Two models more suitable for characterizing the successful reception of a transmission and thereby the capacity of a wireless multi-hop network are introduced by Gupta and Kumar [132]. Under the *protocol model*, a transmission from node i to node j succeeds, if the distance between i and j is smaller than a transmission range r and if no other node which is closer to j than $(1+\epsilon)r, \epsilon > 0$ is transmitting at the same time. According to the less abstract *physical model*, a transmission from i is successfully received by j if the SINR $\gamma_{i,j}$ is greater or equal than a threshold $\gamma^*_{i,j}$:

$$\gamma_{i,j} \geq \gamma^*_{i,j}, \tag{4.6}$$

where $\gamma_{i,j}$ is computed as the fraction of the power received at j when i is transmitting and the sum of background noise and interference (cf. Equation (4.3)).

For networks with n randomly located nodes transmitting all on the same channel, and sending data to a random destination, Gupta and Kumar define the throughput capacity as the average per node throughput feasible under suitable spatial and temporal scheduling schemes. The protocol model allows to show that a network throughput of $\Theta(1/\sqrt{n \log n})$ bps is achievable. In addition to

this rough approximation, the physical model together with a constant value of $\gamma^*_{i,j}$ for all links allows to find tighter bounds for specific scenarios.

While adequate for proving theoretical bounds for the network capacity, both models introduced by [132] are too complex for computing the throughput of a specific network instance. The study of Li et al. [133] therefore considers IEEE 802.11 protocol overhead and localized traffic patterns which are, according to the authors, more likely to occur in large MANETs than completely random traffic flows. In a simulation study, the radio channel is abstracted by assuming that all nodes within a transmission range of 250 m and an interference range of 550 m are able to communicate or interfere respectively. The authors point out the inherent unfairness problems of the IEEE 802.11 channel access mechanism, but also show that large MANETs with localized traffic patterns guarantee a per node throughput close to the theoretical optimum found in [132].

Common to this and other works is that the results can hardly be applied to WMNs where the traffic flows are all either going to or coming from the Internet gateways. Another wireless network specific issue which especially applies for WMNs, is traffic uncertainty. The classical notion of traffic matrix is not suited for WMNs, as the limited sets of mesh clients connected to the mesh routers are highly variable and their traffic profiles are virtually impossible to assess.

One way of dealing with traffic uncertainty is to consider fairness in assigning bandwidth to WMN routes. As typical traffic demands in WMN are elastic, and QoS is not considered explicitly (usually only through lower bounds imposed on the bandwidth assigned to routes), the fair bandwidth allocation approach is able to capture the main traffic characteristic of WMN, where the mesh clients are usually consuming as much bandwidth as the WMN is able to provide. Max-min fairness [113] is one possible definition of fairness. While a number of methods to determine the max-min fair throughput of mesh networks exist, most approaches have deficiencies which makes them unsuitable for realistic mesh networking scenarios. Remedying these deficiencies is the goal of this chapter. For getting an overview on the problem, let us hence review the existing contributions on MMF throughput determination this chapter improves on, before we discuss the

mentioned concepts more thoroughly in Section 4.2.1.

Huang and Bensaou [134] propose an algorithm for determining the max-min fair throughput in an ad-hoc network. However, they do not consider the throughput of end-to-end flows but of links or single-hop flows. Jun and Sichitiu [114] consider a mesh network with end-to-end flows. For actually calculating the per-flow throughput, the *bottleneck collision domain* is determined, where a link's *collision domain* corresponds to the set of this link and all other links on which a parallel transmission would lead to a collision. The bottleneck collision domain is now the collision domain with the highest *nominal load*, i.e. the number of single hop transmissions on the collision domain's links including relayed transmissions. For the case of a WMN where the traffic of all nodes has to be routed through the same Internet gateway, the collision domain of the link to the gateway node will hence be the bottleneck collision domain. The authors argue that in this case, the maximal achievable per flow throughput is in the order of $\mathrm{O}(1/a)$, where a is the average number of non-gateway nodes. Note that Jun and Sichitiu do not really determine the max-min fair throughput of a network but only the capacity of the main bottleneck and hence the minimum throughput.

Aoun and Boutaba [115] use the collision domain concept as defined by [114] in order to determine the max-min fair throughput. This is done by iteratively determining the bottleneck collision domain and fixing the rates of all flows traversing it, i.e. assigning the maximal feasible rate to those flows. Additionally, Aoun and Boutaba introduce the definition of the *effective load* of a collision domain which is lower than the nominal load defined in [114]. The difference of effective load and nominal load is that the effective load considers the possibility of spatial reuse of components belonging to the same collisions domain. While [115] introduces the notation of effective load and demonstrate it using examples, they do not specify an explicit algorithm how to compute it. The algorithm given in [134], however, is actually based on the effective load definition and can be modified to determine the max-min fair throughput in mesh networks with end-to-end flows. A final step towards algorithms suitable for state-of-the-art mesh networks is the work of Akhtar and Moessner [135] which is an extension of [115] for multi-

radio, multi-channel, and multi-gateway mesh networks. However, the authors went back to the concept of the nominal load of a collision domain instead of the effective load introduced by [115].

The validity of using the MMF throughput as a WMN capacity measure is confirmed by a recent contribution to WMN engineering where Luo et al. [136] use a similar but easier to compute optimization criterion: The authors investigate the joint routing, scheduling, rate adaptation, and power control which maximizes the minimal per flow throughput. The authors moreover show that the impact of design decisions observed under this criterion holds for the proportional fair throughput, too. Consequently, this chapter attempts to making the existing MMF algorithms more suitable to realistic scenarios by introducing extensions for multi-gateway, multi-rate, multi-channel, multi-hop mesh networks and thereby contributing a valuable tool for WMN research.

4.2 Max-Min Fair Flow Rate Allocation Algorithms

In the setting described in Section 4.1.2, all nodes $f \in \mathcal{F}$ have a saturated best effort-flow from the Internet, which is routed over path p_f which in turn consists of a number of links with different data rates. The goal is now to find data or flow rates b_f that fulfill the definition of max-min fairness. In the following, first, the earlier mentioned results of [114, 115, 134, 135] will be discussed more thoroughly. Subsequently, the extensions allowing to compute the MMF flow rate allocation for more realistic network instances based on the nominal and effective load definitions are introduced.

4.2.1 Existing Contributions

Let us start the discussion with the definition of a collision domain and its nominal load according to [114]. The *collision domain* $\mathcal{D}_{i,j}$ of link (i, j) corresponds to the set of all links (s, t) which can not be used in parallel to link (i, j). The term “can not be used in parallel" is intentionally chosen rather imprecisely since

the exact definition depends on the underlying MAC technology. In general, a link (s,t) can not be used in parallel to a link (i,j) if the interference from a transmission on link (s,t) alone is strong enough to disturb a parallel transmission on link (i,j). Note that this definition does not include the case that small interferences from multiple parallel transmissions sum up and might together disturb a successful transmission. The concept of collision domains hence greatly reduces the computational complexity at the price of reduced exactness.

Jun and Sichitiu [114] distinguish *symmetric* and *asymmetric* collision domains. In the asymmetric case, a transmission on link (s,t) prevents the successful transmission on (i,j) if the links (s,j) or (i,t) exist, i.e. all one-hop neighbors of j must not transmit and all one-hop neighbors of i must not receive. In the symmetric case, both ends of a transmission are protected, e.g. due to the RTS/CTS mechanism of IEEE 802.11 or the three way hand-shake in the IEEE 802.16 mesh mode. Consequently, a transmission on link (s,t) prevents the successful transmission on (i,j) if one of the links $(i,s),(i,t),(j,s)$ or (j,t) exists. The entire two-hop neighborhood is blocked. In the following, the two cases will be referred to as “asymmetric" and “symmetric" collision definitions.

Let us discuss these different definitions at the example of the topology shown in Figure 4.2. The links carrying the data flows from the gateway nodes 1 and 5 to the nodes 2, 3 and 4, i.e. (1,2), (5,4), (4,3) are *active* and depicted by solid lines. The links (2,3), (3,2), (2,1), (3,4) and (4,5) are called *passive*, as they are not used for routing purposes. For computing the asymmetric collision domain of link (4,3), we need to find all link $(a,b) \in \mathcal{L}$ where either the link $(a,3)$ or $(4,b)$ exists. The symmetric collision domain additionally includes all links (a,b) for which $(4,a)$, or $(b,3)$ exist. For sake of simplicity, let us consider only *active* links which are used for routing purposes. The asymmetric collision domain of (4,3) is now computed as $\mathcal{D}^a_{4,3} = \{(4,3),(5,4)\}$, the symmetric collision domain is $\mathcal{D}^s_{4,3} = \{(4,3),(5,4),(1,2)\}$.

The next required building block is the definition of load. The *nominal load* of a collision domain corresponds to the number of transmissions that take place in a collision domain, where $\zeta_{k,i,j} = 1$ corresponds to a transmission of flow k

Figure 4.2: *Simple example network*

on the hop from node i to node j, i.e. $(i,j) \in p_k$. The number of transmissions $\nu_{i,j}$ of link (i,j) corresponds to the number of end-to-end flows crossing it:

$$\nu_{i,j} = \sum\nolimits_{\{k \in \mathcal{F} | (i,j) \in p_k\}} \zeta_{k,i,j} = \mid \{k \in \mathcal{F} \mid (i,j) \in p_k\} \mid . \tag{4.7}$$

Correspondingly, the nominal load of collision domain $\mathcal{D}_{i,j}$ is given by the number of transmissions in $\mathcal{D}_{i,j}$

$$\mu_{i,j} = \sum\nolimits_{(s,t) \in \mathcal{D}_{i,j}} \nu_{s,t}. \tag{4.8}$$

For the case where all links have the same data rate r, the capacity of the whole collision domain is also r, as only one of its link can be used at a time. Under the fairness constraint, the throughput of any flow traversing at least one link of collision domain $\mathcal{D}_{i,j}$ is upper bound by $r/\mu_{i,j}$. If one computes the load of all collision domains in the network, one obtains the *bottleneck collision domain*, which most strongly restricts the rates of the flows it carries, as the collision domain with the highest nominal load.

Based on this definition of the collision domain throughput, Aoun and Boutaba [115] indicate an algorithm for computing the max-min fair throughput. The principle of the algorithm, which will be called *nominal load based algorithm* (NLBA) in the following, is to iteratively determine the bottleneck collision domain and to allocate the rates of all flows traversing this collision domain. In the next iteration, only the remaining collision domains and flows are considered. The algorithm ends when the rates of all flows are set.

In Algorithm 4.1 the NLBA version proposed by [115] which accounts for

end-to-end flows but is only suitable for networks with homogeneous link rates is shown. It works as follows. Let $\mathcal{F}^*$ be the set of flows without rate allocation, $\psi_{i,j}$ be the percentage of unassigned nominal capacity of collision domain $\mathcal{D}_{i,j}$, and $\mathcal{L}^*$ be the set of links carrying flows with unassigned rates. Then, NLBA yields the max-min fair rate allocation by iteratively allocating the maximal feasible rate to all flows $k \in \mathcal{B}$ crossing the bottleneck collision domain which corresponds to the link $l^\dagger$. This bottleneck rate is computed as the product of the throughput share available for this bottleneck link, $\phi_{l^\dagger}$ and the link rate r. After this assignment, the free capacity, load, and throughput share of the other collision domains are adapted, if they carry one of the fixed flows. All links carrying no load any more are removed from the set of active links, and the flows fixed in this round of the iteration are removed from the set of unassigned flows.

NLBA yields MMF flow rates considering the nominal load of collision domains. Aoun and Boutaba [115] however also introduce the *effective load* of a collision domain. The effective load is lower than the nominal load, as it accounts for the possibility that transmissions in a collision domain can take place in parallel. The example network shown in Figure 4.2 allows to illustrate this difference. Recall that the symmetric collision domain of link (4,3) comprises all active links. The packets to node 2 are sent via gateway 1, the packet to node 3 are forwarded from gateway 5 by node 4 , and flow 4 is also routed over gateway 5. This gives in total 4 transmissions, hence $\mu_{4,3} = 4$, $\phi_{4,3} = 1/4$, and $b_k = r/4 = 13.5$ Mbps for $k = \{2, 3, 4\}$ if all links offer a bandwidth of $r = 54$ Mbps.

The collision domain of (4,3) comprises all active links which means that transmissions on links (1,2) and (5,4) can not take place simultaneous to the transmissions on link (4,3). However, they can take place in parallel to each other. Thus, another possibility to assign the rates would be $b_3 = b_4 = \frac{1}{3}r = 18$ Mbps and $b_2 = \frac{2}{3}r = 36$ Mbps. Then, transmissions from 4 to 3 take place in a third of the time, and for two thirds of the time transmissions from 1 to 2 and from 5 to 4 take place in parallel, the latter one consisting of one half with destination 4 and one half with destination 3. Obviously, this solution leads to a higher total throughput and a higher minimum throughput that is still max-min fair.

Algorithm 4.1 NLBA for single-rate networks [115]

Initialization

1 $\mathcal{F}^* = \mathcal{F}$ ..... all flows are unassigned
2 $\mathcal{L}^* = \{(i,j) \in \mathcal{L} \mid \nu_{i,j} > 0\}$ ..... set of active links
3 for all links $(i,j) \in \mathcal{L}^*$
$\psi_{i,j} = 1$ ..... all links have full capacity
$\mu_{i,j} = \sum_{k \in \mathcal{F}^*} |p_k \cap \mathcal{D}_{i,j}|$ ..... nominal load
$\phi_{i,j} = \psi_{i,j} / \mu_{i,j}$ ..... throughput share per link

While $\mathcal{F}^* \neq \emptyset$

4 $l^\dagger = \arg\min_{(i,j) \in L^*} \phi_{i,j}$ ..... bottleneck link
5 $\mathcal{B} = \{k \in \mathcal{F}^* | p_k \cap \mathcal{D}_{l^\dagger} \neq \emptyset\}$ ..... bottlenecked flows
6 for all $k \in \mathcal{B}$
$b_k = r \cdot \phi_{l^\dagger}$ ..... set bottleneck rates

7 for all links $(i,j) \in \mathcal{L}^*$:
$\psi_{i,j} = \psi_{i,j} - \sum_{k \in \mathcal{B}} |p_k \cap \mathcal{D}_{i,j}| \cdot \phi_{l^\dagger}$ .. adapt free capacity
$\mu_{i,j} = \mu_{i,j} - \sum_{k \in \mathcal{B}} |p_k \cap \mathcal{D}_{i,j}|$ ..... adapt load
$\phi_{i,j} = \psi_{i,j} / \mu_{i,j}$ ..... adapt throughput share

8 $\mathcal{F}^* = \mathcal{F}^* \setminus \mathcal{B}$ ..... adapt set of unassigned flows
9 $\mathcal{L}^* = \{(i,j) \in \mathcal{L} \mid \mu_{i,j} > 0\}$ ..... adapt set of active links

In [115] the effective load of a collision domain is determined by considering pairs of links within a collision domain that can transmit simultaneously and then subtracting the load of the less loaded link from the load of the collision domain. An algorithm how to proceed in more complex cases with many overlapping pairs of links with simultaneous transmissions is not specified.

Huang and Bensaou [134] propose such an algorithm. It however considers max-min fairness among links instead of end-to-end flows. The algorithm is based on finding cliques in the so called *contention graph* $\mathcal{G}_\mathcal{C}$. In $\mathcal{G}_\mathcal{C}$ the active links, i.e. the links actually carrying traffic become nodes and two nodes in the contention graph are interconnected by an edge if parallel transmissions are not possible. Figure 4.3 shows the contention graph of the previously considered

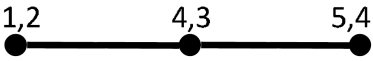

Figure 4.3: *Contention graph for the topology shown in Figure 4.2*

example network. $\mathcal{G}_\mathcal{C}$ maps the three active links of the topology to three nodes. As links (5,4) and (1,2) can be used in parallel, $\mathcal{G}_\mathcal{C}$ is not fully connected but has only two edges, one between nodes (1,2) and (4,3), and one between nodes (4,3) and (5,4). The algorithm for determining the max-min fair rate allocation works on the *clique corpus* $\Omega_\mathcal{C}$ of $\mathcal{G}_\mathcal{C}$[2]. $\Omega_\mathcal{C}$ is now the set of all cliques $\mathcal{C}$ in the contention graph that are not subset of another larger clique.

In the context of mesh networks, a clique in the contention graph corresponds to a set of links whereof no pair can transmit in parallel. In the contention graph shown in Figure 4.3 two cliques are existing, one with links (1,2) and (4,3) and one with links (4,3) and (5,4). Now, the load $\mu_\mathcal{C}$ of a clique $\mathcal{C}$ corresponds to the number of links forming the clique. The algorithm proposed by Huang and Bensaou [134] uses the cliques for determining the effective load and for computing the max-min fair rate allocation analogously to the earlier discussed NLBA. This *effective load based algorithm* (ELBA) is shown in Algorithm 4.2. The functionality of ELBA is very similar to the one of NLBA besides the obvious difference, that it works on the set of unassigned cliques $\Omega_\mathcal{C}$ and assigns in each step the highest possible rate to all flows crossing the bottleneck clique $\mathcal{C}^\dagger$. The problem with ELBA is that it yields a max-min fair rate allocation for one hop networks only and assumes that all link have the same rate r. In the remainder of this section, a modification will be introduced which allows extending ELBA to scenarios with multi-hop flows, as well.

Let us now finally discuss the extension of Akhtar and Moessner [135] for the multi-channel case. If $q_{i,j}$ is the channel assigned to link (i,j), then, the multi-channel collision domain $\mathcal{D}^+_{i,j}$ is the subset of those links in the single channel

[2] A subset of nodes is called a *clique* if an edge exists between any distinct pair of nodes.

Algorithm 4.2 ELBA for single-rate single-hop networks [134]

Initialization
1 $\Omega_C^* = \Omega_C$ ..... all cliques are unassigned
2 for all $\mathcal{C} \in \Omega_C^*$
$\psi_\mathcal{C} = 1$ ..... all cliques have full capacity
$\mu_\mathcal{C} = |\mathcal{C}|$ ..... effective load
$\phi_\mathcal{C} = \psi_\mathcal{C}/\mu_\mathcal{C}$ ..... rate share per link in in clique $\mathcal{C}$

While $\Omega_C^* \neq \emptyset$
3 $\mathcal{C}^\dagger = \arg\min_{\mathcal{C} \in \Omega_C^*} \phi_\mathcal{C}$ ..... bottleneck clique
4 for all $(i,j) \in \mathcal{C}^\dagger$
$b_{i,j} = r \cdot \phi_{\mathcal{C}^\dagger}$ ..... set bottleneck rates

5 for all $\mathcal{C} \in \Omega_C^*$
$\psi_\mathcal{C} = \psi_\mathcal{C} - |\mathcal{C} \cap \mathcal{C}^\dagger| \cdot \phi_{\mathcal{C}^\dagger}$ ..... adapt free capacity
$\mu_\mathcal{C} = \mu_\mathcal{C} - |\mathcal{C} \cap \mathcal{C}^\dagger|$ ..... adapt load
$\phi_\mathcal{C} = \psi_\mathcal{C}/\mu_\mathcal{C}$ ..... adapt rate share

6 $\Omega_C^* = \{\mathcal{C} \in \Omega_C^* | \mu_\mathcal{C} > 0\}$ ... adapt remaining clique corpus

collision domain also using channel $q_{i,j}$:

$$\mathcal{D}_{i,j}^+ = \{(s,t) \in \mathcal{D}_{i,j} \mid q_{i,j} = q_{s,t}\}. \tag{4.9}$$

Besides this slightly different collision domain definition, the algorithm presented in [135] is analogous to the one introduced in [115].

4.2.2 Multi-Hop Multi-Rate Extensions

In the following, two extensions to the previously introduced max-min fair rate allocation algorithms (cf. Algorithms 4.1 and 4.2) will be discussed. First, ELBA will be made suitable for end-to-end multi-hop flows. Second, both NLBA and ELBA will be extended for the case of multi-rate of different but static link rates.

End-to-end flow extension of ELBA

In the original algorithm proposed in [134] the load of a clique is equal to the number of links in the clique independent on the number of flows a link carries. In order to let ELBA take the effects of end-to-end flows into account, the load of a clique $\mathcal{C}$ is changed from the number of links $\mathcal{C}$ to the number of transmissions on the links of the clique. This leads to the following definition of the clique load:

$$\mu_{\mathcal{C}} = \sum_{(i,j)\in\mathcal{C}} \nu_{i,j}. \tag{4.10}$$

Applying this definition to ELBA (cf. Algorithm 4.2), makes three changes necessary. Firstly, the set of unassigned flows, $\mathcal{F}^*$, known from NLBA (cf. Algorithm 4.1) has to be introduced. Secondly, the computation of the initial and of the adapted clique loads in lines 2 and 5 has to be changed according to Equation (4.10). Thirdly, after fixing the rates of the flows crossing the bottleneck clique, the adaptation of the capacity and load of the non-bottleneck cliques has only to be done for the bottlenecked flows. The resulting changes to the algorithm are shown in Algorithm 4.3 together with the extensions for multi-rate networks.

Multi-rate extension of NLBA and ELBA

All previously published theoretical max-min fair share algorithms for mesh networks work for the case where all links in the network use the same data rate. In the following it is described how to let NLBA and ELBA work with different but static link rates, a setting which is closer to reality than the assumption of network-wide equal rates. The multi-rate extension is described at the example of ELBA, but is analogously applied to NLBA.

The key modification is the definition of the clique load. Let us first have a look at the capacity of a clique. In the single-rate algorithm (cf. Algorithm 4.2) this is equal to the nominal link bandwidth. In the multi-rate case, the clique capacity has to be interpreted as a basic unit of time that is shared among the flows running

through a clique. If a flow with rate b_k is transmitted over link (i,j) which uses rate $r_{i,j}$, it requires a percentage of $b_k/r_{i,j}$ of the link's bandwidth and the link is busy with transporting packets of flow k for $b_k/r_{i,j}$ of the time.

Let $\mathcal{K}_{i,j} = \{k \in \mathcal{F} : p_k \cap (i,j) \neq \emptyset\}$ be the set of flows using link (i,j). Then, the fact that (i,j) has to forward all flows in $\mathcal{K}_{i,j}$ translates to this link being active for

$$\upsilon_{i,j} = \sum_{k \in \mathcal{K}_{i,j}} \frac{b_k}{r_{i,j}} \tag{4.11}$$

percent of the time. Extending this to a clique $\mathcal{C}$, gives an activity percentage of

$$\upsilon_{\mathcal{C}} = \sum_{(i,j) \in \mathcal{C}} \sum_{k \in \mathcal{K}_{i,j}} \frac{b_k}{r_{i,j}}. \tag{4.12}$$

Now, let $\mathcal{K}_{i,j} = \mathcal{K}^a_{i,j} \cup \mathcal{K}^u_{i,j}$ be the union of the subset of flows with and the subset without rate allocation. From the obvious condition that a clique can be active to at most hundred percent, i.e. $\upsilon_{\mathcal{C}} \leq 1$, the maximum rate available for unassigned flows is obtained as the fraction of the not yet assigned time and the load of the unassigned flows as

$$b_{\mathcal{C}} = \frac{1 - \sum\limits_{(i,j) \in \mathcal{C}} \sum\limits_{k \in \mathcal{K}^a_{i,j}} \frac{b_k}{r_{i,j}}}{\sum\limits_{(i,j) \in \mathcal{C}} \sum\limits_{k \in \mathcal{K}^u_{i,j}} \frac{1}{r_{i,j}}}. \tag{4.13}$$

The load of a clique may now be defined as

$$\mu_{\mathcal{C}} = \sum_{k \in \mathcal{F}} \sum_{(i,j) \in p_k \cap \mathcal{C}} \frac{1}{r_{i,j}}. \tag{4.14}$$

This and the previously discussed extensions make ELBA suitable for multi-hop multi-rate networks as shown in Algorithm 4.3. The result of the end-to-end flow extension can be found in line 7 where the algorithm adapts the capacity

Algorithm 4.3 ELBA for multi-rate networks

Initialization:

1 $\mathcal{F}^* = \mathcal{F}$ ..... all flows are unassigned
2 $\Omega_C^* = \Omega_C$ ..... clique corpus
3 for all $\mathcal{C} \in \Omega_C^*$
$\psi_\mathcal{C} = 1$ ..... all cliques have full capacity
$\mu_\mathcal{C} = \sum_{(i,j)\in\mathcal{C}} \nu_{i,j}/r_{i,j}$ ..... effective load
$b_\mathcal{C} = \psi_\mathcal{C}/\mu_\mathcal{C}$ ..... achievable per flow throughput

While $\Omega_C^* \neq \emptyset$

4 $\mathcal{C}^\dagger = \arg\min_{\mathcal{C}\in\Omega_C^*} b_\mathcal{C}$ ..... bottleneck clique
5 $\mathcal{B} = \{k \in \mathcal{F}^* |\ p_k \cap \mathcal{C}^\dagger \neq \emptyset\}$ ..... bottlenecked flows
6 for all $k \in \mathcal{B}$
$b_k = b_{\mathcal{C}^\dagger}$ ..... set bottleneck rates

7 for all $\mathcal{C} \in \Omega_C^*$
$\psi_\mathcal{C} = \psi_\mathcal{C} - \sum_{k\in\mathcal{B}} \sum_{(i,j)\in p_k\cap\mathcal{C}} b_{\mathcal{C}^\dagger}/r_{i,j}$ ...adapt free capacity
$\mu_\mathcal{C} = \mu_\mathcal{C} - \sum_{k\in\mathcal{B}} \sum_{(i,j)\in p_k\cap\mathcal{C}} 1/r_{i,j}$ ..... adapt load
$b_\mathcal{C} = \psi_\mathcal{C}/\mu_\mathcal{C}$ ..... adapt achievable throughput

8 $\mathcal{F}^* = \mathcal{F}^* \setminus \mathcal{B}$ ..... adapt set of unassigned flows
9 $\Omega_C^* = \{\mathcal{C} \in \Omega_C^* | \mu_\mathcal{C} > 0\}$ ..... adapt remaining clique corpus

and load of all cliques used by any flow also using the bottleneck clique. Recall that in single-hop Algorithm 4.2, only the cliques sharing a common link with the bottleneck clique required an adaptation.

One result of the multi-rate extension is the computation of the clique load in line 3, where the link rates are taken into account. The other result is found again in line 7. The first statement updates the remaining clique capacities. A flow k that traverses the bottleneck clique $\mathcal{C}^\dagger$ has a data rate of $b_{\mathcal{C}^\dagger}$. Each link (i,j) that transports flow k can be either in the bottleneck clique or not. If yes, flow k occupies a fraction $b_{\mathcal{C}^\dagger}/r_{i,j}$ of link (i,j)'s time. Consequently, the fraction of unassigned time of all cliques $\mathcal{C}$ including link (i,j) is reduced by $b_{\mathcal{C}^\dagger}/r_{i,j}$. The next statement is responsible for reducing the load of a clique by $1/r_{i,j}$ for every

link (i, j) and bottleneck flow using this link.

Algorithm 4.4 NLBA for multi-rate networks

Initialization

1 $\mathcal{F}^* = \mathcal{F}$ ..... all flows are unassigned
2 $\mathcal{L}^* = \{(i,j) \in \mathcal{L} | \ \nu_{i,j} > 0\}$ ..... set of active links
3 for all links $(i, j) \in \mathcal{L}^*$
$\psi_{i,j} = 1$ ..... all links have full capacity
$\mu_{i,j} = \sum_{(g,h)\in\mathcal{D}_{i,j}} \nu_{g,h}/r_{g,h}$ ..... nominal load
$b_{i,j} = \psi_{i,j}/\mu_{i,j}$ ..... achievable per flow throughput

While $\mathcal{F}^* \neq \emptyset$

2 $l^\dagger = \arg\min_{(i,j)\in L^*} b_{i,j}$ ..... bottleneck link
3 $\mathcal{B} = \{k \in \mathcal{F}^* | p_k \cap \mathcal{D}_{l^\dagger} \neq \emptyset\}$ ..... bottlenecked flows
4 for all $k \in \mathcal{B}$
$b_k = b_{l^\dagger}$ ..... set bottleneck rates

5 for all links $(i, j) \in \mathcal{L}^*$:
$\psi_{i,j} = \psi_{i,j} - \sum_{k\in\mathcal{B}} \sum_{(g,h)\in p_k\cap\mathcal{D}_{i,j}} b_{l^\dagger}/r_{g,h}$. adapt free capacity
$\mu_{i,j} = \mu_{i,j} - \sum_{k\in\mathcal{B}} \sum_{(g,h)\in p_k\cap\mathcal{D}_{i,j}} 1/r_{i,j}$ ..... adapt load
$b_{i,j} = \psi_{i,j}/\mu_{i,j}$ ..... adapt achievable throughput

6 $\mathcal{F}^* = \mathcal{F}^* \setminus \mathcal{B}$ ..... adapt set of unassigned flows
7 $\mathcal{L}^* = \{(i,j) \in \mathcal{L} \mid \mu_{i,j} > 0\}$ ..... adapt set of active links

The multi-rate extension for NLBA works in a similar manner and is shown in Algorithm 4.4. Modifying ELBA and NLBA for the case of multiple channels is straightforward. In the contention flow graph edges between links on different channels are simply removed. Otherwise, the algorithms remain the same.

4.3 Comparison of Max-Min Fair Rate Allocations

This section is intended to illustrate the differences between the algorithms ELBA and NLBA and the impact of the collision domain definition. For this purpose, the four different combinations ELBA and NLBA with both symmetric and asym-

metric collision domain definitions are considered and referred as S-ELBA, A-ELBA, S-NLBA, and A-NLBA, respectively. In order to analyze the impact of the load and collision domain definitions, first, an example topology is used. Subsequently, a number of randomly generated mesh network topologies allow to give statistically significant statements by means of Monte Carlo simulations.

The network generation follows the procedure described in Section 4.1.3 with one minor exception: If the assignment of link rates leads to separated network components without a gateway node, one random node is selected as gateway node for this component. An abstraction of a WMN routing algorithm, called *maximum capacity* (MC) routing in the following, is used for establishing the routing structure which consists of trees rooted in the gateway nodes. MC routing establishes a path between each gateway and the neighbor which is connected with the highest link rate. Until all nodes are connected, MC establishes a connection between an already connected node and its not connected highest rate neighbor. This algorithm leads to a not completely arbitrary but also not very sophisticated routing and simply allows to evaluate the performance of a network with an existing routing topology.

Max-min fair rate assignment in an example topology

At the example of a simple network, let us first discuss how the algorithms NLBA and ELBA work and in how far the flow rate allocations differ. The example network under examination is shown in Figure 4.4. Gateways are marked by squares, normal nodes by circles. The color and the width of the lines indicate the rate of the links. Solid lines are used for active links belonging to the routing tree and dotted lines are used for inactive links that are not used but may cause collisions. The per flow rates resulting in each of the four scenarios together with some statistical characteristics are compared in Figure 4.5.

To illustrate the algorithms' workflow, let us focus on S-ELBA. In the first step of the algorithm, the clique comprising links (13,12), (18,13), (6,11), and (12,16) is determined as the bottleneck clique as it enables the network-wide smallest

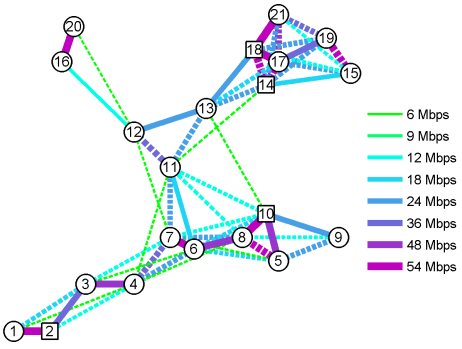

Figure 4.4: *Example network*

throughput of 1.95 Mbps. The flows to nodes 11, 12, 13, 16, and 20 crossing this clique are hence assigned this rate (cf. Figure 4.5). The load of the other cliques is adapted and in the next step, the bottleneck clique is the one containing links (6,11), (10,5), (10,8), (10,9), (13,12), and (18,13). The flows running through this bottleneck clique belong to nodes 5, 6, 7, 8, 9, 11, 12, 13, 16, and 20, of which flows 11, 12, 13, 16, and 20 are already assigned a rate. The still open flows 5, 6, 7, 8 and 9 hence obtain the maximal feasible rate of 2.44 Mbps. The next iteration finds the clique consisting of links (10,5), (18,13), (10,8), (10,9), (6,11), and (13,12) to be the bottleneck. Out of all flows it carries, only the flows 15, 17, 19, and 21 are still open, which are assigned the rate 3.1 Mbps. The next bottleneck clique to be fixed is (10,5), (18,13), (10,8), (10,9), (6, 11), and (13,12), resulting in flows 3 and 4 to obtain 9.22 Mbps. Finally, the clique with links (10,5), (18,13), (10,8), (10,9), (6,11), and (13,12) is considered. Its last open flow, flow 1 obtains 16 Mbps.

Let us now compare the results of the four different algorithms depicted in Figure 4.5. Intuitively, one would expect that in general ELBA produces higher rates than NLBA, simply due to the tighter spatial packing of transmissions. One would also expect that an asymmetric collision definition yields higher rates than

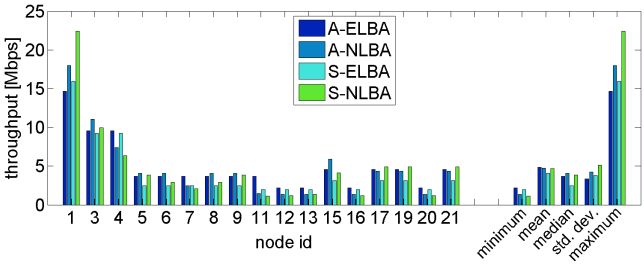

Figure 4.5: *Max-min fair flow throughputs*

a symmetric collision definition, since the links blocked by a transmission in the asymmetric case are a subset of those in the symmetric case. Interestingly, not all nodes benefit as expected. Instead, considering effective instead of nominal load or asymmetric instead of symmetric collision domain definitions mainly increases the minimum throughput. With respect to the maximum throughput, exactly the opposite holds: symmetric collision definition and nominal load lead to a higher maximum throughput. The explanation is that the higher the bottleneck rates are in the first iteration, the more resources are occupied and the less resources remain for the flows in the final iterations. Regarding the mean or aggregate throughput, the results are rather similar, only S-ELBA yields a significantly smaller average throughput. The explanation for this is again the higher minimal throughputs which cause smaller maximal and thereby smaller average throughputs. This phenomenon is also the cause for the increased standard deviation for the case of symmetric collision domain and nominal load definitions which means that the rate allocations are less max-min fair.

Statistical properties of the flow rate assignments

For a more thorough examination of the effects of load and collision domain definition, 100 different network snapshots are generated according to the algorithm

described in Section 4.1.3. For each snapshot, an average of 100 nodes and 10 gateways are placed on a 100×50 grid with a length of 10 m. MMF rate allocations are computed for all networks for each of the four different considered scenarios. The CDFs of the minimum, mean, and maximum rate per generated network obtained for each of the four cases are shown in Figure 4.6.

The representation of the minimum throughput in Figure 4.6(a) allows to see that NLBA leads to clearly lower minimal rates than ELBA. In contrast, the CDFs representing the symmetric and asymmetric collision domain definitions are close by, illustrating that this difference is less significant. Looking at the mean rates (cf. Figure 4.6(b)) shows that A-ELBA clearly produces the highest rates and S-NLBA the by far lowest ones. S-ELBA and A-NLBA are almost identical, i.e., the two effects seem to compensate for each other with respect to the total throughput. The analysis of the maximum rates visualized by Figure 4.6(c) yields a picture just opposite to that for the minimum rates, which is however the reason for the different maximum rates. As ELBA assigns larger minimum rates, less capacity is available for the non-bottlenecked flows and thereby leads to smaller maximum rates than NLBA independent of the collision definition. The impact of the symmetric or asymmetric collision definition is again less significant.

4.4 Concluding Remarks

Facilitating the exchange of data and information, mesh networks will be a key enabler for shifting the communication paradigm from the communication among people to the communication among devices. WMN engineering will hence gain in importance and it is consequently vital to have tools for evaluating the performance of a mesh network. This chapter therefore contributes to this problem by presenting novel insights and methods for the problem of determining max-min fair rates in a mesh network. An overview on the current status of research on max-min fair rate allocations reveals three majors flaws which are remedied. Firstly, the nominal load based NLBA algorithm of Huang and Bensaou [134] is extended in order to obtain a max-min fair rate allocation not only

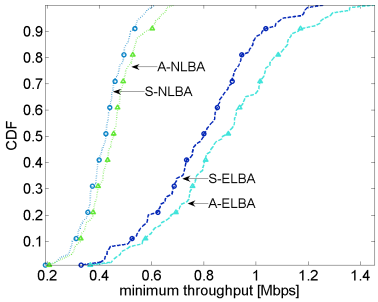

(a) Minimum per flow throughputs

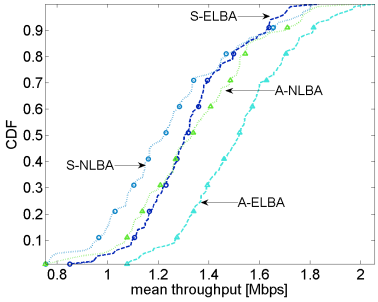

(b) Mean per flow throughputs

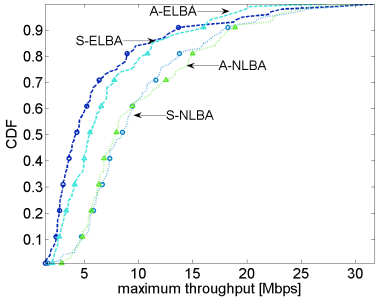

(c) Maximum per flow throughputs

Figure 4.6: *Statistical properties of the obtained per flow throughputs*

among links but also among end-to-end flows. The concept of nominal load is more suited for the analysis of one-hop networks, as it does not account for the possibility of spatial reuse. This effect is considered by the idea of effective load introduced by Aoun and Boutaba [115] which is consequently more suitable for multi-hop mesh networks. Applying this load definition for determining max-min fair rate allocations in a multi-hop mesh network, namely the algorithm ELBA is the second contribution of this chapter. Thirdly are NLBA and ELBA extended for networks with heterogeneous link rates. While this extension seems quite natural, all theoretical mesh networking algorithms work with the assumption of network-wide equal link rates. Such an assumption greatly reduces the modeling and also the computational complexity, but it makes theoretical approaches less suited to represent the real mesh networking world.

Discussing the evaluation of an exemplary network instance allows to illustrate the functionality of both NLBA and ELBA with symmetric and asymmetric collision domains. The differences between the two algorithms and the collision domain definitions observed are statistically significant as well: A comparison of rate allocations achieved for a nominal and effective load definition in randomly generated topologies under the impact of symmetric or asymmetric collision definitions confirms the observations. Thanks to this numerical evaluation it becomes clear that the major impact of using the effective or nominal load definition is on the minimum and maximum rate. The load of the bottleneck clique is smaller than the one of the corresponding bottleneck collision domain. Hence, the minimal assigned per-flow throughput under ELBA is larger than the one of NLBA. This in turn means that under ELBA less capacity is available for the remaining flows, which leads to smaller maximal throughputs, but more balanced flow rate assignments. Symmetric collision domains are larger than asymmetric ones. Hence, similar reasons are responsible that the main impact of a symmetric or asymmetric collision definition is on the mean or total throughput.

Not that this chapter identifies the problem of how to determine collision domains and how to select modulation and coding schemes as critical point. As the focus of this chapter is on the algorithmic dimension, it uses rather simplis-

tic schemes for both problems. This however enables to lay the groundwork for the following chapter which will introduce a more realistic collision domain definition and moreover examine the impact of different methods for selecting modulation and coding schemes more deeply.

5 Optimizing the Wireless Mesh Network Performance via Link Rate Assignment

Talk low, talk slow, and don't talk too much.
John Wayne (1907 - 1979)

Recall from the discussion in the last section that the main WMN use case is to provide Internet access. Especially for this purpose WMNs are no longer only in focus of research, but are increasingly used as Internet access networks in private neighborhoods, small companies, or cities. Although the topology and hardware of the Internet access mesh networks vary strongly, they have one common characteristic: A number of mesh nodes provide Internet access to clients by forwarding traffic from and to a subset of mesh nodes which are connected to the wired backbone and serve as gateways to the Internet. As a result, nodes far away from gateways have to rely on nodes in vicinity of the gateways for forwarding their traffic. Additionally, the WMN traffic pattern, i.e. the bandwidth requirements of the customers served by the mesh nodes is unknown which does not allow implementing network optimization techniques like in traditional networks. The corner stone for the goal of increasing network performance and ensuring the customer satisfaction in WMNs are hence fairness policies guaranteeing a minimum amount of bandwidth for all nodes. Most mechanisms guaranteeing fairness in WMNs, e.g. [20, 136–138], require a deterministic channel access scheme which is able to perfectly allocate the specified number of time slots to a node. While

implementing such algorithms is possible in TDMA-based IEEE 802.16 mesh networks, unplanned community mesh networks use the IEEE 802.11 technology where the channel access is regulated by the random access distributed coordination function (DCF) [54]. Community mesh networks enable cheap near-to ubiquitous Internet access and the popularity of mesh networking initiatives like the German "freifunk" community is consequently increasing. The problem is however that such mesh networks run in general no algorithms striving for fairness and the customer experience is on a best-effort basis only.

An additional challenge for improving the performance of unplanned mesh networks is that the network topology and routing structure, channel assignment, and the transmission output power are dictated by environmental or regulatory constraints. One degree of freedom remains however: Recall from the last chapter that state-of-the art wireless mesh networking technologies (e.g. IEEE 802.11 or IEEE 802.16) provide several modulation and coding schemes which allow transmissions at different data rates at the price of different degrees of sensitivity to interferences. It is hence possible to assign to each link a specific link rate which is kept for the entire operation of the network. The reason why such a dedicated link rate assignment (LRA) is a suitable means for WMN optimization is the following. Most commonly, it is assumed that two nodes communicate at the highest possible data rate for maximizing the throughput, see e.g. [139, 140]. If, in contrast, an MCS with a smaller data rate is used for link x, this on the one hand clearly decreases the link rate. On the other hand it could allow the use of x at the same time as a potentially interfering link, hence, increase the *spatial reuse*.

This trade-off between link data rate and spatial reuse has been neglected by most previous works, as oversimplifying physical layer models are not able to capture the effects of LRA on channel level. Consequently, LRA has not yet been used for planning and optimizing wireless mesh networks. This chapter is therefore dedicated to studying the challenges and opportunities arising from the use of smaller link rates than the maximal feasible ones.

The remainder of this chapter is structured as follows. As the necessary background has already been established in Chapter 4, Section 5.1 just reviews litera-

ture related to the problem of WMN optimization via link rate assignment. The theory behind LRA and a formal framework enabling a systematic study of its effects are introduced in Section 5.2.

While this introductory discussion already points out that LRA may indeed be beneficial for certain links, it is not sufficient for actually assessing the effects on the performance of an entire WMN. This evaluation is subsequently done in two different ways. Section 5.3 reports on the effects of such an LRA strategy on the max-min fair throughput of WMNs, which is an upper bound for the capacity of a WMN with fairness guarantees. This contribution is based on [16]. Results more applicable to realistic deployments on the impact of this LRA strategy in IEEE 802.11 based WMNs with a contention-based channel access scheme which are reviewed in Section 5.4 which is an extension of [22].

These two sections are complemented by Section 5.5, where the MMF traffic engineering objective is formulated as an optimization problem which results in an optimized LRA strategy and optimal channel access schedules. This section contains some insights presented in [2]. Section 5.6 concludes the chapter.

5.1 Related Work

Works related to the problem of optimizing the WMN performance by link rate assignment are also related to the concept of adaptive modulation and coding (AMC). According to Goldsmith [129], the goal of AMC is to enable robust and spectrally-efficient transmissions over time-varying channels by adapting the robustness of a transmission to the channel conditions. A large number of practically implemented algorithms exist which implement this idea by maximizing the link data rate in respect to the channel conditions. The oldest of those rate adaptation algorithms is ARF, proposed by Kamerman and Monteban [141]. Each transmitter using ARF switches to a higher rate after a given number of successful transmissions and switches back to a lower rate after a smaller number of consecutive failures and thereby achieves a higher throughput as if only one link rate is used. This basic principle has been extended by a number of authors, e.g.

by Lacage et al. [139], who propose to adapt the threshold for selecting a higher transmission rate using a binary exponential backoff algorithm. The authors experimentally verify that in terms of one-hop throughput, their AARF algorithm outperforms ARF. Another rate adaptation algorithm building on the basic idea of ARF is RRAA presented by Wong et al. [142]. The authors identify the use of probe packets for estimating the channel quality as major problem and therefore propose to adapt the link rate based on the error rate observed during the most recent transmissions. This observation window is increased with the data rate in order to ensures that the throughput achieved under RRAA is higher than under comparable schemes especially for the case of mobile clients. Note, that the performance of all those algorithms has been evaluated for the one-hop throughput only and does not consider the impact on the overall network throughput.

A first step towards a holistic approach is done by Kim et al. [140] who propose the power and rate control algorithm PRC. The algorithm selects the maximal feasible data rate given the level of interference and reduces the transmit power to the level which is minimally necessary for reaching the SINR threshold of the selected data rate. In a simulation study, PRC maximizes the throughput of transmitter receiver pairs while it uses smaller power levels than comparable schemes. The downside of PRC is however that each receiving node has to feed the perceived interference level back to the sender and that the impact of PRC on multi-hop paths has not been studied. This problem is attacked by Toumpis and Goldsmith [143] who develop a mathematical framework for analyzing how the performance of mobile ad-hoc networks can be optimized. The authors find that increasing the spatial reuse by using lower transmission rates is beneficial for the total network throughput. Due to its complexity, the proposed framework is limited to small network instances and does not allow to give quantitative statements for specific network instances. The question how to exploit spatial reuse for the resource allocation in an IEEE 802.16 mesh network is also studied by Chen et al. [144]. Under the task of resource allocation, the authors understand routing, application flow rate allocation and transmission scheduling. Their study points out how to establish a routing structure organization together with a dedicated

slot assignment in order to enable a higher number of concurrent transmissions and thereby a higher throughput. The authors do however not include the effects of different modulation and coding schemes but assume that all stations are transmitting with the same rate.

More applicable to the problem of link rate allocation in a mesh network is the study of Max et al. [145], who analyze the capacity gain achievable by introducing spatial reuse in WMNs. The authors show that for the case where an omniscient scheduler and a given routing structure exist, it is possible to schedule concurrent transmitters, transmission durations, and rates in order to significantly increase the system throughput. In a similar spirit is the work of Luo et al. [136], who maximize the minimal achievable WMN per flow throughput by solving the joint routing, scheduling, power control and rate adaptation problem.

The downside of this and the other mentioned optimal solutions is however that they are either not applicable to realistic scenarios as they require the modification of given system parameters or that they do not scale to realistic network sizes. Interference modeling is a solution to the first issue but also the reason of the second problem. Actually, Hamida et al. [146] identify the oversimplified physical layer modeling as mainly responsible for unrealistic simulation results. Including the effects of all concurrent transmissions in the interference a transmission is suffering makes the computations arbitrarily complex. The earlier discussed symmetric and asymmetric collision domain definitions in contrast abstract the network to a graph where links exist between nodes which are able to communicate. The classification of nodes which are concurrently able to transmit is done using this graph only and does not consider interferences from nodes outside the communication range. This approach reduces the computational complexity, but introduces an error in comparison to reality. In contrast, Dousse et al. [147] consider all nodes of the network as potential interferers. To represent the efficiency of different MAC protocols, they use a modification of Equation (4.3) where the constant SINR threshold is modified by multiplying the interference $I_{i,j}$ by a weight coefficient $0 \leq w \leq 1$. The authors use this model for proving that under the worst case assumption of all nodes always transmitting, too large values of

w, i.e. bad MAC protocols, result in a not connected network. For the case of WMNs with a CSMA/CA channel access and intermittent traffic, this model is however computationally too expensive, as w is varying in time and space.

The remainder of this chapter therefore introduces a still scalable but more realistic interference-based collision domain definition. Furthermore, it is dedicated to studying the question in how far LRA is suitable for optimizing the performance of a WMN if all other degrees of freedom like node location, transmission output power, or routing structure may not be changed.

5.2 Link Rate Assignment

In the early 1940s, Shannon proved, see e.g. [129], that a code exists which achieves a data rate close to the so called *Shannon capacity*

$$C = W \log_2(1 + \gamma), \tag{5.1}$$

for each transmission with SINR γ over a discrete-time AWGN channel of bandwidth W. In Figure 5.1, the Shannon capacity achievable for a 20 MHz channel, the width of most IEEE 802.11 channels, in dependence of the SINR is shown. The Shannon capacity is on the one hand an upper bound and on the other hand maps the continuous SINR space to continuous data rates. In the case of state-of-the-art wireless transmission technologies, a finite set of MCS $\mathcal{M}$ exists, which enables increasing but discrete data rates for a decreasing SINR. For comparison purposes, Figure 5.1 shows the data rates achieved by the IEEE 802.11 a,g MCS in addition to the Shannon capacity. The target SINRs used for this representation are the ones summarized in Table 4.1.

The representation in Figure 5.1 illustrates the different degrees of sensitivity to interference. Each MCS $m \in \mathcal{M}$ has a unique data rate r_m and a threshold SINR, γ_m^*, which must be exceeded in order to guarantee that the FER for this transmission is small enough. A link which is used with a high data rate supports less concurrently transmitting nodes than a link which is used with a lower data

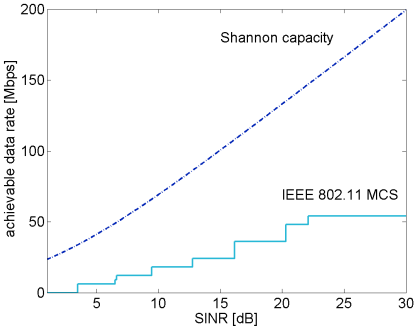

Figure 5.1: *Shannon capacity vs. data rates achievable by IEEE 802.11a,g MCS*

rate as this means a more robust modulation and coding scheme. The trade-off between link rate and transmission robustness is expressed by the minimal required SINR which increases with the link data rate:

$$r_m < r_n \Leftrightarrow \gamma_m^* < \gamma_n^*. \tag{5.2}$$

Given a discrete set of MCS, the link data rates are discrete, too. Using link (i, j) with rate $r_{i,j}$, hence means that an MCS m with $r_m = r_{i,j}$ exists. The condition for a successful transmission introduced in Equation (4.6) extends to

$$\gamma_{i,j} \geq \gamma_{i,j}^* = \gamma_m^*. \tag{5.3}$$

Adaptive modulation and coding addresses the challenge described by Equation (5.2) by dynamically adapting the robustness of a transmission to the channel conditions [129]. An optimal AMC mechanism would allow to use for each transmission the highest data rate which still allows to decode the signal. In analogy to the work of Toumpis and Goldsmith [143], a formal expression of AMC is achieved by introducing the function $\mathcal{Q}$ and thereby mapping the link SINR to a

link data rate provided by $\mathcal{M}$, i.e.

$$\mathcal{Q}(\gamma_{i,j}) = \max_{m \in \mathcal{M}} \{r_m : \gamma_m^* \leq \gamma_{i,j}\}. \tag{5.4}$$

Note that in order to chose the data rate for a transmission via Equation (5.4), the sender i has to predict the SINR at receiver j before actually sending the packet. This is usually done by letting j estimate the channel and feeding this estimate back to i [129]. This approach has however two major problems. On the one hand, a perfect AMC mechanism is not feasible as the SINR is time varying and hardly predictable. As the channel feedback has to strike a balance between real-time information and overhead, the lack of information makes this problem even harder. On the other hand, AMC aims at a per-link optimization and neglects the spatial reuse factor. This fact is also illustrated by Equation (5.2): if a link uses a smaller link rate, the required target SINR decreases and more concurrent transmissions may be tolerated which may be beneficial for the total network throughput. If, in contrast, always the maximal feasible data rate is chosen, this positive effect of increased spatial reuse is minimized.

Those two problems are the motivation for examining the benefits of *static* link rate assignment, i.e. to assign the data rates used by each link for the time of the network operation before the network becomes operational. In this case, the SINR is not available, as nothing about the network traffic and thereby the interference is known. The only available characterization of the link is hence the SNR which depends on the constant path gain only. Using the link SNR, a maximal LRA is achieved by using for each link (i, j) the rate which is given by

$$r_{i,j} = \mathcal{Q}(\gamma'_{i,j}). \tag{5.5}$$

The function $\mathcal{Q}$ is monotonically increasing and the SNR is always larger or equal than the SINR. Therefore, using Equation (5.5), as it has been done in Section 4.3, results in link data rates which are larger or equal to the ones computed by Equation (5.4). Note however that this comes at the price that transmissions

on this link may fail in the presence of concurrent transmissions.

For a more conservative link rate assignment, i.e. for a more robust MCS choice which enables a receiver to successfully decode a transmission despite a certain amount of interference, the link SNR is used together with the *interference buffer* $\Delta\gamma$ is used. The latter can be seen as a safety margin for a certain amount of interference. Using $\Delta\gamma$ together with the SNR as an input for $\mathcal{Q}$ comes at the price of a decreased link rate but increases the spatial reuse by allowing more concurrent transmissions. The optimal interference buffer for link (i, j) guaranteeing the transmission success in the presence of any amount of interference is formally given by

$$\Delta\gamma_{i,j} = \max_{t} \frac{\gamma'_{i,j}(t)}{\gamma_{i,j}}. \tag{5.6}$$

A conservative LRA strategy using the interference buffer is achieved by replacing Equation (5.4) by

$$\mathcal{Q}_{IB}(\gamma'_{i,j}, \Delta\gamma_{i,j}) = \max_{m \in \mathcal{M}} \{r_m : \gamma^*_m \leq \frac{\gamma'_{i,j}}{\Delta\gamma_{i,j}}\}. \tag{5.7}$$

If link (i, j) is operated with $r_{i,k} = \mathcal{Q}_{IB}(\gamma'_{i,j}, \Delta\gamma_{i,j})$, this allows successful transmissions in the presence of an arbitrary number of interfering nodes.

The problem with this approach is that is it not possible to calculate a suitable estimation for a link specific $\Delta\gamma_{i,j}$ without the knowledge of the traffic pattern. The worst case assumption of parameterizing $\Delta\gamma_{i,j}$ such that a link is robust enough to tolerate transmissions from all other nodes would easily lead to link rates of 0. In contrast, if too small a value is used, packets may be lost due to interference. In general, any $\Delta\gamma_{i,j} > 1$ increases the probability of transmission success, but comes at the price of a link rate reduction $\mathcal{R}$ which is calculated as

$$\mathcal{R}(\gamma'_{i,j}, \Delta\gamma_{i,j}) = \mathcal{Q}(\gamma'_{i,j}) - \mathcal{Q}_{IB}(\gamma'_{i,j}, \Delta\gamma_{i,j}). \tag{5.8}$$

As outlined earlier, $\mathcal{R} \geq 0$. Furthermore, $\mathcal{R}$ depends not only on the used interference buffer $\Delta\gamma_{i,j}$, but also on the maximal feasible link rate $r_{i,j} = \mathcal{Q}(\gamma'_{i,j})$, and therefore on $\gamma'_{i,j}$. The reason for the latter fact is that the link rate differences of neighboring MCS are not the same. This is illustrated by Figure 5.1 where it can be nicely seen that the step function representing $\mathcal{M}$ has different heights.

The behavior of $\mathcal{R}$ is visualized in Figure 5.2, which shows the link rate reduction for the SNR range considered in Figure 5.1 and interference buffer values between 0 and 10 dB. Observe first that positive values of $\Delta\gamma_{i,j}$ increase the range where no communication is possible, as the safety margin between the link SNR and the SINR requirements of the most robust MCS can not be guaranteed. The next striking fact is that for some combinations of SNR and $\Delta\gamma_{i,j}$, the link rate is not reduced, i.e. $\mathcal{R} = 0$. This is always the case if the SNR is by more than $\Delta\gamma_{i,j}$ larger than the SINR threshold of the corresponding MCS. Finally, this representation illustrates that $\mathcal{R}$ is not only increasing with $\Delta\gamma_{i,j}$ but also with the SNR, having its maximum of 36 Mbps for links which are very close to the SINR threshold value of the MCS enabling the highest data rate of 54 Mbps and which are reduced to a rate of 18 Mbps only. The reason for this are the higher differences between the data rates for less robust MCS shown by Figure 5.1.

The positive aspects of this link rate reduction, i.e. the increase of the spatial reuse, is illustrated by the following example. If $\Delta\gamma_{i,j} = 5\,\text{dB}$ is used for the considered IEEE 802.11g setting with the path loss given by Equation (4.5), the maximal length of link (i, j) if the least robust MCS, 64-QAM 3/4, is used, decreases from 93.5 to 70.1 m. If on the other hand, for (g, h) with $d_{g,h} = 112$ m the more robust 16-QAM 1/2 instead of 16-QAM 3/4 is used, a parallel transmission of node k with $d_{k,h} = 337$ m will not interfere the transmission on (g, h).

The remainder of this chapter is therefore dedicated to more thoroughly exploring the potentials which lie in the trade-off. This is achieved by examining the potentials of a network-wide value for $\Delta\gamma$ and by discussing how to find a suitable parametrization for such a parameter.

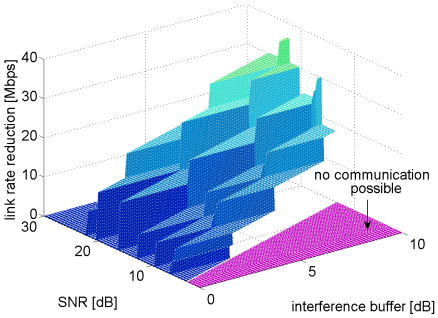

Figure 5.2: *Link rate reductions caused by the use of the interference buffer*

5.3 Effects of Link Rate Assignment under Max-Min Fairness

This section attempts to answer the question in how far using LRA with $\Delta\gamma > 1$ is suitable for increasing the WMN performance if the max-min fair network throughput is used as benchmark. In order to make the results broadly applicable, a channel abstraction which is closer to reality than previously used models and a methodology for studying the sensitivity of MCS optimization to routing mechanisms and network density are introduced. The obtained results demonstrate the inherent optimization potential LRA and point out promising directions for optimized LRA strategies.

5.3.1 A More Realistic Wireless Mesh Network Abstraction

For studying the effects of LRA on end-to-end throughput in WMNs applicable to realistic scenarios, the framework introduced in Sections 4.1.2 and 5.2 is one requirement. Another necessity is an MCS and interference aware collision

domain definition which captures the influence of different link rates on the degree of spatial reuse, a definition which moves the collision domain abstraction closer to reality. Furthermore, abstractions of different routing paradigms allow to examine the sensitivity of capacity results to routing structures.

A more realistic collision domain definition

A channel abstraction which is both computational feasible and closer to Equation (4.3) than the symmetric and asymmetric collision domain definitions introduced in Section 4.2.1 is the *single-interferer collision domain* $\mathcal{D}_{i,j}$. It is defined as the set of all links (a, b) which are using the same channel as (i, j), and where a's transmission causes a too high interference for j to decode a signal from i, or i's transmission causes a too large interference for b to successfully receive a transmission from a:

$$\begin{aligned}\mathcal{D}_{i,j} = \quad & \{(a,b) : \tfrac{P_r^{i,j}}{N+P_r^{a,j}} < \gamma_{i,j}^* \ \vee \ \tfrac{P_r^{a,b}}{N+P_r^{i,b}} < \gamma_{a,b}^*\} \\ & \cap \{(a,b) : q_{a,b} = q_{i,j}\}. \end{aligned} \tag{5.9}$$

Note that with Equation (5.9) the collision domain and the contention graph change if another MCS, i.e. a different SINR threshold is used for (i, j). Using the collision domains, the set of edges $\mathcal{K}$ in the contention graph $\mathcal{G}_\mathcal{C}$, contains all tuples of contending links is defined by $(l_1, l_2) \in \mathcal{K} \Leftrightarrow l_1 \in \mathcal{D}_{l_2} \Leftrightarrow l_2 \in \mathcal{D}_{l_1}$.

With this approach, finding all single-interferer collision domains requires an effort which is proportional to the square of the number of active links. The contention graph can be derived from the set of collision domains with a linear effort, whereas finding all cliques in $\mathcal{G}_\mathcal{C}$ is NP-complete. For the case of medium sized topologies consisting of not more than 100 nodes, a reasonable assumption for any productive WMN, this is however still feasible. Note moreover that the concept of the single-interferer collision domain may be easily extended to n-interferer collision domains, where the interference of up to n nodes is considered. This extension comes at the price of a higher computational effort and is therefore not adopted in order to be able to examine a large number of scenarios.

Abstracting different routing paradigms

The impact of the routing strategy on the network capacity is often neglected. Typical examples for this approach are the earlier mentioned works of [20, 114, 132, 133] which either assume the existence of an arbitrary, or of a shortest path topology. Akyildiz et al. [112] however point out that the WMN throughput increases if e.g. more sophisticated link quality performance metrics are used for establishing the routing topology.

A comparative study of specific routing protocols is not the goal of this chapter, but the question to what degree the effects of LRA depend on the routing paradigm, *is* relevant. For the case of WMNs with more than one Internet gateway, the routing topology connecting each mesh node to one gateway is a forest, consisting of several trees rooted in the gateway nodes. As an abstraction for different routing policies, forests constructed according to three different strategies are considered. *Minimum-hop routing (MH)* serves as an abstraction for a simple ad-hoc routing protocol. Under MH, each node forwards its data to the one of its neighboring nodes which is, in terms of hops, the closest to a gateway. A more sophisticated mesh routing protocol is modeled by *Maximum-capacity routing (MC)* which has already been used in Section 4.3. It establishes a path between each gateway and the neighbor which is connected with the highest link rate. Until all nodes are connected, MC establishes a connection between an already connected node and its not connected highest rate neighbor. For comparison purposes, a non-sophisticated topology is modeled by *Random routing (R)* which establishes routing trees rooted in the gateways, by iteratively connecting each node to a randomly chosen already connected neighbor.

5.3.2 Link Rate Assignment Performance Evaluation

This section investigates the influence of a more conservative MCS assignment on the max-min fair mesh network capacity, which results from a max-min fair flow rate allocation found by NLBA and ELBA introduced in Section 4.2.2. For this purpose, sample network topologies are generated according to the method-

ology discussed in Section 4.1.3. Based on the initial topology with the maximal feasible link rates, for each considered value of $\Delta\gamma$ another topology is created where the the link rates are assigned according to Equation (5.7) together with the considered value of $\Delta\gamma$.

The performance evaluation begins with a simple example network which allows to explain how each network instance is evaluated. In particular, this example illustrates the influence of $\Delta\gamma$ on the link rates, collision domains, and cliques and hence on the maximal achievable throughputs calculated by NLBA and ELBA. After this exemplary discussion, statistically significant statements on the effects of $\Delta\gamma$ are presented.

Effects in an example network

In order to fully understand the methodology of network creation and link rate assignment using $\Delta\gamma$, let us consider a simple example. It consists of 5 nodes whereof nodes 1 and 2 are gateways, and is shown in Figure 5.3. The topology with the maximal feasible link rates, i.e. assigned using $\Delta\gamma = 0\,\text{dB}$ is shown in Figure 5.3(a). The topology with link rates resulting from an interference buffer of $\Delta\gamma = 5\,\text{dB}$ are shown in Figure 5.3(b). Links (5,3) and (3,5) do not meet the tightened requirements for BPSK 1/2 and thus not exist for $\Delta\gamma = 5$ dB.

For determining the routing paths, the minimum-hop paradigm is applied. Recall that in the considered setting, each non-gateway mesh node has one saturated best-effort downlink flow from the Internet. The routing structure is hence such that flows 3 and 4 are routed via gateway 2 and flow 5 is routed via gateway 1. Consequently, only links (5,1), (3,2), and (4,2) are active and shown by solid lines, the remaining links are passive and depicted by dashed lines.

Recall from Section 4.2.2 that the main difference between the nominal and the effective load based algorithms NLBA and ELBA is in the computation of the link loads: NLBA iteratively allocates the maximal feasible rate to the flows crossing the bottleneck collision domain, which is the collision domain with the highest nominal load. ELBA iteratively allocates the maximal feasible rates to

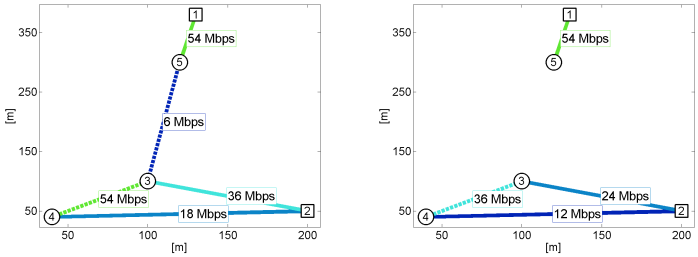

(a) $\Delta\gamma = 0$ dB (b) $\Delta\gamma = 5$ dB

Figure 5.3: *Effects of link rate assignment in an exemplary topology*

the flows crossing the bottleneck clique which is the clique in the contention graph with the highest effective load, where the effective load of a link is smaller or equal than its nominal load. ITherefore, the flows traversing the bottleneck clique are assigned a rate which is larger or equal than the rate assigned to the corresponding bottleneck collision domain rate. In turn, the rates for the flows not crossing the bottleneck clique are smaller or equal than for the case of NLBA, as the bottleneck flows are less throttled and hence occupy a larger percentage of the time. Consequently, ELBA produces more balanced end-to-end flow throughputs than NLBA, which however also results in smaller maximum flow rates and a smaller total network throughput. This effect can also be observed in Table 5.1, where the nominal and effective per-flow throughputs, τ_n, and τ_e resulting in the topologies shown in Figure 5.3 are summarized.

A more conservative MCS assignment strategy, represented by a positive value for $\Delta\gamma$ results in link rates smaller or equal than the maximal feasible rate for this link. Sometimes the link is even not existing as it the case for link (5,3). Due to the increased spatial reuse which results in increased transmission opportunities, the throughput does not necessarily decrease with the link rate, sometimes the per-flow-throughput even increases with $\Delta\gamma$. This is also the case in the example (cf. Table 5.1): If a protection threshold is used for the MCS assignment, the

	$\Delta\gamma = 0$ dB	$\Delta\gamma = 5$ dB
$r_{2,3}$	36 Mbps	24 Mbps
$r_{2,4}$	18 Mbps	12 Mbps
$r_{1,5}$	54 Mbps	54 Mbps
$\mathcal{D}_{2,3}$	$\{(2,3),(2,4),(1,5)\}$	$\{(2,3),(2,4)\}$
$\mathcal{D}_{2,4}$	$\{(2,3),(2,4)\}$	$\{(2,3),(2,4)\}$
$\mathcal{D}_{1,5}$	$\{(2,3),(1,5)\}$	$\{(1,5)\}$
$\Omega_{\mathcal{C}}$	$\{\{(2,3),(2,4)\},\{(2,3),(1,5)\}\}$	$\{\{(2,3),(2,4)\},\{(1,5)\}\}$
$\tau_n(3)$	9.82 Mbps	8 Mbps
$\tau_e(3)$	12 Mbps	8 Mbps
$\tau_n(4)$	13.09 Mbps	8 Mbps
$\tau_e(4)$	12 Mbps	8 Mbps
$\tau_n(5)$	39.27 Mbps	54 Mbps
$\tau_e(5)$	36 Mbps	54 Mbps

Table 5.1: *Effects of LRA for the topologies depicted in Figure 5.3*

maximal achievable throughput of node 5 increases to 54 Mbps under both load definitions, as the rate of link (1,5) remains unchanged at 54 Mbps, but a transmission of 1 is not disturbing the transmission of 2 to 3 any more. Obviously, flows 3 and 4 pay the price for the throughput increase of node 5. Both the nominal and effective throughput of node 3, 9.82 and 12 Mbps, and of node 4, 13.09 and 12 Mbps, are cut down to 8 Mbps. $\tau_n(3)$ is decreased to a smaller degree than $\tau_n(4)$ although the link rate (2,3) is reduced more heavily than the rate of link (2,4). This is due to the fact that node 3 does only need to share the available capacity with node 2 and no longer with node 5. The collision domain of link (2,4) remains however unchanged. This effect is not observable for the effective throughput, as the bottleneck clique $\{(2,3),(4,2)\}$ remains the same.

Analyzing the overall network throughput shows that an assignment of the maximal feasible link rates results in an average nominal throughput of 20.73 Mbps which is slightly higher than the effective average throughput of 20 Mbps. If link rates are assigned with $\Delta\gamma = 5$ dB, both average throughputs increase to 23.33 Mbps. Due to the small number of flows, this increase is modest but already

demonstrates the potential of LRA. The next section will therefore be dedicated to a more thorough analysis of the effects of MCS choice in larger topologies.

Effects in larger networks

The previously introduced framework is now applied to investigating the influence of a more conservative MCS assignment on the max-min fair mesh network capacity. For this purpose, the effects of using $\Delta\gamma = \{0, 1, \ldots, 10\}$ dB in WMNs with 50 mesh nodes whereof 5 are gateways are considered. Keeping the number of nodes constant in each topologies allows an easier comparison as number of traffic flows remains constant, too. Experiments with other parameterizations showed that the exact throughput results are topology-dependent, but that qualitative statements and trends are comparable.

To investigate the sensitivity of LRA to external factors, the influence of network density, the adaptation of the routing structure, and the connectivity of the topology are considered. Sample topologies with link rates assigned using different values of $\Delta\gamma$ are constructed for the following three scenarios:

- *Scenario A*: In a square area of 1000 m $\times$ 1000 m, sparse network instances are generated with grid lengths $l_F = 20\,\text{m}$ and $l_G = 200\,\text{m}$. To keep the number of nodes constant for all sample networks, only topologies are considere where all mesh nodes are connected to the gateways for $\Delta\gamma = 0\,\text{dB}$. No protection threshold is used for the most robust MCS in order to avoid isolated nodes for $\Delta\gamma > 0\,\text{dB}$. Therefore, all links exist for all link rate assignments, i.e. all values of $\Delta\gamma$. If the SNR of a link is smaller than the SINR threshold of the most robust MCS plus the protection threshold, it is nevertheless kept operating at the lowest rate. As a consequence, the routing forest determined for the maximal feasible link rates can be used for more conservative assignment strategies, too.

- *Scenario B*: In a square area of 1000 m $\times$ 1000 m, sparse networks with $l_F = 20\,\text{m}$ and $l_G = 200\,\text{m}$ which are connected for $\Delta\gamma = 0\,\text{dB}$ are cre-

ated. The protection threshold is used for all MCS. As illustrated by Figure 5.2, this restricts the range of SNR values for which a communication is possible. A result of this are a smaller number of links for larger values of $\Delta\gamma$ and thereby nodes which are not connected to the Internet any more. Another consequence of this is that the routing forests have to be recomputed for each link rate assignment.

- *Scenario C*: In order to consider dense networks, network instances are created in a 750 m $\times$ 750 m square and $l_F = 15\,\text{m}$ together with $l_G = 150\,\text{m}$ is used. Additionally, only topologies where all nodes have an Internet connection for $\Delta\gamma = 10\,\text{dB}$ are considered. The interference buffer is used for all links, consequently, the number of links decreases for increasing values of $\Delta\gamma$. Therefore, the routing forest is recomputed for each link rate assignment.

In the following, first, general insights in the effect of link rate assignments on the average network throughput are shown, before, subsequently, some details are analyzed more closely.

The average network throughput

Recall from the discussion in Section 4.1.4 that the average MMF network throughput, i.e. the throughput averaged over all end-to-end flows is a suitable metric for studying trends of more conservative link rate assignment strategies, i.e. increasing values of $\Delta\gamma$. This metric is represented in Figure 5.4. The average MMF network throughput for each considered scenario averaged over 200 different randomly generated network instances together with the corresponding 95% confidence intervals is shown. The representation using three subfigures, line styles, and markers allows to compare the effects of more robust link rate assignment under different scenarios, load definitions, and routing paradigms respectively and illustrates the number of dimensions of the design space. In the following, those different dimensions are addressed one by one.

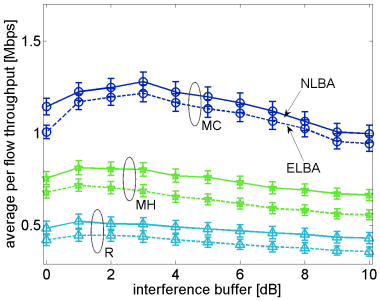

(a) Scenario A

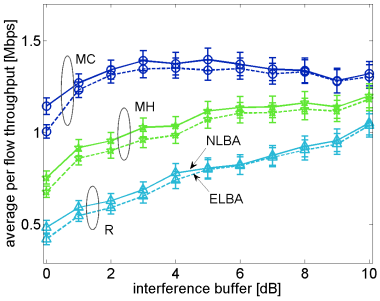

(b) Scenario B

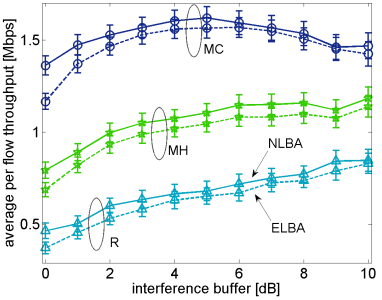

(c) Scenario C

Figure 5.4: *Average max-min fair end-to-end flow throughput*

Let us start with a comparison of the results obtained in the different scenarios. The influence of $\Delta\gamma$ on the average network in Scenario A (cf. Figure 5.4(a)) is significantly weaker than in Scenario B and C (cf. Figures 5.4(b) and 5.4(c)). The difference of the throughputs obtained in Scenarios A and B seems strange as the only difference between the considered network instances is the connectivity: using a more robust link rate assignment, link (i, j) may not exist in Scenario B, if its SNR is smaller than the requirements of BPSK 1/2 plus $\Delta\gamma$, while it is kept operating with the 6 Mbps provided by BPSK 1/2 in Scenario A. This small difference causes however some nodes to lose their Internet connection for higher values of $\Delta\gamma$ and is the reason for the increasing average throughput in Scenario B. The disconnected nodes stop competing for the shared medium, the still connected nodes can increase their throughput, and the overall system throughput is increased, an effect which does not occur in Scenario A. This effect is also the reason for the larger positive effect of $\Delta\gamma$ in Scenario C. Additionally, the node deployment is denser and hence the proportion of short, i.e. high data rate links is larger than in Scenarios A and B. Moreover is the deployment area smaller and the routing paths have on average a smaller number of hops which causes the absolute throughput values shown in Figure 5.4(c) to be larger than the ones in Figure 5.4(a) and 5.4(b).

Next, let us compare the effects of the different routing policies. Observe first that out of all considered routing paradigms, maximum-capacity routing achieves the highest throughput, as it maximizes the used link rates. Minimum-hop routing results in a higher average throughput than random routing, as the number of used hops and thereby the number of potential bottleneck-links is minimized. Those effects are observable in all figures, i.e. scenarios.

A closer look reveals that in Scenario A the MH and R routing paradigms do not only show a smaller throughput but also a smaller positive effect of $\Delta\gamma$, while this is not the case for Scenarios B and C. The cause for this difference is that in Scenario A, the routing topologies are not adapted to the link rate assignment and that long links which operate near the minimal SINR threshold are not affected by the positive effects of $\Delta\gamma$. The proportion of these links among the routing

links and consequently the optimization potential of $\Delta\gamma$ is larger for MC than for MH and R routing. In Scenarios B and C, in contrast, the routing topologies are recomputed for each new link rate assignment. Therefore, the random routing paradigm bears a greater optimization potential than the other paradigms as it benefits the most from the increasing probability that a randomly chosen link is contending with a smaller set of other links. This effect holds to a weaker degree for the more efficient MH routing and is only valid as long as the link rates do not become too small or too many nodes are disconnected.

Another routing-specific effect is that a critical value of $\Delta\gamma$ maximizing the average network throughput exists for each scenario and routing paradigm. A too large value of $\Delta\gamma$ results in a high number of unconnected nodes and links operating at the lowest rate and hence decreases the average per-flow throughput. The figures illustrate that for MH and R routing in Scenarios B and C, this critical value is larger than 10 dB. MC routing in contrast optimizes the per-flow-throughput by choosing high-rate links, the critical value is thus much smaller for this paradigm. If the routing structure is not adapted to the new link rates (cf. Figure 5.4(a)) MC benefits most from a conservative link rate assignment. MH and R use a higher percentage of low data rate links, which are not protected against interferences and thus profit less from the increased spatial reuse.

Next, consider the difference between the throughputs computed by NLBA and ELBA. As we already saw in Section 4.3, NLBA assigns very small throughputs to flows crossing links with large collision domains and consequently very large rates to all non-bottlenecked flows. In the considered scenarios this behavior results in a higher average network throughput than the one computed by ELBA which assigns more balanced flow rates. A more important fact is however that both load definitions show the same overall effects of $\Delta\gamma$'s influence even if some of the computed flow throughputs are numerically different.

Finally, let us concentrate on the influence of an increasing value of $\Delta\gamma$. The results illustrate that using $\Delta\gamma > 0$ dB for MCS assignment is always suitable for increasing the network throughput, although this effect is weaker if the routing is not optimized and low data rate bottleneck links are kept for connectivity reasons

(cf. Figure 5.4(a)). In contrast, if the routing forest is adapted to the new link rates (cf. Figures 5.4(b) and 5.4(c)), the throughput increases are larger. Especially for the non-throughput optimized MH and R routing paradigms, a high protection threshold enables significant performance gains in terms of average throughput. Observe however also that this throughput increase is limited, as the price for smaller collision domains and thereby more channel access time is a smaller link rate. This interdependency will subsequently be studied in more detail.

A closer look on the per flow throughput

The representation of the average network throughput shown in Figure 5.4 does not permit to judge how an increase is achieved. Examining the CDFs for all effective end-to-end flow throughputs collected in the 200 considered topologies in Figure 5.5 allows a more thorough analysis. In order to simplify the presentation, only results for the effective load definition, two scenarios, and two routing paradigms are shown. This restriction still allows to illustrate the points of interest while it increases the clarity of the presentation. For sake of readability, the x-axis is logarithmically scaled. This is necessary due to the highly variant flow rate distribution: For $\Delta\gamma = 10\,\text{dB}$, e.g. there is always one out of the 200 considered network snapshots, where one node is the only child of a gateways node, no other node is interfering its transmission, and its associated flow consequently achieves the highest throughput of 54 Mbps. To furthermore increase the readability of the representation, only 3 of the 11 considered CDFs are depicted with bold lines, the remaining CDFS are shown with light lines only.

Let us analyze Figure 5.5(a) first. It represents Scenario B where the protection threshold $\Delta\gamma$ is used for all MCS. Therefore, some links do not exist any more for higher values of $\Delta\gamma$. As the CDF of the per-flow throughputs for $\Delta\gamma = 10\,\text{dB}$ illustrates, this results in not connected topologies, i.e. nodes with zero throughput. The exact value of the probability for a node to be disconnected depends on the network density but exists for all routing paradigms. Since isolated nodes do not compete for time shares on the channel, all not isolated nodes

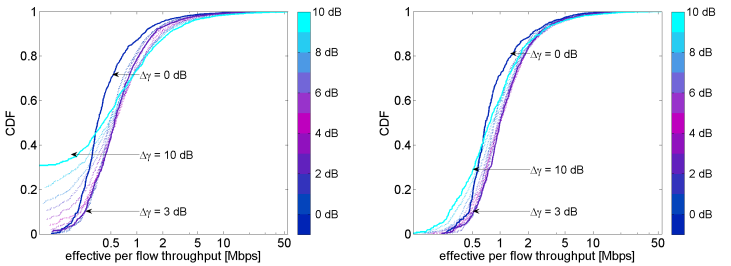

(a) Scenario B, MH routing

(b) Scenario C, MC routing

Figure 5.5: *Effective per flow throughput for Scenarios B and C*

have more opportunities to access the channel and are thus able to increase their throughput. Figure 5.4(b) illustrates that this effect increases the average per-flow throughputs, as long as the number of isolated nodes is not too large. The CDF for $\Delta\gamma = 3\,\text{dB}$ and other values in the middle of the range considered for values of $\Delta\gamma$ demonstrate however also that medium values of $\Delta\gamma$ are suitable for a more balanced throughput increase.

The results obtained for Scenario C (cf. Figure 5.5(b)) are suitable for addressing another detail. We saw earlier that for each routing paradigm and topology type a critical value of $\Delta\gamma$ maximizing the average network throughput exists. The average throughputs for Scenario C shown in Figure 5.4(c) illustrate that for MC routing this critical value is somewhere in $[4, 6]$ dB. The CDFs shown in Figure 5.5(b) demonstrate that as long as $\Delta\gamma$ is below the critical value (cf. CDF for $\Delta\gamma = 3\,\text{dB}$), the throughput of nearly all flows is increased in comparison to $\Delta\gamma = 0\,\text{dB}$. This is due to a moderate protection threshold causing only links with an SNR very close to the MCS threshold, contending with a large number of other links, to decrease their rate. This altruistic "behavior" of a small number of potential bottleneck links is advantageous for the entire network. If in contrast a value of $\Delta\gamma$ above the critical threshold is used (cf. CDF for $\Delta\gamma = 10\,\text{dB}$), all links use a data rate one or several levels below the theoretically feasible fastest

one. For the set of considered MCSs this may result in significant raw bit rate reductions (cf. Table 4.1) which can not be compensated by increased channel access time and thus causes small flow throughputs. MC routing uses the highest proportion of high data rate links for which the reductions are most severe and is thus more sensitive to this problem than the other routing paradigms.

All in all, the performance evaluation reveals a topology dependent but positive effect of $\Delta\gamma$ on the average network throughput. If max-min fair flow rate allocation can be guaranteed by means of a perfect channel access mechanism, assigning link rates more conservatively than necessary is always advisable. The problem with this result is however that these idealistic assumptions are hardly achievable in realistic networks. The next section is therefore dedicated to investigating the potentials of $\Delta\gamma$ under less ideal conditions.

5.4 Effects of Link Rate Assignment in an IEEE 802.11 Setting

The results discussed in the last section emphasize the positive effect of $\Delta\gamma$ on the average max-min fair network throughput. The problem with this metric is however that the results hardly apply to reality, as a truly MMF flow allocation can be achieved only in networks where the radio resource can be optimally used e.g. by a TDMA channel access. IEEE 802.11 mesh networks in contrast utilize a a contention based channel access scheme, thus the resource allocation is not perfect. This section is therefore dedicated to exploring if and to which degree LRA with $\Delta\gamma > 1$ is beneficial in networks with a random access scheme. Therefore, first an analytical framework is introduced which allows to derive a collision-avoiding parameterization for $\Delta\gamma$. The costs and benefits of this parameterization are assessed both analytically and by means of a simulation study.

5.4.1 An Analytical Approach to Optimized Link Rate Assignment

This section explains how LRA may be used for optimizing the performance of a random access WMN. For this purpose, a parameterization for the interference buffer $\Delta\gamma$ protecting a transmission against interference from a given number of interferers is derived. This protection comes at the price of a reduced link rate, therefore, subsequently, a framework for analyzing the impact of this approach on the network throughput is derived.

Finding a collision avoiding value for $\Delta\gamma$

The location of the mesh nodes may again be modeled as a point process $\Phi = \{X_i\}$, where the node locations are given by $\{X_i\}$. If Φ is a stationary Poisson process with density λ, two key properties hold: (1) The number of points in a bounded Borel set of size A, $\Phi(A)$, follows a Poisson distribution with mean λA, and (2) the number of points in disjoint sets are independent, see e.g. Stoyan et al. [130]. As outlined earlier, a Poisson process is insofar not quite suitable to model a WMN, as it allows the mesh points to be arbitrarily close to each other. In contrast to other point processes, the properties of the Poisson process allow however to derive the CDF of the interference I seen by an arbitrary receiver $r \in \Phi$. This will be done in the following.

The interference seen by r is computed as the sum of the sending powers received from the nodes z in the set of interferers $\mathcal{Z}$ which are transmitting at the same time as the node s which actually transmits a packet to r. In the remainder of this section, an analytical expression for I under the assumption that the nodes in $\mathcal{Z}$ are the Z closest interferers to r, where $Z = |\mathcal{Z}|$ will be derived. Consequently, first, a CDF of the distance of r's kth nearest neighbor is derived, which allows to obtain the CDF of the distance of r's kth nearest interferer.

Property (1), i.e. the fact that the number of points in a subset of Φ are Poisson distributed allows to calculate the CDF of the distance of an arbitrary point r's kth nearest neighbor. This is the point of Φ whereof the distance to r, L_k, is

larger than the distance between r and $k-1$ other points of Φ. The CDF of L_k is hence given by the probability that the circle around r with radius L_k, $C(r, L_k)$ contains at least k points of Φ, cf. Figure 5.6(a) for $k = 3$ nodes. Formally, this may be expressed as [130]

$$\begin{aligned} F_{L_k}(x) &= P(L_k \leq x) = 1 - P(\Phi(C(r,x)) \leq k-1) \\ &= 1 - \sum_{j=0}^{k-1} \frac{(\lambda\pi x^2)^j e^{-\lambda\pi x^2}}{j!}. \end{aligned} \tag{5.10}$$

In a similar manner the CDF of the distance L_k^* to the kth nearest *interferer* of r is obtained as the probability that in the area with maximal distance x to node r, $A_r^*(x)$, where possible interferers might lie in, at least k interferers are located:

$$F_{L_k^*}(x) = P(L_k^* \leq x) = 1 - P(\Phi(A_r^*(x)) \leq k-1). \tag{5.11}$$

Whether $A_r^*(x)$ is different from $C(r,x)$ and which value it actually adopts, depends on the MAC layer functionality. Expressions for $A_r^*(x)$ will be derived later in this section, let us now continue with using Equation (5.11) for expressing a probability for the amount of interference r has to suffer.

Without a detailed knowledge of the WMN traffic pattern, it is unknown which nodes actually disturb a transmission. A worst case assumption is that the Z nodes of Φ closest to the receiver are interfering. With Equation (4.1), this allows to obtain an upper bound for the interference viewed by any receiver $r \in \Phi$ as

$$I = \sum_{k=1}^{Z} P_r^{z_k,r} = P_t \beta \sum_{k=1}^{Z} L_k^{*-\alpha}. \tag{5.12}$$

Furthermore, the CDF of I is given by

$$F_I^Z(x) = P(I \leq x) = P(\sum_{k=1}^{Z} L_k^{*-\alpha} \leq \frac{x}{P_t \beta}). \tag{5.13}$$

The above considerations allow to find a network wide value of $\Delta\gamma$ which guarantees collision free transmissions if link rates are obtained from using this value with Equation (5.7). Recall from Equation (4.3) and (4.2), that a perfect value of $\Delta\gamma$ is lower bounded by

$$\Delta\gamma \geq \frac{N_0 + I}{N_0} \Leftrightarrow \Delta\gamma \geq 1 + \frac{I}{N_0}, \tag{5.14}$$

where the random variable I represents the interference disturbing the transmission between any nodes $s, r \in \Phi$, and N_0 stands for the thermal noise.

Combining Equation (5.14) and Equation (5.13) allows to compute the probability $P^Z_{\Delta\gamma}(x)$ of a collision free operation in the presence of Z interferers if the interference buffer is chosen to be $\Delta\gamma = x$:

$$\begin{aligned} P^Z_{\Delta\gamma}(x) &= P(\Delta\gamma = x \geq 1 + \frac{I}{N_0}) \\ &= P(I \leq N_0 \cdot (x-1)) = F^Z_I(N_0 \cdot (x-1)). \end{aligned} \tag{5.15}$$

Using the condition of a collision free operation described by Equation (5.14) and if the Z interferers are the Z closest nodes, a collision avoiding value of $\Delta\gamma$ is obtained as

$$\Delta\gamma \geq 1 + \frac{1}{N_0} \sum_{k=1}^{Z} P_t \beta L_k^{*-\alpha} \tag{5.16}$$

If only one node z is interfering, Equation (5.16) gives a lower bound for the distance $L_S(\Delta\gamma)$ between the receiving node r and z so that the interference can still be tolerated if $\Delta\gamma$ is used for LRA:

$$\Delta\gamma \geq 1 + \frac{P_t \beta L_1^{*-\alpha}}{N_0} \Leftrightarrow L_1^* \geq \sqrt[\alpha]{\frac{P_t \beta}{N_0(\Delta\gamma(1) - 1)}} =: L_S(\Delta\gamma). \tag{5.17}$$

In other terms, the transmission between s and r will be successfully terminated, if z is not in the area of potential interferers with outer radius $L_S(\Delta\gamma)$,

$A_r^*(L_S(\Delta\gamma)$, i.e. L_1^* is larger than $L_S(\Delta\gamma)$. Considering this, the probability for a collision free operation may hence be derived from Equations (5.11), (5.13) and (5.15) as

$$\begin{aligned} P_{\Delta\gamma}^1(x) &= F_I(N_0(x-1)) = 1 - F_{L_1^*}(L_S(x)) \\ &= \begin{cases} 1 & \text{if } L_S(x) \leq L_1^* \\ e^{-\lambda A_r^*(L_S(x))} & \text{otherwise .} \end{cases} \end{aligned} \tag{5.18}$$

For computing $A_r^*(L_S(x)))$, which in turn allows the computation of $P_{\Delta\gamma}^Z(x)$ and for assessing L_k^*, the MAC layer functionality has to be considered. For IEEE 802.11 mesh networks, three different cases have to be distinguished and consequently three different expressions for $A_r^*(x)$, denoted ${}^aA_r^*(x)$, ${}^bA_r^*(x)$, ${}^cA_{r,s}^*(x)$ respectively will be derived.

The simpler variant of the IEEE 802.11 DCF consists of carrier sense multiple access with collision avoidance (CSMA/CA) [54]. In this case (a), a possible interferer could be arbitrary close to r, as it senses the channel prior to the transmission of s, and starts its transmission during the transmission of s. As a further refinement and protection against collision during a transmission from sender s to receiver r, s can transmit a "request to send" (RTS) frame which r answers by a "clear to send" (CTS) frame. All stations overhearing either the RTS or the CTS do not disturb the transmission. In this case, there is hence a minimum distance between an interferer and r, as no node which has heard either the RTS or the CTS is transmitting. The assumption (b) that only nodes which were not able to decode the CTS of r are not interfering is an assumption which greatly simplifies the computation of A_r^*. Dropping this assumption and accounting for the fact that (c), both the receivers of the CTS and of the RTS do not interfere the transmission from s to r, requires a more extensive computation.

(a) RTS/CTS is not used As previously outlined, a potential interferer could be arbitrarily close, i.e. $L_k = L_k^*$ and ${}^aA_r^*(x) = C(r,x)$. This is illustrated by Figure 5.6(a) where the shaded circle does indicates both the area where at

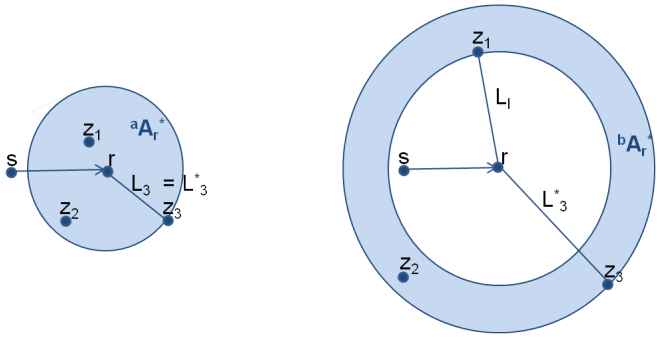

(a) Plain CSMA/CA (b) CSMA/CA with RTS/CTS, simple model

Figure 5.6: *Possible interferer locations for the IEEE 802.11 DCF*

least 3 neighbors of r and 3 interferers of the transmission from s to r can lie in. Calculating the CDF of the interference and the probabilities of collision fraa operation is hence straightforward using Equations (5.12) – (5.18).

The mean value of the distance to the kth nearest interferer is identical to the mean distance of the kth nearest neighbor. Following Thompson [148], this allows to obtain an estimation $\tilde{\Delta}\gamma(Z)$ for $\Delta\gamma(Z)$ by computing

$$E[L_k^*] = E[L_k] = \int_0^\infty x f_{L_k}(x)\mathrm{d}x = \frac{(2k)!k}{\sqrt{\lambda}(2^k k!)^2}. \tag{5.19}$$

and using this result in Equation (5.16)

$$\tilde{\Delta}\gamma(Z) \geq 1 + \frac{P_t\beta}{N_0}\sum_{k=1}^{Z}\left(\frac{\sqrt{\lambda}(2^k k!)^2}{(2k)!k}\right)^\alpha. \tag{5.20}$$

(b) Only the CTS blocks the channel If RTS and CTS are used, all stations overhearing either the RTS or the CTS do not disturb the transmission. A worst-case assumption is that only nodes which did not receive the CTS are possibly interfering. This assumption is illustrated by Figure 5.6(b), where the shaded area where at least 3 interferers of the transmission from s to r lie in, ${}^{b}A_r^*$, is not a circle as in Figure 5.6(a), but a ring, which results from the fact that all nodes within a circle around r did receive the CTS and are hence not interfering. For compatibility and robustness reasons, those command messages are encoded by the most robust available MCS m_C [54]. It is consequently possible to derive a lower bound for the distance between the receiver and any of its interferers z_k, L_k^*. Under the assumption that a too small SINR is the only reason for not receiving the CTS, L_k^* may be lower bounded as follows:

$$\begin{aligned} \gamma_{r,z_k} < \gamma_{m_C}^* \quad &\Leftrightarrow \quad \frac{P_t \beta L_k^{*-\alpha}}{N_0 + I_{r,z_k}} < \gamma_{m_C}^* \\ &\Leftrightarrow \quad L_k^* > \sqrt[\alpha]{\frac{P_t \beta}{\gamma_{m_C}^* (N_0 + I_{r,z_k})}}. \end{aligned} \tag{5.21}$$

Command messages are short. The probability that no interference is present if the CTS is sent, is high, and therefore $I_{r,z_k} = 0$ is a reasonable assumption for Equation (5.21). Under the assumption of symmetric path gains, this leads to a lower bound for the distance to any interferer as the distance to any node which was not able to decode the CTS

$$L_k^* > \sqrt[\alpha]{\frac{P_t \beta}{\gamma_{m_C}^* N_0}} =: L_I, \tag{5.22}$$

which is the inner radius of the ring where the potential interferers might lie in shown in Figure 5.6(b). Taking this into account, the CDF of the distance L_k^* to the kth nearest interferer is given by the probability that there are at least k nodes of Φ in the ring where all points of the plane lie which are closer to the receiver

r than x, but farther away than L_I. Applying this to Equation (5.10) results in

$$\begin{aligned} F_{L_k^*}(x) &= 1 - P(\Phi(C(r,x) \setminus C(r,L_I)) \leq k-1) \qquad (5.23) \\ &= \begin{cases} 0 & \text{if } x \leq L_I \\ 1 - \sum_{j=0}^{k-1} \frac{(\lambda\pi(x^2-L_I^2))^j e^{-\lambda\pi(x^2-L_I^2)}}{j!} & \text{otherwise .} \end{cases} \end{aligned}$$

The equations (5.12) – (5.18) allow to obtain expressions for the interference, its CDF and the collision probabilities if a specific value for $\Delta\gamma$ is used. What is however more worthwhile is having a closer look at the probability for a collision free operation in the presence of $Z = 1$ interferer. Combining Equations (5.18) and (5.23) results in

$$\begin{aligned} P_{\Delta\gamma}^1(x) &= F_I(N_0(x-1)) = 1 - F_{L_1^*}(L_S) \\ &= \begin{cases} 1 & \text{if } L_S \leq L_I \\ e^{\lambda\pi(L_S^2-L_I^2)} & \text{otherwise .} \end{cases} \end{aligned} \qquad (5.24)$$

The interpretation of Equation (5.24) is as follows. As no node is sending which has decoded the CTS of r, the distance between any interferer and r has to be greater than L_I. For a successful reception, there must however also exist a circle with a radius $L_S \geq L_I$ around r where the interferer z does not lie in. The closer the link SNR is to the SINR threshold of the selected MCS, the larger must this circle be. Any positive value for the interference buffer decreases this distance. As soon as it is smaller than L_I collision avoidance can be guaranteed.

The condition guaranteeing collision avoidance in the presence of one interferer, i.e. $P_{\Delta\gamma}^1(x) = 1$ and therefore an expression for a value of the interference buffer for collision free link rate assignment from Equation (5.16) develops to

$$\Delta\gamma(1) \geq \frac{L_I^{-\alpha} P_t \beta}{N_0} + 1 = \gamma_{m_C}^* + 1. \qquad (5.25)$$

Due to the non-linear interdependency of interferer distance and interference

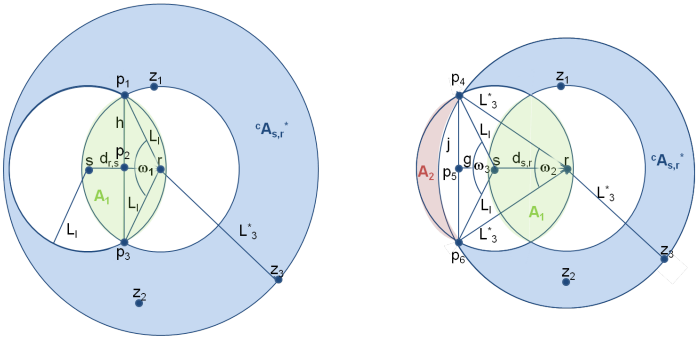

(a) Case 1 (b) Case 2

Figure 5.7: *Possible interferer locations if RTS/CTS is used, realistic model*

strength, a closed form analytical expression and a geometrical interpretation for $P^Z_{\Delta\gamma}(x)$ with $Z > 1$ follow in a similar manner, but are more complex to derive. Likewise, a collision avoidance value $\Delta\gamma(Z)$ for $Z > 1$ can be computed.

(c) Both RTS and CTS block the channel Including the fact that in addition to nodes which did hear the CTS, the nodes which did correctly decode the RTS are not interfering the transmission from s to r, results in a more complicated shape of the region ${}^cA^*_r$ where interferers may lie in. As illustrated by Figure 5.7, this area may be computed as

$$\begin{aligned} {}^cA^*_r(x) &= C(r,x) \setminus \{C(r,L_I) \cup C(s,L_I)\} \\ &= x^2\pi - \left[2L_I^2\pi - A_1 - A_2\right]. \end{aligned} \tag{5.26}$$

If $x > d_{r,s} + L_I$ (Case 1, depicted in Figure 5.7(a)), $A_2 = 0$. It is hence a special case of Case 2 illustrated in Figure 5.7(b). For sake of readability, the components required for computing A_1 are illustrated in Figure 5.7(a) only, but

hold for Case 2 as well.

Observe that the area A_1 is symmetric, as it is the intersection of two circles with the same radius L_I. The connection of the two points of intersection, p_1, and p_3, is consequently the perpendicular bisector of the connection of s and r. It is hence possible to compute A_1 as the 2 times multiple of the area of the circular segment of $C(r, L_I)$ whereof the angle is given by ω_1, and the chord length by h. In turn, the area of this segment is obtained as the difference of the area of the circular sector of $C(r, L_I)$ with angle ω_1 and the triangle $\Delta\ p_1 r p_3$

$$A_1 = 2(L_I^2 \frac{\omega_1}{2} - \frac{1}{4} d_{r,s} h). \tag{5.27}$$

The triangle $\Delta\ p_1 r p_2$ is a rectangled one, consequently the Pythagorean theorem can be applied for computing h as

$$\left(\frac{h}{2}\right)^2 + \left(\frac{d_{r,s}}{2}\right)^2 = L_I^2 \Rightarrow h = \sqrt{4L_I^2 - d_{r,s}^2}. \tag{5.28}$$

From Equation (5.28) and the law of cosines applied for $\Delta\ p_1 r p_3$, an expression for ω_1 follows as

$$\omega_1 = \arccos\left(\frac{2L_I^2 - h^2}{2L_I^2}\right) = \arccos\left(\frac{d_{r,s}^2}{2L_I^2} - 1\right). \tag{5.29}$$

For the computation of A_2, let us now have a look at Figure 5.7(b). It shows that A_2 can be computed as the difference between the area of the circular segment of $C(s, L_I)$ whereof the angle is given by ω_3, and the chord length by j, and the area of the circular segment of $C(r, x)$ whereof the angle is given by ω_2, and the chord length by j. Both circular segment areas can be computed as the difference between the corresponding circular sector and the triangles spanned

by the points of intersection of $C(s, L_I)$ and $C(r, L_I)$,p_4 and p_6, respectively:

$$\begin{aligned} A_2 &= (L_I^2 \frac{\omega_3}{2} - \frac{1}{2} jg) - (x^2 \frac{\omega_2}{2} - \frac{1}{2} j(d_{r,s} + g)) \\ &= L_I^2 \frac{\omega_3}{2} - x^2 \frac{\omega_2}{2} + \frac{1}{2} j d_{r,s}. \end{aligned} \tag{5.30}$$

The distance between s and p_5, g is not needed for the final computation of A_2. The remaining variables are again obtained by means of trigonometry. The angle ω_2 results from applying the law of cosine to the triangle $\Delta\ p_4 r s$ as

$$\omega_2 = 2 \arccos \left(\frac{x^2 + d_{s,r}^2 - L_I^2}{2 x d_{s,r}} \right). \tag{5.31}$$

Using the law of cosine in the triangle $\Delta\ p_4 r p_6$ allows to compute j, the distance between p_4 and p_6 as

$$\omega_2 = \arccos \left(\frac{2L_k^{*2} - j^2}{2L_k^{*2}} \right) \Rightarrow j = \sqrt{2L_k^{*2}(1 - \cos \beta)} \tag{5.32}$$

The law of cosine applied to the triangle $\Delta\ p_4 s p_6$ results in

$$\omega_3 = \arccos \left(\frac{2L_I^2 - j^2}{2L_I^2} \right) = \arccos \left(1 - \frac{j^2}{2L_I^2} \right). \tag{5.33}$$

Putting Equations (5.27) – (5.33) in Equations (5.11) and (5.18) allows to compute $F_{L_k^*}$ and thereby also the probabilities $P_{\Delta\gamma}^Z(x)$ and the thresholds for $\Delta\gamma$. Note that while the more exact expressions for $P_{\Delta\gamma}^1(x)$ and $\Delta\gamma(1)$ derived by Equations (5.24) and (5.25), respectively, hold in this case, too, the probability of a collision free operation will be larger or equal than the one resulting from Equation (5.24), as the area enclosed by ${}^cA_{s,r}^*(L_S)$ is smaller than the one enclosed by ${}^bA^*(L_S)$. The price for this more exact calculation is however that it is not generally valid but depends on the distance between s and r.

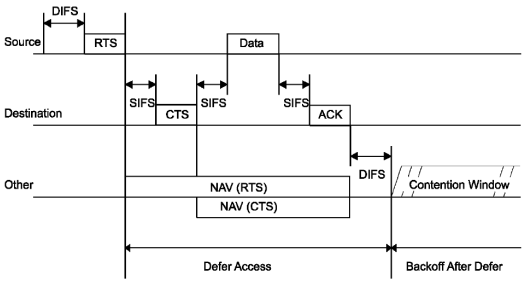

Figure 5.8: *RTS/CTS/data/ACK and NAV setting [54]*

Influence of $\Delta\gamma$ on the per-link throughput

This section assesses the advantages and disadvantages of using the interference buffer for link rate assignment in terms of achievable link throughput. Due to the MAC and PHY layer overhead, the achievable link throughput is significantly smaller than the raw data. If the RTS/CTS exchange is not used, the link throughput reductions are straightforward. Let us hence focus on the more interesting case where RTS and CTS are used. The computation of the NAV (network allocation vector) shown in Figure 5.8 taken from the IEEE 802.11-2007 standard [54] illustrates that in this case, the time required for sending data packets using the standardized 802.11 DCF mechanism may be significantly larger than the time required for actually sending the bits over the channel.

In the optimal case, i.e. if everything is working as intended, a rough model of the time $t_{tx}(p, m)$ required for transmitting a packet with p payload bits and MCS m is given by [54]

$$\begin{aligned} t_{tx}(p,m) &= \text{DIFS} + t_{bo} + \delta(p_{\text{RTS}}, m_C) + \text{SIFS} + \delta(p_{\text{CTS}}, m_C) \\ &\quad + \text{SIFS} + \delta(p,m) + \text{SIFS} + \delta(p_{\text{ACK}}, m). \end{aligned} \tag{5.34}$$

In this formula, t_{bo} denotes the optional time the node backs off before it sends

the CTS. If the channel is sensed as free, the CTS is sent immediately, hence $t_{bo} = 0$. Otherwise, t_{bo} is uniformly distributed between 0 and CW multiples of aSlotTime, where CW is varying between aCWmin and aCWmax, depending on the backoff stage. The time required for sending p payload bits over the channel, $\delta(p, m)$, depends on the used MCS m and on the used PHY layer. For the case of OFDM, it can be computed as [54]

$$\begin{aligned} \delta(p,m) &= T_{PREAMBLE} + T_{SIGNAL} \\ &\quad + T_{SYM} \cdot \lceil (16 + 8 \cdot p + 6)/N_{DBPS}(m)) \rceil. \end{aligned} \tag{5.35}$$

The number of coded bits per OFDM symbol, $N_{DBPS}(m)$ is increasing with the data rate r_m. RTS and CTS messages are sent using the most robust MCS, m_C which is supported by all stations, while the ACK is sent using the same modulation scheme used for the data packet.

Observe that Equation (5.34) is only valid, if the transmitting node does not encounter any problems. However, three different problems which are subsequently described may affect the packet transmission in various ways and consequently increases the transmission time. (1) A packet could be detected during backoff. In this case, which is denoted by db for *disturbed backoff*, the backoff counter will be frozen and continues to decrement as soon as the channel is sensed idle again for a time DIFS. (2) The RTS/CTS exchange could fail, i.e. a *signaling failure*, sf, could occur. This type of failure is detected by the sending node if no CTS was received during the CTS Timeout interval after the RTS was sent. (3) A *data failure*, df, could happen i.e. the node does not receive an acknowledgment during the ACKTimeout interval after having sent the data packet. In this case, the entire RTS/CTS exchange procedure has to be repeated. If during a MAC layer packet transmission attempt, more than 7 signaling failures or more than 4 data failures occur, the packet will be discarded [54].

The average network throughput using the correct probabilities for each event could be derived as proposed by Bianchi [149]. As these formulas are valid for the case of saturated throughput only, let us concentrate on the effect of the

type of failure which the use of the interference buffer may prevent. RTS and CTS are always sent with the most robust MCS [54]. The *df* failure is hence the only failure which can be avoided by a more robust MCS choice. If l data failures occur during the transmission of p payload bits, the time required for $l+1$ backoff phases with increasing contention windows, t_{bo}^{i}, the time for l failed data exchanges and for one successful one have to be added. All in all, the required transmission time increases to [54]

$$\begin{aligned} t_{tx}^{df}(p,m,l) &= \sum_{i=1}^{l+1} t_{bo}^{i} + l \cdot \big[\text{DIFS} + \delta(p_{\text{RTS}}, m_C) + \text{SIFS} \\ &\quad + \delta(p_{\text{CTS}}, m) + \text{SIFS} + \delta(p,m) + \text{ACKTimeout}\big] \\ &\quad + \text{DIFS} + \delta(p_{\text{RTS}}, m_C) + \text{SIFS} + \delta(p_{\text{CTS}}, m_C) \\ &\quad + \text{SIFS} + \delta(p,m) + \text{SIFS} + \delta(p_{\text{ACK}}, m). \end{aligned} \tag{5.36}$$

In order to derive a model for the effects of $\Delta\gamma$ on the average network throughput, let us assume that data failures are the only events which could occur. This is insofar justified as the interference buffer has no positive influence on the occurrence of the other events and the focus of this chapter is on studying the impact of the MCS choice. For the case where all data packets have the same amount of payload, p_l, and with a probability of ρ, that exactly $l = 1$ data failure occurs during a transmission, probability theory allows to compute the throughput $\tau(m)$ under MCS m as

$$\tau(m) = \frac{p_l}{(1-\rho)t_{tx}(p_l,m) + \rho t_{tx}^{df}(p_l,m,1)}. \tag{5.37}$$

Note that the goal of this model is not to include the effect of a varying number of data failures or the interdependency of ρ, the used MCS, and the network environment. Instead, Equation (5.37) is intentionally kept simple in oder to illustrate the double-edged influence of a $\Delta\gamma > 1$ which both increases the transmission times and reduces the *df* failure probability.

5.4.2 Link Rate Assignment Performance Evaluation

This section contains results from a simulation study complementing the theoretical results of Section 5.3.2. The channel model Equation (4.1) is parametrized according to Equation (4.5). In order to move this model closer to a realistic mesh network, the ambient noise N_0 is set to the product of the thermal noise spectral density, -174 dBm/Hz, a typical receiver noise figure $F_N = 7.5$ dB and the channel bandwidth $W = 20$ MHz, i.e. $N_0 = -93.5$ dBm. The noise figure characterizes the quality of the transceiver. In the optimal case, $F_N = 0$ dB. For typical mesh transceivers, Hiertz et al. [150], indicate $F_N = 5$ dB and $F_N = 10$ dB as low and high values, $F_N = 7.5$ dB is hence a representative in-between value. Note that the only difference to the more abstract channel model used in Section 5.3.2, is that the probability of successfully decoding a transmission decreases, i.e. the length of a link with a given data rate gets shorter.

Collision probability and per-link throughput

Let us first analyze the interdependency between the probability of a collision-free operation, $P^Z_{\Delta\gamma}(x)$, and a specific value of $\Delta\gamma$. In Figure 5.9(a) this analysis is illustrated for the case of $Z = 1$ interferer and for different network densities corresponding to one node per circle of 10 to 50 m radius. The probability for collision free operation is the highest for a small node density, and also increases with increasing values of $\Delta\gamma$. Additionally, $\Delta\gamma(1) = 5.1$ dB guaranteeing a collision-free operation for the case of $Z = 1$ interferer derived from Equation (5.25) is shown. Results obtained from both models for computing the possible interferer area for cases (b) and (c) discussed in Section 5.4.1 are shown.

For case (a), Equation (5.20) allows to derive an estimation for a suitable parameterization of $\Delta\gamma$ for the considered densities. For the case where the $1 \leq z \leq 10$ nearest neighbor is interfering, this results in interference buffer values between 25 and 90 dB. The results presented in Section 5.3.2 underline however that such values are too high to be beneficial for the network throughput. A collision avoidance parameterization of $\Delta\gamma$ is hence not reasonable for this case.

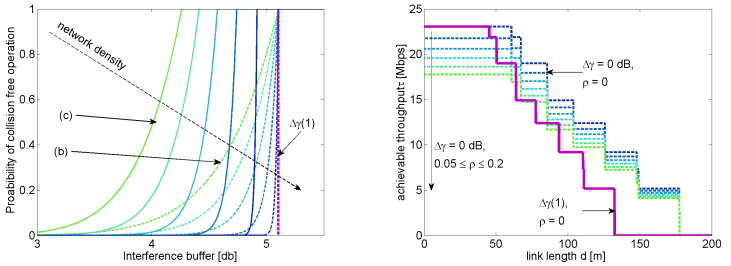

(a) Probability of collision free operation

(b) Average throughput with 1.5 kB payload

Figure 5.9: *Analysis of the interference buffer impact*

As a result, the probabilities $P^{Z}_{\Delta\gamma}$ resulting from the $\Delta\gamma$ values used for the representation shown in Figure 5.9(a) for case (a) are significantly smaller than the probabilities resulting in cases (b) and (c) and therefore not shown.

Note that the results of this figure hold for an ideal Poisson field only. It is insofar difficult to apply its statements to WMNs, as the number of neighbors in a WMN with the same density is always smaller. The probabilities shown in Figure 5.9(a) are thus a mere general guideline and have to be adapted in order to give quantitative values for a given deployment. The qualitative statement, i.e. the interference buffer becoming more important for collision avoidance with an increasing number of nodes or higher node activity is however directly applicable.

Packet collisions decrease the e2e throughput. Consequently, $\Delta\gamma$ has a positive influence on the throughput, but also a negative one, as it decreases the link data rate. In order to analyze which values of $\Delta\gamma$ are suitable, Figure 5.9(b) illustrates the effect of data failures on the link throughput. For this purpose, the feasible link length without interference buffer is computed for each of the 8 available MCS according to the used path gain model. The throughputs for the case that with probability $0 \leq \rho \leq 0.2$ each data packet encounters one data failure are calculated using Equation (5.37) and shown with dashed lines.

The solid line depicts the resulting throughputs if link rates are assigned using $\Delta\gamma(1) = 5.1$ dB. Recall that the model is based on the assumption that all failures which could occur are data failures caused by one interfering node. If $\Delta\gamma(1)$ is used for link rate assignment, the collision probability is hence 0, if only one interferer may occur.

This representation allows to see that the quantitative negative impact of failures on the throughput of short, i.e. high data rate links is larger than on longer, low data rate links. This is due to the fact that the RTS/CTS exchange, which is done with the slowest link rate, has to be repeated. The time penalty of a failure in comparison to a data transmission is hence larger for fast links than for slow ones. Consequently, using $\Delta\gamma(1)$ for link rate assignment is most beneficial for high data rate links. For links with a medium link rate, this pays only if the collision probability and thereby the loss of transmission efficiency is high. In the case of links with a length over 130 m, the use of $\Delta\gamma(1)$ for link rate assignment would even result in a throughput of 0, as those links could simply not be used anymore. Note that the analysis presented in Figure 5.9(b) is valid for one hop only. For obtaining similar results for a non-idealistic multi-hop network, a simulation is better suited than an analysis. The next section therefore studies $\Delta\gamma$'s effects in a simulated multi-hop environment.

Effects of $\Delta\gamma$ in an RTS/CTS based WMN deployment

In order to examine in how far the benefits of $\Delta\gamma$ for the max-min fair network throughput hold in a more realistic setting, too, the remainder of this section reports on a performance evaluation of LRA with $\Delta\gamma$ of a WMN with a contention based access scheme. The necessary simulation study has been carried out with the simulator USE which has been developed at the Chair of Communication Networks at the University of Würzburg.

USE models the signal propagation by computing the received signal strength and the amount of cumulative interference according to Equation (4.5). For the MAC layer, the 802.11-2007 stack is implemented and all necessary constants

are set for the OFDM PHY given in [54]. As upper layer protocols, IP and UDP are used. At randomly distributed times within the first simulation second, each of the non-gateway nodes starts an application layer CBR flow of 10 Mbps from the Internet representing its customer demands. Recall from Figure 5.4 that the average per flow throughput is below 2 Mbps. Parameterizing the application layer data rate with 10 Mbps allows hence to obtaine a throughput comparable to the MMF throughput. USE has a time resolution of 5 μs. In order to examine a large amount of design points, simulation results are obtained from the first 30 seconds of the network lifetime. As the routing topology is considered to be static, the initial transient period is completed after at most one second. Results gathered before this time are discarded.

Effects in a small topology The first simulation study this section reports on has been carried out with a Java version of USE which enables per packet logging. This approach does not scale for the topologies with 50 nodes used in Section 5.3.2. Hence, 200 network samples consisting of 3 gateways and 15 mesh access points are considered. All numerical values shown in the following are obtained as averages over the 200 different samples and are depicted with the corresponding 95% confidence intervals. The network creation methodology discussed in Section 4.1.3 is used to randomly generate network topologies with a fixed number of nodes placed in a square area of 400 m $\times$ 400 m. As grid lengths, l_G =100 m and $l_F = 20\,\mathrm{m}$ are used.

For each constructed topology, values of $\Delta\gamma = \{0, 1, \ldots, 10\}$ dB are used for LRA. As illustrated in Figure 5.9(b), long links which exist in topologies with $\Delta\gamma = 0$ dB, might be assigned a zero link rate for $\Delta\gamma > 0$ dB as their SNR is smaller than the smallest SINR threshold plus the interference buffer. In this case, the routing has to be recomputed for each link rate assignment. Recall from the discussion of Figure 5.4 that this reorganization of the topology is responsible for a significant throughput increase. If, in contrast, the routing topology is not reorganized, this allows to study the undiluted effect of $\Delta\gamma$ and the results are applicable to cases where the routing topology can not be changed. For this

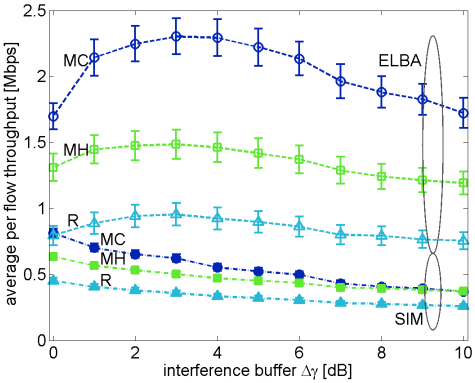

Figure 5.10: *Max-min fair share vs. simulated average per flow throughput*

purpose, long links which are already using the slowest rate for $\Delta\gamma = 0$ dB are kept operating at this rate for all values of $\Delta\gamma$. This procedure is similar to the one used for Scenario A in Section 5.3.2. After the link rate assignment, the routing topology is established using the routing algorithms MC, MH and R discussed in Section 5.3.1.

In Figure 5.10 the average max-min fair share throughput (computed with ELBA introduced in Section 4.2.2 and labeled "ELBA") and simulated network throughput (labeled "SIM") are shown in dependence of the $\Delta\gamma$ value used for LRA. Results for each of the used routing protocols are labeled accordingly. This representation illustrates several aspects: Firstly, the less efficient resource utilization in a random access network compared to a perfect channel access schedule enabling a MMF resource utilization is depicted by the significant difference between the max-min fair throughput and the simulated one. Observe that the relative differences between the routing protocols are similar under both evaluation techniques. Secondly, the representation of the MMF throughputs shows the effect we already observed in Section 5.3.2: For each network configuration,

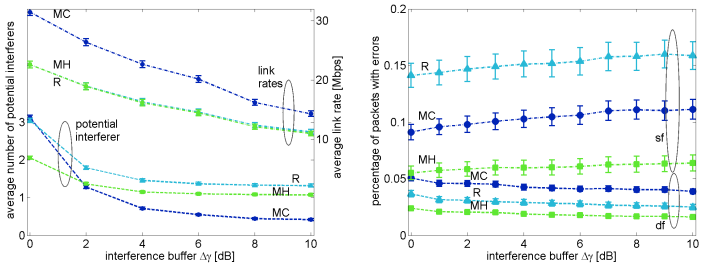

(a) Topological effects (b) Failure rates

Figure 5.11: *Impact of the interference buffer on topology and failure rates*

there is a value of $\Delta\gamma > 0$ dB which is able to maximize the network throughput, as the relation between link rates and spatial reuse is optimized. Moreover, the throughput increase is stronger for the MC protocol. This is due to the fact that this paradigm prefers links with the highest data rate for which more robust link rate assignment is the most advantageous (cf. Figure 5.9(b)).

Surprisingly, no positive effect of the interference buffer is observable for the *simulated* network throughput. The average network throughput is instead decreasing and the decrease is moreover strongest for the MC protocol. The reason for this is the effect of $\Delta\gamma$ on the network topology which is illustrated in Figure 5.11(a). The y-axis on the left represents the average number of potential interferers each node has to cope with. This term denotes all mesh nodes which could interfere the transmission to the node. The right y-axis shows the average data rate of the routing links. This representation allows to see that in dependence of the routing protocol, the number of hidden nodes is reduced by over 50% for $\Delta\gamma = 10$ dB. As in turn, the link rate is decreased by roughly 50% it is evident that for large values of $\Delta\gamma$, the link rate reduction can not be compensated any more by the increased channel access time.

Using the average link rates and number of interferers shown in Figure 5.11(a) for a calculation neglecting the MAC layer overhead yields that for $\Delta\gamma = 0$ dB

and the MC routing protocol, the nodes have on average an available link capacity of $32/(3+1) = 7$ Mbps in comparison to $26/(2+1) = 8.7$ Mbps when $\Delta\gamma = 2$ dB is used. This result does however contrast the results from Figure 5.10, where a decrease of the average throughput for increasing $\Delta\gamma$ is shown. The reason for this phenomenon is illustrated in Figure 5.11(b). The figure shows the number of packets which suffer data and signaling failures in relation to the number of transmitted packets and thereby shows again a double edged influence of $\Delta\gamma$. Observe that the percentage of signaling failures is both larger than the number of data failures and is additionally increasing with $\Delta\gamma$. The latter phenomenon is due to the fact that data packets are longer on the channel, the probability of a concurrent transmission of a signaling and a data packet is hence increasing. Figure 5.11(b) shows also that the number of data failures is in fact decreasing with $\Delta\gamma$ which is again to a higher degree the case for the MC protocol than for the other ones. This effect can however not compensate the reductions of throughput which are due to the reduced link rates and the increased number of signaling failures. The total throughput is hence decreasing.

All in all, the effect of $\Delta\gamma$ on the average throughput in this investigated scenario is negative, as the amount of decreased collision probability simply does not compensate for the link rate reductions. Moreover, the percentage of data failures can never decrease to zero, as long as there are still links operating at the lowest data rate. The potential of conservative link rate assignment is thus larger in denser and larger topologies where the routing structure is adapted to the link rate assignment, i.e. where only links with a safety margin of $\Delta\gamma$ between the link SNR and the MCS SINR threshold exists. Networks where the same MCS is used for data transmission and RTS/CTS would also profit more from this method than the considered configurations. In medium sized WMNs where fairness can not be guaranteed and the routing topology is given, it is hence advisable to assign link rates using $\Delta\gamma = 0$ dB.

Effects in larger networks In order to evalute the impact of $\Delta\gamma$ on the network throughput for the scenarios studied in Section 5.3.2, a C++ version of

USE which does not enable a per-packet logging and thereby sacrifies details for speed, is used. Results from this experiment are shown in Figure 5.12. For a better comparison, the computed average max-min fair share (labeled "ELBA") are again shown along with the simulatively obtained network throughputs (labeled "SIM") in dependence of the $\Delta\gamma$ value used for LRA. Results for each of the used routing protocols are labeled accordingly. The MMF throughputs are the same which have already been shown in Figure 5.4. To ease the comparison among the methodologies, the scale of all y-axis in the subfigures of Figure 5.12 is the same as in Figure 5.4.

The first striking fact is again the significant difference between the throughputs obtained for the different evaluation metrics which is due to the previously observed less efficient resource utilization of the random channel access. An effect which has also been previously discussed is the topology-dependent effect of $\Delta\gamma$ on the simulated network throughput. Let us discuss these issues on a per-scenario basis. For the case of Scenario A, which corresponds to the setting examined with the Java version of USE, no node can become disconnected, as all links are kept operating with the slowest available MCS even if their SNR is smaller than the link target SINR plus the interference buffer. That is the reason why $\Delta\gamma$ has only a marginal influence on the max-min fair throughput of the MH and R topologies as they use a high percentage of slow links whereof the rate is not affected by the use of the interference buffer. The same reason is responsible for the fact that $\Delta\gamma$ has no positive effect on the simulated network throughput, as the interference buffer can not protect transmissions which are done using the smallest MCS. What is more surprising is the negative effect of $\Delta\gamma$ on the throughput achievable in MC topologies which contrasts the positive effect of $\Delta\gamma$ on the MMF throughput.

The reason for this is illustrated by Figure 5.11(a), but has also been previously discussed. MC routing uses a significantly higher share of high data-rate links than the other routing paradigms and therefore the data rates of the links used for routing data are most heavily reduced. As it is also illustrated by Figure 5.11(a) this phenomenon is accompanied by a similar reduction of potential interferers.

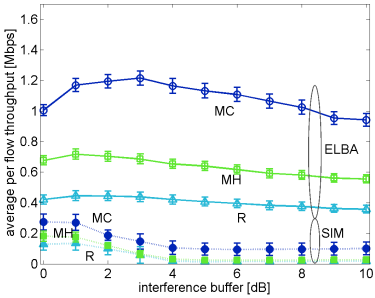

(a) Scenario A

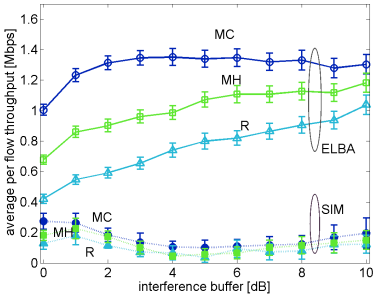

(b) Scenario B

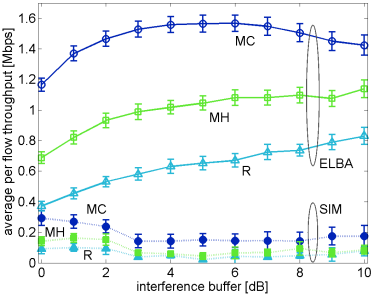

(c) Scenario C

Figure 5.12: *Max-min fair share vs. simulated average per flow throughput*

For the case of a perfect channel access, the increased spatial reuse is able to pay off the link rate reduction, as more concurrent transmissions can be scheduled. If the channel is used in a random access manner in contrast, this is not the case.

Let us now focus the results obtained in Scenarios B and C (cf. Figures 5.12(b) and 5.12(c)). In Scenario B, representing the case where a large percentage of the routing links is so long that the smallest data rate has to be used, the MMF throughput is strongly increasing with $\Delta\gamma$ as large values of the interference buffer result in isolated nodes which do not compete for the channel access any more, thereby increasing the throughput of the other nodes. This holds for the simulated throughput, too, but the effect is weaker. As this increase of the average per flow throughput comes along with a high number of starving flows, the local maximum at $\Delta\gamma = 1$ dB for MH and R routing is more interesting. This is caused by the fact that those links which just meet the SINR requirements for their MCS and are thereby very sensitive to concurrent transmissions, reduce their data rate or are not used any more, which pays off in terms of total network throughput. Note that the average throughput achieved under the MC routing algorithm is not increased as in this case, many high data rate links are used which suffer most under the rate reduction, and consequently, the topology is not reorganized.

In Scenario C, the node density is higher and consequently, the percentage of low data rate links is smaller than in Scenario A and B. Hence, not only the MC, but also the R routing paradigm use more high than low data rate links and the benefits resulting from the use of the interference buffer on the throughput are not existing for these routing topologies. In contrast, the throughput achieved under MH has a local maximum for $\Delta\gamma = 2$ dB which is due to the reorganization of the routing structure which now avoids the use of very tightly assigned link rates. Observe that again, the link rates tend to increase for larger values of $\Delta\gamma$.

Repeating the same simulation in a setting without RTS/CTS, yields similar results. One may thus infer that using the interference buffer for link rate assignment is a suitable method for increasing the efficiency of random access WMNs, too, at least if only small values for $\Delta\gamma$ are chosen and if the routing structure is adapted so that only links with a certain small safety margin are used.

5.5 Link Rate Assignment for Max-Min Fair Flow Optimization

The last sections illustrated that using one value of $\Delta\gamma$ for a network-wide more robust than necessary link rate assignment. They however also showed that more sophisticated link rate assignment strategies taking into account the individual link characteristics are necessary. This section therefore describes the maximization of the WMN capacity as an optimization problem where link rate assignment and transmission scheduling are degrees of freedom. This problem introduces modeling challenges which are not present in classical network optimization problems, as the problem formulation is not only complicated by the characteristics of the wireless communication channel, but also by the traffic uncertainty. The former problem is addressed by contributing a mixed-integer programming (MIP) model determining the feasible space for the link capacity reservation vectors, i.e. feasible transmission schedules, link rates, and the resulting throughputs, under the constraint that the traffic matrices that could be used for performance engineering are unknown. In analogy to the approach of Section 5.3, this problem is handled by considering max-min fairness in assigning bandwidth to WMN routes and by introducing algorithms for solving the non-convex MMF problems given a feasible link capacity reservation space. Introducing the mentioned models and algorithms, requires more variables than the ones introduced in Section 4.1.2. In the following, those additional variables will be discussed prior to the actual algorithm description and performance evaluation.

5.5.1 Additional Notation

Recall that a WMN is abstracted as the set of nodes $\mathcal{N}$, and the set of links $\mathcal{L}$. The start and end node of a link $l \in \mathcal{L}$ is denoted by $s(l)$ and $e(l)$, respectively, that is, when $l = (i, j), i, j \in \mathcal{N}$ then $s(l) = i$ and $e(l) = j$. Further, $\chi^+(i)$ and $\chi^-(i)$ denote, respectively, the sets of outgoing and incoming links from/to node $i \in \mathcal{N}$. The set of all links incident to node i, is given by $\chi(i) = \chi^+(i) \cup \chi^-(i)$.

In analogy to the scenario described in Section 4.1.2, in a network with the set of MCS $\mathcal{M}$, link l exists if and only if $\gamma'_l \geq \gamma^*_m$ for at least one $m \in \mathcal{M}$. With the channel model from Equation (4.5), this is equivalent to $d_{i,j}$ being smaller or equal than at least one of the feasible link lengths summarized in Table 4.1.

In order to model the temporal network dynamics, let the total time of network operation be partitioned by a set of time slots $\mathcal{T}$. Each slot $t \in \mathcal{T}$ represents a time interval of length Δt where a specified subset of nodes can successfully transmit at the same time which translates to links being active at the same time. The subsets of links active in consecutive time slots $t \in \mathcal{T}$ are specified by a scheduling solution. The total time of network operation is hence given by $\Delta t|\mathcal{T}|$. The network operation is described by the following variables:

Y_{lt} binary variable indicating whether link l is scheduled to be active in time slot $t \in \mathcal{T}$. If a link is active, then its SINR must be larger than the target SINR of the used MCS, i.e. Equation (4.6) must be satisfied for the SINR threshold of the appropriate MCS.

y^m_{lt} binary variable indicating whether link l is active and uses MCS m in time slot $t \in \mathcal{T}$.

X_{it} binary variable indicating whether node i transmits (is active) in time slot $t \in \mathcal{T}$.

x^m_{it} binary variable indicating whether node i transmits using MCS m in time slot $t \in \mathcal{T}$.

M^m_l nonnegative integer variable indicating which MCS is used by link l in all time slots.

r_{lt} nonnegative rate of link l achieved in time slot $t \in \mathcal{T}$, determined by the used MCS.

c_l nonnegative integer capacity of link l, equal to the total volume of data that can be send on link l during the time of the network operation.

Together with the previously introduce notation, these variables allow now to describe WMN optimization models.

5.5.2 Modeling the Link Capacity Space

This section is devoted to modeling feasible sets of radio link capacity reservations. For this purpose MIP formulations, that is, systems of linear equalities and inequalities in continuous and integer variables are used. Pioro et al. [2] discuss four different possibilities to abstract a WMN. The introduced formulations are applicable for networks where each node has one or more transceiver, where one or more MCS are used, and where the nodes are or are not constrained to utilize the entire transmission capability of one time slot on one link. The authors point out that all models are independent of any particular optimization objective formulations and are in this sense general.

In the remainder of this section, the WMN model introduced in [2] which describes the previously discussed situation is described. It models a WMN where the transmission output power is given, and where each link shall be statically assigned a link rate which is kept for the entire operation of the WMN. Each node has only one transceiver, but this transceiver may use different MCSs. The constraints of such a system are described by the following system of equations:

$$\sum_{m \in \mathcal{M}} M_l^m = 1 \qquad l \in \mathcal{L} \tag{5.38a}$$

$$y_{lt}^m \leq M_l^m \qquad l \in \mathcal{L}, m \in \mathcal{M}, t \in \mathcal{T} \tag{5.38b}$$

$$Y_{lt} = \sum_{m \in \mathcal{M}} y_{lt}^m \qquad l \in \mathcal{L}, t \in \mathcal{T} \tag{5.38c}$$

$$\sum_{l \in \chi(i)} Y_{lt} \leq 1 \qquad i \in \mathcal{N}, t \in \mathcal{T} \tag{5.38d}$$

$$\sum_{l \in \chi^+(i)} y_{lt}^m = x_{it}^m \qquad i \in \mathcal{N}, m \in \mathcal{M}, t \in \mathcal{T} \tag{5.38e}$$

$$X_{it} = \sum_{m \in \mathcal{M}} x_{it}^m \qquad i \in \mathcal{N}, t \in \mathcal{T} \tag{5.38f}$$

$$y_{lt}^m \frac{P_r^{s(l),e(l)}}{N_0 + \sum_{i \in \mathcal{N} \setminus \{s(l)\}} P_r^{i,e(l)} X_{it}} \geq y_{lt}^m \gamma_m^* \qquad l \in \mathcal{L}, t \in \mathcal{T} \tag{5.38g}$$

$$c_l = \Delta t \sum_{t \in \mathcal{T}} \sum_{m \in \mathcal{M}} r_m y_{lt}^m \qquad l \in \mathcal{L}. \tag{5.38h}$$

The constraints assure that

(5.38a) every link selects one MCS.

(5.38b) the MCS used by a link in any time slot in which the link is active must be the one selected for this link.

(5.38c) $Y_{lt} = 1$ if, and only if, link l is active and uses one of the available MCSs.

(5.38d) at most one link incident to a node can be active in any time slot.

(5.38e) node i is active in time slot t with MCS m, if exactly one link outgoing from node i is active this time slot t and uses m.

(5.38f) $X_{it} = 1$ if, and only if, node i is active and uses one of the available MCSs.

(5.38g) the SINR constraint (see Equations (4.3) and (4.6)) does hold. If link l is active in time slot t with MCS m i.e., if $y_{lt}^m = 1$ and thereby $Y_{lt} = 1$, then its SINR must be greater or equal to the SINR threshold of MCS m.

(5.38h) the total effective capacity of link l is the sum of its capacities over all time slots and MCSs.

Two modifications

For obtaining solutions from Formulation (5.38), two modifications, both concerning Equation (5.38g), are necessary, which will be subsequently discussed.

Observe first that Equation (5.38g) is not linear but bi-linear. It can be made linear by introducing additional binary variables z_{lit}^m to express the product $y_{lt}^m \cdot X_{it}$, i.e., $z_{lit}^m = 1$ if both y_{lt}^m and X_{it} are equal to 1, and 0, otherwise. This is achieved using the constraints:

$$z_{lit}^m \geq y_{lt}^m + X_{it} - 1 \qquad i \in \mathcal{N}, l \in \mathcal{L}, t \in \mathcal{T}, m \in \mathcal{M} \tag{5.39a}$$

$$z_{lit}^m \leq y_{lt}^m,\ z_{lit}^m \leq X_{it} \qquad i \in \mathcal{N}, l \in \mathcal{L}, t \in \mathcal{T}, m \in \mathcal{M}. \tag{5.39b}$$

In addition, Equation (5.38g) is changed to

$$N_0 y_{lt}^m + \sum_{i \in \mathcal{N} \setminus \{s(l)\}} P_r^{i,e(l)} z_{lit}^m \leq \frac{1}{\gamma_m^*} P_r^{s(l),e(l)} y_{lt}^m \qquad l \in \mathcal{L}, t \in \mathcal{T}, m \in \mathcal{M}. \tag{5.40}$$

A simplification of the interference model is the second important modification and leads to a significant decrease of the time needed to solve the related optimization problems. In Equation (5.38g) a full interference model is assumed. However, it is possible to reasonably simplify it like discussed in Section 5.3.1, and to consider only single-interferer collision domains. Recall that the idea of

this simplification is to assume that if any subset of nodes $\mathcal{D} \subseteq \mathcal{N} \setminus \{s(l)\}$, when simultaneously active, interferes with transmission on link l then transmission on link l is already interfered when a single node of $\mathcal{D}$ is active. Certainly, in general this is not the case and therefore may lead to network capacity overestimation.

In order to formally incorporate the simplified interference model in Equation (5.38), the following constraint replaces Equation (5.38g):

$$y_{lt}^m \frac{P_r^{s(l),e(l)}}{N_0 + P_r^{i,e(l)} X_{it}} \geq y_{lt}^m \gamma_m^* \quad l \in \mathcal{L},\ t \in \mathcal{T},\ i \in \mathcal{N} \setminus \{s(l)\}, m \in \mathcal{M}. \tag{5.41}$$

Now it is possible to rewrite (5.41) in a linear form :

$$y_{lt}^m + X_{it} \leq 1, \quad l \in \mathcal{L}\ t \in \mathcal{T},\ i \in \mathcal{D}_l^m, \tag{5.42}$$

where

$$\mathcal{D}_l^m = \{i \in \mathcal{N} \setminus \{s(l)\} :\ \frac{P_r^{s(l),e(l)}}{N_0 + P_r^{i,e(l)}} < \gamma_m^*\}. \tag{5.43}$$

5.5.3 Max-Min Fair Optimization of Demand Flows

The Formulation (5.38) defines a feasible set $\Gamma \subseteq \mathbf{R}^{|\mathcal{L}|}$ of link capacity reservations $c = (c_l : l \in \mathcal{L})$. Based on this link capacity space, the following formulation allows a MMF flow optimization which is also applicable to all other models presented in [2] or other imaginable WMN configurations.

Recall from Section 4.1.2 that $\mathcal{P} = \{p_1, p_2, \ldots, p_F\}$ is the set of paths which connect the F non-gateway nodes and the G gateway nodes. Each such path p_f is supposed to carry the entire downstream flow or throughput of node $f \in \mathcal{F}$ which is routed via one specific gateway node $g \in \mathcal{G}$. Each path p_f is a subset of links, i.e., $p_f \subseteq \mathcal{L}$, $f = 1, 2, \ldots, F$. For each link $l \in \mathcal{L}$, the set of all indices of paths in $\mathcal{P}$ that contain this link will be denoted by $\mathcal{I}_l = \{f :\ l \in p_f,\ 1 \leq f \leq F\}$. According to Ogryczak et al. [151], this notation allows to formulate the MMF

flow optimization problem as follows:

$$\text{lexmax} \quad [(\tau_1, \tau_2, \ldots, \tau_F)] \tag{5.44a}$$

$$c \in \Gamma \tag{5.44b}$$

$$\sum_{f \in \mathcal{I}_l} \tau_f \leq c_l \qquad l \in \mathcal{L}. \tag{5.44c}$$

In Equation (5.44a), $[\tau] = ([\tau]_1, [\tau]_2, \ldots, [\tau]_F)$ denotes the vector $\tau = (\tau_1, \tau_2, \ldots, \tau_F)$ sorted in non-decreasing order, so that objective (5.44a) consists in lexicographical maximization of the sorted vector of path-flows ($[\tau]_1 \leq [\tau]_2 \leq \ldots \leq [\tau]_F$). The lexicographic order used for this purpose is defined as follows. Let $\tau' = (\tau'_1, \tau'_2, \ldots, \tau'_F)$ and $\tau'' = (\tau''_1, \tau''_2, \ldots, \tau''_F)$ be two vectors representing flow throughputs. Vector τ' is lexicographically greater than vector τ'', $\tau' >_{lex} \tau''$, if there exists an index k, $0 \leq k \leq F$, such that $\tau'_j = \tau''_j$ for all $j \leq k$ and $\tau'_{k+1} > \tau''_{k+1}$. Consequently, τ' is lexicographically greater or equal than τ'', $\tau' \geq_{lex} \tau''$, if $\tau' >_{lex} \tau''$ or $\tau' = \tau''$. If $[\tau^*]$ is now a solution of Problem (5.44), then $[\tau^*]$ is lexicographically greater or equal than all other ordered flow throughputs resulting from a feasible link capacity reservation.

Problem (5.44) can be solved sequentially through the so called *conditional means approach* [151]. The idea of the approach is to express *optimization criteria*, i.e. the consecutive entries of vector $[\tau]$ and maximize them one by one, keeping the previously optimized entries at their optimal values. Based on this idea, Ogryczak et al. [151] describe the max-min fair flow allocation algorithm (MMFFA) which needs F steps for iteratively maximizing the fth smallest flow throughput, where f is increasing from 1 to F.

The optimization space Γ which is required as input for the MMFFA is obtained from the problem description (5.38) together with the two discussed interference modeling approaches, which will be denoted by *full* and *simplified* interference in the following. The full interference model is the one resulting from Equation (5.38) with the constraint (5.38g) replaced by Equations (5.39) and (5.40). The resulting link capacity space is therefore denoted by Γ^{FI}_{static},

as Equation (5.38) describes the static link rate assignment problem. If now the simplified interference model is applied and constraints Equations (5.39) and (5.40) are substituted by Equation (5.42), the resulting capacity space is denoted as Γ^{SI}_{static}. The corresponding MMF optimization problems are obtained by replacing $\mathcal{C}$ in the generic MMF problem (5.44). If $\Gamma := \Gamma^{FI}_{static}$, the problem will be called *Problem SA/FI*. If $\Gamma := \Gamma^{SI}_{static}$ it is denoted by *Problem SA/SI*.

The subproblems which have to be solved in the consecutive steps of MMFFA for the problems SA/FI, and SA/SI are NP-hard. According to Capone et al. [152], it is possible to considerably simplify them by using so called compatible sets. The concept of *compatible sets* (CS) is somewhat opposed to the one of collision domains, as a compatible set defines a feasible transmission scheme which is a group of simultaneous link transmissions along with the associated data rates, such that the corresponding SINR requirements are satisfied. For a detailed derivation of the CS formulation, please refer to [2]. Roughly speaking does it allow to consider non-compact formulations of the MMF problems based on lists $\mathcal{J}$ of compatible sets. To do that, the whole time of network operation has to be considered. Continuous variables define the portion of the network operation time utilized by the transmission scheme defined by each compatible set $j \in \mathcal{J}$. The difference between the previously discussed time slot (TS) formulation, the CS formulation yields better results as it allows for a more fine grained resource allocation. This is however due to the limited number of time slots only. TS with a sufficiently large number of time slots will give the same results as CS. The price to pay for bot the increased number of time slots and the CS formulation is however a significantly increased complexity.

5.5.4 Performance Comparison of the Optimization Algorithms

This section contains results obtained from the LP and MIP models implemented using Visual C++ under Windows XP, and executed on a single core Intel 2.4 GHz CPU with 3.92 GB RAM using the CPLEX 11.0 LP/MIP solver. As a

comparison, results from a simple heuristics are shown. This heuristic is based on LRA using $\Delta\gamma$ as discussed in Section 5.2: For each considered network snapshot, the existing links are assigned rates using $0 \leq \Delta\gamma \leq 5\,\text{dB}$ and the MMF per flow throughputs are computed by NLBA and ELBA. Out of the MMF flow throughput resulting from different values of $\Delta\gamma$, the one with the highest minimal throughput is chosen. The heuristic as well as the algorithms NLBA and ELBA are implemented in MATLAB under Windows XP and executed on a dual core Intel 3.16 GHz CPU with 3.72 GB RAM. In the following, these approaches are compared in terms of running times of the algorithms, the resulting MMF vectors, and the assigned link rates.

For solving the MMF optimization problems, the 6 different randomly generated example topologies shown in Figure 5.13 are used. The topologies are created by a binomial point process on a grid with 30×30 points in a similar way as discussed in Section 4.1.3. Both sparse and dense topologies created in a square with length 750 and 1050 m, respectively, are considered. For the sparse topologies shown in Figures 5.13(a)-5.13(d), a grid length of $d_x = 25$ m is used. With a probability of $p_f = 0.02$ and $p_g = 0.003$, each grid point is selected to be a non-gateway, or a gateway-node, respectively. For the dense topologies depicted in Figures 5.13(e)-5.13(f), $d_x = 30$ m, and the probabilities $p_f = 0.04$ and $p_g = 0.006$ are used. Paths rooted in the gateways are established by the MC routing protocol. The representation used in Figure 5.13 is the same which has been used earlier: mesh routers are represented by circles and mesh gateways by squares. Routing links are depicted by solid lines, all other links by dotted lines. The link colors used in Figure 5.13 moreover visualize the link rates resulting from a LRA with $\Delta\gamma = 0\,\text{dB}$. The link rates are captured by the colors and line widths which are summarized by the legend shown in Figure 5.13(a).

Let us start the discussion by comparing the times required for solving the two different variants of the MMF problem. These are summarized in Table 5.2. The first three columns of the table describe the considered networks and contain the network name, number of nodes, and number of links. The remaining four columns show the time the algorithms require for solving the two considered

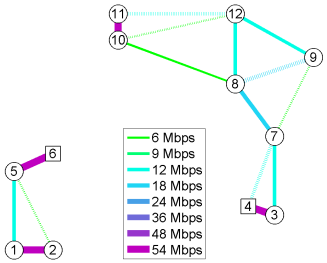

(a) $S1$

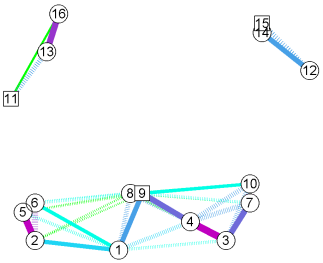

(b) $S2$

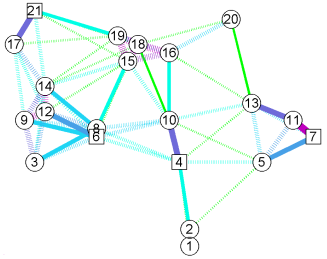

(c) $S3$

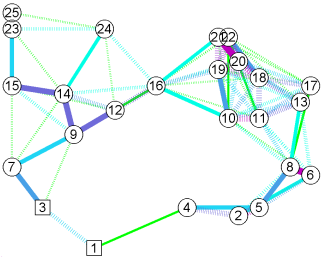

(d) $S4$

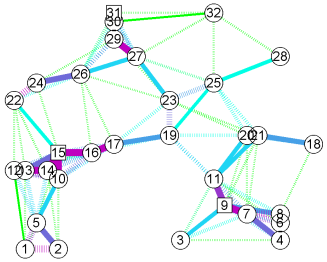

(e) $D1$

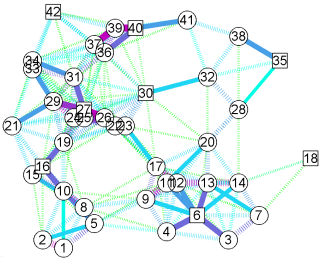

(f) $D2$

Figure 5.13: *Considered example networks*

network			Problem SA			
			TS		CS	
name	N	L	FI	SI	FI	SI
$S1$	12	10	3 sec	7 sec	7 sec	$<$ 1 sec
$S2$	16	13	1 h 13 min	17 sec	2 min 48 sec	1 min 12 sec
$S3$	21	17	3 h*	10 sec	19 min 59 sec	7 min 20 sec
$S4$	25	23	3 h*	30 sec	3 h*	3 h*
$D1$	32	29	3 h*	39 min 33 sec	3 h*	3 h*
$D2$	42	34	3 h*	48 min 53 sec	3 h*	3 h*

Table 5.2: *Run times, where "3h*" means not solvable within 3h*

problems SA/FI, and SA/SI with both TS and CS. Note that some results are marked with an asterisk. Those are the cases that were not solved within a time limit of three hours. Increasing the number of time slots and using a larger set of MCS increases the throughput of the minimal flow, but also the running time [2]. For this evaluation the number of considered time slots is set to 10 and the number of MCS is set to 8, in accordance to the MCS available for IEEE 802.11g.

As expected, the solution time increases with both the number of nodes and the density of the network. The obtained results confirm moreover the difficulty of the FI cases, thus justifying the simplified interference model. Moreover are the larger network instance not solvable by the CS formulation. The reason is that they require a branch-and-price algorithm, while for TS a branch-and-cut algorithm available in CPLEX is sufficient. The time required for computing the MMF solution for the NLBA/ELBA heuristics for all the considered topologies was in the worst case equal to 90 seconds, and in most cases much smaller. Thus the running time for the heuristics is not explicitly given.

Note that a time limit of 3 hours is in general to low for a network operator which aims at optimizing a WMN deployment. Under the guarantee that the effort is suitable for increasing the customer satisfaction and thereby the revenue, running times increasing up to a day are acceptable. For quickly assessing the approximate capacity of an intended combination of router deployments, this effort is not tolerable in contrast. Let us hence discuss if the results provided by

			Problem SA					
network			TS		CS		ELBA	NLBA
name	N	L	FI	SI	FI	SI	SI	SI
$S1$	12	10	0.6	0.6	0.73	0.73	0.66	0.97
$S2$	16	13	1.2	1.2	1.5	1.5	1.2	0.94
$S3$	21	17	0.9*	1.2	1.26	1.41	1.19	0.78
$S4$	25	23	0.15*	0.15	0.21*	0.22*	0.22	0.15
$D1$	32	29	0.0*	0.6	0.72*	0.74*	0.80	0.46
$D2$	42	34	0.0*	1.2	1.25*	1.26*	1.44	0.66

Table 5.3: *Maximal minimum flow [Mbps]*

the significantly faster heuristics are good enough for this purpose.

In Table 5.3, the bandwidths of the minimum flow resulting as a solution of the problems SA/FI, and SA/SI, provided by the TS and CS formulation along with the results from the heuristics and the throughput computed by NLBA and ELBA, are presented. As before, the cases that were not solved within a 3 hour time limit are marked with an asterisk.

Observe that the results obtained by CS are better than the results obtained by TS. This fact is self-explanatory, as the CS formulation allows for a more fine grained resource allocation. Another fact that might have been considered obvious is that results for SI are better than those for FI. This is due to the higher amount of interference disturbing a transmission which is considered by the FI, but not by the SI formulation. Even if the SI results are hence more different from the performance of a realistic WMN, simplifying the interference model was sometimes the only way to obtain a non-zero feasible result.

Comparing the results found by the heuristic method to the results found by the exact methods yields first that the results provided by ELBA are, except for $S1$, which has a particular shape and also results the FI formulation to be faster than SI (cf. Table 5.2) always superior to the ones found by NLBA. The reason for this is just the earlier observed more balanced flow assignment of ELBA which results in larger minimal but smaller maximal throughputs. Moreover are the results found by ELBA larger or equal than the optimal results found by the

TS formulation. The reason for the worse FI results is that often the exact algorithm times out, thus the obtained solution is not optimal. But even in the cases where the optimal solution does not time out, the bandwidth of the minimal flow found by ELBA is larger. The reason for this is the earlier discussed less optimal resource allocation of the TS formulation. For $S1$–$S3$ for which the CS formulation was solvable, the throughputs achieved by ELBA are significantly smaller. The outcome of this comparison is hence that the flow rate assignment found by ELBA is acceptable if a solution shall be found within a small amount of time. If more time is available, the CS formulation yields significantly better results.

Finally, let us discuss the outcome of the optimal and the heuristic solutions at the example of $S2$ in more detail. The x-axis of Figure 5.14(a) represents the 13 flows of the network ordered by increasing MMF throughput. The left y-axis visualizes the time needed to solve each MMF step to optimality. The y-axis on the right illustrates the throughputs obtained as optimal result from solving SA/SI via CS and results returned by ELBA and NLBA.

The results should be read as follows. The first value of the x-axis represents the minimum flow, the second entry contains the second minimum flow, etc. Observe that the heuristics do not provide optimal solutions in terms of max-min fairness, but result in larger maximal throughputs at the price of smaller minimal throughput. Thus, if a MMF rate assignment is the goal, as far as it is possible with respect to the running time, the exact approach should be used in order to solve the problem. Note that the time needed to solved the consecutive steps of MMFFA decreases. The reason is that the feasible capacity region is continuously diminished by additional constraints after each step of the algorithm.

The reason why the minimal per flow throughput, which is the optimization goal of MMFFA is significantly superior to the throughputs found by NLBA and ELBA is explained by the link rates which are assigned by the optimal solution. In Figure 5.14(b), the rates for all actives links of $S3$ found by using different values of $\Delta\gamma$ are compared against the optimal solution. The links are ordered by increasing link rate assigned for $\Delta\gamma = 0\,\text{dB}$. This representation confirms the earlier stated hypothesis that a network-wide value of $\Delta\gamma$ is inadequate. The

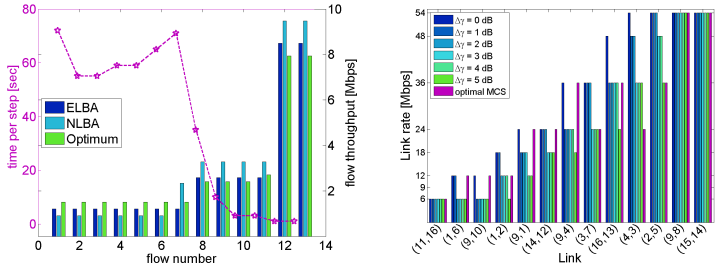

(a) MMF throughputs (b) Assigned link rates

Figure 5.14: *Comparison of optimal and heuristic results for S2*

example illustrates moreover that it is not straightforward to derive the link rates from characteristics like link lengths, collision domain size, distance to gateway nodes, or forwarding load. Systematically carrying out experiments similar than the one shown in Figure 5.14(b) is hence a promising research opportunity, as this will point out directions for finding new, better heuristics for networks where the optimal solutions do not provide results any more.

5.6 Concluding Remarks

In this chapter the potentials of a more conservative link rate assignment for increasing the performance of WMNs have been studied. This contribution breaks new ground, as prior works have never considered how the trade-off between link data rate and spatial reuse, i.e. smaller per-link throughput vs. higher number of parallel possible concurrent transmission may be used for WMN optimization. A key reason for this fact is the complexity of the problem which is overcome by the newly introduced methodology, whereof the heart is abstracting LRA by means of the interference buffer $\Delta\gamma$.

As a first step, the advantages and disadvantages of more conservative MCS

selection strategies, i.e. increasing values of $\Delta\gamma$ on the MMF network throughput has been investigated. The impact of $\Delta\gamma$ on the MMF throughput computed according to two considered different analytical load definitions is comparable. A result of this study is hence that using slightly more robust modulation and coding schemes than necessary is a suitable mechanism for increasing the overall MMF network throughput. Additionally, the results point out that for each network configuration an optimal protection threshold increasing the maximal achievable max-min fair throughput of all end-to-end flows can be found.

As most WMNs are operating with a contention based channel access scheme, as a second step, the effects of $\Delta\gamma$ in a random access IEEE 802.11 WMN have been examined. Stochastic geometry enables to analytically derive parametrization for the interference buffer $\Delta\gamma$ in order to find a collision minimizing link rate assignment for contention-based WMNs. In contrast to the theoretical benefits of this method in terms of increased link throughput, a simulation study reveals that an increase of $\Delta\gamma$ has significantly smaller positive effects on the throughput in realistic environments. The reason for this is that the type of failures which can be avoided using a more robust MCS have only a small share of the overall failure rate and their reduction does not pay in terms of throughput increase.

As a third step, a MIP formulation characterizing the link data rate capacity space and transmission scheduling within time slots and thereby allowing to formulate the maximization of the MMF throughput as an optimization has been introduced. A numerical study illustrates that assigning MCS on a per link basis allows for significantly larger minimum flow throughputs than LRA with a network-wide identical value of $\Delta\gamma$. The price for this throughput difference is the running time efficiency of the optimal solution approaches. It is still acceptable for small and medium sized networks, but significantly worse for larger network instances. The approach of using the heuristic approach for quickly assessing the estimated network capacity and subsequently using the optimal solution for the final network configuration is hence most promising.

Together, the three contributions prove a double edged impact of more robust link rate assignment for mesh networks. While a network-wide more robust

LRA is advantageous in networks where fairness can be guaranteed by means of a deterministic channel access, it allows only a marginal failure reduction in networks with a random channel access scheme. However, even in such networks it is advisable to assign the link rates with a small positive value for $\Delta\gamma$ in order to maximize the average network throughput. The analysis of the optimal solutions demonstrate the potential of a per-link LRA, as some links benefit to a higher degree from a protection than others. The value of this chapter is hence also that it points a way towards a previously unknown but very promising WMN optimization direction.

6 Conclusions

I do not think that the wireless waves that I have discovered will have any practical application.
Heinrich Hertz (1857 - 1894)

Pushing the digital frontier by integrating the Internet more seamlessly in the every day life will be one of the great challenges of the next decade. To this end, incorporating more facets of the physical world is as important as enabling a more flexible, cheap, widely available Internet access. In contrast to the above cited opinion of Hertz, wireless communication will be the key enabling technology for improving the Internet-connectivity of both, "things" and people.

This monograph was dedicated to the study of the two types of wireless networks which are considered most appropriate for attaining those goals. While wireless sensor networks enhance the Internet's reach by providing data about the properties of the environment, wireless mesh networks extend the Internet access possibilities beyond the wired backbone. Both WSNs and WMNs strongly differ from the conventional, well-researched network types. This on the one hand necessitates introducing and evaluating the viability of innovative performance evaluation metrics, but on the other hand opens the opportunity for novel optimization approaches.

Even if traditional networking metrics like packet loss, or delivery speed are still of interest for analytical wireless sensor networking research, accurately modeling the energy consumptions is the key issue. The WSN research pioneers hence came up with models describing the communication costs in terms of energy consumptions. Since then, countless contributions to WSN engineer-

ing were built on these models, as it has been a common understanding that the *quantitative* exactness of communication costs is less relevant for theoretical research. At the other end of the spectrum, researchers aim at modeling the sensor node energy consumptions on chip level. Systematically studying the effect of such results on the analysis of large scale WSN deployments has however never been done, a deficiency which is remedied by this monograph. A comparison of energy minimizing routing topologies created according to more theoretical or more hardware-oriented energy consumption models revealed a multitude of differences and thereby proved the utmost importance of exactly modeling the communication costs.

This study was completed by a more thorough examination of the impact of the MAC layer efficiency on the daily energy consumptions of a sensor node. The introduction of this factor, which captures the amount of time a sensor node transceiver actually has to be active for fulfilling its communication duties, is a further merit of this work. Previously, theoretical works assumed a perfectly efficient MAC layer enabling the sensor node to just spend energy on receiving a packet, without being forced to additionally listen to the channel. Including the effects of a more realistic, lower efficiency is however suitable for inversing the answer to the question whether a WSN design option increases the energy-efficiency or not. If results applying to a realistic setting are required, this factor has always to be included.

These considerations enabled to attack another, less abstract problem. Turning visions like the Internet of Things into reality, and seamlessly integrating sensor networks in the Internet, requires a standardized communication layer. IEEE 802.15.4 together with ZigBee might play this role, but is only slowly accepted by the WSN community. The root cause for this non-acceptance is that neither IEEE 802.15.4 nor ZigBee have been designed for large multi-hop networks with regularly sleeping devices. A potpourri of problems results from this design paradigm and blocks the way towards standards-based WSNs. Clearing this way by identifying and presenting simulatively verified solutions for overcoming three of the blocking barriers is another contribution of this work.

Firstly, this monograph showed how the network initialization can be successfully and efficiently carried out, if the IEEE 802.15.4 procedure is slightly modified. Secondly, it presented an adaptation of the ZigBee routing layer allowing a fast, reliable multi-hop data delivery in a network with periodically sleeping nodes. And thirdly, it introduced a self-organizing distributed sleep-scheduling solution which works atop the IEEE 802.15.4 MAC layer and thereby maintains the standard compliance while enabling to efficiently operate large scale low-power IEEE 802.15.4 sensor networks.

For wireless mesh networks, both energy efficiency and the need for a standardized communication layer are of minor interest, whereas the network performance is more in the center of interest. This is most often indicated in terms of capacity which in turn is best characterized by the end-to-end throughput. Due to the increasing WMN complexity involving not only multiple link rates, but also multiple Internet gateways and due to the WMN immanent fairness paradigm, estimating the capacity of state-of-the-art WMNs is non-trivial. The algorithms for computing the max-min fair network throughput introduced by this work are hence a valuable tool for wireless mesh network engineering, as they allow indicating an upper bound for the capacity achievable under fairness constraints. The additional value of these algorithms is that they enable assessing the impact of different collision domain and link load definitions provided by the literature.

The max-min fair network throughput is the first metric which is used for thoroughly studying the impact of systematically assigning more robust link rates than actually necessary, thereby allowing to exploit the trade-off between spatial reuse and per-link throughput. As this is a novel idea for WMN optimization, the introduction of an analytical formulation was necessary. This enabled to show that a network-wide slightly more conservative link rate assignment than necessary increases the throughput of a WMN where max-min fairness is guaranteed by a dedicated channel access scheme. For the case where all mesh nodes compete for the channel access, and fairness is not given, a link rate assignment paradigm protecting each transmission against one interferer has been derived by means of stochastic geometry. A simulation study revealed, however, that the

price for this collision protection in terms of decreased link rate throughput is too high in order to make the approach beneficial for the end-to-end throughput.

Finally, the suitability of dedicated link rate assignment for optimal WMN configurations has been proven. A mixed integer programming solution enabled to determine the optimal combination of link rate assignment and channel access schedule with the goal of maximizing the max-min fair network throughput. The resulting optimization space is huge, consequently, only small network instances could be optimized. The results do however point out that more sophisticated link rate assignment schemes merit the effort of the research community, as they are suitable for significantly increasing the network performance.

Together, the contributions of this monograph can be definitively seen as one step of the journey towards the Internet of the future. This step consists of providing novel insights on both modeling and optimizing, both wireless sensor and wireless mesh networks which are indispensable for integrating the Internet more tightly in our daily life. Despite its technical depth, this monograph was only able to scratch the surface of the vast optimization space which might be exploited for making WSNs and WMNs even more valuable for the future Internet. The additional merit of this monograph is hence that it fosters the fundamental understanding of these complex wireless network types and thereby encourages researchers to set off for new shores.

Nomenclature

General

d	(transmission) distance
$d_{i,j}$	euclidean distance between nodes i and j
d_0	reference distance
P_t	transmission output power
T	basic time unit or clock of the network
$P(Y)$	probability of event Y
F_X	CDF of random variable X
$E[X]$	mean, or expected value of random variable X

The following variables are unique within the sensor, or mesh networking context, only.

WIRELESS SENSOR NETWORKS

Chapter 2: Energy Consumption Modeling

c	channel characteristics
$E(d)$	amount of energy required for transmitting and receiving a bit over a distance d
E_0	distance-independent energy consumptions required for transmitting a bit
$E_t(c, d)$	amount of energy required for a transmitting a bit over a distance d over the channel characterized by c

E_r	distance-independent energy consumptions required for receiving a bit
t_{bit}	time required for transmitting a bit
$E_{norm}(d)$	normalized transmission costs
η	drain efficiency of the power amplifier
t_i^t	fraction of T node i spends in transmit state
t_i^r	fraction of T node i spends in receive state
t_i^s	fraction of T node i spends in sleep state
$P_t^{el}(P_t)$	electrical (input) power required for a transmission with output power P_t
P_r^{el}	electrical power required for receiving
P_s^{el}	electrical power required in sleep state
E_i^{radio}	daily radio-related energy consumptions of node i
Π_i	number of packets sent by node i during T
λ	number of packets each node creates during T
ξ_i	number of children node i has in the routing tree
t_{dat}	time required for sending or receiving a data packet
t_{disc}	time required for discarding a packet
ε	MAC layer efficiency
Ξ_i	number of packets node i receives during T
ϑ_{ji}	boolean variable expressing whether messages sent by j are overheard by i
l	length of WSN deployment square
ρ	density of WSN deployment

Chapter 3.2: IEEE 802.15.4 Association

t_{scan}	time spent for a channel scan
a	association retry interval
t_{alt}	altruistic period
dep	deployment strategy of the sensor network
θ	average node degree

ν	activity ratio of a duty cycling sensor node
σ	coefficient of variation of node activation time
T_0	initial tolerance time
$rand$	randomization of a
gr	greedy association
alt	altruistic association
s_A	association success
t_A	association time
E_A	association energy consumptions
$e_x(y)$	main effect of factor x on metric y
$e_{xy}(z)$	interaction effect of factors x and y on metric z

Chapter 3.3: Smooth AODV

g	guard interval of smooth AODV
L_T	LLF threshold of smooth AODV
n_c	number of LLFs observed by smoot AODV
p_l	packet length
Δt	packet inter send time
n_A	number of AODV packets each node has to send
t_{sim}	simulation duration
E_b	amount of energy required for until one bit reaches the sink
δ	e2e delay, time required until a packet reaches the sink
h	number of hops between source and sink

Chapter 3.4: CLS

o_{uv}	temporal offset between nodes u and v
d_{min}	lower bound for temporal offset
d_{max}	upper bound for temporal offset
δ_1	base delay component of δ under CLS
δ_2	intra-node delay component of δ under CLS
δ_3	inter-node delay component of δ under CLS

WIRELESS MESH NETWORKS

Chapter 4.1: Formal Description of a WMN

$\mathcal{N}$	set of mesh nodes
N	number of mesh nodes
$\mathcal{L}$	set of links
L	number of links
(i, j)	link between nodes i and j
$r_{i,j}$	data rate of link (i, j)
$q_{i,j}$	channel assigned to link (i, j)
$\mathcal{F}$	set of non-gateway mesh nodes
F	number of non-gateway mesh nodes
$\mathcal{G}$	set of gateway mesh nodes
G	number of gateway mesh nodes
$\mathcal{P}$	set of static routing paths
p_f	(routing) path between node f and its gateway node
$P_r^{i,j}$	power received at node j when i is transmitting
P_t	transmission output power
$P_g^{i,j}$	path gain between i and j
α	path loss exponent
K	unitless constant capturing antenna characteristics and the average channel attenuation
β	simplification for path loss model: $\beta = K d_0^{\alpha}$
N_0	ambient noise power
I	interference
$I_{i,j}$	interference a transmission from i to j has to suffer
$\mathcal{Z}$	set of interferers
Z	number of interferers
$\mathcal{M}$	set of available MCS

$\gamma'_{i,j}$	SNR of a transmission from i to j
$\gamma_{i,j}$	SINR of a transmission from i to j
γ^*_m	SINR requirement of MCS m
$\gamma^*_{i,j}$	SINR requirement of link (i,j)
$\Phi = \{X_i\}$	point process modeling the mesh node locations
l_F	grid length for positions of the non-gateway mesh nodes
l_G	grid length for positions of the gateway mesh nodes

Chapter 4.2: MMF Flow Rate Allocation

b_f	(application layer) rate of flow f
$\mathcal{D}_{i,j}$	collision domain of link (i,j)
$\mathcal{D}^+_{i,j}$	multi-channel collision domain of link (i,j)
$\zeta_{k,i,j}$	binary variable indicating if a transmission of flow k takes the hop from node i to node j
$\nu_{i,j}$	number of transmissions on link (i,j)
$\mu_{i,j}$	nominal load of collision domain $\mathcal{D}_{i,j}$
$\psi_{i,j}$	percentage of unassigned nominal capacity of $\mathcal{D}_{i,j}$
$\phi_{i,j}$	throughput share of link (i,j)
$\mathcal{F}^*$	set of flows without rate allocation
$\mathcal{L}^*$	set of links carrying flows with unassigned rates
$l^\dagger$	bottleneck link
$\mathcal{B}$	set of bottlenecked flows
$\mathcal{C}$	clique
$\mathcal{G}_\mathcal{C}$	contention graph
$\Omega_\mathcal{C}$	clique corpus
$\mu_\mathcal{C}$	effective load of $\mathcal{C}$
$\psi_\mathcal{C}$	free capacity of $\mathcal{C}$
$\phi_\mathcal{C}$	rate share per link in $\mathcal{C}$
Ω^*_C	set of unassigned cliques
$\mathcal{C}^\dagger$	bottleneck clique
$\mathcal{K}_{i,j}$	set of flows using link (i,j)

$\mathcal{K}^a_{i,j}$	set of flows using link (i,j) having a rate allocation
$\mathcal{K}^u_{i,j}$	set of flows using link (i,j) without rate allocation
$\upsilon_{i,j}$	activity percentage of link (i,j)
$\upsilon_{\mathcal{C}}$	activity percentage of $\mathcal{C}$
$b_{\mathcal{C}}$	maximum rate available for unassigned flows in $\mathcal{C}$

Chapter 5.2: Link Rate Assignment

W	channel bandwidth
C	Shannon capacity
$\mathcal{Q}$	function mapping link SINR to link data rate
$\Delta\gamma$	(network-wide) interference buffer
$\Delta\gamma_{i,j}$	interference buffer of link (i,j)
$\mathcal{Q}_{IB}$	function mapping link SINR, and interference buffer to link data rate
$\mathcal{R}$	link rate reduction
$\mathcal{K}$	set of edges in the contention graph $\mathcal{G}_{\mathcal{C}}$

Chapter 5.3: LRA under MMF

$\tau_n(f)$	nominal throughput of flow f
$\tau_e(f)$	effective throughput of flow f

Chapter 5.4: LRA under IEEE 802.11

m_C	MCS used for sending RTS and CTS messages
L_k	distance to a node kth nearest neighbor
$C(p,x)$	circle around point p with radius x
L^*_k	distance to a node kth nearest interferer
$A^*_r(x)$	area with maximal distance x to node r, possible interferers might lie in
${}^aA^*_r(x)$	$A^*_r(x)$ if the channel access is plain CSMA/CA
${}^bA^*_r(x)$	$A^*_r(x)$ if RTS/CTS is used, and only the CTS blocks the channel

${}^{c}A_r^*(x)$	$A_r^*(x)$ if RTS/CTS is used, and both RTS and CTS block the channel
$L_S(\Delta\gamma)$	if $\Delta\gamma$ is used for LRA, lower bound for the distance to one interferer which can still be tolerated
$L_I(\Delta\gamma)$	lower bound for the distance to any interferer if RTS/CTS is used
$\tilde{\Delta}\gamma(Z)$	estimation for $\Delta\gamma(Z)$
A_1, A_2	circle segments required for computing ${}^{c}A_r^*(x)$
ω_1, ω_2	angles required for computing ${}^{c}A_r^*(x)$
g, h, j	distances required for computing ${}^{c}A_r^*(x)$
$t_{tx}(p, m)$	time required for transmitting a packet with payload p and MCS m
t_{bo}	backoff time
ρ	probability of one df failure during a transmission
$\tau(m)$	throughput achieveable under MCS m
F_N	receiver noise figure

Chapter 5.5: LRA for MMF Throughput Optimization

$s(l)$	start node of link l
$e(l)$	end node of link l
$\chi(i)$	set of all links incident to node i
$\chi^+(i)$	set of outgoing links of node i
$\chi^-(i)$	set of incoming links to node i
$\mathcal{T}$	set of timeslots
Δt	length of a timeslot
Y_{lt}	binary variable indicating whether link l is active in time slot t
y_{lt}^m	binary variable indicating whether link l is active in time slot t and uses MCS m
X_{it}	binary variable indicating whether node i is active in time slot t

x_{it}^m	binary variable indicating whether node i in time slot t in time slot t and uses MCS m
M_l^m	nonnegative integer variable indicating which MCS is used by link l in all time slots
r_{lt}	nonnegative rate of link l achieved in time slot t
c_l	nonnegative integer capacity of link l
z_{lit}^m	binary variable expressing the product $y_{lt}^m \cdot X_{it}$
Γ	feasible set of link capacity reservations
Γ_{static}^{FI}	Γ for static link rate assignment and the full interference model
Γ_{static}^{SI}	Γ for static link rate assignment and the simplified interference model
$\mathcal{I}_l$	indices of paths that contain link l
$[\tau]$	lexicographically sorted vector of path-flows
$\mathcal{J}$	lists of compatible sets
d_x	grid length used for topology generation
p_f	probability for a grid point to be a non-gateway mesh node
p_g	probability for a grid point to be a gateway mesh node

Acronyms

AARF	adaptive ARF (rate adaptation algorithm)
A-ELBA	ELBA with asymmetric collision domains
AMC	adaptive modulation and coding
A-NLBA	NLBA with asymmetric collision domains
AODV	ad hoc on-demand distance vector routing
AP	access point
APL	application layer
APS	application support sub-layer
AR	adaptive resynchronization
ARF	auto rate fallback (rate adaptation algorithm)
ASK	amplitude phase shift keying
AWGN	additive white Gaussian noise
B.A.T.M.A.N	better approach to mobile adhoc networking
BPSK	binary phase shift keying
CAP	contention access period
CBR	constant bit rate
CDF	cumulative probability distribution function
CFP	contention free period
CLS	cross-layer sleep scheduling algorithm
CPU	central processing unit
CS	compatible sets (approach)
CSMA/CA	carrier sense multiple access/collision avoidance
CSS	chirp spread spectrum

db	disturbed backoff
DC	direct current
DCF	distributed coordination function
df	data failure
DQPSK	differential quadrature phase shift keying
DSL	digital subscriber line
DSSS	direct sequence spread spectrum
e2e	end-to-end
ELBA	effective load based algorithm
ESN	environmental sensor network
FER	frame error rate
FFD	full-function device
FI	full interference (model)
GFSK	Gaussian frequency-shift keying
GTS	guaranteed time slot
HM	hardware-oriented model for transmission energy consumptions
IEEE	Institute of Electrical and Electronics Engineers
IETF	Internet Engineering Task Force
IP	Internet protocol
ISM band	industrial, scientific and medical band
LLF	link layer feedback
LP	linear programming
LRA	link rate assignment
MAC	medium access control
MANET	mobile ad hoc network
MC	maximum capacity (routing algorithm)
MCS	modulation and coding scheme
MH	minimum hop routing
minH^{-}	minimum hop topology for minimal feasible output powers

minH$^+$	minimum hop topology for maximal feasible output powers
MIP	mixed-integer programming
MMF	max-min fair
MMFFA	max-min fair flow allocation algorithm
MPSK	m-ary phase shift keying
MTE	minimum total energy tree
NAC	neighbor aware resynchronization
NAV	network allocation vector
NLBA	nominal load based algorithm
NWK	network layer
OFDM	orthogonal frequency-division multiplexing
OLSR	optimized link state routing
O-QPSK	offset quadrature phase shift keying
PAN	personal area network
PDR	packet delivery ratio
PHY	physical layer
PMP	point-to-multipoint
PRC	power and rate control algorithm
QoS	qualiy of service
R	random routing
RAM	random-access memory
RFD	reduced-function device
RFID	radio-frequency identification
RRAA	robust rate adaptation algorithm
RREP	route reply message
RREQ	route request message
RRER	route error message
RTS/CTS	request to send / clear to send (handshaking)
S-ELBA	ELBA with symmetric collision domains
sf	signaling failure

SI	simplified interference (model)
SINR	signal to interference and noise ratio
S-NLBA	NLBA with symmetric collision domains
SNR	signal to noise ratio
TCP	transmission control protocol
TDMA	time division multiple access
TM	theoretical model for transmission energy consumptions
TS	time slot (approach)
UDP	user datagram protocol
UWB	ultra-wide band
WMN	wireless mesh network
WPAN	wireless personal area network
WS	wakeup signal
WSN	wireless sensor network
ZDO	ZigBee device object

Bibliography of the Author

— Journals —

[1] R. Pries, D. Staehle, B. Staehle, and P. Tran-Gia, "On Optimization of Wireless Mesh Networks using Genetic Algorithms," *International Journal On Advances in Internet Technology*, vol. 1&2, July 2010.

[2] M. Pióro, M. Żotkiewicz, B. Staehle, D. Staehle, and D. Yuan, "On Max-Min Fair Flow Optimization in Wireless Mesh Networks," *Ad Hoc Networks, Special Issue on Models and Algorithms for Wireless Mesh Networks*, 2011, to appear.

[3] B. Staehle, F. Wamser, M. Hirth, D. Stezenbach, and D. Staehle, "AquareYoum: Application and Quality of Experience-Aware Resource Management for YouTube in Wireless Mesh Networks," *PIK - Praxis der Informationsverarbeitung und Kommunikation*, 2011, to appear.

— Conference Papers —

[4] B. Emmert and A. Binzenhöfer, "Efficient Link Failure Detection and Localization using P2P-Overlay Networks," in *Proceedings of the First International Workshop on Dependable and Sustainable Peer-to-Peer Systems*, Vienna, Austria, April 2006.

[5] B. Emmert and O. Jorns, "Prepaid Peer-to-Peer Services," in *Proceedings of the 6th IEEE International Conference on Peer-to-Peer Computing*,

Cambridge, UK, September 2006.

[6] B. Staehle, T. Hoßfeld, M. Kuhnert, and N. Vicari, "Enabling the Sleep Mode in Non-beaconed 802.15.4 Multihop Networks - A Simulative Investigation," in *Proceedings of the 6. GI/ITG KuVS Fachgespräche Drahtlose Sensornetze*, Aachen, Germany, July 2007.

[7] B. Emmert, A. Binzenhöfer, D. Schlosser, and M. Weiß, "Source Traffic Characterization for Thin Client Based Office Applications," in *Proceedings of the 13th EUNICE Open European Summer School and IFIP TC6.6 Workshop on Dependable and Adaptable Networks and Services*, Twente, the Netherlands, July 2007.

[8] B. Staehle and D. Staehle, "Impact of Energy Models on Energy Efficient Sensor Network Routing," in *Proceedings of the 4th IEEE International Conference on Mobile Ad-hoc and Sensor Systems*, Pisa, Italy, October 2007.

[9] D. Schlosser, A. Binzenhöfer, and B. Staehle, "Performance Comparison of Windows-based Thin-Client Architectures," in *Proceedings of the 2007 Australasian Telecommunication Networks and Applications Conference*, Christchurch, New Zealand, December 2007.

[10] B. Staehle, A. Binzenhöfer, D. Schlosser, and B. Boder, "Quantifying the Influence of Network Conditions on the Service Quality Experienced by a Thin Client User," in *Proceedings of the 14. GI/ITG Konferenz Messung, Modellierung und Bewertung von Rechen- und Kommunikationssystemen*, Dortmund, Germany, April 2008.

[11] B. Staehle, T. Hoßfeld, N. Vicari, and M. Kuhnert, "A Cross-Layer Approach for Enabling Low Duty Cycled ZigBee Mesh Sensor Networks," in *2008 International Symposium on Wireless Pervasive Computing*, Santorini, Greece, May 2008.

[12] B. Staehle, “A Closer Look at the Association Procedure in Low Power 802.15.4 Multihop Sensor Networks,” in *Proceedings of the 7. GI/ITG KuVS Fachgespräche Drahtlose Sensornetze*, Berlin, Germany, September 2008.

[13] ——, “Optimizing the Association Procedure for Low-Power 802.15.4 Nonbeacon Sensor Networks,” in *Proceedings of the 2009 IFIP International Conference on Networking*, Aachen, Germany, May 2009.

[14] R. Pries, D. Staehle, M. Stoykova, B. Staehle, and P. Tran-Gia, “A Genetic Approach for Wireless Mesh Network Planning and Optimization,” in *Proceedings of the First International Workshop on Planning and Optimization of Wireless Communication Networks*, Leipzig, Germany, 2009.

[15] ——, “Wireless Mesh Network Planning and Optimization through Genetic Algorithms.” in *Proceedings of the Second International Conference on Advances in Mesh Networks*, Athens, Greece, June 2009.

[16] B. Staehle, D. Staehle, and R. Pries, “Effects of Link Rate Assignment on the Max-Min Fair Throughput of Wireless Mesh Networks,” in *Proceedings of the 21st International Teletraffic Congress*, Paris, France, September 2009.

[17] B. Staehle, D. Staehle, R. Pries, M. Hirth, A. Kassler, and P. Dely, “Measuring One-Way Delay in Wireless Mesh Networks - An Experimental Investigation,” in *Proceedings of the 4-th ACM Workshop on Performance Monitoring and Measurement of Heterogeneous Wireless and Wired Networks*, Tenerife, Canary Islands, Spain, October 2009.

[18] D. Schlosser, B. Staehle, A. Binzenhöfer, and B. Boder, “Improving the QoE of Citrix Thin Client Users,” in *Proceedings of the 2010 IEEE International Conference on Communications*, Cape Town, South Africa, May 2010.

[19] M. Hirth, B. Staehle, F. Wamser, R. Pries, and D. Staehle, "QoE Prediction for Radio Resource Management," in *Proceedings of the 6th International Conference on Testbeds and Research Infrastructures for the Developement of Networks & Communities*, Berlin, Germany, May 2010.

[20] D. Staehle, B. Staehle, and R. Pries, "Max-Min Fair Throughput in Multi-Gateway Multi-Rate Mesh Networks," in *Proceedings of the 2010-Spring IEEE Vehicular Technology Conference*, Taipei, Taiwan, May 2010.

[21] B. Staehle, M. Hirth, R. Pries, F. Wamser, and D. Staehle, "YoMo: A YouTube Application Comfort Monitoring Tool," in *Proceedings of the 2010 Workshop on Quality of Experience for Multimedia Content Sharing*, Tampere, Finland, June 2010.

[22] B. Staehle, D. Staehle, and R. Pries, "Effects of Link Rate Assignment in IEEE 802.11 Mesh Networks," in *Proceedings of the 16th European Wireless Conference*, Lucca, Italy, 2010.

[23] B. Staehle and D. Staehle, "Starting Up Multi-Gateway WSNs," in *Proceedings of the 6th International Wireless Communications and Mobile Computing Conference*, Caen, France, June 2010.

[24] B. Staehle, F. Wamser, R. Pries, D. Staehle, C. Mannweiler, A. Klein, J. Schneider, and H. Schotten, "Application- and Context-Aware Radio Resource Management for Future Wireless Networks," in *Proceedings of the 2010 joint ITG, ITC, and Euro-NF Workshop "Visions of Future Generation Networks"*, Würzburg, Germany, August 2010.

[25] B. Staehle, M. Leimbach, and D. Staehle, "Tuontu: A Tool for Evaluating the Impact of Wireless Sensor Network Design Alternatives," in *Proceedings of the 9. GI/ITG KuVS Fachgespräche Sensornetze*, Würzburg, Germany, September 2010.

[26] R. Pries, V. Wendel, B. Staehle, and D. Staehle, “Genetic Algorithms for WMN Planning,” in *Proceedings of the 13-th ACM International Conference on Modeling, Analysis and Simulation of Wireless and Mobile Systems*, Bodrum, Turkey, October 2010.

[27] D. Fu, B. Staehle, R. Pries, and D. Staehle, “On the Potential of IEEE 802.11s Intra-Mesh Congestion Control,” in *Proceedings of the 13-th ACM International Conference on Modeling, Analysis and Simulation of Wireless and Mobile Systems*, Bodrum, Turkey, October 2010.

[28] B. Staehle, M. Hirth, R. Pries, F. Wamser, and D. Staehle, “Aquarema in Action: Improving the YouTube QoE in Wireless Mesh Networks,” in *Proceedings of the 2011 Baltic Congress on Future Internet Communications*, Riga, Latvia, February 2011.

General References

[29] Bundesverband Informationswirtschaft, Telekommunikation und neue Medien e.V., “Erstmals mehr als 50 Millionen Deutsche im Internet,” Presseinformation, April 2011.

[30] A. Goldsmith, “The Next Wave in Wireless Technology: Challenges and Solutions,” Keynote held at 16th European Wireless Conference, Lucca, Italy, April 2010.

[31] G. P. Fettweis, F. Denzin, N. Michailow, K. Schlöder, D. Seul, I. Wolff, and E. Zimmermann, “M2M - Maschine-zu-Maschine- Kommunikation,” VDE-Positionspapier, February 2011.

[32] IEEE Computer Society, “IEEE Standard for Information Technology – Telecommunication and information exchange between systems – Local

and metropolitan area networks – Specific requirements. Part 15.4: Wireless Medium Access Control (MAC) and Physical Layer (PHY) Specifications for Low-Rate Wireless Personal Area Networks (WPANs)," September 2006.

[33] ZigBee Alliance, "ZigBee Specification," Document 053474r17, January 2008.

[34] J. Kahn, R. Katz, and K. Pister, "Next Century Challenges: Mobile Networking for "Smart Dust"," in *Proceedings of the 5th Annual ACM/IEEE international Conference on Mobile Computing and Networking*, Seattle, WA, USA, August 1999.

[35] W. Heinzelman, A. Chandrakasan, and H. Balakrishnan, "Energy-Efficient Communication Protocol for Wireless Microsensor Networks," in *Proceedings of the 33rd Hawaii International Conference on System Sciences*, Maui, HI, USA, January 2000.

[36] J. Hill, R. Szewczyk, A. Woo, S. Hollar, D. Culler, and K. Pister, "System Architecture Directions for Networked Sensors," in *Proceedings of the 9th International Conference on Architectural Support for Programming Languages and Operating Systems*, Cambridge, MA, USA, 2000.

[37] N. Gershenfeld, R. Krikorian, and D. Cohen, "The Internet of Things," *Scientific American*, vol. 291, no. 4, 2004.

[38] J. Rabaey, J. Ammer, J. da Silva Jr, and D. Patel, "PicoRadio: Ad-hoc Wireless Networking of Ubiquitous Low-Energy Sensor/Monitor Nodes," in *Proceedings of the IEEE Computer Society Workshop on VLSI 2000*, Orlando, FL, USA, April 2000.

[39] I. F. Akyildiz, W. Su, Y. Sankarasubramaniam, and E. Cayirci, "A Survey on Sensor Networks," *IEEE Communications Magazine*, vol. 40, no. 8, August 2002.

[40] C. Intanagonwiwat, R. Govindan, and D. Estrin, "Directed Diffusion: A Scalable and Robust Communication Paradigm for Sensor Networks," in *Proceedings of the 6th Annual ACM/IEEE International Conference on Mobile Computing and Networking*, Boston, MA, USA, August 2000.

[41] K. Langendoen, "Medium Access Control in Wireless Sensor Networks," in *Medium Access Control in Wireless Networks, Volume II: Practice and Standards*. Nova Science Publishers, 2007.

[42] J. Yick, B. Mukherjee, and D. Ghosal, "Wireless Sensor Network Survey," *Computer Networks*, vol. 52, no. 12, 2008.

[43] S. Kim, S. Pakzad, D. Culler, J. Demmel, G. Fenves, S. Glaser, and M. Turon, "Health Monitoring of Civil Infrastructures Using Wireless Sensor Networks," in *Proceedings of the 6th International Conference on Information Processing in Sensor Networks*, Cambridge, MA, USA, April 2007.

[44] D. Doolin and N. Sitar, "Wireless Sensors for Wildfire Monitoring," in *Proceedings of the 2005 SPIE Symposium on Smart Structures & Materials*, San Diego, CA, USA, March 2005.

[45] T. He, S. Krishnamurthy, L. Luo, T. Yan, L. Gu, R. Stoleru, G. Zhou, Q. Cao, P. Vicaire, J. A. Stankovic, T. F. Abdelzaher, J. Hui, and B. Krogh, "VigilNet: An Integrated Sensor Network System for Energy-Efficient Surveillance," *ACM Transactions on Sensor Networks*, vol. 2, no. 1, 2004.

[46] G. Wittenburg, K. Terfloth, F. Villafuerte, T. Naumowicz, H. Ritter, and J. Schiller, "Fence Monitoring - Experimental Evaluation of a Use Case for Wireless Sensor Networks," in *Proceedings of the 4th European Conference on Wireless Sensor Networks*, Delft, The Netherlands, January 2007.

[47] J. Hart and K. Martinez, "Environmental Sensor Networks: A Revolution in the Earth System Science?" *Earth-Science Reviews*, vol. 78, July 2006.

[48] D. Goense, J. Thelen, and K. Langendoen, "Wireless Sensor Networks for Precise Phytophthora Decision Support," in *Proceedings of the 5th European Conference on Precision Agriculture*, Uppsala, Sweden, June 2005.

[49] G. Virone, A. Wood, L. Selavo, Q. Cao, L. Fang, T. Doan, Z. He, R. Stoleru, S. Lin, and J. Stankovic, "An Assisted Living Oriented Information System Based on a Residential Wireless Sensor Network," in *Proceedings of the First Transdisciplinary Conference on Distributed Diagnosis and Home Healthcare*, Arlington, VA, USA, April 2006.

[50] K. Lorincz, D. J. Malan, T. R. Fulford-Jones, A. Nawoj, A. Clavel, V. Shnayder, G. Mainland, M. Welsh, and S. Moulton, "Sensor Networks for Emergency Response: Challenges and Opportunities," *IEEE Pervasive Computing*, vol. 3, no. 4, October 2004.

[51] I. Akyildiz, D. Pompili, and T. Melodia, "Underwater Acoustic Sensor Networks: Research Challenges," *Ad Hoc Networks*, vol. 3, February 2005.

[52] I. Akyildiz and E. Stuntebeck, "Wireless Underground Sensors Networks: Research Challenges," *Ad Hoc Networks*, vol. 4, no. 6, July 2006.

[53] MEMSIC Inc., "IRIS - Wireless Measurement System," Datasheet.

[54] IEEE Computer Society, "IEEE Standard for Information Technology – Telecommunications and information exchange between systems – Local and metropolitan area networks – Specific requirements. Part 11: Wireless LAN Medium Access Control (MAC) and Physical Layer (PHY) Specifications," June 2007.

[55] ——, "IEEE Standard for Information Technology – Telecommunication and information exchange between systems – Local and metropolitan area

networks – Specific requirements. Part 16: Air Interface for Broadband Wireless Access Systems," IEEE Computer Society, May 2009.

[56] J. Al-Karaki and A. Kamal, "Routing Techniques in Wireless Sensor Networks: A Survey," *IEEE Wireless Communications*, vol. 11, no. 6, December 2004.

[57] K. Akkaya and M. Younis, "A Survey on Routing Protocols for Wireless Sensor Networks," *Ad Hoc Networks*, vol. 3, no. 3, May 2005.

[58] Y. Yu, R. Govindan, and D. Estrin, "Geographical and Energy Aware Routing: A Recursive Data Dissemination Protocol for Wireless Sensor Networks," UCLA Computer Science Department, Tech. Rep. UCLA/CSD-TR-01-0023, May 2001.

[59] J. Jones and M. Atiquzzaman, "Transport Protocols for Wireless Sensor Networks: State-of-the-Art and Future Directions," *International Journal of Distributed Sensor Networks*, vol. 3, no. 1, 2007.

[60] J. Paradiso and T. Starner, "Energy Scavenging for Mobile and Wireless Electronics," *IEEE Pervasive Computing*, vol. 4, no. 1, 2005.

[61] C. Chiasserini and M. Garetto, "Modeling the Performance of Wireless Sensor Networks," in *Proceedings of the 23rd Conference of the IEEE Communications Society*, Hong Kong, China, March 2004.

[62] S. Lindsey and C. Raghavendra, "PEGASIS: Power-Efficient Gathering in Sensor Information Systems," in *Proceedings of the 2002 IEEE Aerospace Conference*, Big Sky, MT, USA, March 2002.

[63] T. Melodia, D. Pompili, and I. Akyildiz, "On the Interdependence of Distributed Topology Control and Geographical Routing in Ad Hoc and Sensor Networks," *IEEE Journal on Selected Areas in Communications*, vol. 23, no. 3, March 2005.

[64] W. Heinzelman, A. Chandrakasan, and H. Balakrishnan, "An Application-Specific Protocol Architecture for Wireless Microsensor Networks," *IEEE Transactions on Wireless Communications*, vol. 1, no. 4, 2002.

[65] Q. Wang, M. Hempstead, and W. Yang, "A Realistic Power Consumption Model for Wireless Sensor Network Devices," in *Proceedings of the 3rd Annual IEEE Conference on Sensor, Mesh and Ad Hoc Communications and Networks*, Reston, VA, USA, September 2006.

[66] Texas Instruments, "CC1000 Single Chip Very Low Power FRF Transceiver," Data sheet.

[67] ——, "2.4 GHz IEEE 802.15.4 / ZigBee-ready RF Transceiver," Data sheet.

[68] M. Haenggi, "The Impact of Power Amplifier Characteristics on Routing in Random Wireless Networks," in *Proceedings of the 2003 Global Telecommunications Conference*, San Francisco, CA, USA, November 2003.

[69] O. Landsiedel, K. Wehrle, and S. Götz, "Accurate Prediction of Power Consumption in Sensor Networks," in *Proceedings of the 2nd IEEE Workshop on Embedded Networked Sensors*, Sydney, Australia, May 2005.

[70] J. Polastre, J. Hill, and D. Culler, "Versatile Low Power Media Access for Wireless Sensor Networks," in *Proceedings of the 2nd International Conference on Embedded Networked Sensor Systems*, Baltimore, MD, USA, 2004.

[71] B. Bougard, F. Catthoor, D. C. Daly, A. Chandrakasan, and W. Dehaene, "Energy Efficiency of the IEEE 802.15.4 Standard in Dense Wireless Microsensor Networks: Modeling and Improvement Perspectives," in *Proceedings of the 2005 Conference on Design, Automation and Test in Europe*, Munich, Germany, March 2005.

[72] Q. Wang and W. Yang, "Energy Consumption Model for Power Management in Wireless Sensor Networks," in *Proceedings of the 4th Annual IEEE Communications Society Conference on Sensor, Mesh and Ad Hoc Communications and Networks*, San Diego, CA, USA, June 2007.

[73] MEMSIC Inc., "MICA2 Wireless Measurement System," Data sheet.

[74] J. Molina-Garcia-Pardo, A. Martinez-Sala, M. Bueno-Delgado, E. Egea-Lopez, L. Juan-Llacer, and J. García-Haro, "Channel Model at 868 MHz for Wireless Sensor Networks in Outdoor Scenarios," in *Proceedings of the 2005 International Workshop on Wireless Ad-hoc Networks*, London, UK, May 2005.

[75] M. Haenggi, "Twelve Reasons not to Route over Many Short Hops," in *Proceedings of the 2004-Fall IEEE Vehicular Technology Conference*, 2004.

[76] HART Communication Foundation, "WirelessHART Technical Data Sheet," HCF_LIT-89 Revision 1.0B, May 2007.

[77] Moteiv Corporation, "Tmote Sky: Ultra Low Power IEEE 802.15.4 Compliant Wireless Sensor Module," Data sheet.

[78] Dust Networks, "SmartMesh-XT M2135 2.4 GHz Long Range Mote," Data sheet.

[79] MEMSIC Inc., "TelosB Mote Platform," Data sheet.

[80] ——, "MICAz - Wireless Measurement System," Data sheet.

[81] ——, "Imote2 - High-Performance Wireless Sensor Network Node," Datasheet.

[82] WISEBED, "Deliverable D1.3: Final Hardware Installation," May 2010.

[83] IEEE Computer Society, "IEEE Standard for Information Technology – Telecommunication and information exchange between systems – Local and metropolitan area networks – Specific requirements. Part 15.4: Wireless Medium Access Control (MAC) and Physical Layer (PHY) Specifications for Low-Rate Wireless Personal Area Networks (LR-WPANs)," October 2003.

[84] ——, "IEEE Standard for Information Technology – Telecommunications and information exchange between systems – Local and metropolitan area networks – Specific requirements Part 15.4: Wireless Medium Access Control (MAC) and Physical Layer (PHY) Specifications for Low-Rate Wireless Personal Area Networks (WPANs) Amendment 1: Add Alternate PHYs," August 2007.

[85] ——, "IEEE Standard for Information Technology – Telecommunications and information exchange between systems – Local and metropolitan area networks – Specific requirements. Part 15.4: Wireless Medium Access Control (MAC) and Physical Layer (PHY) Specifications for Low-Rate Wireless Personal Area Networks (WPANs) Amendment 2: Alternative Physical Layer Extension to support one or more of the Chinese 314-316 MHz, 430-434 MHz, and 779-787 MHz bands," April 2009.

[86] ——, "IEEE Standard for Information Technology – Telecommunications and information exchange between systems – Local and metropolitan area networks – Specific requirements. Part 15.4: Wireless Medium Access Control (MAC) and Physical Layer (PHY) Specifications for Low-Rate Wireless Personal Area Networks (WPANs) Amendment 3: Alternative Physical Layer Extension to support the Japanese 950 MHz bands," April 2009.

[87] J. Zheng and M. J. Lee, *Sensor Network Operations.* IEEE Press, 2004, ch. A Comprehensive Performance Study of IEEE 802.15.4.

[88] I. Ramachandran, A. K. Das, and S. Roy, "Analysis of the Contention Access Period of IEEE 802.15.4 MAC," *ACM Transactions on Sensor Networks*, vol. 3, no. 1, 2007.

[89] M. Petrova, J. Riihijärvi, P. Mähönen, and S. Labella, "Performance Study of IEEE 802.15.4 Using Measurements and Simulations," in *Proceedings of the 2006 IEEE Wireless Communications and Networking Conference*, Las Vegas, NV, USA, April 2006.

[90] J.-S. Lee, "Performance Evaluation of IEEE 802.15.4 for Low-Rate Wireless Personal Area Networks," *IEEE Transactions on Consumer Electronics*, vol. 52, no. 3, August 2006.

[91] B. Latré, P. D. Mil, I. Moerman, B. Dhoedt, and P. Demeester, "Throughput and Delay Analysis of Unslotted IEEE 802.15.4," *Journal of Networks*, vol. 1, no. 1, May 2006.

[92] M. Kohvakka, M. Kuorilehto, M. Hännikäinen, and T. D. Hämälinen, "Performance Analysis of IEEE 802.15.4 and ZigBee for Large-scale Wireless Sensor Network Applications," in *Proceedings of the 3rd ACM International Workshop on Performance Evaluation of Wireless Ad Hoc, Sensor and Ubiquitous Networks*, Terromolinos, Spain, October 2006.

[93] C. Perkins, E. Belding-Royer, and S. Das, "Ad hoc On-Demand Distance Vector (AODV) Routing," RFC3561, July 2003.

[94] V. Rao and D. Marandin, "Adaptive Backoff Exponent Algorithm for Zigbee (IEEE 802.15.4)," in *Proceedings of the 6th International Conference on Next Generation Teletraffic and Wired/Wireless Advanced Networking*, St.Petersburg, Russia, May 2006.

[95] S. Shin, H. Park, S. Choi, and W. Kwon, "Packet Error Rate Analysis of ZigBee under WLAN and Bluetooth Interferences," *IEEE Transactions on Wireless Communications*, vol. 6, no. 8, August 2007.

[96] J. Lee, Y. Su, and C. Shen, "A Comparative Study of Wireless Protocols: Bluetooth, UWB, ZigBee, and Wi-Fi," in *Proceedings of the 33rd Annual Conference of the IEEE Industrial Electronics Society*, 2007.

[97] E. Pinedo-Frausto and J. Garcia-Macias, "An Experimental Analysis of Zigbee Networks," in *Proceedings of the 33rd IEEE Conference on Local Computer Networks*, Montreal, QC, Canada, October 2008.

[98] A. Law and W. Kelton, *Simulation Modeling and Analysis*. McGraw-Hill Higher Education, 1997.

[99] R. Mathew and M. Younis, "Energy-Efficient Bootstrapping Protocol for Sensor Networks," in *Proceedings of the 2003 International Conference on Wireless Networks*, Las Vegas, NV, USA, June 2003.

[100] F. Barsi, A. Bertossi, F. Sorbelli, R. Ciotti, S. Olariu, and C. Pinotti, "Asynchronous Training in Wireless Sensor Networks," in *Proceedings of the 3rd International Workshop on Algorithmic Aspects of Wireless Sensor Networks*, Wroclaw, Poland, July 2007.

[101] F. Zhang, F. Wang, B. Dai, and Y. Li, "Performance Evaluation of IEEE 802.15.4 Beacon-Enabled Association Process," in *Proceedings of the 22nd International Conference on Advanced Information Networking and Applications*, Okinawa, Japan, March 2008.

[102] F. Cuomo, S. D. Luna, U. Monaco, and T. Melodia, "Routing in ZigBee: Benefits from Exploiting the IEEE 802.15.4 Association Tree," in *Proceedings of the 2007 IEEE International Conference on Communications*, Glasgow, Scotland, June 2007.

[103] I. Chakeres and L. Klein-Berndt, "AODVjr, AODV simplified," *ACM SIGMOBILE Mobile Computing and Communications Review*, vol. 6, no. 3, 2002.

[104] S. Tao, W. Wei, L. Xu-Dong, and L. Jian-Wei, "AODVjr Routing Protocol with Multiple Feedback Policy for ZigBee Network," in *Proceedings of the IEEE 13th International Symposium on Consumer Electronics*, Kyoto, Japan, May 2009.

[105] A. Khayyat and A. Safwat, "The Synchronized Peer-to-Peer Framework and Distributed Contention-Free Medium Access for Multihop Wireless Sensor Networks," *Journal of Sensors*, vol. 2008, 2008.

[106] G. Anastasi, M. Conti, M. Francesco, and A. Passarella, "Energy Conservation in Wireless Sensor Networks: a Survey," *Ad Hoc Networks*, vol. 7, no. 3, 2009.

[107] W. Ye, F. Silva, and J. Heidemann, "Ultra-Low Duty Cycle MAC with Scheduled Channel Polling," in *Proceedings of the 4th International Conference on Embedded Networked Sensor Systems*, Boulder, CD, USA, 2006.

[108] T. R. Park and M. J. Lee, "Power Saving Algorithms for Wireless Sensor Networks on IEEE 802.15.4," *IEEE Communications Magazine*, vol. 46, no. 6, June 2008.

[109] A. Giusti, A. Murphy, and G. Picco, "Decentralized Scattering of Wake-up Times in Wireless Sensor Networks," in *Proceedings of the 4th European Conference on Wireless Sensor Networks*, Delft, The Netherlands, January 2007.

[110] G. Anastasi, M. Conti, M. Di Francesco, and A. Passarella, "An Adaptive and Low-latency Power Management Protocol for Wireless Sensor Networks," in *Proceedings of the 4th ACM International Workshop on Mobility Management and Wireless Access*, Malaga, Spain, October 2006.

[111] M. Younis and K. Akkaya, "Strategies and Techniques for Node Placement in Wireless Sensor Networks: A Survey," *Ad Hoc Networks*, vol. 6, no. 4, 2008.

[112] I. Akyildiz, X. Wang, and W. Wang, "Wireless Mesh Networks: A Survey," *Computer Networks*, vol. 47, no. 4, 2005.

[113] D. Bertsekas and R. Gallager, *Data Networks*. Prentice-Hall, 1987.

[114] J. Jun and M. L. Sichitiu, "The Nominal Capacity of Wireless Mesh Networks," *IEEE Wireless Communications*, vol. 10, no. 5, October 2003.

[115] B. Aoun and R. Boutaba, "Max-Min Fair Capacity of Wireless Mesh Networks," in *Proceedings of the 2006 IEEE International Conference on Mobile Adhoc and Sensor Systems*, Vancouver, BC, Canada, October 2006.

[116] R. Bruno, M. Conti, and E. Gregori, "Mesh Networks: Commodity Multihop Ad Hoc Networks," *Communications Magazine, IEEE*, vol. 43, no. 3, March 2005.

[117] M. Conti and S. Giordano, "Multihop Ad Hoc Networking: The Reality," *IEEE Communications Magazine*, vol. 45, no. 4, April 2007.

[118] S. Corson, "Mobile Ad hoc Networking (MANET): Routing Protocol Performance Issues and Evaluation Considerations," RFC 2501, January 1999.

[119] calsoft labs, "Wireless 802.11s Mesh Networks, a Techno Commercial Overview," White Paper, 2010.

[120] P. Serrano, C. J. Bernardos, A. D. L. Oliva, and I. Soto, "Lessons Learned from the Deployment of a Multihop IEEE 802.11g Testbed Using COTS Devices," in *Proceedings of the 16th European Wireless Conference*, Lucca, Italy, April 2010.

[121] T. Clausen and P. Jacquet, "Optimized Link State Routing Protocol (OLSR)," RFC 3626, October 2003.

[122] A. Neumann, C. Aichele, M. Lindner, and S. Wunderlich, "Better Approach To Mobile Ad-hoc Networking (B.A.T.M.A.N.)," RFC Experimental, April 2007.

[123] G. Hiertz, D. Denteneer, S. Max, R. Taori, J. Cardona, L. Berlemann, and B. Walke, "IEEE 802.11s: the WLAN Mesh Standard," *IEEE Wireless Communications*, vol. 17, no. 1, February 2010.

[124] IEEE Computer Society, "IEEE P802.11s/D9.0 Draft STANDARD for Information Technology - Telecommunications and information exchange between systems - Local and metropolitan area networks- Specific requirements. Part 11: Wireless LAN Medium Access Control (MAC) and Physical Layer (PHY) specifications Amendment 10: Mesh Networking," February 2011.

[125] ——, "IEEE Standard for Information Technology – Telecommunication and information exchange between systems – Local and metropolitan area networks – Specific requirements. Part 15.5: Mesh Topology Capability in Wireless Personal Area Networks (WPANs)," May 2009.

[126] M. Lee, R. Zhang, C. Zhu, T. Park, C. Shin, Y. Jeon, S. Lee, S. Choi, Y. Liu, and S. Park, "Meshing Wireless Personal Area Networks: Introducing IEEE 802.15.5," *IEEE Communications Magazine*, vol. 48, no. 1, January 2010.

[127] IEEE Computer Society, "IEEE Standard for Information Technology – Telecommunication and information exchange between systems – Local and metropolitan area networks – Specific requirements. Part 16: Air Interface for Broadband Wireless Access Systems," IEEE Computer Society, June 2004.

[128] R. Sombrutzki, A. Zubow, M. Kurth, and J. Redlich, "Self-Organization in Community Mesh Networks: The Berlin RoofNet," in *Proceedings of the*

First Workshop on Operator-Assisted (Wireless Mesh) Community Networks, Berlin, Germany, September 2006.

[129] A. Goldsmith, *Wireless Communications*. Cambridge University Press, 2005.

[130] D. Stoyan, W. Kendall, J. Mecke, and D. Kendall, *Stochastic Geometry and its Applications*. Wiley New York, 1995.

[131] N. Abramson, "The ALOHA System - Another Alternative for Computer Communications," Storming Media, April 1970.

[132] P. Gupta and P. Kumar, "The Capacity of Wireless Networks," *IEEE Transactions of Information Theory*, vol. 46, no. 2, March 2000.

[133] J. Li, C. Blake, D. De Couto, H. Lee, and R. Morris, "Capacity of Ad Hoc Wireless Networks," in *Proceeding of the 7th ACM SIGMOBILE Annual International Conference on Mobile Computing and Networking*, Rome, Italy, July 2001.

[134] X. L. Huang and B. Bensaou, "On Max-Min Fairness and Scheduling in Wireless Ad-Hoc Networks: Analytical Framework and Implementation," in *Proceedings of the 2001 ACM Symposium on Mobile Ad Hoc Networking & Computing*, Long Beach, CA, USA, October 2001.

[135] N. Akhtar and K. Moessner, "On the Nominal Capacity of Multi-radio Multi-channel Wireless Mesh Networks," *Computer Communications*, vol. 31, 2008.

[136] J. Luo, C. Rosenberg, and A. Girard, "Engineering Wireless Mesh Networks: Joint Scheduling, Routing, Power Control and Rate Adaptation," *IEEE/ACM Transactions on Networking*, vol. 18, no. 5, October 2010.

[137] B. Aoun and R. Boutaba, "Max-Min Fair Capacity of Wireless Mesh Networks," in *Proceedings of the 2006 IEEE International Conference on Mobile Adhoc and Sensor Systems*, Vancouver, BC, Canada, October 2006.

[138] R. Vannier and I. Lassous, "Towards a Practical and Fair Rate Allocation for Multihop Wireless Networks based on a Simple Node Model," in *Proceedings of the 11-th ACM International Conference on Modeling, Analysis and Simulation of Wireless and Mobile Systems*, Vancouver, BC, Canada, October 2008.

[139] M. Lacage, M. H. Manshaei, and T. Turletti, "IEEE 802.11 Rate Adaptation: A Practical Approach," in *Proceedings of the 7-th ACM International Conference on Modeling, Analysis and Simulation of Wireless and Mobile Systems*, Venice, Italy, October 2004.

[140] T. Kim, H. Lim, and J. Hou, "Improving Spatial Reuse through Tuning Transmit Power Carrier Sense Threshold, and Data Rate in Multihop Wireless Networks," in *Proceedings of the 12th Annual International Conference on Mobile Computing and Networking.* Los Angeles, CA, USA, September 2006.

[141] A. Kamerman and L. Monteban, "WaveLAN-II: A High-Performance Wireless LAN for the Unlicensed Band," *Bell Labs Technical Journal*, vol. 2, no. 3, 1997.

[142] S. Wong, H. Yang, S. Lu, and V. Bharghavan, "Robust Rate Adaptation for 802.11 Wireless Networks," in *Proceedings of the 12th Annual International Conference on Mobile Computing and Networking*, Los Angeles, CA, USA, September 2006.

[143] S. Toumpis and A. Goldsmith, "Capacity Regions for Wireless Ad Hoc Networks," *IEEE Transactions on Wireless Communications*, vol. 2, no. 4, 2003.

[144] L.-W. Chen, Y.-C. Tseng, Y.-C. Wang, D.-W. Wang, and J.-J. Wu, "Exploiting Spectral Reuse in Routing, Resource Allocation, and Scheduling for IEEE 802.16 Mesh Networks," *IEEE Transactions on Vehicular Technology*, vol. 58, no. 1, January 2009.

[145] S. Max, E. Weiss, and G. Hiertz, "Benefits and Limitations of Spatial Reuse in Wireless Mesh Networks," in *Proceedings of the 10-th ACM International Conference on Modeling, Analysis and Simulation of Wireless and Mobile Systems*, Chania, Crete Island, Greece, October 2007.

[146] E. B. Hamida, G. Chelius, and J.-M. Gorce, "On the Complexity of an Accurate and Precise Performance Evaluation of Wireless Networks Using Simulations," in *Proceedings of the 11-th ACM International Conference on Modeling, Analysis and Simulation of Wireless and Mobile Systems*, October 2008.

[147] O. Dousse, F. Baccelli, and P. Thiran, "Impact of Interferences on Connectivity in Ad Hoc Networks," *IEEE/ACM Transactions on Networking*, vol. 13, no. 2, 2005.

[148] H. Thompson, "Distribution of Distance to Nth Neighbour in a Population of Randomly Distributed Individuals," *Ecology*, vol. 37, no. 2, April 1956.

[149] G. Bianchi, "Performance Analysis of the IEEE 802.11 Distributed Coordination Function," *IEEE Journal on Selected Areas in Communications*, vol. 18, no. 3, 2000.

[150] G. R. Hiertz, S. Max, Y. Zhang, T. Junge, and D. Dentenee, "IEEE 802.11s MAC Fundamentals," in *Proceedings of the First IEEE International Workshop on Enabling Technologies and Standards for Wireless Mesh Networking*, Pisa, Italy, October 2007.

[151] W. Ogryczak, M. Pióro, and A. Tomaszewski, "Telecommunications Network Design and Max-Min Optimization Problem," *Journal of Telecommunications and Information Technology*, vol. 3, no. 3, 2005.

[152] A. Capone, G. Carello, I. Filippini, S. Gualandi, and F. Malucelli, "Routing, Scheduling and Channel Assignment in Wireless Mesh Networks:

Optimization Models and Algorithms," *Ad Hoc Networks*, vol. 8, no. 6, August 2010.

ISSN 1432-8801